Cranfield University

THEOKLIS NIKOLAIDIS

WATER INGESTION EFFECTS ON GAS TURBINE ENGINE PERFORMANCE

SCHOOL OF ENGINEERING

PhD THESIS

Cranfield University

SCHOOL OF ENGINEERING

PhD THESIS

Academic Year 2007-2008

THEOKLIS NIKOLAIDIS

WATER INGESTION EFFECTS ON GAS TURBINE ENGINE PERFORMANCE

Supervisor: P. Pilidis

October 2008

ABSTRACT

Although gas turbine engines are designed to use dry air as the working fluid, the great demand over the last decades for air travel at several altitudes and speeds has increased aircraft's exposure to inclement weather conditions. Although, they are required to perform safely under the effect of various meteorological phenomena, in which air entering the engine contains water, several incidents have been reported to the aviation authorities about power loss during flight at inclement weather. It was understood that the rain ingestion into a gas turbine engine influences the performance of the engine and particular the compressor and the combustor.

The effects of water ingestion on gas turbine engines are aerodynamic, thermodynamic and mechanical. These effects occur simultaneously and affect each other. Considering the above effects and the fact that they are time-dependent, there are few gas turbine performance simulation tools, which take into account the water ingestion phenomenon.

This study is a new research of investigating theoretically the water ingestion effects on a gas turbine performance. It focuses on the aerodynamic and mechanical effects of the phenomenon on the compressor and the combustor. The application of Computational Fluid Dynamics (CFD) is the basic methodology to examine the details of the flow in an axial compressor and how it is affected by the presence of water. The calculations of water film thickness, which is formed on the rotor blade, its motion (direction and speed) and the extra torque demand, are provided by a code created by the author using FORTRAN programming language. Considering the change in blade's profile and the wavy characteristics of the liquid film, the compressor's performance deterioration is calculated.

The compressor and combustor's deterioration data are imported to a gas turbine simulation code, which is upgraded to calculate overall engine's performance deterioration. The results show a considerable alteration in engine's performance parameters and arrive at the same conclusions with the relevant experimental observations.

Keywords: Simulation, Film, Deterioration, Rain, Adverse Weather.

ACKNOWLEDGEMENTS

Thank you God, I did it I never thought I would (**but I wanted so much**)!

I feel lucky for being a student of Cranfield University and meeting very interesting people. It was a wonderful experience, which has really broadened my mind.

I would like to seize this opportunity to thank the following people for their help and support throughout this project:

I wish to express my gratitude to my supervisor and mentor, Professor Periclis Pilidis for his continuous support, in every aspect, over these years. Without his consultation and assistance, I would have hardly completed successfully this work.

Dr Joao Amaral Teixeira, who was tirelessly discussing about my work. His help on the CFX analysis was invaluable. I always remember his friendliness and his good sense of humour.

Mr Chris Freeman from Rolls-Royce plc for his ideas and guidance about my study.

Dr Vasillios Pachidis, who was always available for discussion and suggestions.

Dr John Williams, former of Cambridge University, for his willingness to discuss about my project and welcome me to the “water ingestion community”.

Mrs Anita Beal of the Library Students Offsite Services, whose support and understanding helped me overcome all the difficulties of being a part-time student and made me feel very much a part of the university. She tirelessly responded to my request for articles.

Dr Les Oswald (Cranfield High Performance Computer Team) and Dr Julian Turnbull (former of Cranfield High Performance Computer Team) for their support on logging on and using CFX, while being off-campus.

Finally, I dedicate this work to my beloved wife Louisa and my children Eirini, Efstratios and Marietta who always stood by me. They were next to me when I wanted it and they did not when I did not want it.

TABLE OF CONTENTS

ABSTRACT i

ACKNOWLEDGEMENTS ii

TABLE OF FIGURES vii

TABLE OF TABLES xii

TABLE OF EQUATIONS xiii

Nomenclature xv

1 Introduction 1

1.1 Background 1

1.2 Performance Simulation 2

2 Project Objectives 4

3 Thesis Structure 5

4 Literature Review 7

4.1 Problem Identification 7

4.2 Atmospheric Water 12

4.3 Water Droplet Behaviour 18

4.3.1 Water Droplets in High-Speed Airflow 18

4.3.2 Droplet Splashing – Deposition – Film Formation 24

4.3.3 Water Evaporation 31

4.4 Intake 38

4.4.1 Scoop effect 38

4.5 Compressor 40

4.5.1 Water Film Formation and Motion 40

4.5.1.1 Water Droplet Trajectories 41

4.5.1.2 Forces Acting on Deposited Water Droplets 42

4.5.1.3 Water Film Thickness 47

4.5.1.4 Water Film Wavy Characteristic 51

4.5.2 Tip clearance effects 54
4.5.3 Effects on Compressor Performance 54
4.6 Combustor 60
4.6.1 Effects on Combustor Performance 60
4.7 Turbine 66
4.8 Engine Control 66
4.9 Engine Protection against Water Ingestion 67
4.10 Concluding Remarks 68
5 Project Methodology 70
6 CFD of an Axial Flow Compressor 72
6.1 Compressor Model – Mesh Generation 72
6.1.1 Grid Checks 74
6.2 CFD Parameters 75
6.3 Application of CFD 77
6.3.1 Process Overview 77
6.3.2 Test Strategy 80
6.3.2.1 Blade Rotational Speed Factor 81
6.4 Water Film Computation 82
6.4.1 Span-wise (Radial) Movement 84
6.4.2 Chord-wise Movement 86
6.4.3 Torque calculation 88
6.4.4 Water Film Characteristics 89
6.5 CFD Results 91
6.5.1 Lagrangian Tracking Model 92
6.5.2 Water Deposition on Blade Surface 93
6.5.3 Effects of Water Ingestion Parameters 95
6.5.3.1 Effect of Ingested Water Mass 95
6.5.3.2 Effect of droplet diameter 98

6.5.3.3 Effect of water droplet speed 102
6.5.4 Effect of rotational speed 105
6.6 Compressor Performance Results 107
6.6.1 Isentropic Efficiency (ETA) 107
6.6.2 Pressure Ratio (PR) 109
6.6.3 Non-dimensional Mass Flow (WAC) 110
6.6.4 Water Evaporation 111
6.7 Data Processing 112
6.8 FILM_MOTION Results Validation 115
6.9 Concluding Remarks 118
7 Water Ingestion - Engine Performance Simulation 123
7.1 The Turbomatch Code 123
7.2 The Turbomatch Code with Water Ingestion Capability 125
7.2.1 Intake 127
7.2.2 Compressor 128
7.2.3 Combustor 130
7.2.4 Turbine - Nozzles 135
7.2.5 Mixing Components 136
7.3 Performance Results 136
7.3.1 PCN Handle 138
7.3.2 TET Handle 145
7.4 Code's Limitations 148
7.5 Code Validation 149
7.6 Concluding Remarks 155
8 Discussion 156
8.1 Compressor 156
8.1.1 Water Deposition 156
8.1.2 Liquid Water Film Thickness 156

8.1.3 Liquid Water Film Motion 158
8.1.4 Compressor's Performance 159
8.2 Combustor 163
8.3 Engine Performance Simulation 164
8.3.1 PCN Handle 164
8.3.2 TET Handle 166
9 Conclusions – Further Work 170
9.1 Conclusions 170
9.1.1 Methodology 170
9.1.2 Application of CFD 171
9.1.3 Engine Performance Simulation 173
9.2 Further Work 175
REFERENCE 179
APPENDICES 191
A Compressor Blading Data A-1
B Off-campus Connection with Cranfield HPC B-1
C Creation of Computational Domain C-1
D FILM_MOTION Flowchart D-1
E Forecast Function E-1
F Turbomatch Results Spreadsheet F-1
G Water Ingestion Module Flowchart G-1

TABLE OF FIGURES

Figure 4-1: Inclement Weather In-flight Shutdown Aircraft Events 9

Figure 4-2: CMF56-3 Fan and Booster Cross Section 10

Figure 4-3: Certification Standard Atmospheric Rain Concentration (gr of water/m^3 of air) 16

Figure 4-4: Raindrop Size Distribution: (a) Contribution to the Total Number of Raindrops from each 0.5 mm Diameter Interval, (b) Contribution to the Total LWC from each 0.5 mm Diameter Interval. 17

Figure 4-5: Vertical Profile of LWC for the 10^{-8} Probability LWC of 18.9 gr/m^3 . 18

Figure 4-6: Modes of droplets disintegration. Above: Bag break-up. Down: Shear break-up 20

Figure 4-7: Droplet Break-Up Criteria at Descent Idle Airflow Velocity Range .. 21

Figure 4-8: Droplet break-up Regimes: (a) bag break-up (b) shear or boundary layer break-up (c) Sheet break-up and (d) catastrophic break-up 22

Figure 4-9: Parameters Governing the Impact of a Liquid Drop 25

Figure 4-10: Limits for Splashing and Deposition of Droplets 28

Figure 4-11: Droplet impingement on a wavy Film 29

Figure 4-12: Droplet Impingement 30

Figure 4-13: Deposited Mass Fraction and Composition Ratio of the Secondary Droplets 31

Figure 4-14: Temperature-specific volume water diagram 32

Figure 4-15: Water T-S Diagram 32

Figure 4-16: Droplet Trajectories in an Axial-Flow Compressor 34

Figure 4-17: Vapour Mass Fraction Vs Compressor Length 34

Figure 4-18: Scoop Factor Effect 39

Figure 4-19: Droplet Trajectories Estimation 41

Figure 4-20: Droplet Trajectories for Different Rotor Speed 42

Figure 4-21: Water Droplet Trajectories for Different Stagger Angle and Zero Friction Force 45

Figure 4-22: Laminar Film Flow Friction Factor (K) over a Rotating Surface 46

Figure 4-23: Film Thickness Parameter 47

Figure 4-24: Water Ligament Formation and Break-up at the Blade Trailing Edge 48

Figure 4-25: HPC Running Line Movement due to Water Ingestion 57

Figure 4-26: Combustor Pressure Loss Factor change 61

Figure 4-27: Combustor Temperature Increase Factor 62

Figure 4-28: Water Flow in the Combustor 62

Figure 4-29: Combustor Efficiency Deterioration due to Ingested Water 64

Figure 4-30: V-shaped Guide Vanes at Diffuser 66

Figure 6-1: 3D View of Compressor IGV & 1st Stage 74

Figure 6-2: 3D View of Axial Flow Compressor Model 75

Figure 6-3: CFD Work Flowchart 79

Figure 6-4: Water Ingestion Parameters 81

Figure 6-5: 3D Computational Domain 83

Figure 6-6: Water Mass Deposition on Rotor Pressure Surface 83

Figure 6-7: Water Film Span-wise Motion 85

Figure 6-8: Rotor Blade Pressure Surface Regions 91

Figure 6-9: Water mass deposition for (a):1000, (b):5000, (c):10000, (d):15000 and (e):20000 water droplets 93

Figure 6-10: Water Mass Deposition on Rotor Blade (BUILDUP units: kgr/sec) 94

Figure 6-11: Water Film Thickness (m) for 30% water/air, D_w=1 mm 95

Figure 6-12: Water Film Thickness Change (m) for 4% to 30% Increase of Ingested Water (idle speed, D_{dr}=1 mm, $V_{dr\text{-}rel}$=0) 96

Figure 6-13: Water Film Thickness Increase due to Ingested Water Mass 96

Figure 6-14: Increase of Water Film Thickness (%) due to Ingested Water Mass 97

Figure 6-15: Torque Increase due to Ingested Water Mass 98

Figure 6-16: Build-up Mass Change for Different Droplets Size (0.003mm to 3mm, for 2% water/air, V_w=150m/sec) 99

Figure 6-17: Water vapour change for different droplets size (0.003mm to 3mm, for 2% water/air, V_w=150m/sec) 100

Figure 6-18: Water Build-up Mass Variation for Different Droplet Sizes 101

Figure 6-19: Water Build up Mass Difference when Ingestion Speed changes 102

Figure 6-20: Build up Mass and Torque Variation when Droplet Ingestion Speed Reduces 103

Figure 6-21: Air Axial Velocity Reduction due to Water Ingestion 104

Figure 6-22: Water Film Exit Speed when Droplet Ingestion Speed Varies 105

Figure 6-23: Water Film Thickness Change due to Angular Speed 106

Figure 6-24: Water speed angle change due to angular speed 107

Figure 6-25: Efficiency Deterioration due to Ingested Water Mass 108

Figure 6-26: ETA – WAC Deterioration due to Ingested Water Mass 108

Figure 6-27: PR Deterioration due to Ingested Water 109

Figure 6-28: PR – WAC Deterioration due to Ingested Water 110

Figure 6-29: WAC Deterioration due to Ingested Water 111

Figure 6-30: Water Vapour, Outlet Total Temperature Change due to Ingested Water 111

Figure 6-31: Compressor ETA Deterioration Processed Data 113

Figure 6-32: PR Deterioration Processed Data 113

Figure 6-33: WAC Deterioration Processed Data 114

Figure 6-34: Torque Increase Processed Data 115

Figure 6-35: Film Thickness Measurements and Theoretical Calculations 116

Figure 6-36: Water Axial Exit Speed Vs Ingested Water 117

Figure 6-37: Water Ingestion Parameters Influence on Torque Demand 119

Figure 6-38: Performance Parameters Change due to Ingested Water 120

Figure 7-1: WAG property in the Turbomatch Result File 126

Figure 7-2: Turbomatch Case Selector Error Message.....127

Figure 7-3: Linear Lagrange Interpolation.....129

Figure 7-4: Burner ETA Deterioration due to Ingested Water 132

Figure 7-5: Burner Total Pressure Loss Increase due to Water Ingestion 133

Figure 7-6: Turbomatch Result File.....138

Figure 7-7: Compressor Map under Water Ingestion Condition (PCN handle)139

Figure 7-8: Operating Point Movement due to Water Ingestion 139

Figure 7-9: Surge Margin Decrease due to Water Ingestion.....141

Figure 7-10: Compressor ETA deterioration due to water ingestion (PCN handle) 142

Figure 7-11: Detail of Compressor ETA deterioration (PCN handle).....142

Figure 7-12: Compressor Work Increase due to Ingested Water.....143

Figure 7-13: Fuel Flow Increase due to Ingested Water for % of Evaporation 144

Figure 7-14: % Difference in Fuel Flow between Full and No Water Evaporation Cases.....144

Figure 7-15: Engine Speed Reduction under Water Ingestion Condition (TET handle) 145

Figure 7-16: Compressor Map under Water Ingestion Condition (TET handle)146

Figure 7-17: Compressor ETA Variation under Water Ingestion Condition (TET handle) 146

Figure 7-18: Percentage Deterioration of Net and Specific Thrust with Water Ingestion (TET handle).....147

Figure 7-19: SFC Increase due to Water Ingestion (TET handle).....148

Figure 7-20: PR Vs N due to Water Ingestion.....150

Figure 7-21: Error in %PR and %N change due to Water Ingestion between Simulated and Experimental Results 151

Figure 7-22: Torque Experimental Measurements and Simulation Results under Water Ingestion Condition.....152

Figure 7-23: Loss of Pressure Rise due to Water Ingestion–Experimental and Theoretical Data.....153

Figure A-1: Siemens V94.3A Geometry A-3
Figure A-2: 1st Rotor DCA Blading Scratch Data A-5
Figure A-3: 1st Rotor Blade Theta Angle Vs Axial Location A-6
Figure A-4: 1st Rotor Blade Thickness Vs Axial Location A-6
Figure A-5: IGV Blade Smoothing A-7
Figure A-6: IGV Blade 3D View A-7
Figure A-7: 1st Rotor 3D View A-8
Figure A-8: 1st Stator 3D View A-8
Figure A-9: IGV Blade Grid A-9
Figure A-10: 1st Rotor Blade Grid A-9
Figure B-1: PuTTY Log on Screen B-1
Figure B-2: PuTTY SSH Protocol B-2
Figure B-3: PuTTY SSH Tunnelling B-3
Figure C-1: 3D View of Compressor IGV & 1st Stage C-3
Figure C-2: Mid Span Grid Surface C-3
Figure C-3: Meridional Grid Surface C-4
Figure C-4: 3D Axial Flow Compressor Model C-4
Figure D-1: FILM_MOTION Flowchart D-2
Figure D-2: FILM_MOTION Screen View D-4
Figure F-1: Turbomatch Spreadsheet File – Water Ingestion Variables Definition F-1
Figure F-2: Turbomatch Spreadsheet File – Variables Definition for Intake and Burner F-2
Figure F-3: Turbomatch Spreadsheet File F-2
Figure G-1: Turbomatch Water Ingestion Flowchart G-2

TABLE OF TABLES

Table 4-1: Equations Used to convert Rain Rate (Rr: mm/hr) to LWC (Mw: gr/m3) 14

Table 4-2: Dry air and water constant values in Cp polynomial calculations .. 37

Table 6-1: J79-GE-17 Compressor Design Parameters 73

Table 6-2: Water Ingestion Parameters Variation due to change of Water Droplet Diameter 101

Table 6-3: Water Ingestion Parameters and Simulation Qualitative Results 119

Table 7-1: Turbomatch Station Vector Items 124

Table 8-1: Theoretical and Experimental Results 168

Table A-1: Siemens V94.3A design parameters A-1

Table A-2: Siemens V94.3A Geometric Characteristics A-2

Table A-3: Blading Data for the 1st rotor and 1st stator A-4

Table C-1: J79-GE-17 Design Parameters C-1

Table C-2: Siemens V34 – J79 Compressor Scaling Parameters C-2

TABLE OF EQUATIONS

Equation 4-1: LWC Probability Equation 13

Equation 4-2: Rain Intensity Level Vs Probability of Occurrence 15

Equation 4-3: Drag Force exerted by Air on a Water Droplet 19

Equation 4-4: Drag Force - Drag Coefficient 19

Equation 4-5: Drag Coefficient Calculation 19

Equation 4-6: Drag Coefficient Calculation 19

Equation 4-7: Drag Coefficient Calculation 19

Equation 4-8: Drag Coefficient Calculation 19

Equation 4-9: Weber Number Definition 20

Equation 4-10: Water Mass Mean Droplet Diameter after Break-Up 23

Equation 4-11: Ohnesorge Number Definition 27

Equation 4-12: Oh, We and Re Relation 27

Equation 4-13: K Splashing Parameter definition 27

Equation 4-14: Laplace Number (La) Definition 29

Equation 4-15: Droplet Rate Evaporation 35

Equation 4-16: Gas Constant Factor for Moist Air 36

Equation 4-17: Molecular Weight for Moist Air 36

Equation 4-18: Gamma Factor for Moist Air 36

Equation 4-19: Cp Polynomial Calculation 36

Equation 4-20: Specific Heat Factor for Moist Air 37

Equation 4-21: Fully non-dimensional Mass Flow and Speed Parameters 37

Equation 4-22: Non-dimensional Mass Flow and Speed Correlations for Moist Air 37

Equation 4-23: Friction Force on a Liquid Water Mass 44

Equation 4-24: Friction Factor Calculation 46

Equation 4-25: Water Film Acceleration 48

Equation 4-26: Water Film Thickness on Rotor Blade 50
Equation 4-27: Water Film Thickness Calculation 50
Equation 4-28: Friction Factor Estimation 52
Equation 4-29: Equivalent Sand Grain Roughness Equation 53
Equation 4-30: Power Demand due to Water 60
Equation 4-31: Pressure Loss Factor Definition 61
Equation 4-32: Temperature Increase Factor Definition 62
Equation 6-1: Mass Continuity Equation 85
Equation 6-2: Water Film Steady Flow Equation 85
Equation 6-3: Zero Pressure Gradients Equation 85
Equation 6-4: Navier-Stokes Equation in Span-wise Direction 86
Equation 6-5: Centrifugal Force Equation 86
Equation 6-6: Centrifugal Force – Mass Equation 86
Equation 6-7: Film Thickness Equation 86
Equation 6-8: Water Film Span-wise Velocity 86
Equation 6-9: Wall Shear Stress Equation 87
Equation 6-10: Continuity Equation in Chord-wise Direction 87
Equation 6-11: Chord-wise “Mass Component” Equation 88
Equation 6-12: “Mass Components” Equation 88
Equation 6-13: Water Torque Equation 89
Equation 6-14: Equivalent Sand-Grain Roughness Equation 90
Equation 6-15: Compressor Isentropic Efficiency Equation 107
Equation 7-1: Linear Lagrange polynomial 129
Equation 7-2: Combustor Mass and Energy Balance Equation 133
Equation 7-3: Manipulated Formula of Mass and Energy Balance Equation 134
Equation 7-4: Combustor Fuel Flow Equation 134
Equation 7-5: Surge Margin Definition 140

Nomenclature

Symbols

Chapter 4

A_o: free stream area (m)

A_1: intake highlight area (m)

α_{iD}: impingement angle of primary droplets (deg)

C_{pa}: air specific heat capacity (J/Kg K)

C_{iD}: velocity of primary droplets (m/sec)

CV: mass vapour per unit mass of dry air

CL: mass liquid per unit mass of dry air

D_{iD}: diameter of primary droplets (m)

D_w: diameter of drop (m)

D_{mw}: mean diameter of drop (m)

F_d: drag force exerted by air (Nt)

F_f: Friction Force (Nt)

F_I: Inertia Force (Nt)

G: Film local water mass flow rate per unit width of film (kg/sec m)

h_{fg}: Latent heat of evaporation (J/kg)

K: Splashing Parameter

k: Friction Factor (1/sec)

K: Non-dimensional friction factor ($K=k/\omega$)

k_s: Equivalent sand grain roughness

k_{CLA}: Arithmetic centreline average roughness

La: Laplace number

MW_w: Water molecular weight=18.015

MW_a: Air molecular weight=28.96

MW: Molecular weight

Oh: Ohnesorge number

P: Power (kW) or Probability

P_j: Joint Probability

P_t: Duration Probability

Rr: Rain Rate (mm/hr)

Ro: Universal gas constant (8.31 KJ/mole °K)

R_{fac}: Ratio of mixture gas constant R_{moist} to that of dry air R_{air}

R_{air}: 287.05 J/kgr °K

R_w: 461.5 J/kgr °K

Re: Reynolds number

T_a: Air temperature (°K)

T_d: Droplet temperature (°K)

V_a: Air velocity (m/sec)

V_w: Droplet velocity (m/sec)

We: Weber Number

WAR_{molar}: The ratio of water to air by the number of moles,

W: Mass flow (kg/sec)

Chapter 6

a: Height of the grid cell (m)

b: Length of the grid cell (m)

E: Node area wall (m^2)

m_K: Mass of deposited water moving to the K computational index (span wise direction) (kg/sec)

m_I: Mass of deposited water moving to the I computational index (chord wise direction) (kg/sec)

$\dot{m}$: The water mass rate (kgr/sec)

M_b (or M_w): Build-up (i.e. deposited) mass (kg/sec)

M: Water deposited mass (kg) at equilibrium condition

R: Radius of the node (m)

u: Water mass velocity to the span-wise direction (m/sec)

v: Water mass velocity to the chord-wise direction

V_θ Blade's tangential speed (m/sec)

Chapter 7

COMPW: Compressor work (W)

CM: Corrected mass flow

CN: Relative non-dimensional speed

DP: Design Point

ETA: Efficiency

FP_l: Pressure Loss Factor

FT_l: Temperature Increase Factor

f: Fuel/air ratio

FN: Net Thrust (Nt)

h: Enthalpy (kJ)

ke: Kinetic energy (kJ)

m_a: Air mass flow (kg/sec)

m_w: Water mass flow (kg/sec)

m_f: Fuel mass flow (kg/sec)

N: Rotational speed (rpm)

PR: Pressure ratio

RelHum: Relative Humidity

SFC: Specific Fuel Consumption (kg/kW h or kg/Nt h)

SFN: Specific Thrust (Nt sec/kg)

SM: Surge Margin

TRQW: Compressor torque due to liquid water (Ntm)

TURBW: Turbine work (W)

WAC: Non-dimensional mass flow (kg √K/kPa sec)

X: Liquid water quality

Greek Symbols

β: Stagger angle

Γ: Diffusion coefficient for water vapour in air

γ: Ratio of specific heat

δ: Film thickness (m)

η: Deposited mass fraction

θ: Total energy (J)

λ_a: Air conductivity

μ_w: Liquid water dynamic viscosity (10^{-3} kg/m sec)

μ_a: Air viscosity (1.8 10^{-5} kg/m sec)

μ: Viscosity (dynamic: kg/m sec, kinematic m^2/sec)

ξ: Composition ratio

ρ_l: Water density (998 kg/m^3)

ρ_a: Air density (1.2 kg/m^3)

σ_w: Water Surface Tension (0.07 Nt/m)

φ: Fuel equivalence ratio

Subscripts

a: air

w: water

st: steam

m: mixture

Abbreviations

APU: Auxiliary Power Unit

AD: Airworthiness Directive

BD: Brick Data

B.C.: Boundary Conditions

CFD: Computational Fluid Dynamics

DCA: Double Circular Arc

EASA: European Aviation Safety Agency

HPC: High Pressure Compressor

HWC: Hail Water Concentration

LHV: Low-Heating Value

LPC: Low Pressure Compressor

LWC or Mw: Liquid Water Concentration

MSL: Mean Sea Line

MLP: Modified Linear Profile

MS: Microsoft

NTSB: National Transportation Safety Board

PAC: Physical Advection Correction

VBV: Variable Bleed Valve

VWC: Vapour Water Content

WAR: Water to air ratio (injection or humidity)

WAG: Water to air ratio (ingestion of liquid water due to rain)

1 Introduction

This chapter discusses the background, the current state of water ingestion simulation and the reasons, which led to commence this project.

1.1 Background

Over the last decades, the development of aviation demanded improved propulsion systems that would be able to boost aircraft's ability to fly higher and faster. This enabled the design of new engines like the high-bypass turbofan or turboprop, etc. Although gas turbine engines are designed to use dry air as the working fluid, the great demand for air travel at several altitudes and speeds has increased aircraft's exposure to inclement weather conditions. However, they are required to perform safely under the effect of various meteorological phenomena, which air entering the engine contains water.

Up to the early 80's, several incidents have been reported to the aviation authorities about power loss during flight at inclement weather. It was understood that the rain ingestion into a gas turbine engine influences the performance of the compressor, combustor, turbine and nozzle. This performance deterioration may result in flameout or shutdown of the engine.

The aviation authorities and the jet engines manufacturers decided to study the problem in depth and take all the necessary measures. They devoted their full resources to investigate the incidents, to evaluate any threat to the flight safety and, finally, to propose the necessary changes to the existing certification regulations. They noticed that the majority of the incidents referred to large high bypass ratio engines and they occurred at low power settings (i.e. descent or approach flight phases). By mid-1991, engine modifications had been developed and tested, which aimed to improve the engine's rain ingestion capability. The aviation authorities issued new water ingestion certification regulations and the engine manufacturers complied with them, showing that the matter was of extreme interest.

Nevertheless, it seems that the resulted modifications and their application in the engine's design have not fully resolved the problem. In 2002, a new incident occurred although the engines involved in it, had incorporated all the design modifications. Currently, the aviation authorities and the jet engines manufacturers are working again on the effect of water ingestion trying to explore it in depth evaluating all the parameters, like the so-called scoop factor.

Many in-flight and on-ground tests have been undertaken by engines manufacturers to establish the water ingestion conditions. These tests were necessary, albeit expensive. However, another satisfactory way to establish the

tests conditions is to use analytical or computational procedures for calculating the components performance deterioration. When the power loss incidents became relatively frequent, the demand for engine test under water ingestion conditions was increased. At the same time, the increase of computer capability and the low development cost made feasible the creation of water-ingestion simulation codes, mainly by the gas turbine industry. However, there is not a great deal of published information and the way used to model the effects. In any case, the complexity of the phenomenon has driven to the conclusion that only simulation combined with experimental testing can assure the accurate prediction of gas turbine performance.

Without doubt, both the engine's manufacturers and the aviation authorities have made a considerable effort to address the rain ingestion effects. Their growing concern about the operation in adverse weather conditions is fully justified. However, there are still open items in the process of investigating the rain ingestion effects, which should be resolved for enhancing the aviation safety.

1.2 Performance Simulation

When rain is ingested into an engine, the water droplets impinge on the blade where they splash and part of their mass deposit on the blade. The deposit liquid water forms a film, which moves radially outwards under the influence mainly of the inertia forces. The film concentrates at the tip clearance and part of it disintegrates. Although evaporation may occur in the last stages of compressor, the largest part of this liquid water will move downstream to the burner, where it evaporates. Rundown of the engine or even flameout are caused. The effects of water ingestion on gas turbine engines are aerodynamic (air shear force increase, change of velocity triangle in the compressor), thermodynamic (heat and mass transfer, temperature distortion, change of gas properties in the working medium) and mechanical (demanded torque increase, blade vibration, change of structural load). These effects occur simultaneously and affect each other.

Considering the above effects and the fact that they are time-dependent, it is understood that it is difficult to simulate accurately the phenomenon of water ingestion. Several commercial performance simulation codes include only the thermodynamic effects of water, which are closely related to water injection (fine droplets evaporation and neglecting any aerodynamic or mechanical effect). Nevertheless, there are published water ingestion simulation analyses, which focused on specific areas of the phenomenon and neglected some others. Hence, extensive work has been done on the time-dependent nature of the phenomenon and on its aerodynamic effects. Furthermore, engine's behaviour with ingested water in transient mode of operation has been examined.

Although the mechanical effects of water ingestion dominate the engine's performance, they have not been examined thoroughly. In the analytical or computational methods of investigating the phenomenon, the torque increase has not been calculated. The water film formation on the compressor rotor blade has been estimated assuming that it moves under the influence of the centrifugal force and neglecting the shearing action of the airflow or the momentum of the subsequent deposited droplets.

2 Project Objectives

In this chapter, the objectives of this research project are described. Furthermore, the milestones that have to be achieved are presented.

It is well understood that the long-term goals are completed by the teamwork of several researchers. This project may be included in a broader research, which has the objective of developing a computer code that will enable in the future the simulation of water ingestion effects on gas turbine engines. The combined effects of water ingestion are currently observed only in large-scale engine tests and are engine-geometry dependent. This code will encapsulate the complex processes and the component interactions. Therefore, the manufacturers will be able to detect engine's vulnerability to water ingestion during the design early stages and they will manage to improve its design reducing the manufacturing cost. Furthermore, it will contribute to the aviation safety because the engine will be examined in a variety of weather conditions.

Having said this, **the objective of this research project is to investigate and quantify the performance deterioration of a gas turbine engine due to water ingestion**. The specific milestones in the context of this work are:

- the identification of the parameters that affect water flow in a gas turbine engine under water ingestion conditions.
- the evaluation of their impact on engine's operation.
- the investigation of engine's major components performance deterioration due to water ingestion, and mainly the compressor and the combustor.
- the development of a simulation code to account for the effects of water ingestion and its integration with the Turbomatch simulation tool.

Apart from the primary objective, a secondary one is to upgrade Turbomatch code in the way the user manipulates its results. The code used to export its results in a MS Excel spreadsheet but after its last improvement, this function is inoperative.

3 Thesis Structure

The thesis consists of nine chapters, which are subdivided into several sections and subsections. Chapters 1, 2 and 3 (**1: Introduction, 2: Thesis Objectives** and **3: Thesis Structure**) are self-explanatory.

The broader literature review performed in the context of this work is included in **Chapter 4 - Literature Review.** The scope of this chapter is to present the breadth and depth of the water ingestion phenomenon as it has been illustrated in the published literature. The literature review is focused on areas, which have been identified that affect the phenomenon. Thus, *Section 1 - Problem Identification* covers the aviation history of rain ingestion incidents/accidents and their investigation of the aviation authorities. *Section 2 - Atmospheric Water* covers the nature of atmospheric water and the weather threat analysis. *Section 3 - Water Droplet Behaviour* analyses the processes, which take place when rain is ingested by a gas turbine engine. Furthermore, the effects on engine's performance in the individual components are described in *Section 4 – Intake*, *Section 5 – Compressor*, *Section 6 – Combustor*, *Section 7 – Turbine*, and *Section 8 – Engine Control*. Finally, *Section 9 – Engine Protection against Water Ingestion* introduces several methods either proposed by engineers or taken by the jet engine manufacturers against the water ingestion effects.

Chapter 5 - Project Methodology explains the methodology that is used in the context of this research. Bearing in mind the project's objectives and the literature review, there is a description of the used methods. The application of Computational Fluid Dynamics (CFD) is the basic methodology to examine the details of the flow in an axial compressor and how it is affected by the presence of water. Furthermore, FORTRAN programming language is utilized to develop a simulation tool to account for the water ingestion effects.

Chapter 6 - CFD of an Axial Flow Compressor refers to the modelling of the compressor flow field under water ingestion conditions. The scope of this chapter is to investigate the compressor's performance deterioration due to water ingestion. More analytically, the *Section 6.1 - Compressor Model – Mesh Generation* covers the topic of the creation the computational grid. In *Section 6.2 - CFD Parameters* and *Section 6.3 - Application of CFD,* the analysis of the factors used to solve the fluid flow and the simulation strategy is discussed. *Section 6.4 - Water Film Computation* covers the topic of the numerical approach, which is used to evaluate the liquid water film thickness and its motion on an axial flow compressor rotor blade under water ingestion conditions. The change in blade's profile and surface is imported in CFD, which calculates the change in the performance parameters of the compressor stage. Afterwards, *Section 6.5 - CFD Results* presents the outcome of the computational analysis. By changing the water ingestion parameters, the results for water film formation on the rotor blade and the demanded water torque are

exported. Moreover, *Section 6.6 - Compressor Performance Results* and *Section 6.7 - Data Processing* explain in detail the compressor's performance deterioration based on blade profile change and surface roughness model. Data for pressure ratio, non-dimensional mass flow and efficiency deterioration are analysed. Finally, *Section 6.8 - FILM_MOTION Results Validation* discusses the topic of validation of the FILM_MOTION code, which was carried out based on experimental observations.

Chapter 7 - Water Ingestion - Engine Performance Simulation refers to the modelling of water ingestion effects and its integration in a gas turbine performance code. First, in *Section 7.1 - The Turbomatch Code,* the computer program developed by Cranfield University to facilitate design and off-design point performance calculations for gas turbine engines is presented. *Section 7.2 - The Turbomatch Code with Water Ingestion Capability* covers thoroughly the way the effects of water ingestion are simulated and how the Turbomatch code integrates these effects. A new module, which includes new subroutines, has been added and calculates the deterioration, which is caused due to engine's operation in rain conditions. To be more specific, four new subroutines calculate the pressure ratio, non-dimensional mass flow and efficiency deterioration in the compressor and efficiency and pressure loss rise in the combustor when they operate with ingested water. Furthermore, the extra torque needed by the compressor to accelerate the liquid water film, which is formed on the blade, is also calculated and added to the compressor work. Therefore, the performance deterioration of a gas turbine engine due to water is modelled and the results are explained in detailed in *Section 7.3 - Performance Results*. Lastly yet importantly, *Section 7.4* – Code's Limitations and *Section 7.5 – Code Validation* discuss the limitations in the use of the code and its validation under water ingestion mode of operation.

Chapter 8 – Discussion includes the discussion for the results produced by the theoretical approach. It also presents experimental values, which compared with the simulation outcome, provide the relevant justification. The chapter focuses on three key areas of interest in the context of this research. *Section 8.1 – Compressor* discusses thoroughly the effects of ingested water on the compressor. It includes the water deposition phenomenon, an analysis for the liquid water film thickness and its motion and finally a general outcome for the compressor's performance. Moreover, *Section 8.2 – Combustor* covers the topic for the combustor component, while *Section 8.3 - Engine Performance Simulation* describes analytically the engine's overall performance deterioration.

Finally, **Chapter 9 – Conclusions – Further Work** summarizes the conclusions, observations and the limitations of this study. A number of recommendations for the potential further work are also suggested, which the author believes that they will strengthen a relevant future study.

4 Literature Review

The scope of this work is the investigation of water ingestion effects on gas turbine engine. The literature review performed in the context of this work is focused on areas, which have been detected that affect the phenomenon. Thus, the literature review includes the aviation history of adverse weather incidents/accidents and their investigation of the aviation authorities. It is also contains the area of atmospheric water, the processes which take place when rain is ingested by a gas turbine engine, and finally, the effects on engine's components.

4.1 Problem Identification

Over the last decades, the development of aviation has been accompanied by an outstanding improvement of the new aircrafts propulsion. This enabled the design of new engines (turbofan, turboprop etc). These engines boosted aircraft's ability to fly higher and faster. The increased demand for air travel at several altitudes and speeds has increased aircraft's exposure to inclement weather conditions. Up to the early 80's, several incidents have been reported to the aviation authorities about power loss during flight at inclement weather. It was understood that the rain ingestion into a gas turbine engine deteriorated its performance. When the water quantities were quite large like a flight through heavy rain, serious incidents or even fatal accidents occurred.

On 4th of April 1977, a DC-9 equipped with two Pratt & Whitney JT9D-7A engines crashed due to engine power loss while it was flying through a severe storm. The crew attempted an emergency landing but it was not successful and the aircraft crashed. The National Transportation Safety Board (NTSB) investigated the accident and revealed that the engines lost their power due to water ingestion. The aircraft had been flying through heavy rain and hail for about 2.5 minutes, immediately before it lost complete engine thrust. This happened as the engines ingested large amounts of precipitation causing a decrease to their rotational speed. In the meantime, the aircraft was descending from 17,000 to 14,000 ft and the engine's power settings were presumably at idle (regular setting for descend). With the loss of rotational speed, HPC on both engines destabilized and began to stall severely because of water ingestion. The pilot's reaction to the reduction in engines' rotational speed was to increase power setting and this made things even worse as the engines did not respond [Kissel, (1979)].

On 12th of June 1980, a SA 226TC Metro II aircraft, powered with two Garrett TPE331 engines, was descending out of 6,000 ft through heavy rain. The pilots reported a double power loss (due to flameout) and they tried to restart without

success. The aircraft could not recover and struck a muddy field. The National Transportation Safety Board (NTSB) investigated the accident and concluded that the cause was the massive water ingestion into both engines [NTSB, (1980)].

In 1984, General Electric engine manufacturer investigated the occurrences of compressor stalls most happened in rain conditions [Russell and Victor, (1984)]. For this reason, the engines, which had stalled in service, were checked in the test cell. The test results showed that the ingested water caused a loss of stall margin. It was found that water impinged on the coils of the compressor inlet temperature sensor and it was giving a false indication of the air inlet temperature. The latter affects the position schedule of the compressor variable stators. Therefore, their position did not corresponded to this of the current operating condition, leading the engine to compressor stall. Russell and Victor, (1984) highlighted the fact that the resulting temperature error could be in excess of 5°C relative to the air temperature at the compressor inlet.

Two events with CFM56 engines are reported in Volk, (1992). In August 1987, a Boeing 737-300, powered by two CFM56-3 engines, faced a similar situation when both engines lost their power due to flameout during descent flight through heavy rain and hail. After a few seconds, crew managed to restart both engines and the aircraft landed safely. The investigation revealed that the two engines had flamed out simultaneously at 8900 ft, 289 KIAS, 15°C TAT, at idle descend power. The crew reported that there was heavy rain and hail shower. There was no damage to the engines but the aircraft surfaces had several dents due to the hailstones.

The other incident with a similar aircraft happened on 24th of May 1988 in New Orleans. This time, a Boeing 737-300, was descending from 35,000ft through severe rain, hail and turbulence conditions at 16,500ft, 267KIAS, -29°C TAT. The aircraft experienced a dual engine flameout at about 16,200ft due to water ingestion and the crew was able to start the Auxiliary Power Unit (APU), which restored the electrical power, at about 10,500 ft. The pilots attempted to restart the engines, but neither engine produced more than idle power. Finally, following emergency procedures, they landed the aircraft on a grass strip. Ground inspection revealed over-temperature damage in one engine's turbine due to the unsuccessful restart attempts in the rain and hail. The other engine was removed and tested thoroughly without having any problem. The investigation revealed that the incident was a result of flight through heavy rain and hail.

Following the above dual-engine flameout event, the FAA, taking into consideration that these happened at low power settings, tried to ensure that the engine would continue to operate in the presence of heavy concentrations of rain and hail. For this, on 27th of May 1988 the FAA issued Telegraphic

Airworthiness Directive (AD) T88-11-51, with which the minimum engine fan speed should be 40%, when 737 aircraft, equipped with CFM56 engines, flies in or near heavy rainfall. This AD was superseded on 14th of June 1988, by AD T88-13-51, which raised the minimum speed limitation to 45%.

At the same time, CMF International (General Electric Aircraft Engines and SNECMA) devoted their full resources to investigate the events and to identify ways to improve the CFM56-3 engine's water ingestion capability [Volk, (1992)]. They carried out research on the raindrop break-up behaviour and trajectories, developed new facilities for inclement weather testing, engine ground and in-flight test. Volk, (1992) presents some statistical data, which show that 48 aircraft power-loss events, related to inclement weather, have resulted in in-flight shutdowns, over the 10-year period from 1 Jan 1980 to 31 Dec 1989 (figure 4-1). The author mentioned that not only all the engine manufacturers were involved but also there were approximately equal numbers of power loss events in inclement weather for each one. The author, as a Senior Staff Engineer of General Electric Aircraft Engines, declares, "*Investigation of operation in inclement weather is an area of much activity within the industry at the present time*" [Volk, (1992), pg 239].

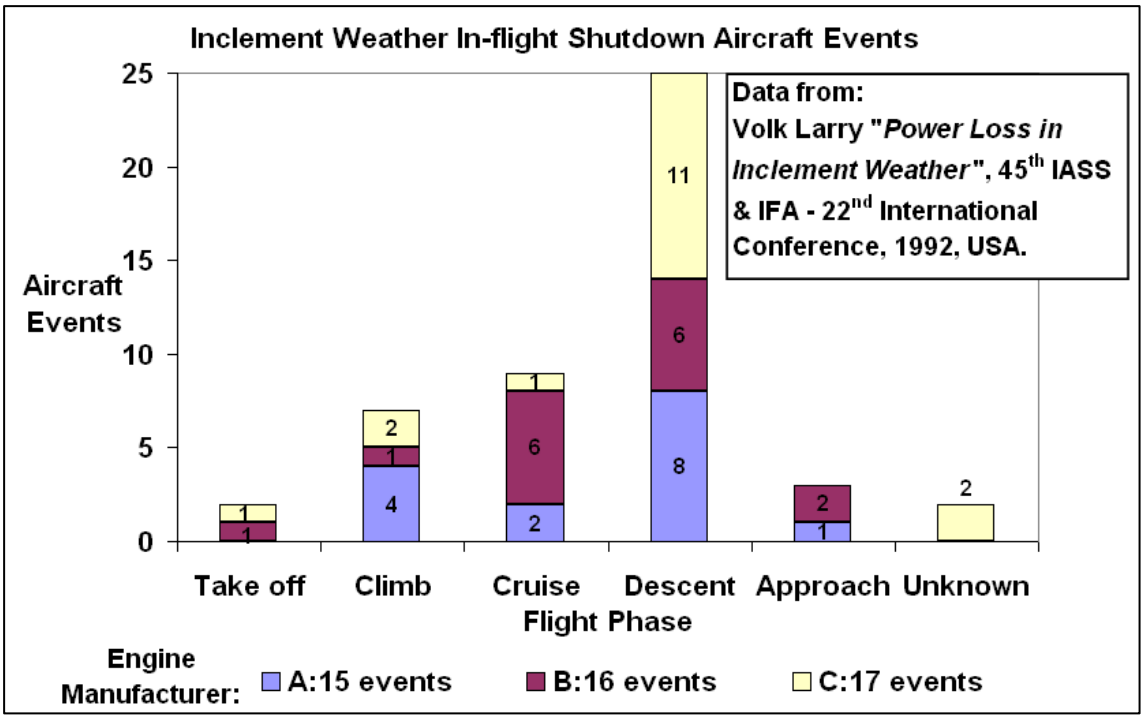

Figure 4-1: Inclement Weather In-flight Shutdown Aircraft Events 1 Jan 1980-31 Dec 1989 [Volk, (1992)]

By mid-1991, CFM had developed and tested engine modifications that were designed to improve the rain and hail ingestion capability of the CFM56. These modifications included a cutback fan/booster splitter fairing, an improved variable bleed valve (VBV), an elliptical spinner, and a revised schedule for VBV

operation (figure 4-2) [Volk, (1992)]. As a result, in 1993, AD T88-13-51 was superseded by AD 93-05-05, which eliminated the limitation of 45% minimum engine fan speed imposed by AD T88-13-51.

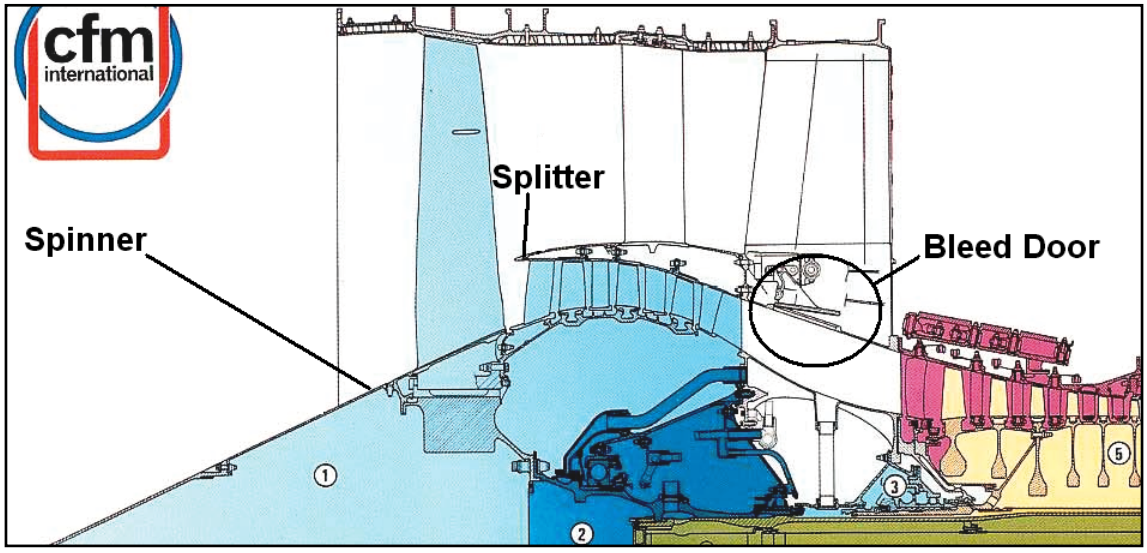

Figure 4-2: CMF56-3 Fan and Booster Cross Section (initial photo courtesy of CFM)

Engine manufacturers complied with the new regulations, showing that the matter was of extreme interest. It is worth noting that Rolls-Royce plc, developed enhanced water ingestion tests requirements due to the fact that the basic certification requirements does not expose the engine to transient operation [Jackson, (1997)].

Back in 1987, the Aerospace Industry Association (AIA) initiated a study of natural icing effects of high-bypass ratio turbofan engines, which revealed that operation in inclement weather could lead to power-loss [Volk, (1992)]. At that time, Boeing had already begun additional adverse weather studies and after its recommendation, a separate AIA committee (AIA Inclement Weather Committee) was formed in 1988 to further investigate the incidents, to evaluate any threat to the flight safety and, finally, to propose the necessary changes to the existing certification regulations.

The committee searched all the records from both engine and airframe manufacturers trying to collect any relevant data. It was found that the majority of the incidents referred to large high bypass ratio (greater than 2.0) engine powered aircraft due to the fact that these engines were newly designed and provided better documentation [Kirk, (1990)]. The author, although he does not clearly state the period, reports that over 200 incidents involving power loss on high bypass ratio engines were found to have occurred during flight in inclement weather conditions. Although data are not presented analytically, it is mentioned that the majority of the events have occurred during descent or approach flight phases. Therefore, Kirk, (1990) and Volk, (1992) share the view that during these flight phases the aircraft faces the highest possibility of power loss when

adverse weather exists. At these phases, the engines operate at low power settings.

Moreover, the AIA Inclement Weather Committee argued that the water ingestion requirements of Federal Aviation Regulation (FAR - 33.77c) could not adequately deal with the adverse weather conditions indentified by the committee [Volk, (1992)]. In August 1996, the FAA initiated studies for the new rain and hail-ingestion certification standards. The new engine certification standard, 14 Code of Federal Regulations Section 33.78, "Rain and Hail Ingestion," went into effect on 26th of March 1998 [FAA, (1998)]. This standard requires that "*all engines be capable of acceptable operation when subjected to sudden encounters with certain specified atmospheric concentrations of rain for 3 continuous minutes and hail for 30 continuous seconds, without experiencing flameout, rundown, continued or non recoverable surge or stall, or loss of acceleration and deceleration capability*" [FAA, (1998) section 33.78]. The specified atmospheric concentrations and size distribution of rain and hail varied according to altitude. For rain, the highest specified water content was 20 gr/m^3 of air from sea level to 20,000 feet.

It is noteworthy that the National Transportation Safety Board (NTSB) and FAA reviewed the CFM test data after the compliance of AD 93-05-05 and the results indicated that the CFM56 hardware improvements exceeded the new FAA certification standards in Section 33.78 for rain and hail ingestion [NTSB, (2005)].

One may think that after these investigations and the resulted modifications in the engine's design, the effects of rain ingestion would be negligible. However, on 16th of January 2002 a Boeing 737-300 (Garuda Indonesia Airlines – flight 421), equipped with two CFM56-3-B turbofan engines, experienced a dual-engine flameout (power loss) while it was flying through heavy precipitation approaching to the city of Yogyakarta in Indonesia. The pilots attempted unsuccessfully many times to restart the engines and finally performed an emergency landing into the Solo River on Java Island [NTSB, (2005)]. It is highlighted that in this accident both CFM56 engines had incorporated all these hardware modifications induced by AD 93-05-05 and described above.

The great concern of NTSB is expressed in a letter to FAA, sent in 31st of August 2005 and signed by its chairman Mark Rosenker [NTSB, (2005)]. In this letter, the Safety Board highlights that "*because the flight 421 accident clearly demonstrates that meteorological conditions exist that can cause engine flameout if a turbofan-powered aircraft inadvertently encounters them, the Safety Board is concerned about the validity of the current certification standard. The Board notes that the current standard is based on service and atmospheric data gathered in the 1980s and that significant technological advances in weather prediction have occurred since then. Furthermore, the*

Board notes that important technological advances in meteorology have occurred since 1996 that have given rise to a significant amount of new atmospheric data and that aircraft engine service experience has increased significantly since the rule was issued" [NTSB, (2005) pg 4].

Because of this accident, FAA has participated from summer 2004 in a panel from industry experts to review the current turbofan-engine certification standards for rain and hail ingestion. Their objectives include the investigation of the rain/hail environments encountered during the in-service events and the recommendation of revisions to the current certification standard. It is worth noting that European Aviation Safety Agency (EASA) agrees currently with FAA about the procedures for rain ingestion certification tests [EASA, (2007)].

In conclusion, over the last decades, the growing concern of gas turbine industry about the adverse weather conditions is fully justified. Without doubt, the water ingestion has pronounced effects on engine's operation. It can be argued that the growing aviation market requires the development of defence mechanisms against inclement weather conditions. Both, the engine's manufacturers and the aviation authorities, have made a considerable effort to address the rain ingestion effects. However, there are still open items in this process, which should be sorted out. This is necessary for the aviation safety.

4.2 Atmospheric Water

It is known that water may be present in the atmosphere in many forms. Water can be in vapour, liquid or solid (ice) form, in a variety of shapes and sizes and of course in different concentrations. Thus, there exists a variety of ways, in which a gas turbine engine may ingest large quantities of water. Some of them are high humidity air, flight through rain and storm and/or ice crystal clouds, or even water spray formation during taking off from rough runways with puddles of water. Moreover, flight during icing conditions enables ice formation in aircraft's surfaces, which under several circumstances may enter the engine. Consequently, the specific effects of water ingestion in the operation of gas turbine engines will depend on the elemental forms of water. These forms of water should be studied thoroughly in order to determine the possible effects on engine performance and operability.

Water vapour is always present to some extent in the atmosphere. The Vapour Water Content (VWC) is expressed in water vapour mass per volume of air (gr/m^3). Absolute humidity, relative humidity and specific humidity are different ways to express the water content in a volume of air. Absolute humidity is the quantity of water in a particular volume of air. It is an inconvenient definition because absolute humidity value changes as air pressure changes. Relative humidity is defined as the ratio of the partial pressure of water vapour in a

gaseous mixture of air and water vapour to the saturated vapour pressure of water at a given temperature. Relative humidity is expressed as a percentage. Specific humidity is the ratio of water vapour to humid air (dry air plus water vapour) in a particular volume of air.

Liquid Water Concentration (LWC) is the quantity of liquid water in air, expressed in water mass per volume of air (gr/m^3). However, the definition of water-air mass ratio is widely used in the gas turbine studies because it transfers in a better way the idea of mixture mass flow of the engine. Furthermore, water-air mass ratio is a non-dimensional parameter and it is more convenient in the thermodynamic cycle modelling.

The liquid water entering the engine may be a result of rain, inlet condensation, droplet suspension or liquid spray. Condensation can occur under conditions of high inlet velocity and humidity, because the reduced static temperature causes the water vapour to condense into fine droplets. Liquid suspension is the product of natural condensation, which creates fine water droplets. Solid water can be in the form of hail, ice crystals or snow. In any case, its concentration is referred to as the Hail Water Concentration (HWC), which is the quantity of solid water mass in a given volume of air (gr/m^3).

The analysis of the in-flight power loss events due to inclement weather presented in the previous section shows that heavy rain and hail are far the most serious threats. Considering that this project focuses on the effects of rain ingestion, the remaining literature review will concentrate to the liquid water phase.

Boeing Company, one of the biggest aircraft manufacturers, has conducted a thorough study to refine rain and hail water concentration at the worldwide worst-case locations for rain and hail. The study took place in support of the AIA, after the B737-300 power loss events and based on probability analysis. Its objective was to quantify for a known location in the world the probability to occur a rain (or hail) of a given intensity Moravec B. and Patnoe, (1996b), Patnoe and Moravec B., (1996a).

Water concentration (LWC) is used to describe the level of intensity of rain and hail. LWC is described as a function of probability: $LWC=f(P_j, P_t)$ where P_j is the joint probability of a rain occurring at a given point and of a given LWC being equalled or exceeded at that point. P_t is the duration probability, and the case of rain, is assumed 1.0, which means that, at that phase, any rain duration can be experienced by an airplane. P_j is expressed symbolically:

$$Pj = P(storm \cap LWC) = P(storm)\ X\ P(LWC / storm)$$

Equation 4-1: LWC Probability Equation Patnoe and Moravec B., (1996a)

where P(storm) is the probability of a storm occurring at a given point and at a given instant, P(LWC/storm) is the conditional probability of a given LWC value occurring at that point and time given the occurrence of the storm.

To evaluate the liquid water content (LWC: gr/m^3) during a rainfall, its equivalent to a given rainfall rate (Rr: mm/hr) must be known. Studies, based on probability analysis, have defined equations to connect rainfall rates with LWC. Because the probability for a given LWC varies significantly as a function of location, these studies have used data from locations where the most intense rain and storms have been observed. All of them define a power law relationship between LWC (Mw in meteorology terminology) and Rr. Table 4-1, shows the Mw-Rr relations used in the rain analysis. Typically, Rr and Mw are measured independently, but at the same time and location.

Source	Mw-Rr Equation	Locations where data were collected
Jones, D.M.A., *Rainfall Drop-Size Distribution and Radar Reflectivity*, Res. Rept No. 6, Urbana: Meteor. Lab., Illinois State Water Survey, 1956.	**$Mw = 0.052\ (Rr)^{0.95}$**	Illinois
Mueller, E.A., and A. L. Sims, *Investigation of the Quantitative Determination of Point and Areal Precipitation by Radar Echo Measurements*, Tech Rep. ECOM-00032-F, Illinois State Water Survey, Urbana, 88 pp, 1966	**$Mw = 0.0528\ (Rr)^{0.95}$**	Miami
Willis, P.T., *Functional Fits to Some Observed Drop Size Distributions and Parameterizations of Rain*, J. Atmos. Sci., 41, pg 1648-1661, 1984.	**$Mw = 0.062\ (Rr)^{0.913}$**	Hurricanes Anita & Frederic
Atlas D., *Advances in Radar Meteorology*, Vol 10, 1964, Academic Press, NY.	**$Mw= 0.052\ (60Rr)^{0.97}$**	Illinois (Intense Thunderstorms)

Table 4-1: Equations Used to convert Rain Rate (Rr: mm/hr) to LWC (Mw: gr/m3)

The first three sources are cited in Patnoe and Moravec B., (1996a). Atlas (1964) equation differs from the others in table 4-1, but Kissel, (1979) comments that it is applicable for intense thunderstorms. Anyway, the point is that by using Rr values the LWC can be estimated for a given location.

Patnoe and Moravec (1996a and b) collected data from a number of studies about the intensity levels of rain. They analyzed several parameters like the rain duration, its rate, in a number of stations at various locations, taken over a ten-year period. For their study, they took into consideration only the data for 1-min rain duration. They also assumed that the probability of a LWC to exceed a given value is calculated by dividing the annual average number of occurrences of 1-min by the number of minutes in a year. The larger the sample population, the minimum is the error. For example, if, of all the 1-min rains in a location, a Rr=2.5 mm/min is measured to have occurred 11 times annually, then the LWC can be calculated by using Mueller and Sims equation from table 4-1:

$$LWC = 0.0528 \cdot Rr^{0.95} = 0.0528 \cdot \left(2.5 \cdot 60 \, {}^{mm}\!/_{hr}\right)^{0.95} \Rightarrow LWC = 6.2 \, {}^{gr}\!/_{m^3}$$

The probability value is calculated by taking the number of 1-min occurrences divided by the number of minutes in a year:

$$P(LWC) = \frac{\text{number of occurrences}}{\text{minutes in a year}} = \frac{11}{365.25 \cdot 24 \cdot 60} = 2.1 \cdot 10^{-5}$$

Further examples and detailed references can be found in Moravec B. and Patnoe, (1996b), Patnoe and Moravec B., (1996a) and AGARD, (1995). It is noteworthy that the work presented in AGARD, (1995) agrees with the above methodology and it obviously uses data from Patnoe's and Moravec's (1996a and b) study.

Following a detailed analysis, the authors conclude in the following empirical relationship for the intensity levels of rain (LWC) as a function of P_j:

$$LWC = 1.526 \cdot \ln\left({}^{2.32 \cdot 10^{-3}}\!/_{Pj}\right)$$

Equation 4-2: Rain Intensity Level Vs Probability of Occurrence

Thus, they plot the rain curve with the various data points. At probability levels of 10^{-7}, 10^{-8} and 10^{-9}, the corresponding LWC values are 15.3, 18.9, and 22.4 gr/m^3 respectively.

Moravec and Patnoe (1996b) suggest LWC levels for the engine certification requirements. Their approach is based on the expected life of an airplane type and the probability of experiencing a severe rainstorm. The latter is defined on a flight cycle basis. It may be stated that airplanes exposed to extreme rain conditions during all phases of flight and a flight hour basis would be more appropriate. However, as it has been presented, engine power losses have occurred during low power operation on descent.

Furthermore, Moravec and Patnoe (1996b) chose a LWC level on the P_j of 10^{-8} per flight cycle. They argued that it was unlikely an airplane type to experience this level (or higher) of rain over its entire service life, which was assessed to be approximately 10^8 flight cycles. They included in their estimation some mitigating factors such as weather avoidance and the fact that three minutes (hence P_t<1.0) rain duration was chosen. Consequently, the highest concentration was calculated to 18.9 gr/m^3 (P_j=10^{-8}/flight cycle). Finally, the value of LWC = 20 gr/m^3 was proposed. The recommendation was accepted by FAA, which issued new certification requirements (14 Code of Federal Regulations Section 33.78, "Rain and Hail Ingestion) [FAA, (1998)], and went into effect on 26th of March 1998. EASA, (2007) also has adopted the same certification requirements (figure 4-3).

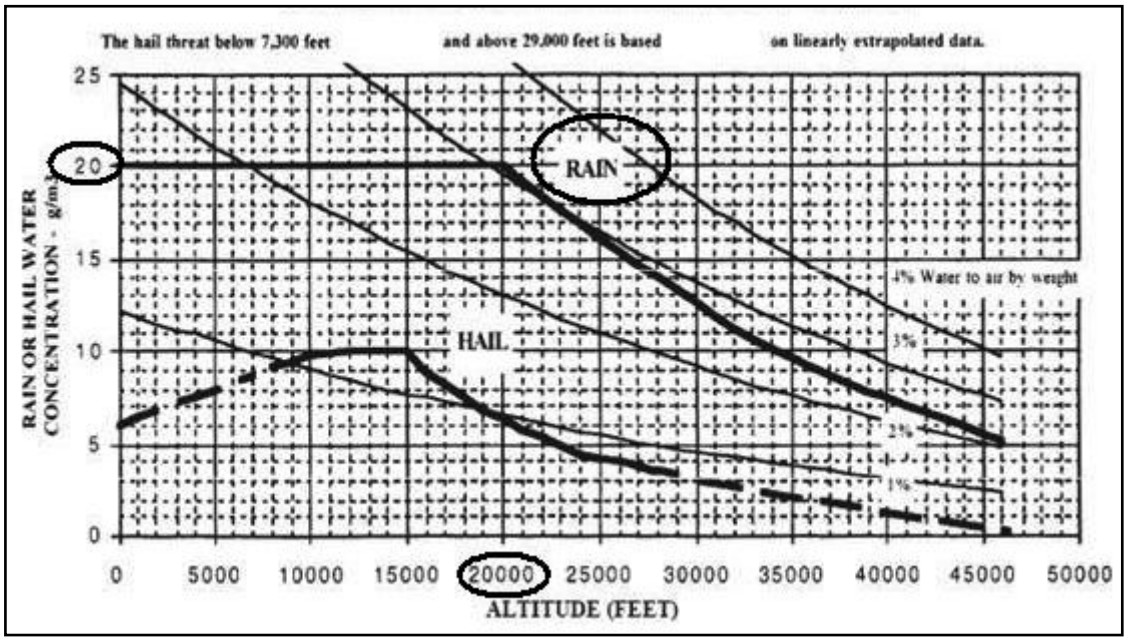

Figure 4-3: Certification Standard Atmospheric Rain Concentration (gr of water/m^3 of air) [EASA, (2007)]

However, it can be mentioned that the proposed certification values do not account for in-flight aerodynamic effects. At descent flight, the combination of aircraft's high speed and the low power settings results in an increase in water concentration at the engine's inlet because the engine's capture stream tube is smaller than its projected area. This is called "scoop factor" and it is analysed in the next sections. Moravec and Patnoe (1996b) hold the view that the proposed rain requirements will be more severe than the current regulation when these aerodynamic effects have been considered.

Another important aspect of the weather threat analysis is the raindrop size distribution. Based on the extensive work of Tattelman and Willis, (1985), Moravec and Patnoe (1996a) share the view that for the 42-minutes world record rainfall rate of 15.8 gr/m^3 (22nd of June 1947), the 72% of the rain drops are between 0.5 and 2.0 mm. The mean drop size is 1.4 mm in diameter. Approximately 75% of the total water is from drops with diameters between 1.5 and 3.9 mm (figure 4-4).

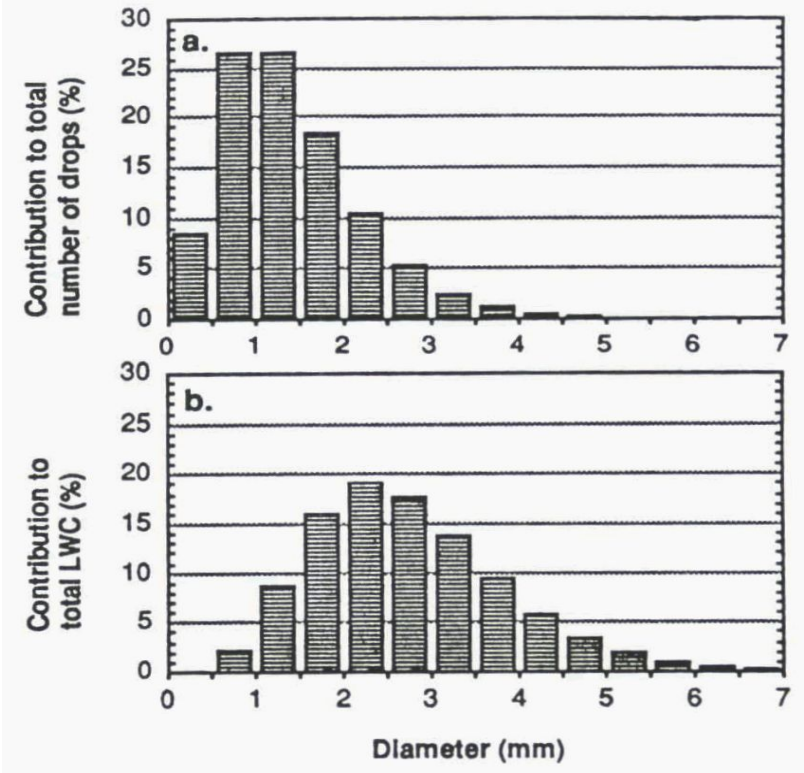

Figure 4-4: Raindrop Size Distribution: (a) Contribution to the Total Number of Raindrops from each 0.5 mm Diameter Interval, (b) Contribution to the Total LWC from each 0.5 mm Diameter Interval [Tattelman and Willis, (1985)].

Kissel, (1979) confirms the above droplet distribution. He reports that measurements of typical rain droplet diameters in storms indicated that the droplets are between 0.5 mm and 3 mm with the peak occurring at 1 mm. This is similar to the views of Russell and Victor, (1984), who mention that cloud-droplets size values vary from 0.1 mm-0.2 mm under light rain, to very large 2.0mm-3.0mm in heavy rain. Consequently, the value of 1 mm for water droplet diameter is representative of a typical heavy rain occurrence.

Another important aspect of the weather threat analysis is the vertical distribution of rain LWC in the atmosphere. Tattelman and Willis, (1985) include this data in their work. Figure 4-5 presents the vertical profile of 18.9gr/m^3 LWC for the 10^{-8} probability. It is observed that LWC is constant from the surface to 20,000 ft Mean Sea Line (MSL) and drops off after this altitude. Hence, altitudes below 20,000 ft should be considered in rain threat evaluation.

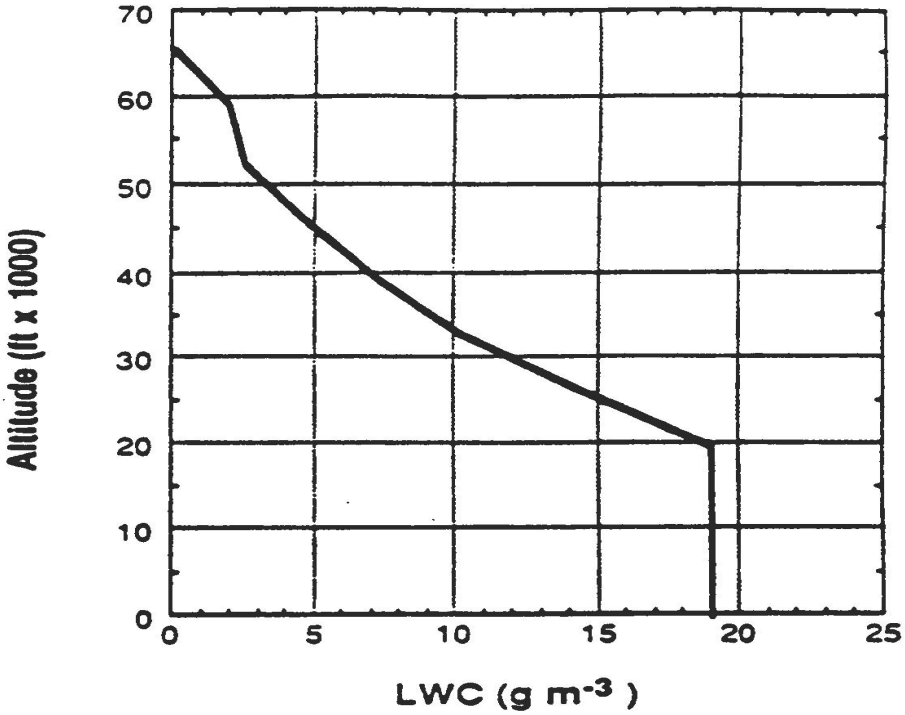

Figure 4-5: Vertical Profile of LWC for the 10^{-8} Probability LWC of 18.9 gr/m^3 [Tattelman and Willis, (1985)]

4.3 Water Droplet Behaviour

In order to investigate the effects of water ingestion on a gas turbine engine, it is necessary to understand and account for the effects of rain droplets as they enter the engine inlet. Water droplets are affected by the high-speed airflow, they break-up, splash or deposited on the blades, form films, which may disintegrates. These phenomena are analysed in the following sections.

4.3.1 Water Droplets in High-Speed Airflow

As rain droplets enter the inlet of the engine, there is a relative velocity between air and water (V_a-V_w). This relative velocity causes a viscous drag force (F_d) that tends to accelerate the droplets to equal their speed with that of air. The surface tension force (σ_w), which holds together the droplet mass, counterbalances the drag force. When this force becomes sufficiently large, it overcomes the surface tension force and the droplets disintegrate into smaller droplets.

Neglecting gravity, water droplet motion (of mass m and diameter D_w) is governed by the following classical law equation:

$$F_d = m\frac{d(V_a - V_w)}{dt}$$

Equation 4-3: Drag Force exerted by Air on a Water Droplet

The drag coefficient C_D can be enabled to express F_d:

$$F_d = \frac{1}{2}C_D\pi\frac{D_w^2}{4}\rho_a(V_a - V_w)^2$$

Equation 4-4: Drag Force - Drag Coefficient

C_D depends on a number of factors. In AGARD, (1995) is referred that in case of spherical drops bigger than 10 μm, C_D is calculated based on droplet's Reynolds Number (Re):

$$C_D = 24/Re \qquad Re < 1$$

$$C_D = \left(21.64/Re\right) + 2.36 \qquad 1 < Re < 10, \qquad Re = \frac{\rho_a(V_a - V_w)D_w}{\mu_a}$$

$$C_D = \left(21.942/Re^{0.718}\right) + 0.324 \qquad Re > 10$$

Equation 4-5: Drag Coefficient Calculation [AGARD, (1995)]

Park and Chang, (2000) adopts the above model for the C_D calculation. Pinkus O., (1983) studies the motion of steam droplets through a blade channel and he proposes a different drag coefficient calculation:

$$C_D = 24/Re \qquad (Re < 0.6)$$

$$C_D = 0.05 \cdot e^{\left(6.193 \cdot Re^{-0.1496}\right)} \qquad (0.6 < Re < 1500)$$

$$C_D = 0.398 \qquad (Re > 1500)$$

Equation 4-6: Drag Coefficient Calculation [Pinkus O., (1983)]

A wide range of authors [Oliveira et al. (2002), Morsi and Alexander, (1972), Valentine and Decker, (1995b)] use Wallis (1969) correlation:

$$C_D = \frac{24}{Re}\left(1 + 0.15 \cdot Re^{0.687}\right) \qquad Re > 1000$$

$$C_D = 0.44 \qquad Re < 1000$$

Equation 4-7: Drag Coefficient Calculation [Wallis, (1969)]

Finally, White (2006) suggests a single drag coefficient formula, which is applicable over a wide range of Re:

$$C_D = 0.4 + (24/Re) + \frac{6}{1 + \sqrt{Re}} \quad \text{for} \quad Re < 2 \cdot 10^5$$

Equation 4-8: Drag Coefficient Calculation [White (2006)]

In general, for airflow in a gas turbine, water droplet deformation will occur because drag force dominates on the surface tension force (σ_w). This affects C_D estimation because droplet is no longer spherical. In AGARD (1995), this is addressed by importing a correction factor on C_D calculation (equation 4-5): 1.0 for $We/\sqrt{Re}$ = 0 and 1.7 for $We/\sqrt{Re}$=0.79 with linear interpolation between these values. The relative importance of aerodynamic and surface tension forces is expressed by the non-dimensional Weber number (We), which is defined as:

$$We = \frac{\rho_a D_w \left(V_a - V_w\right)^2}{\sigma_w}$$

Equation 4-9: Weber Number Definition

Park and Chang (2000) also adopt the correction factor to account for droplet's deformation. Weber number depends on the liquid nature (for water σ_w=0.07 Nt/m), the flow characteristics and the droplet's diameter D_w. The importance of $We/\sqrt{Re}$ factor will be analysed in the next section.

Generally, break-up of a droplet occurs when the internal viscous forces exceed the surface tension forces due to droplet distortion. In case of a droplet entering a high-speed airflow, viscous force F_d is sufficiently larger than surface tension σ_w and tends to break the original droplets into smaller droplets.

When a droplet is subjected to airflow, it is initially flattened to an ellipsoid. Depending on the magnitude of the internal forces, droplet may be converted into a bag shape. When a critical relative velocity is reached, it is blown out into a hollow bag, which develops until it ruptures, producing fine small droplets. This is classified as bag (or hat) break-up. In case of high velocity air stream, the magnitude of the aerodynamic forces is quite high and the droplet is deformed into a saucer shape until it rapidly disintegrates into smaller droplets. This is called shear break-up. Liu (2000) describes in detail the two break-up mechanisms, which are shown in figure 4-6.

Figure 4-6: Modes of droplets disintegration. Above: Bag break-up. Down: Shear break-up [Liu (2000)]

In both break-up mechanisms, the initial stage of the process involves a flattening of the droplet into a disc shape, normal to the flow direction. The whole process depends on the aerodynamic and surface tension forces, which their ratio is the Weber number. Hence, the disintegration mode is closely related to We and it will be the same at similar We.

Kennedy and Roberts (1990) refer to the two aforementioned types of break-up modes. They experimentally estimated the diameter of the liquid droplet, which is subject to disintegration. Their work is thought to be very precious because a part of it focused on rain droplet break-up at descent flight conditions. A test facility was constructed and liquid water droplets were accelerated due to entrance in high-speed airflow. It generated droplets with diameters ranging from 0.5 mm to 3.0 mm. Air velocity varied from 20 m/sec up to 124 m/sec and water droplet could be greater than 45 m/sec. The produced relative velocity simulated rain ingestion at descent idle in flight.

The authors report that shear type break-up occurs for droplet's diameter greater than 0.6 mm over the entire idle descent velocity range. They correlate the shear break-up process with the We/√Re parameter, which remains almost constant for the idle descent velocity range. They also observe that shear type break-up occurs when We/√Re=0.79, which corresponds to We>10. Hat type break-up is recorded at lower air velocities and We/√Re=0.4 (We<10). In figure 4-7, a plot is presented for We/√Re parameter and it is used as a break-up criterion by a wide range of researchers.

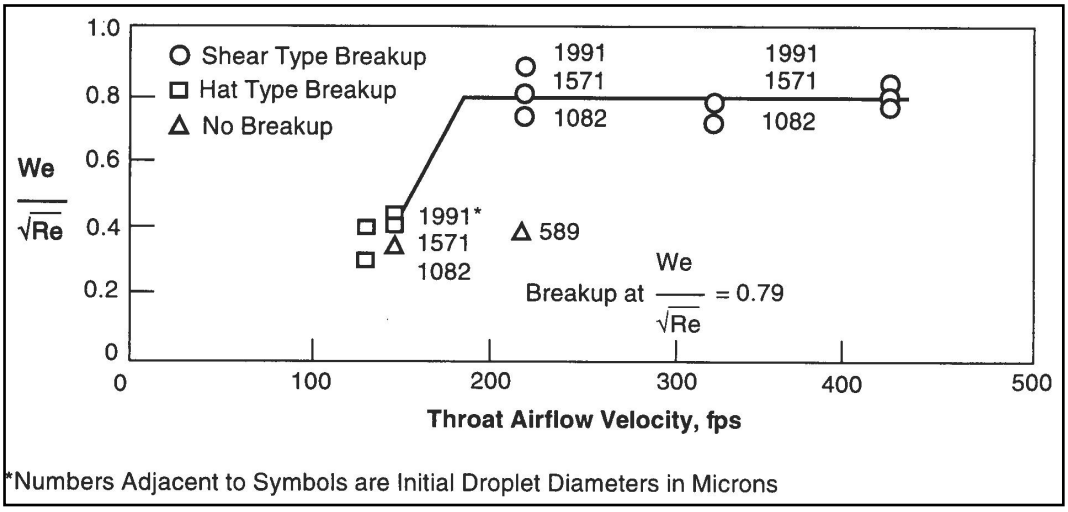

Figure 4-7: Droplet Break-Up Criteria at Descent Idle Airflow Velocity Range [Kennedy and Roberts, (1990)]

It is worth noting that AGARD (1995) adopts the above view. It is commented that at descent flight under rain conditions, the parameter We/√Re will be higher than the critical value of 0.79 and its rate of change will be d(We/√Re)/dt>30. This implies than not only there is a high relative velocity between air and water

but also there is no sufficient time for the hat type break-up. Hence, shear break-up is typical at descent flight under rain ingestion conditions.

Lee and Reitz (2000) refer to four break-up regimes depending on the relative velocity between a drop and the surrounding gas. Thus, apart from “bag” and “shear” break-up, “sheet” and catastrophic break-up mode are also mentioned. The latter takes place at sufficiently high air velocities where the drop experiences a large dynamic pressure change on its surface. That causes a flattening in the form of a sheet, which breaks into smaller fragments. Finally, this process produces fine droplets. Figure 4-8 illustrates the four break-up regimes.

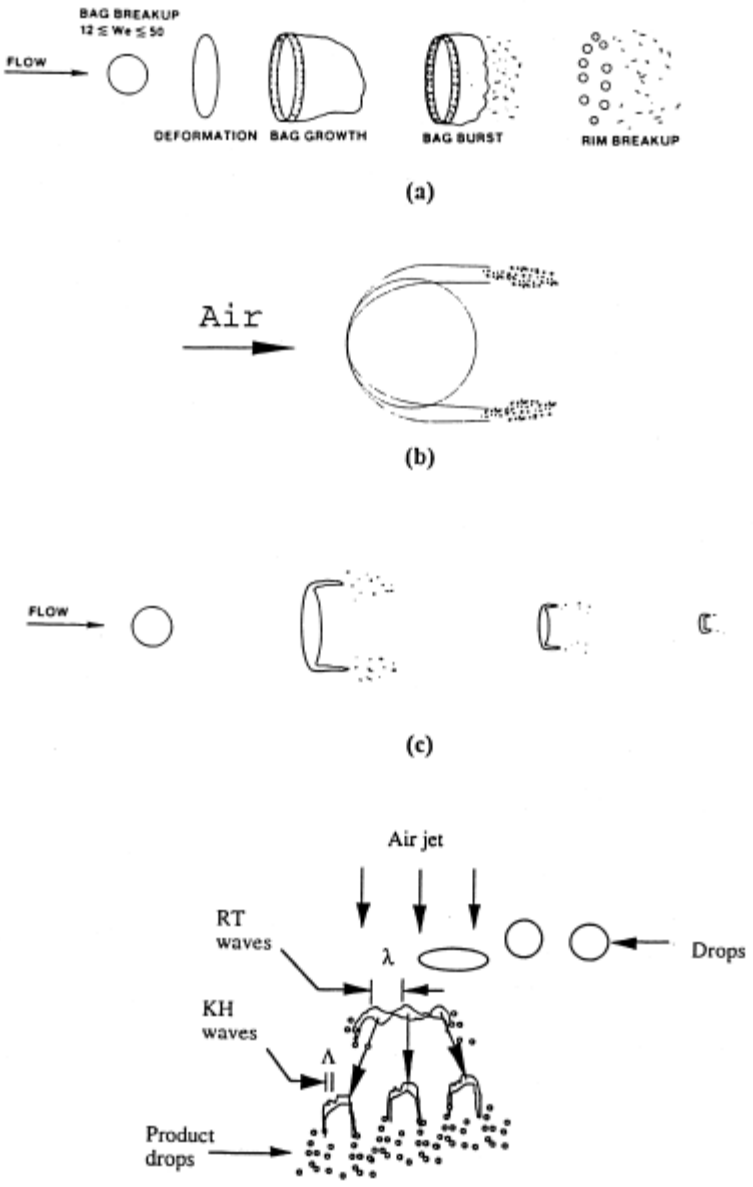

Figure 4-8: Droplet break-up Regimes: (a) bag break-up (b) shear or boundary layer break-up (c) Sheet break-up and (d) catastrophic break-up [Lee and Reitz, (2000)]

Lee and Reitz (2000) also notice that significant drop distortion and oscillation takes place starting at We~1. They share the view with Kennedy and Roberts, (1990) about the We criterion for the break-up type. They confirm that the bag break-up mode begin at We=12. It is also noted that in the intermediate We number range a combined bag and shear type break-up takes place.

Gelfand (1996) refers to “bag”, “bag stamen” and “chaotic” type of disintegration of a liquid drop subjected to a gas flow. It notes that bag type break-up at We~40-60 transforms into the “bag stamen” type. In this regime, the main mass of liquid is concentrated in the central liquid stamen, which has one axis with the gas flow direction. Further increase of We number (We>60) causes a “chaotic” type break-up, in which the deformation of the droplets progresses into a thin disk through the formation of a liquid body. At very high We numbers “explosive” drop break-up occurs.

Varga et al. (2003) agree with the definition of catastrophic break-up type. Based on their extensive work, they confirm that the transitions between the break-up modes depend on the value of the We. The authors experiment with water and ethanol break-up process and they observe that bag break-up is encountered in the range 12<We<80 while shear break-up occurs for We>80, and catastrophic break-up, generally occurs for We>350.

The extensive literature on droplet break-up at high-speed airflow is well represented in Varga et al. (2003). Hsiang and Faeth (1992) report data for Weber numbers ranged from 0.5 to 1000 with Reynolds numbers from 300 to 1600. Joseph et al. (1999) describe the sequence of the basic stages of drop break-up at high Weber and Reynolds numbers. Firstly, the flattening of the droplet takes place, because of application of the pressure forces around the droplet. Secondly, there is a radially outward boundary layer flow from the nose of the drop to its equator, and thirdly, the liquid accumulates in a thin ring at the equator, due to its motion from the nose of the drop. Lastly, droplet blows off from the rings into smaller droplets and even mist.

AGARD (1995) also describes a method of estimating the resulting droplet sizes after the break-up process. An empirical equation is introduced based on the work of Anderson W.H. and Wolfe H.E., for the mass mean diameter (D_{wm}):

$$D_{wm} = \left[\frac{136 \cdot \mu_w \cdot \sigma_w^{3/2} \cdot D_w^{1/2}}{\rho_a^{\,2} \cdot \rho_w^{1/2} \cdot (V_a - V_w)^4} \right]^{1/3}$$

Equation 4-10: Water Mass Mean Droplet Diameter after Break-Up

It is also stated that the droplet size distribution can be calculated by using the Rosin-Rammler distribution function. Kennedy and Roberts (1990) support that rain droplets break-up into smaller droplets, whose average diameter equals to

approximately 0.125 mm. Further literature research of the subject is beyond the scope of this project and it is not presented.

In conclusion, at airflow conditions similar to these at idle descent flight, shear or catastrophic type break-up will occur. These types of break-up mechanism produce smaller droplets than the other types. Fine droplets are subjected to lower inertial force and consequently they can follow the air streamlines. This implies that water concentration is reduced due to the alleviation of scoop effect. The latter is analysed in section 4.4.1.

4.3.2 Droplet Splashing – Deposition – Film Formation

Depending on the circumstances under which a drop impact occurs, many different cases may be distinguished. The outcome of a collision depends on the properties of the drop, of the impacted surface and of the fluid, which the drop traverses before impact. The impact velocity and the geometric characteristics of the surface also affect the phenomenon. For this subject, there is an extensive literature by many researchers, which is justified by the practical importance of droplet impact on a surface. At this section, the basic theory of droplet collision is discussed, and only few papers are cited comparing with the number of papers existing in this particular field.

Rein (1993) describes in detail all the possible parameters, which governs the liquid drop impact (figure 4-9). In order to compare any results, the different conditions must be considered in depth.

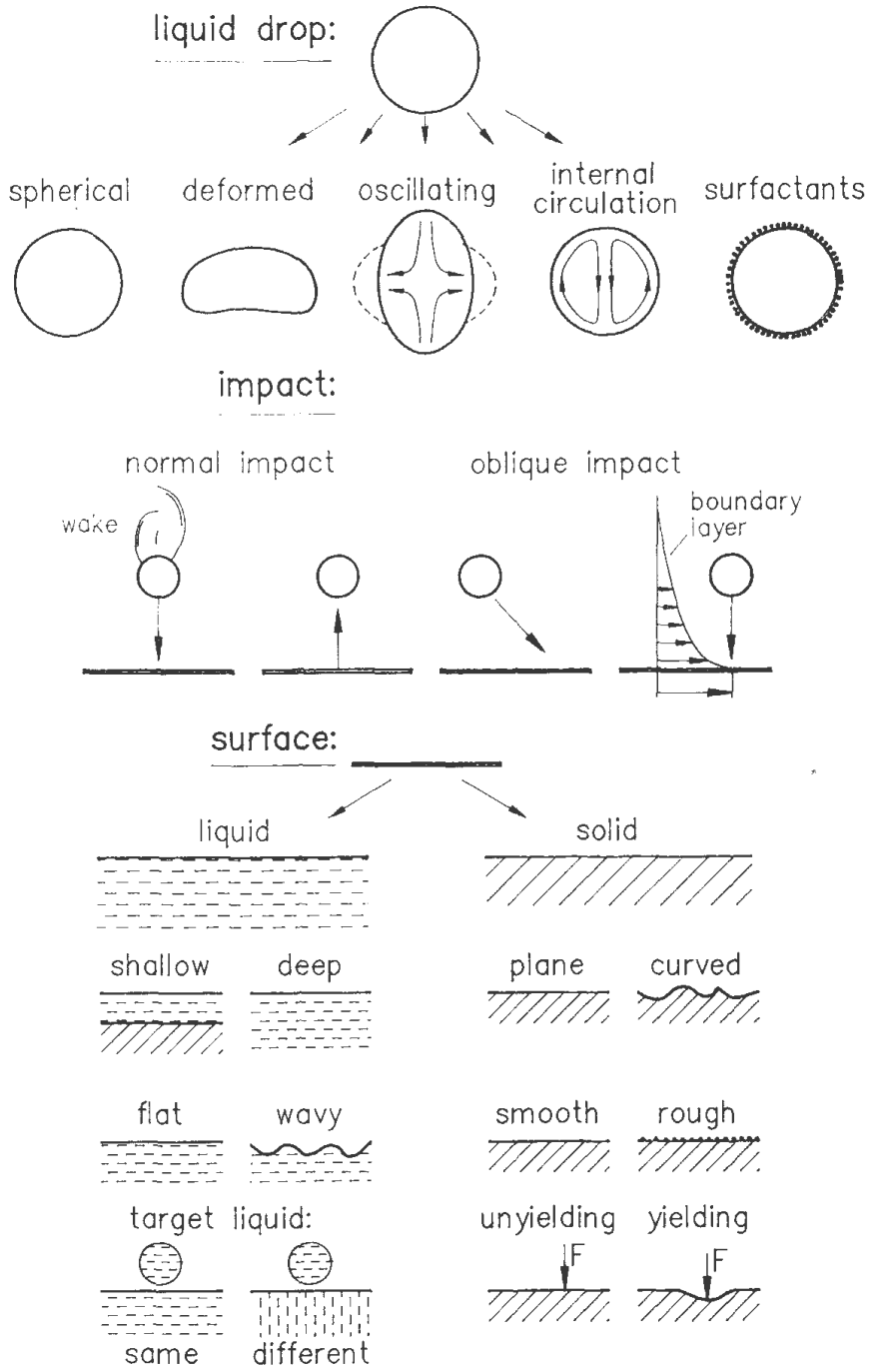

Figure 4-9: Parameters Governing the Impact of a Liquid Drop [Rein, (1993)]

The shape of a liquid drop can take several forms. In the majority of the theoretical and numerical calculations, drops are assumed spherical. This is also the case in experimental work, although the shape of drops moving through a fluid will always be rendered slightly ellipsoidal by aerodynamic forces. Drop oscillation may be the cause for its deformation.

The impacted surface can be either solid or liquid. When it is liquid, it is assumed deep enough. In this case, the bottom does not affect the process of

drop impact. Rein (1993) reports that when droplets impinge on thin liquid surfaces the splashing characteristics are similar to these impacting on solid surfaces.

Rein (1993), Mundo Chr. et al. (1995), Yarin and Weiss (1995) and Sikalo S. et al. (2002) refer that when a liquid droplet impacts on a solid and dry surface there are two possible basic outcomes. Droplet may deposit on the surface and form a liquid film. Alternatively, droplet may splash and secondary droplets may form, which is likely to happen in high energetic impacts. Rioboo et al. (2001) by considering a wide range of droplet velocities and diameters, suggest six different outcomes.

The first outcome is “deposition”, in which the drop is deformed and stays on the surface. The second is called “prompt splash” and it means that the droplets are ejected directly from the region between the surface and the liquid in the spreading phase of the lamella (the expanding liquid disk). The third is “corona splash” and takes place when a corona is formed during the spreading phase and eventually breaks-up into droplets. The fourth outcome is called “receding break-up” and occurs when the droplets are left on the surface during the receding phase of the impact. The fifth one is the “rebound” and it is self-explanatory. The last one is the “partial rebound” where part of the drop stays attached to the surface while some part rebounds.

Since deposition and spreading/splashing are regarded to be the basic droplet-impinging outcome, their analysis follows in detail. During the initial stage of impact, the drop is merely deformed and compressed at its base. After a contact is formed between a drop and a solid surface, the liquid normally starts spreading out. The kinetic energy of the drop influences spreading largely. A smooth motion of the liquid that results in the formation of a thin liquid disc is characteristic of low-speed impacts. At higher impact velocities the jetting motion leads to a disintegration of the liquid and splashing occurs. The threshold between spreading and splashing has been the topic for many researches.

Splashing occurs whenever the droplet disintegrates into two or more secondary droplets. A key feature is the crown, which is formed and the tiny droplets ejected from the rim of the crown. Rein (1993) argues that the droplet’s kinetic energy and its surface tension determine the splashing threshold. The ratio of the kinetic energy to the surface energy is expressed by the Weber number (We), defined in the preceding section. He is also states that threshold depends on other properties of the drop (i.e. viscosity), which is not presented in the Weber number, and on properties of the surface (i.e. roughness). Hence, he concludes that a critical Weber number alone does not supply a splashing threshold.

For this reason, Stow and Hadfield (1981), Bussmann M. et al. (2000), Chandra and Avedisian (1991) attempt to evaluate the surface roughness effect on the splashing threshold. They share the view that this parameter has a strong influence on splashing. The parameters that can affect the splash mechanism are the droplet impact velocity and angle, droplet size, viscosity and surface tension. To account for the viscous and surface tension effects, Mundo Chr. et al. (1995) introduce the Ohnesorge number, which represents the ratio of viscous force to interfacial tension force:

$$\mathrm{Oh} = \frac{\mu}{\sqrt{\rho \sigma \mathrm{D}}}$$

Equation 4-11: Ohnesorge Number Definition

Bearing in mind the We and Re definitions (equations 4-9 and 4-5 respectively), the relation between Oh, We and Re is expressed by the following equation:

$$\mathrm{Oh} = \frac{\sqrt{\mathrm{We}}}{\mathrm{Re}}$$

Equation 4-12: Oh, We and Re Relation

The authors use energy and mass conservation to determine the splashing – deposition threshold, in their theoretical approach to the deposition – splashing of a droplet. They focus on the task to express splashing as a function of the Oh and Re numbers of the impinging droplet. In their experimental work, they succeed to correlate the Oh and Re numbers for which splashing occurs and they define the K parameter:

$$\mathrm{K} = \mathrm{Oh} \cdot \mathrm{Re}^{1.25}$$

Equation 4-13: K Splashing Parameter definition

Mundo Chr. et al. (1995) conclude that if K>57.7 then splashing occurs, whereas K is less than 57.7 complete deposition takes place. Their results for splashing threshold are illustrated in figure 4-10.

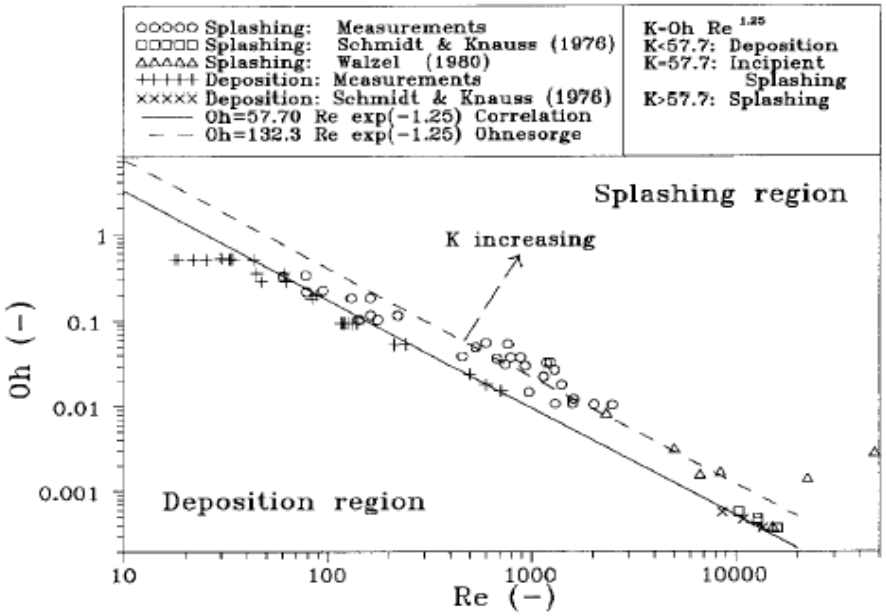

Figure 4-10: Limits for Splashing and Deposition of Droplets [Mundo Chr. et al. (1995)]

Thus, the outcome of an impact (whether splashing or deposition occur) depends on the Re and Oh numbers, which represent the fluid properties and kinematics impact parameters. It can be easily understood that in case of rain droplets ingestion in a gas turbine engine, splashing will occur since the Re number is considerable high leading to values of K higher than 57.7. Tan and Barlett (2003) adopt the above model for the splashing threshold and report that rain droplet splashing under inclement weather conditions is quite possible due to the high relative droplet-air velocity encountered. Thus, it is a high energetic impact whenever it takes place (inlet or compressor blade). The author thinks that, in cases the water impacts on a compressor rotor blade, the droplets splash producing fine droplets with high velocity magnitude. This is concluded by studying experiments, where high energetic impact takes place for K parameter values well above the critical value of 57.7.

Samenfink et al. (1999) study the droplet interaction with shear-driven liquid films. They investigate the mechanism of droplet splashing and the characteristics of the deposited mass fraction on a liquid film. They confirm that a large number of different parameters govern the droplet impingement and the following process of secondary droplet generation. It seems that the momentum of the incoming droplet and the properties of the impacted liquid influence largely the process. The most important parameters of the primary droplets are the velocity C_{iD}, the diameter D_{iD} and the impingement angle α_{iD} (figure 4-11, for clarification, figure's notation is followed).

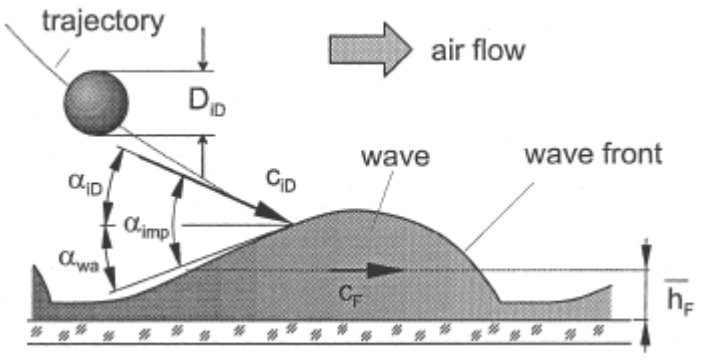

Figure 4-11: Droplet impingement on a wavy Film [Samenfink et al. (1999)]

Assuming that the liquid surface consists of the same liquid as the droplets, the important properties are the density ρ_{lq}, the viscosity μ_{lq}, and the surface tension σ_{lq}. The parameters of the liquid film, which are necessary to describe the impingement process are the mean film height $\bar{h}_F$, the mean film velocity C_F, and due to the waviness the wave angle α_{wa}. The authors introduce dimensionless numbers to reduce the number of parameters and variables and to generalize the results of these investigations. Hence, they define the Laplace number (La) and the momentum parameter of the primary droplets s_{cd}:

$$La = \frac{\rho_{lq} \cdot \sigma_{lq} \cdot D_{iD}}{\mu_{lq}^2}$$

Equation 4-14: Laplace Number (La) Definition

S_{cd} expresses the ratio of the original droplet's velocity to the minimum velocity in which the destruction process starts. Additional dimensionless parameters are the normalized film height $h^* = \bar{h}_F / D_{iD}$ and the impingement angle α_{imp}, representing the sum of the angle of the primary droplets and the wave angle (figure 4-11).

Samenfink et al. (1999) propose that complete deposition takes place when $s_{cd}<1$, while splashing occurs for $s_{cd}>1$. They also argue that the deposited mass fraction increases significantly with a decreasing impact angle, down to a value of $\alpha_{iD} \approx 30°$. At this point, the deposition rate exceeds 90% when droplets injection velocity is 30 m/sec. The primary droplets diameter varies from 5 µm to 80 µm. Consequently, at steep angles, the most possible outcome is splashing and the entrainment of the secondary droplets in the airflow. A representative graphic is shown in figure 4-12.

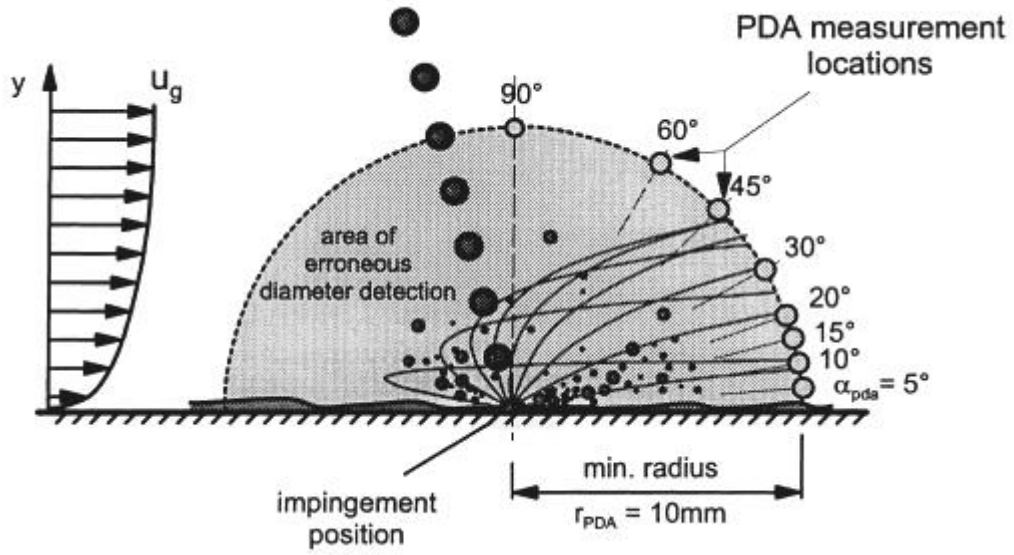

Figure 4-12: Droplet Impingement [Samenfink et al. (1999)]

Furthermore, they demonstrate that the film thickness has an influence on the deposited mass. When the liquid film is thicker, deposited mass fraction (η) increases. The composition ratio (ξ), which is the ratio of primary to secondary droplets volume flux, is influenced by the film thickness and the impact angle. Due to a better mixing of impinging droplet and film with decreasing impact angles the composition ratio decreases as well. The authors notice that for impact angles smaller than 30° the composition ratio rises again. They attribute that to the wavy surface structure of the shear-driven film. The above are plotted in figure 4-13.

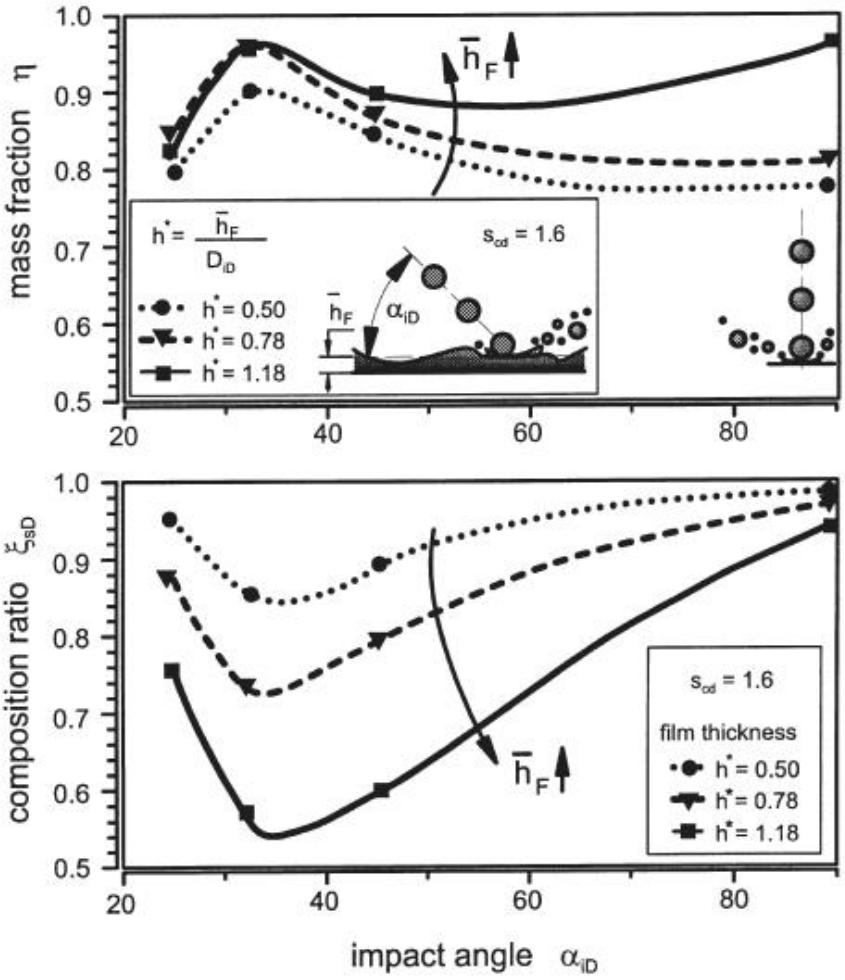

Figure 4-13: Deposited Mass Fraction and Composition Ratio of the Secondary Droplets [Samenfink et al. (1999)]

Samenfink et al. (1999) examine in detail the effects of liquid water droplet impaction on a liquid film and their results are verified for fine droplets (5 µm to 80 µm) and primary droplets velocity up to 30 m/sec. However, the author believes that, their results should be used only in a qualitative way when a case of water droplets impinging on a compressor rotor blade is considered. The relative speed of droplet and blade is quite higher than the described experiment as the droplet diameter as well. On the other hand, it gives a clear view of the processes, which take place when water droplets impact on a blade and a liquid film is formed by the preceding droplets.

4.3.3 Water Evaporation

Water may exist in both liquid and vapour phase over a wide range of temperatures. Figure 4-14 illustrates the temperature-specific volume diagram for water showing the liquid, two phase liquid vapour, and vapour regions.

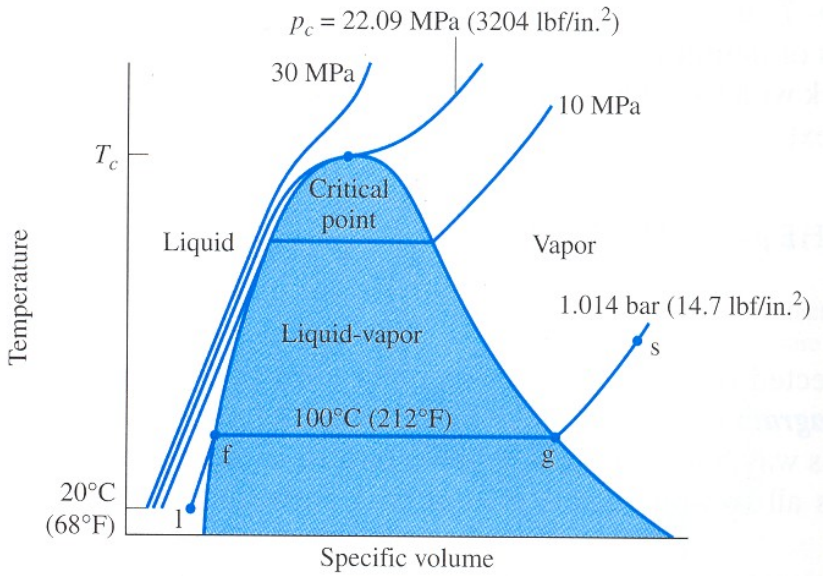

Figure 4-14: Temperature-specific volume water diagram [Moran and Shapiro (2000)]

There are constant pressure lines, which are called isobars. The temperature, at which a phase change takes place at a given pressure, is called saturation temperature and the pressure, saturation pressure. For each saturation pressure there is a unique saturation temperature and conversely. When liquid water is heated at constant pressure, it turns into vapour with a considerable increase in specific volume. At a pressure of 1.014 bars and temperature of 100 °C, water evaporates to steam if heat is supplied. This energy requirement is the latent heat of evaporation, and under these conditions, it is accompanied by a considerable increase in volume by a factor of 1,600 [Moran and Shapiro (2000)]. The higher the pressure, the higher the temperature at which evaporation takes place.

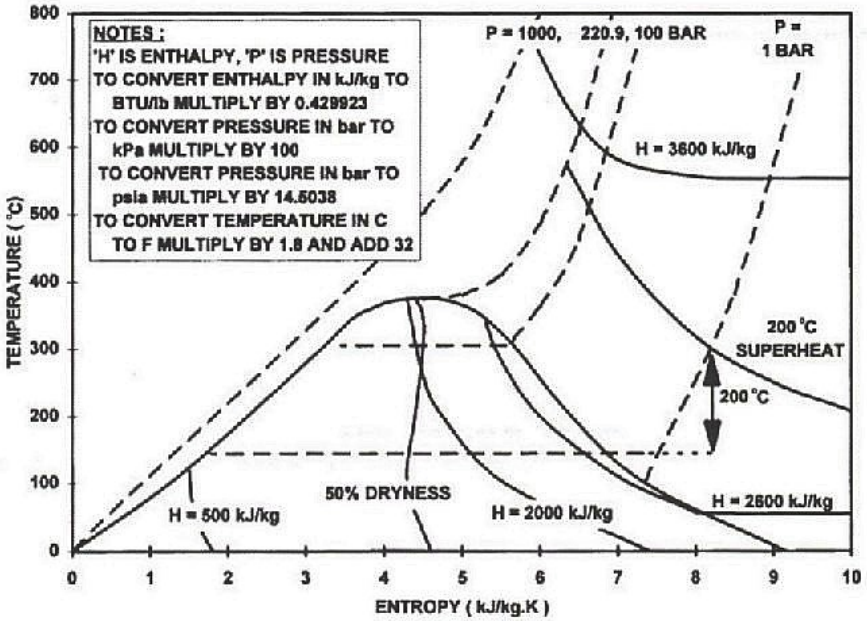

Figure 4-15: Water T-S Diagram [Walsh and Fletcher (1998)]

The properties of water in a Temperature-Entropy diagram (T-S) (this is also called a Mollier diagram) are plotted in figure 4-15. It is worth mentioning the triple point at 0 °C, where water may exist as solid (ice), liquid and vapour. At fixed pressure, heat input to liquid water increases the temperature until it crosses the saturated liquid line, when the boiling temperature is reached. Further heat input evaporates liquid water at constant temperature moving towards the saturated vapour line. In this line, evaporation is completed, and additional heat input will increase the temperature and steam will become superheated.

In case of an axial flow compressor, heat absorption will cause a reduction in the inlet temperature. Furthermore, the presence of vapour in the fluid flow increases the mixture mass flow. These have a beneficial effect on the performance of the engine. This is what happens in case of water injection in a gas turbine engine. Fine droplets are injected in a controllable way and they easily evaporate into steam, improving engine's performance. On the other hand, in case of operation under adverse weather condition, liquid water enters into the engine possibly in large quantities and in big diameter droplets. At the same time, complex aerodynamic and mechanical effects take place, resulting in performance deterioration.

Numerous works has been accomplished on the subject of the heat transfer between water droplets and a co-current gas. The resulted evaporation strongly depends on the residence time to transfer heat to water, on droplet size and temperature. Extensive work has been done on the phenomenon of evaporation when water is injected in a gas turbine engine. Presenting thoroughly the parameters of water evaporation is out of the scope of this project. Therefore,

the subsequent section aims to spot just few remarks, which the author has frequently met over the literature search.

For an aero-engine, the residence time of a water droplet in a compressor is very small (few seconds). Consequently, heat exchange and mass transfer between the air and the liquid surface are very low. Quandt, (1996) argues that water droplets larger than 10 μm may pass through the compressor into the combustor. In his theoretical work, he holds the view that the water drop will evaporate at the last stages of the compressor, where high pressures and temperatures are present.

Extensive work on the evaporation in an axial-flow compressor was carried out by Loebig et al. (1998). They investigated, both theoretically and experimentally, the effects of water-methanol injection on an Allison T56 turbo-shaft engine. In their theoretical part of their work, the numerical analysis was based on solutions of 3-D compressor flow equations. The streamline curvature method was used for the solution of the flow field. The computation included the 3-D droplet trajectories, droplet evaporation characteristics and droplet impingement locations on both the hub and casing surfaces of the compressor. The code does not take into account the droplet impingement on the blades.

The authors conclude that droplets with diameter greater than 50 μm impinged on the inner casing wall. The smaller droplets followed the airflow very closely (figure 4-16).

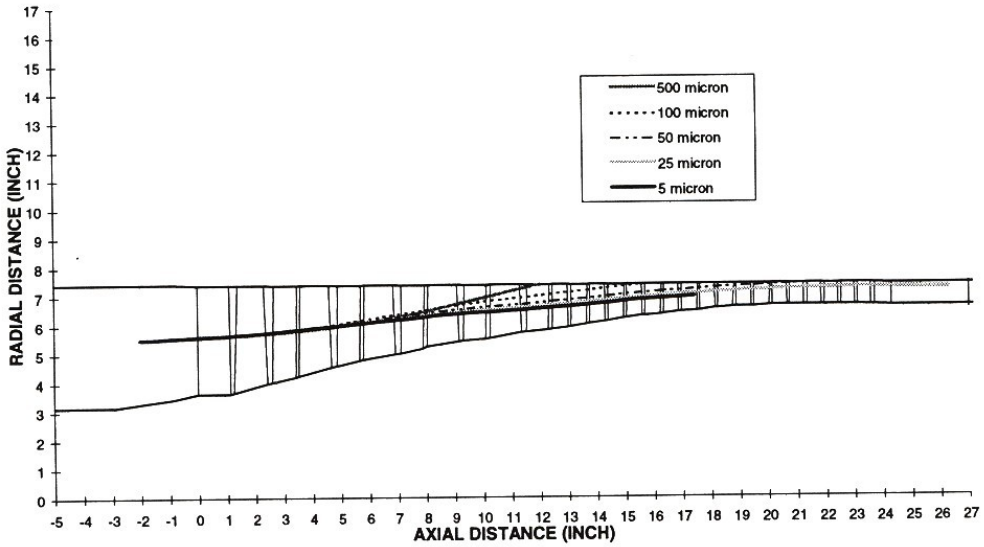

Figure 4-16: Droplet Trajectories in an Axial-Flow Compressor [Loebig et al. (1998)]

In figure 4-17, the vapour mass fraction is plotted as a function of the compressor's axial length. The authors remark that the droplets with diameter of 0.2 mm do not evaporate contrary to the very fine droplets of 25 μm. It is

highlighted that these droplets evaporate 30% at the last stages of the compressor.

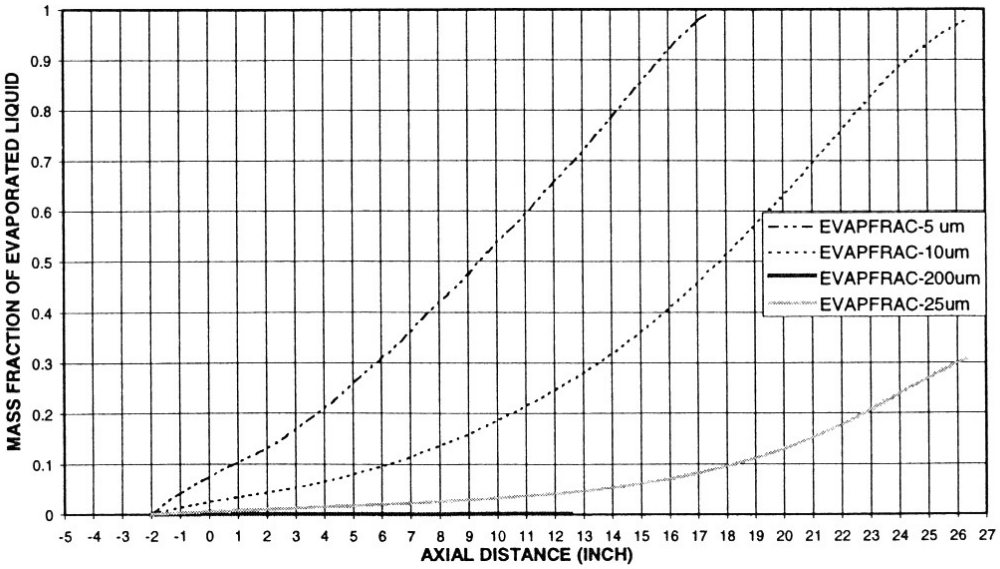

Figure 4-17: Vapour Mass Fraction Vs Compressor Length [Loebig et al. (1998)]

Qun Zheng et al. (2003) theoretically evaluate the time for a given droplet to evaporate in an axial compressor. They conclude that for an axial air velocity in order of 10^2 m/sec, which is typical for a modern compressor, the maximum staying time of droplet is generally in order of 0.01 sec (considering the compressor length about 1 m). Thus, over this time all the droplets below the size of 0.02 mm will evaporate. The authors comment that smaller droplets can achieve a better evaporative effect. They also note that droplets smaller than 0.005 mm can move along the streamlines causing rapid evaporation with the least disturbance to airflow.

As far as the droplet evaporation model is concerned, a considerable number of works adopt Spalding's evaporation model [Spalding (1979)]. Following this analysis, the rate of change of a spherical droplet radius r_d is given by the following equation:

$$\frac{dr}{dt} = \frac{\rho\Gamma}{r}\ln\left(\frac{1+CV}{1+CL}\right)$$

Equation 4-15: Droplet Rate Evaporation [Spalding (1979)]

Γ is the diffusion coefficient for water vapour in air, ρ is the humid air density and CV-CL is the mass vapour – liquid per unit mass of dry air respectively Horlock (2001), White and Meacock (2003), AEA (2002a), Mathioudakis and Roumeliotis (2006) use the above model to their theoretical calculations.

The presence of water vapour in the working fluid influences its properties. The air-water mixture has a different molecular weight (MW) and thus, ratio of specific heat (γ) relative to that of dry air. This condition affects the engine's thermodynamic cycle. The gas constant R of a single constituent or a mixture equals to $R=R_o/MW$, where Ro is the universal gas constant (8.31 KJ/mole °K). In case of a mixture, R is calculated by the mass averaged of the gas constant of the constituents. Hence, the ratio R_{fac} of mixture gas constant R_m to that of dry air R_a (=287.05 J/kgr °K), equals:

$$R_{fac} = \frac{R_m}{R_a} = \frac{Ro}{MW_m \ R_a}$$

Equation 4-16: Gas Constant Factor for Moist Air

MW_m is the molecular weight of moist air. By considering that the molecular weight of water is 18.015 and that of dry air is 28.96, MW_m can be related to water to air ratio by mass (WAR) with the following equation:

$$MW_m = \frac{1}{\left(\frac{WAR}{18.015} + \frac{1 - WAR}{28.96}\right)}$$

Equation 4-17: Molecular Weight for Moist Air

Similarly, the ratio of specific heats of air-water mixture (gamma factor) can be obtained as the mass averaged of the ratio of specific heats of the constituents. Hence, the gamma factor ratio of moist to dry air is:

$$\gamma_{fac} = \frac{\gamma_m}{\gamma_a} = \frac{WAR_{molar}\,\gamma_w + (1 - WAR_{molar})\gamma_a}{\gamma_a}$$

Equation 4-18: Gamma Factor for Moist Air

In the above equation, WAR_{molar} is the ratio of water to air by the number of moles, and equals: $WAR_{molar}=WAR\cdot(28.96/18.015)$.

Furthermore, the presence of gaseous water in air alters the specific heat at constant pressure Cp, since it depends on temperature and the nature of the fluid. Cp of water and dry air for a given temperature can be calculated using the following polynomial:

$$Cp = A_0 + A_1T_Z + A_2T_Z^2 + A_3T_Z^3 + A_4T_Z^4 + A_5T_Z^5 + A_6T_Z^6 + A_7T_Z^7 + A_8T_Z^8 + A_9T_Z^9 + A_{10}T_Z^{10}$$

Equation 4-19: Cp Polynomial Calculation [Walsh and Fletcher (1998)]

T_z is the static temperature divided by 1000.0 and A_i are constants and they are given in the following table:

	Dry Air	Water
A_o	0.992313	1.937043
A_1	0.236688	-0.967916
A_2	-1.852148	3.338905
A_3	6.083152	-3.652122
A_4	-8.893933	2.33247
A_5	7.097112	-0.819451
A_6	-3.234725	0.118783
A_7	0.794571	0
A_8	-0.081873	0
A_9	0.422178	2.860773
A_{10}	0.001053	-0.000219

Table 4-2: Dry air and water constant values in Cp polynomial calculations [Walsh and Fletcher (1998)]

Consequently, the specific heat factor Cp_{fac} can be calculated by averaging the mixture constituents on a molar basis:

$$Cp_{fac} = \frac{Cp_m}{Cp_a} = \frac{WAR_{molar}\, Cp_w + (1 - WAR_{molar})\, Cp_a}{Cp_a}$$

Equation 4-20: Specific Heat Factor for Moist Air

The quasi-dimensionless parameters group are usually involved to plot components' map. In this case, it is assumed that the working fluid's nature does not change, i.e. γ, R and Cp are constant. However, as it is described above, this is not valid for the water ingestion, and for this case, fully non-dimensional parameters should be invoked:

$$W\sqrt{R\,T}\,/\,(D^2\,P\,\sqrt{\gamma}) \qquad N\,D/\sqrt{\gamma\,R\,T}$$

Equation 4-21: Fully non-dimensional Mass Flow and Speed Parameters

Consequently, by using equations 4-16 and 4-18 the following correlations can be extracted and should be used in cases where water vapour is present in the airflow:

$$\left(\frac{W\sqrt{T}}{P}\right)_m = \left(\frac{W\sqrt{T}}{P}\right)_a \sqrt{\frac{\gamma_a}{\gamma_m}}\sqrt{\frac{R_m}{R_a}} \quad \text{and} \quad \left(\frac{N}{\sqrt{T}}\right)_m = \left(\frac{N}{\sqrt{T}}\right)_a \sqrt{\frac{\gamma_a}{\gamma_m}}\sqrt{\frac{R_a}{R_m}}$$

Equation 4-22: Non-dimensional Mass Flow and Speed Correlations for Moist Air

By considering that $MW_m<MW_a$, it is concluded that $R_m>R_a$ and $\gamma_m<\gamma_a$. Thus, from equation 4-22, in case of moist air the non-dimensional mass flow parameter increases while the non-dimensional speed decreases relative to the dry air values.

In conclusion, it can be argued that water evaporation in a wet compression process has been investigated from a wide range of researchers. They arrive at the same conclusion that evaporation has a beneficial effect on the gas turbine engine performance under specific conditions. Furthermore, it is confirmed that fine droplets evaporate more easily and efficiently. However, it should be highlighted that in case of water ingestion, the effects of any evaporation are diminished by the aerodynamic and mechanical consequences. Apart from that, evaporation rates are certainly lower since the rain droplets are bigger than the sizes considered in water injection studies. Droplet break-up cannot result in very fine droplets, adequate to evaporate before the entrance to the combustor. Hence, in the author's view, when rain ingestion phenomena are examined, the thermodynamic effects on the compressor can be neglected.

4.4 Intake

Engine's intake is the first component the rain droplet meets. The inlet's geometry influences largely the water entering the gas generator. The intake highlight area is one of the parameters, which controls the scoop factor (is analysed in the next section). Apart from that, the majority of rain droplets impacts on the intake's spinner. After the impact, they may enter the by-pass duct or the engine core. The design of the spinner can lead to lower water concentration in the engine core. It can be recalled that this was included in CFM modifications for increasing CFM56 engines water ingestion capability (chapter 4, section 4.1).

Another important parameter on the water ingestion effects is the droplet velocity as it enters the intake. Its influence on droplet break-up and splashing has been analysed in the previous section. High-speed droplets break-up into smaller secondary droplets.

Although there is extensive published work on the velocity of water droplets in an accelerating airflow, little data have been found on rain droplets' velocity entering an engine at flight conditions. Russell and Victor, (1984) did experimental work on the subject and measured the droplet's velocity levels at the intake throat by using a laser velocity meter. They observe that the water velocity values range from 35 m/sec to 170 m/sec for droplets larger than 1 mm, while the fine droplets (<0.3 mm) accelerate to the air stream velocity levels.

4.4.1 Scoop effect

It is well known that gas turbine engine inlets are designed to achieve the minimum spillage drag for a wide range of the expected operational velocities. For this reason, the size of inlet area is designed to provide an optimum mass flow ratio. A critical parameter for the intake design is the ratio of free stream

area (A_o) to the intake highlight area (A_1) (figure 4-18). It is referred in AGARD (1995) that for a subsonic transport aircraft, the A_o/A_1 value is approximately 0.8 to 1.0 in the cruise speed.

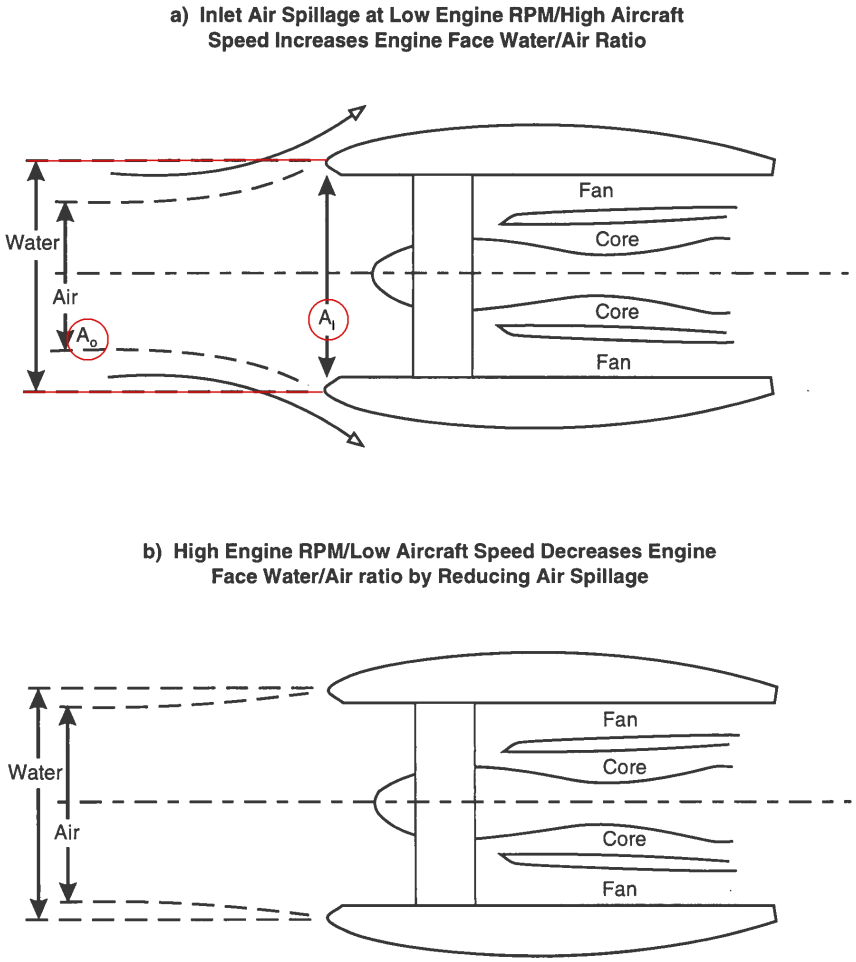

Figure 4-18: Scoop Factor Effect [AGARD, (1995)]

Under descent conditions, the aircraft typically flies with high speed and needs to slow down. Therefore, its engine works in idle settings (low air mass flow) and it is unable to swallow all the air entering the engine-inlet highlight area. Thus, part of the airflow creates a spilling flow because it is forced to flow around the engine's nacelle. However, under rain conditions, the water droplets, because of their inertia, cannot follow the spillage flow. Instead of it, they follow straight-line trajectories and enter into the engine, increasing the water to air mass flow ratio. The concentration ("scooping") of water droplets is known as the scoop effect.

In case of supersonic intakes designed mostly for military aircrafts, scoop effect may be alleviated by the bleeds and bypasses ducts. Furthermore, shock waves change substantially the static pressure (before and after the shock

wave) so that the resultant differential velocity between a droplet and the airflow will disintegrate the former, as it has been described in the previous section.

The author, as an F-4 aircraft maintenance engineer, experienced once the scoop effect. It was the case of an aircraft performed an emergency landing during light rain. The problem focused on one engine, which, after a sudden knock, it vibrated with an over-temperature indication at the same time. After landing and the engines' shutdown, an inspection of the first compressor stages took place for detecting foreign or domestic object damage (i.e. the engineer enters the inlet and crawls across the intake to the compressor). The author observed that the majority of the inlet's surface was wet and there was liquid water concentration at the lower part of the inlet duct. However, there was no evidence of water at the compressor's blades. Presumably, the ingested water quantity evaporated in the compressor. Furthermore, after the engine's shutdown, the heat of the combustor is transferred upstream as well and increases the compressor temperature.

It is mentioned in chapter 4 (section 4.2) that the proposed values for rain certification tests do not account for the scoop effects. Moravec and Patnoe (1996b) recommend that these effects should be included in the proposed rain requirements and extensive research should be initiated. However, there is no quantitative data in the open literature about the percentage increase of water-air ratio attributed to scoop effect. The only data are sourced from Kennedy and Roberts (1990) work, in which they report that at low power during descend in storm, the scooping effect can increase the water-air ratio at the engine nacelle inlet to 260% percent of the ambient levels existing in the storm. Nevertheless, they do not explain the calculation of this value. Presumably, the percentage of spillage flow is estimated and then it is taken into account altering the water-air ratio.

4.5 Compressor

The published research of water effects on gas turbine engine performance has mainly focused on the compressor component. This is fully justified by considering that the compressor suffers the effects first, since it is directly exposed to water ingestion. Consequently, in the subsequent sections a detail description of the processes taking place in this component is presented.

4.5.1 Water Film Formation and Motion

The total amount of ingested water in a gas turbine engine depends on the scoop factor and the flight velocity. When rain droplets enter the engine, they may impact on the inlet spinner, on the engine casings, on the fan blade or they may pass through the fan blade row and enter the core engine. Large droplets,

because of their inertia, are less able to follow the air streamlines. As a result, they will impact on the blades and form a liquid film.

4.5.1.1 Water Droplet Trajectories

The tracking of droplet trajectories in the airflow helps to predict the deposition mechanism on the compressor blades. It is reported in AGARD (1995), that droplets bigger than 70 μm are captured by the blades and form a liquid film. The idea is plotted in figure 4-19. The aerodynamic forces on the droplets with the diameter of 10 μm affect their motion and they may pass the blade row.

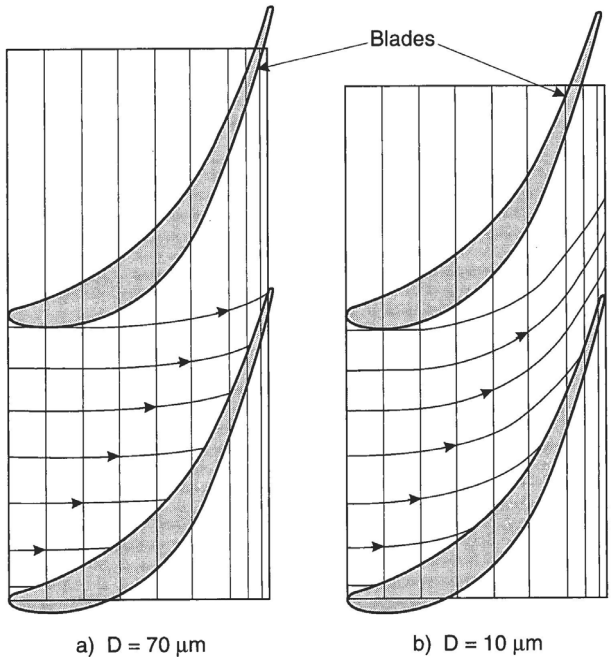

Figure 4-19: Droplet Trajectories Estimation [AGARD, (1995)]

Extensive work on the water droplet collection on a booster rotor was carried out by Das et al. (2006). Their numerical investigation included the effects of rotational speed on the water collection efficiency and it was based on Computational Fluid Dynamics (CFD) method and the solution of the compressible Reynolds Averaged Navier Stokes (RANS). The Lagrangian approach was used to track the water droplets in the flow field and the one-way coupling was used to simulate the effects of momentum and energy exchange between the flow and the droplets. Droplets were injected with zero absolute velocity, which, in the rotor frame of reference, was equal to rotor speed towards the blade pressure surface. In addition to that, it was assumed that all the droplets deposited on the blade after they impinged on its surface.

The authors argue that the percentage of the deposited droplets increases at lower rotational speeds. At these speeds, the droplets impinge on the rotor blade pressure-side at the leading edge region after they have crossed several blade passages. As the rotor speed increases, the impingement locations move

towards the trailing edge. Finally, at high speeds some of the droplets manage to cross the passage without impinging on the blades. Figure 4-20 shows the water droplets trajectories for a range of rotational speed.

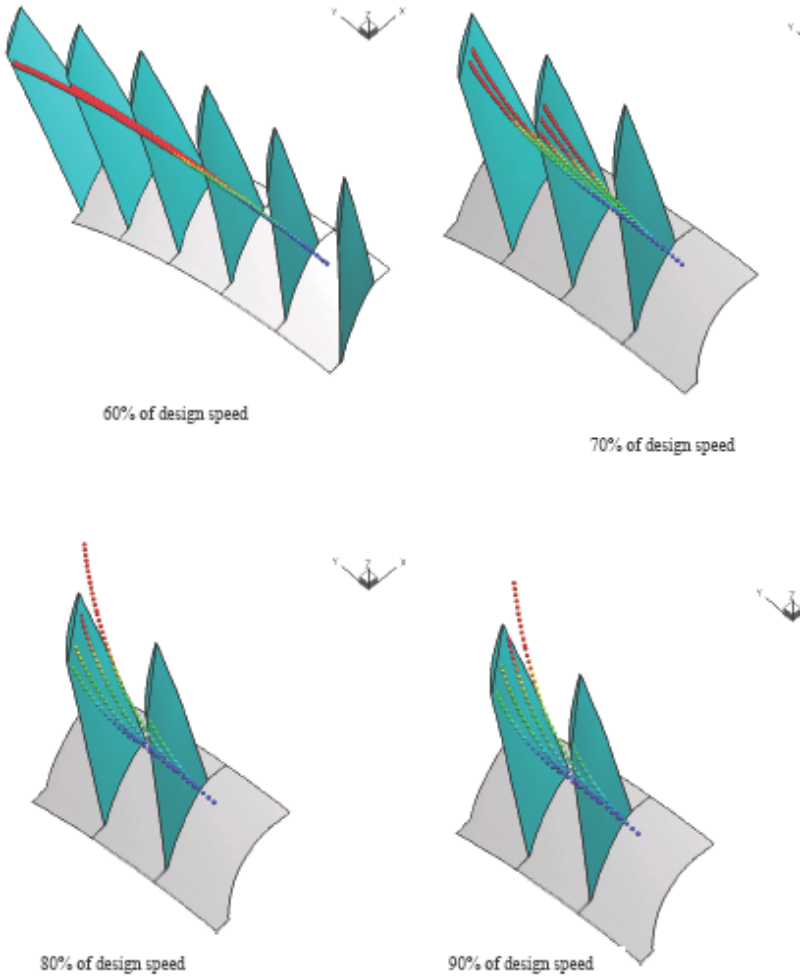

Figure 4-20: Droplet Trajectories for Different Rotor Speed [Das et al. (2006)]

Das et al. (2006) conclude that the deposited droplet mass is higher at the leading edge near the tip and at the lowest rotor speed. They also note that only very few droplets impinge the leading edge of the rotor blade suction surface. However, their research focuses only on fine droplets of D_w=30 μm. This is a basic parameter of the impingement process. It is certain that larger droplets will impinge on the blade pressure surface even at high rotational speeds.

4.5.1.2 Forces Acting on Deposited Water Droplets

It has been noted that when water droplets enter the compressor, they impinge on the rotor blade and form a liquid film. The latter moves under the influence of the following forces:

- The inertia force, which comprises the Centrifugal and Coriolis components, resulted from the blade rotation,
- The blade-water film friction force,
- The total interfacial air-water film force, which is composed of the aerodynamic shear force due to airflow, and the force generated as the subsequent deposited droplets decelerate, and
- The aerodynamic force due to the pressure gradient,

In addition to these, water viscosity also retards its motion. The inevitable non-uniformities of the wall (grooves etc) enhance the blade-water film friction force. The latter tends to split the cohering water film into individual currents.

Many researchers have investigated the motion of water film on a turbomachinery blade. They share the view that the centrifugal force is the dominant force in the radial direction and the aerodynamic force due to the pressure gradient is negligible for the turbomachinery flow field. However, they differ about the friction force calculation and almost nobody takes into account the force due to the succeeding deposited droplets deceleration.

Gardner (1963) investigated the viscous flow of a liquid on a rotating flat surface with a shear stress exerted by a flowing gas stream along the surface and normal to the radial direction. He assumed that firstly, the pressure gradient had no effect on the film flow and secondly there was no radial shear force due to the secondary flow. Moreover, he did not take into account any friction force and noted that the gas shear stress will depend on the presence of the liquid film because the liquid would not be free of ripples. He states that for this particular research, where $Re<400$, the viscous equation of motion would apply as for the dry case. Gardner argues that the value of liquid axial velocity is controlled by air shear stress, while the value of liquid radial velocity by the centrifugal force. He concludes that the liquid film flows towards the tip of the surface and its motion is influenced mostly by the rotational speed.

Gyarmathy (1962) studied the water film motion on a steam turbine blade. He focused on the film thickness and its velocity calculations. He assumed that there was no velocity component perpendicular to the blade because a very thin water film in laminar flow was considered. He also took for granted that on stator blades the governing forces are the pressure gradient and interfacial shear force, while centrifugal force predominates on the rotor blades.

The author proposes that the film thickness on a rotor blade depends on the rotational speed, the liquid mass flow and its physical properties. On stator blades, the gas drag coefficient influences the calculation. He also estimates that the film moves almost radially (4°-7° from radial direction). He extends its

calculation to the water film motion on the casing walls, in which the pressure gradient is taking into account for a steam turbine case. He estimates that the water film thickness between two stator blades for 0.4 kgr/sec liquid water flow can be in the order of 90 μm. It is worth noting that this value would be different for a compressor because the pressure gradient is not the same.

Kirillov and Yablonik (1968) model a steam turbine rotor blade as a flat plate and analyse the motion of water on the plate for different stagger angles (stagger or setting angle (β): the angle of blade chord relative to the axial direction). They include the friction force in their calculations assuming that it acts in the opposite direction to the water velocity relative to the blade, with magnitude proportional to the water speed (equation 4-23). They declare, however, that the form of the liquid water (droplet, rivulet or film) influences the actual magnitude of the friction force. Kirillov and Yablonik (1968) also neglect the aerodynamic drag supporting that it is small in comparison with the centrifugal and Coriolis forces. The frictional force per unit mass of water is assumed to be given by:

$$F_f = -k \cdot V_w$$

Equation 4-23: Friction Force on a Liquid Water Mass

V_w is the liquid water velocity relative to the surface and k is a constant, termed the “friction factor”. It becomes non-dimensional when K=k/ω, where ω is the angular velocity. Kirillov and Yablonik (1968) support that K takes values between 0 and 1.

However, Williams and Young (2006) disagree and support that K can be significantly bigger than 1.0. Nevertheless, they augment the view that the limiting case of K=0 (zero friction force) is still worth considering because it defines the water movement when controlled only by inertia. Williams and Young (2006) carry out extensive work on the subject of deposited water trajectory over a compressor blade surface. Their analysis includes the effect of all the forces acting on the liquid water droplet and it actually extends the work of Kirillov and Yablonik (1968) by considering water motion on a rotor blade of arbitrary shape. They also assume that when the water deposits on the blade, it looses all its momentum and it starts its motion from rest relative to the plate.

The authors show that for the case where K=0 and stagger angle β=0 the Coriolis force acts normal to the plate surface and does not affect the water motion. The latter centrifugal force is the only force acting radially and the film moves outward to the tip. When β is negative (i.e. compressor blades case while β is positive in turbine blades), the effect of the Coriolis force is more pronounced and tends to displace the water to the blade trailing edge (it is clear that in case of the turbine blades this force is towards the leading edge). Their

analysis for these conditions agrees with the results of Kirillov and Yablonik (1968) as it is shown in figure 4-21.

However, the authors acknowledged that the extra momentum in the axial direction added to the film by the further deposited water droplets is not taken into account. This effect would clearly augment the tendency of the trajectories to move towards the trailing edge.

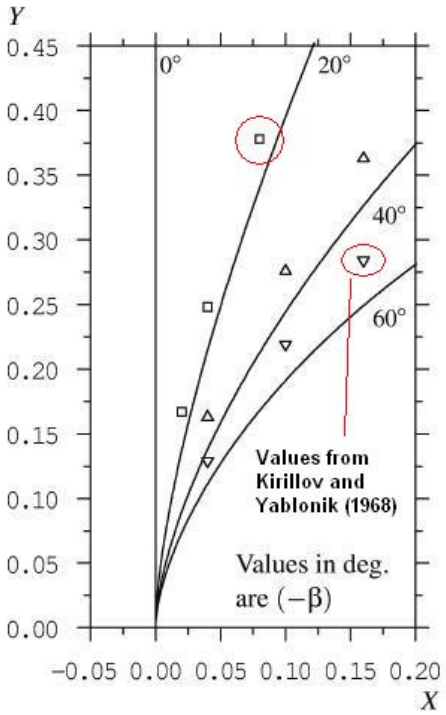

Figure 4-21: Water Droplet Trajectories for Different Stagger Angle and Zero Friction Force [Williams and Young, (2006)]

Williams and Young (2006) examine the case where there is a high friction force (K>>1). They mention that when K is large the water follows a radial trajectory and the effects of stagger angle changes are counterbalanced. It is also calculated that the maximum deviation of the droplet's trajectory from the radial direction is 8°. Therefore, they conclude that blades having a high friction surface (i.e. roughness), enhance the tendency of water to move radially under the influence of centrifugal force.

Williams and Young (2006) extend their study to the non-dimensional friction factor (K) calculation. They share the view that K depends on the form of water (droplet, rivulets or film) and its estimation with some confidence is feasible only when a laminar film is considered. They show that for the limiting case of β=0, K is calculated from the following equation:

$$K = \left(\frac{3 \cdot Re_{cent}}{Re_{film}^2} \right)^{1/3}$$

$$Re_{cent} = \frac{r^2 \cdot \omega \cdot \rho_w}{\mu_w} \qquad \text{and} \qquad Re_{film} = \frac{G}{\mu_w}$$

Equation 4-24: Friction Factor Calculation [Williams and Young, (2006)]

Re_{cent} is a centrifugal Reynolds number, Re_{film} is a film Reynolds number, ω is the angular velocity, r is the radius, ρ_w and μ_w is the liquid water density and dynamic viscosity respectively, and G is the local water mass flow rate per unit width of film. The variation of K with Re_{film} for various values of Re_{cent} is plotted in figure 4-22:

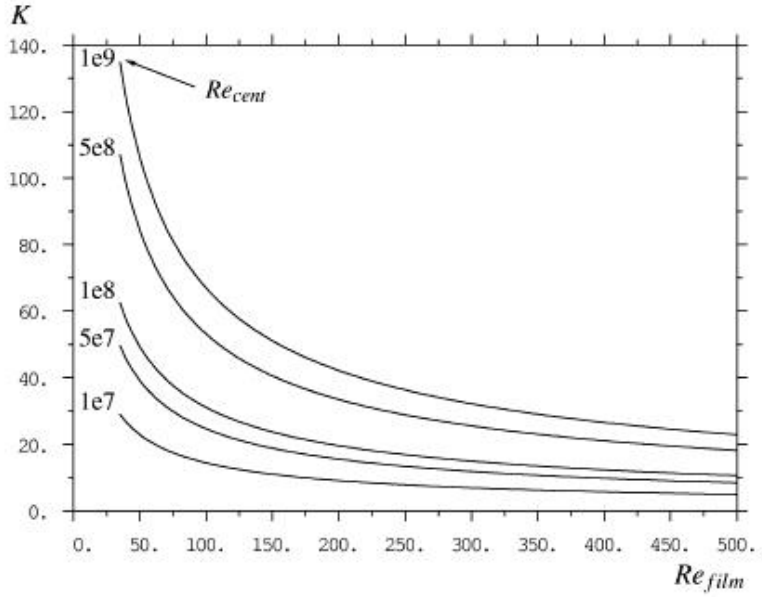

Figure 4-22: Laminar Film Flow Friction Factor (K) over a Rotating Surface [Williams and Young, (2006)]

It is noteworthy that K increases when the rotational speed of the blade increases (i.e. Re_{cent}>5 10^7).

Williams and Young (2006) examine the effect of the aerodynamic pressure force, which acts both in axial and radial direction. The authors confirm that this force does not influence the droplet's motion because its magnitude is small, compared with the other forces. In a compressor, the pressure rises through a blade passage and this implies that a pressure force acts on the droplet towards the leading edge. The authors also study the influence of the aerodynamic shear force. They assume that it acts predominantly in the axial direction and depends on the form of water film. They conclude that the aerodynamic shear force can influence the water trajectories and displace them towards the trailing edge. However, they do not give details about the drag coefficient estimation

and how it is affected by the presence of the water film. In addition to that, their analysis does not include the momentum of subsequent deposited water droplets, which further increases the axial force.

Williams and Young (2006) confirm that water droplet trajectories are mostly influenced by the inertia forces (centrifugal and Coriolis), the frictional force between the blade's surface - water film, and the aerodynamic shear force. The most important parameters are the blade stagger angle, the friction coefficient and the initial water velocity on the blade.

4.5.1.3 Water Film Thickness

The thickness of liquid film flows are of great interest for many engineering applications. In the field of gas turbine engines, it is considered in the combustor design process. In case of water ingestion conditions, the water film, which is formed on the compressor blades, is of primary importance because it is a basic parameter for the mechanical and aerodynamic effects. However, there is not detailed data in the literature, about water-film thickness estimation on the compressor blades.

Experimental data for the film thickness are presented in AGARD (1995). By using Pratt and Whitney internal research measurements, the film thickness parameter C_D/δ_{film}, (C_D is the drag coefficient of water on plate) is illustrated in figure 4-23:

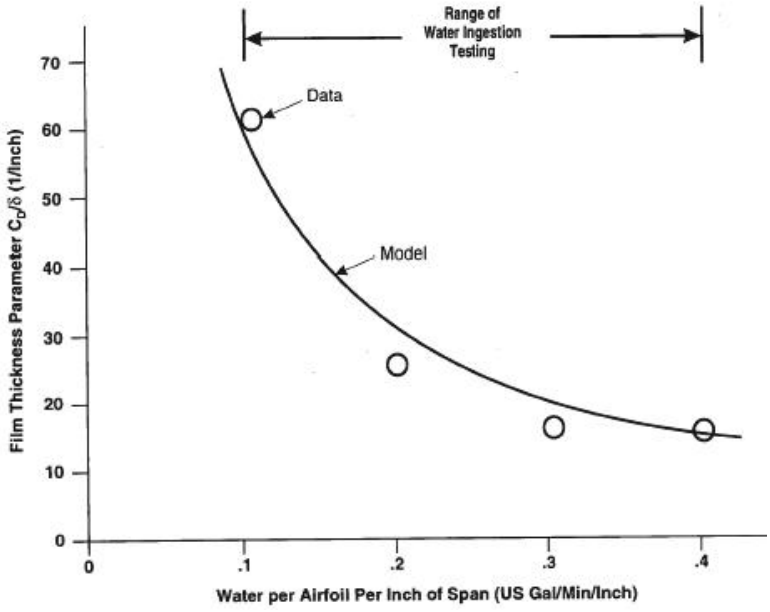

Figure 4-23: Film Thickness Parameter [AGARD, (1995)]

It is shown that the film thickness parameter C_D/δ_{film} is a function of the available blade surface. It is contended that δ_{film} is measured during water ingestion

engine tests without presenting a theoretical calculation for it. Finally, water film acceleration is estimated by the following equation:

$$\frac{dV_{film}}{dt} = \frac{U^2}{r} - \frac{C_D}{\delta_{film}} V_{film}^2$$

Equation 4-25: Water Film Acceleration [AGARD (1995)]

It is also reported that the film breaks-up at the blade trailing edge and the produced droplets are greater than 2.5 mm. However, it is not available any other data. Ulrichs and Joos, (2006) present an opposing view about the secondary droplets size. In their study, they observe that the resulting droplets are of the order of 30 μm, although only fine droplets are injected at the inlet of the compressor cascade.

The ligament formation and its break-up at the blade's trailing edge, producing secondary droplets, demonstrated in figure 4-24:

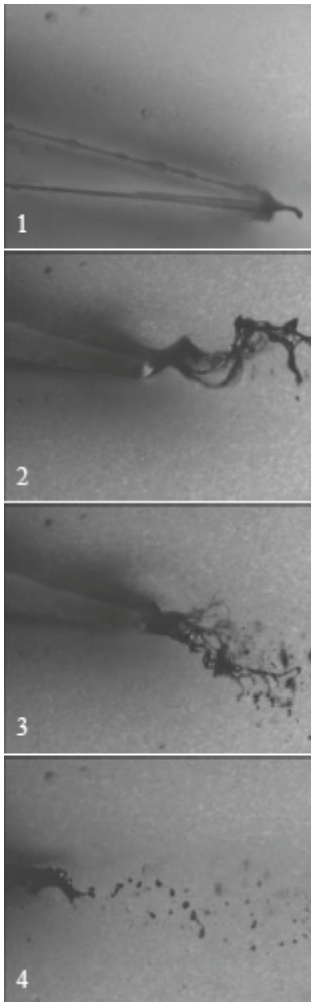

Figure 4-24: Water Ligament Formation and Break-up at the Blade Trailing Edge [Ulrichs and Joos (2006)]

It is evident that the wavy water film under the influence of air shear force moves towards the blade's trailing edge. At this point, the film accumulates and when it reaches a certain size, it breaks-up forming a ligament. This ligament develops in the main flow direction, where it further breaks-up to secondary droplets. The authors support that the air stream velocity is the dominant parameter for the formation of these ligaments. The higher the velocity the shorter the ligaments are because the destabilization and the break-up occur earlier. Their results are confirmed by Varga et al. (2003), in which the secondary droplet's size approaches approximately 20 μm with increasing velocity of the coaxial air stream. However, it is noteworthy that these researches focus on fine injected droplets. Thus, the contradiction with the data in AGARD (1995) presented above, may be justified considering that the latter data refer to large rain droplets and higher air stream velocities.

Bong-Hwa and Gene (1987) study the co-current steam-liquid film flow in a low-pressure steam tunnel. Their objective is to investigate the effects of water flow

rate and its temperature on the turbine blades. They declare that there are three different flow regimes: rivulet, continuous and atomized (shed droplet) film flow. The discrete rivulets characterize the rivulet flow while the liquid film covers the entire wall surface in case of the “continuous” regime. In the “atomized” regime, droplets are transferred by the driving steam (or gas) flow.

Bong-Hwa and Gene (1987) propose the film thickness depends on the water properties (surface tension, density and viscosity), the interfacial shear force between liquid film and co-current air, and the water flow rate. In their experiments, the authors observe that film thickness (δ) alters with the steam flow (Q) and its velocity (V_{st}). They present that for V_{st}=325 m/sec, δ increases from 16 μm to 56 μm as Q increases by 6 X (100 to 600 cc/min). They also show that δ increases as V_{st} decreased in constant Q. For example, at Q=200 cc/min, δ increases from 21.6 μm to 251 μm (12 X) as V_{st} decreases from 325 to 105 m/sec.

Gyarmathy (1962) attempts to describe the water film thickness by the following equation, considering only the centrifugal force in the radial equation and air shear force in the axial:

$$\delta = \left(\frac{3 \cdot \mu_w}{\rho_w^2} \cdot \frac{m_w}{r \cdot \omega^2} \right)^{1/3}$$

Equation 4-26: Water Film Thickness on Rotor Blade [Gyarmathy (1962)]

r is the radius of the point on the blade, ω is the angular velocity and m_w is the water mass flow rate per unit of width.

Williams and Young (2006) suggest that the film thickness can be calculated by the following equation:

$$\overline{V}_w = \frac{\rho_w \delta^2}{3 \cdot \mu_w} \cdot F_I \Rightarrow \delta = \sqrt{\frac{3 \cdot \mu_w \cdot \overline{V}_w}{\rho_w \cdot F_I}}$$

Equation 4-27: Water Film Thickness Calculation [Williams and Young (2006)]

$\overline{V}_w$ is the mean water velocity and F_I is the inertia force (centrifugal and Coriolis) per unit of mass. The authors ignore the aerodynamic shear force but they take into account the friction force for the calculation of the mean water velocity.

The author in Nikolaidis Th. et al. (2008) suggests a film thickness estimation based on the dominant effect of centrifugal force and the aerodynamic shear force. This work extends that of Gyarmathy (1962) considering the momentum effect of the further deposited water droplets. The latter increases the aerodynamic shear force due to airflow. Moreover, this work emphasizes the

point of demanded compressor torque due to water droplets acceleration, which is the root for the mechanical effects of water ingestion. Detail description is presented in chapter 6, subsection 6-4.

4.5.1.4 Water Film Wavy Characteristic

Many researchers have investigated the water film formation on the blades of steam turbines. The increasing concern is justified by the fact that the liquid film alters the geometric characteristics of the blade (i.e. its profile). Furthermore, air shear force and water droplets momentum cause waves in water film's surface. The wavelet characteristics are not stable and they usually result in water film breakdown and the formation of "dry spots" and/or rivulets. The effects of the described features on the fluid flow are similar to these of rough blade surfaces, which are known to develop considerably larger skin friction coefficients when compared to smooth surfaces. The thickening of boundary layer is noticed in both cases resulting in an increase in blockage and reducing the aerodynamic performance of the blade. Consequently, the roughness effect of wavy water films on co-current airflow can be compared with that caused by a blade with rough surface.

It is known that for a surface, the roughening effect on the flow does not only depend on the mean height or grain size but also on the form of the grains and their distribution on the surface. Nikuradse (1933) defined the sand-grain roughness parameter and measured the relation of close-packed natural sand grains of nominally uniform diameter by investigating their effect on airflow. The concept of equivalent sand grain roughness k_s was firstly introduced by Schlichting, (1936) and it is the height of standard sand roughness that would produce the same effects on the flow as the roughness of interest.

Wurz (1976) indentify that the interfacial shear stress, which is the mean drag acting at the wavy film-gas interface, consists of skin friction and form drag. Two different approaches can be used for its calculation. The first one is by measuring the air velocity profiles in the boundary layer. The second is by the momentum-integral equation for two-dimensional compressible boundary layers. In any case, Wurz (1976) argues that the interfacial shear stress is not the same under dry and wet conditions.

Wurz (1976) experimentally investigates the liquid film flow on a flat plate under the influence of high-speed co-current airflow. He compares the air velocity profiles between wet and dry plate and observes that the liquid film causes a velocity defect, shifting the velocity profiles towards higher roughness Reynolds numbers. He claims that the presence of the liquid film increases the shear stress by approximately 30% in comparison with the dry wall condition. He also examines the film thickness values for air velocity Ma=1.2 – 2.4 and confirms that air velocity affects film thickness (20 μm to 40 μm). Finally, he calculates

the equivalent sand-grain roughness (computed from Re), and compares it with the mean film thickness. The most important point of his research is its conclusion that the ratio of equivalent sand-grain roughness to the mean water-film thickness is almost constant and equals to 1.5. Hence, the roughness effect of wavy water films on co-current airflow can be compared with the effect of sand-roughened walls.

Wurz (1970) also examines the same effect in a low velocity range. In the subsonic test from 0.18-0.6 Mach number range, he shows that the described ratio is 1.25 to 2.0. Therefore, it seems that the ratio is almost unaffected by the change of air velocity. The author does not comment on the remarkable similarity of this ratio over the range of the air velocity. Another key feature is that his experiments are conducted in low rainfall rates, which produce low film thickness values.

Extensive work on the phenomenon of film formation on a flat plate under the influence of a co-current steam-flow has been done in the University of Michigan. Hammitt et al. (1975a), Hammitt et al. (1975b), and Hammitt et al. (1981) focus on the film thickness measurements. Their objective is to investigate the behaviour and the stability of thin liquid film formed on the turbine blades during high velocity steam flow. The authors note that the shear force generated by the high velocity steam (gas) flow drives the liquid film. They justify their view that the liquid film is within the laminar range, supporting that the film is thin (10 μm to 100 μm), and its velocity is small relatively to this of steam. Hence, it is assumed that the film has a linear velocity profile i.e. it is a "Couette flow". The authors also support that the liquid film velocity profile could be accurately calculated if the interface shear (and droplet deposition) is known. For this, the "friction factor" (f) between the steam and the liquid water is required. They also remark that inadequate information exists concerning the friction factor between a liquid and high-velocity gaseous phase, even if surface waves were not generated, which is generally not a realistic assumption.

However, Hammitt et al. (1981) show that the "friction factor" f may be estimated by the following experimental formula:

$$f = \left(0.0007 + 0.0625 \times Re_v^{-0.32}\right) \times \left(1 + 0.025 \times Re_l\right)$$

Equation 4-28: Friction Factor Estimation [Hammitt et al. (1981)]

Re_l and Re_v are the liquid and vapour Reynolds numbers. The characteristic lengths here are the film thickness and the hydraulic channel diameter and it is assumed adiabatic conditions for the film. This factor depends upon film wavelet characteristics, just as it depends upon relative roughness in convectional pipe flow. Cohen and Hanratty (1968) report that the effective friction factor for such a wavy film flow, is somewhat greater than for comparable pipe flow.

In Michigan University tests, liquid water is injected near the leading edge of the plate at known rates and it flows under the influence of a steam flow. Its values vary from 50 μm to 200 μm for water flow rate 5 to 60 cm^3/min. By assuming that the gas shear force equals to liquid shear force at the interface, and the velocity profile in the film flow is linear, a theoretical estimation of film thickness is feasible. It is found that measurements of the film thickness are almost double the values of the theoretical calculations. The authors attribute the error to the interface shear-force estimation and they confirm that there is indeed a friction factor between liquid film and high-velocity gas. It is added that the surface wavelet formation compose the most important feature of film flow regimes, because they usually result in film breakdown and the formation of presumably “dry spots” and/or rivulets, which further influence the friction factor and consequently the interfacial shear force.

The idea of the roughening effect of water droplets on aircraft wings has widely been used by several researchers. Thompson B. et al. (1995), Thompson B. and Jang J. (1996), Haines and Luers (1983), Luers and Haines (1983), Khodadoust A. and Bragg M.B. (1995), Ashenden R. et al. (1996a), Valentine and Decker (1995a), and Bilanin (1987) investigate the performance deterioration of airfoils under the influence of rain.

Ashenden R. et al. (1996b), Haines and Luers (1983) attempt to evaluate the aerodynamic penalty of heavy rain on an aircraft wing. Their effort focuses on the airfoil roughness caused by the momentum of droplets, which disturb water film surface, and the waves developed on the water film surface under wind shear stress. They find that the performance degradation of an aircraft wing under rainfall conditions could be significant. The roughness associated with drop impact produce a 37% loss in maximum lift at 100 mm/h rainfall. Accordingly, film waviness causes losses in maximum lift from 11% to 30%, depending on the rainfall rates. However, their results lack experimental validation. Qualitatively, rain on an airfoil can produce the same aerodynamic deterioration as the fixed-element roughness does.

Koch and Smith (1976) determine the value of equivalent sand-grain roughness k_s. They propose that the equivalent sand grain k_s can be related to the arithmetic centreline average roughness k_{CLA} with the relation:

$$k_s = 6.2 \cdot k_{CLA}$$

Equation 4-29: Equivalent Sand Grain Roughness Equation

Their conclusion based on the usage of measurements of k_s values for several standard sandpapers made by Spiedel (1954) cited in Koch and Smith (1976). The above equation is in reasonable agreement with the experimental results of Young (1950) cited in Koch and Smith (1976).

It is concluded that a key feature of the liquid water film, which is formed on the compressor blade, is that it causes a roughness effect. This is a result of its wavy characteristics. The consequence is the performance deterioration of the blade. Furthermore, the liquid film roughness effect is related to the equivalent sand-grain roughness. The latter is a basic tool, which is widely used on the field of investigating the effects of roughness.

4.5.2 Tip clearance effects

Tip clearance is an important parameter in the compressor's operation and performance. When the clearance is large, the loss of mass flow causes efficiency deterioration and the operating point moves towards the surge line. The lower value of tip clearance is limited by the mechanical requirement of avoiding rubbing between blade and compressor casing. The clearance introduced in the compressor's design undergoes substantial changes under different conditions of operation. Furthermore, as the engine becomes aged, it becomes larger and increases the secondary losses. At the design process, a nominal clearance of 2.0% - 3.5% of blade height can be met.

Under water ingestion condition, the water is centrifuged and moves towards the casing. The film of water at the casing wall moves by the shearing action of the airflow. As long as the clearance is not filled, the film will continue to grow as water is added to it. When the clearance becomes filled then additional water will be splashed back into the blade span.

Bose and Murthy (1994) investigate the influence of water ingestion on the blade clearance. They build a code (WINCLR), which provides a scheme for obtaining the performance and the blade clearance for an axial-flow compressor working under given operating and water ingestion conditions. The authors conclude that the blade clearance is affected by the presence of water and the change in compressor's performance is substantial. They argue that the extent of changes in performance and clearance increases with an increase in the mass fraction of water entering the compressor. Numerically, they report that the blade clearance at the 1st rotor blade reduces from 0.123 mm to 0.1 mm when water is ingested.

4.5.3 Effects on Compressor Performance

The compressor (or the fan in case of turbofan engine - their behaviour towards this condition is the same) is the first component of the engine, which is directly exposed to water ingestion. Hence, the effects are more pronounced and several researchers have investigated them.

Extensive theoretical and experimental work has been done in Purdue University. The subject of water ingestion effects on a gas turbine engine has

been investigated thoroughly for several years. Murthy (1996b) and Murthy (1996a) presents a detail review of the research done in Purdue University and has dealt with the areas of water ingestion from puddles on runways, the instrumentation setting for pressure and temperature measurement in an air-water mixture, tests on axial flow compressors and combustors and time-dependent performance of turbofan engines.

A small axial flow compressor with 2.5 pressure ratio is used for the experimental part of the work. Murthy and Ehresman (1984) and Murthy et al. (1986) give a description of the test rig. Water mass fraction ranges from 1 to 10%, the mean volumetric droplet size at entry to the compressor from 20 to 600 μm, and the rotational speed ranges from 60 to 100% design speed. They observe that when the water is drained out the engine accelerated satisfactorily in the transient mode. On the other hand, when the water enters the burner, the effect on engine's performance is more significant.

The requirements for the water ingestion tests are established in Murthy and Ehresman (1989). Transient engine performance with water ingestion is discussed in Haykin and Murthy (1988), Murthy et al. (1986), Haykin and Murthy (1987a). In Murthy and Mullican (1993b) and Murthy and Mullican (1990) the transient performance of a fan-compressor unit with water ingestion is analysed. For this case, a code has been developed (WINCOF-I), which calculates the performance parameters for a given water ingestion condition on a time-dependent basis. The authors justify that by arguing that the phenomenon of water-process in the compressor is not progressively uniform in the various stages.

In Murthy and Mullican (1993b) and Murthy and Mullican (1993a), the authors discuss the transient performance of a generic fan engine with water ingestion. They focus on the case, in which the mass fraction of water is instantly changed form 2.0% to 8.0%, under design operating conditions. They also present a model for the motion of water droplets on the compressor blade. The code takes into account only the centrifugal force ignoring the shearing action of the airflow.

The main conclusions of the above research can be summarized:

- The aerodynamic changes and the water displacement from the blades affect greatly the compressor's performance.
- Heat and mass transfer become significant when residence time and overall pressure ratio are large.
- The liquid water over blade surfaces and in blade passages causes modifications in deviation and momentum loss.

- Small quantities of water (1%) are sufficient to cause performance deterioration and these changes do not vary linearly depending upon the amount of water.

- The liquid water mass fraction has a great influence on the effects of water ingestion. Particularly, the form of water and its size (diameter and its distribution for droplets, and thickness for films) are very important and the effects may vary for the same water quantity.

- Simple scaling laws cannot be established for the various effects of water ingestion.

- An engine suffering water ingestion probably does not attain a steady state, even if the ingestion is steady and persists for long time (>60 sec).

- The liquid film can affect sensors at the engine casing giving erroneous data to the engine control system.

- The thrust and the specific fuel consumption show an increasing deterioration with an increase in the mass fraction of water.

- When the ingested water mass fraction increases, the low-pressure turbine becomes incapable of driving the fan under certain conditions of operation.

It is noteworthy that the authors state that the performance deterioration depends on the physical size of the engine. The water distribution and its behaviour are different between a small and a large engine. The differences do not scale with geometry in a simple way because of the heat and mass transfer of the droplets.

In the above research, the aero-thermodynamic effects of water ingestion on a time-dependent basis are thoroughly investigated. A limited number of researchers have assessed the transient operation of gas turbine engine under rain conditions. However, in the author's view the mechanical effects are underestimated. Although the water droplets centrifugation and the film formation on the compressor's casing are calculated, their effect on the rotational speed is not taken into account. In the author's view, the rundown of the engine is of primary importance because it is the first warning indication of water ingestion.

AGARD (1995) describes that under rain conditions the compressor operates closer to the surge line. Heat and mass transfer between gaseous and liquid phases takes place in the compressor but with a low rate, since residence time is small (fractions of sec). Water evaporates mainly in the combustor because the temperature is quite high. The increased volume of water vapour occupies

the burner and displaces air, acting as a throttle to the compressor, which means that even smaller quantity of air enters into the combustor with constant fuel mass flow rate. Thus, in the final stages of the compressor, the air axial velocity increases and bearing in mind the rotor speed, the angle of attack decreases (i.e. the known velocity triangle is modified). A reduced angle of attack results in a drop in compressor's efficiency and consequently, the mass flow deteriorates moving the operating point closer to surge. It should be highlighted that the above condition describes the aero-thermodynamic processes, which take place in the compressor-combustor components. It is thought that the mechanical effects are far more dominant because the water centrifugation precedes any other aero-thermodynamic process. Thus, the engine's rundown should be taken into consideration in any case.

Santa (2000) clearly demonstrates in figure 4-25 the movement of running line towards the surge line as the water fraction increases. The author attempts to examine the water ingestion phenomenon and deals with its mathematical modelling. He focuses on the thermodynamic effects and assumes that evaporation occurs in the combustion chamber. Santa (2000) argues that the operating point of the compressor moves towards the surge line, i.e. there is a reduction in surge margin. This is attributed to the fact that, due to evaporation, the increase of the air-water volume causes a reduction in air mass flow, in the same way explained in the previous paragraph. However, it is believed that aerodynamic and mechanical effects should be always taken into consideration. Evaporation is the principal factor in cases of water injection or fog boosting to improve the cycle efficiency of industrial engines. On the other hand, rain ingestion involves large water droplets and the effect of evaporation is less important compared with the aerodynamic and mechanical effects.

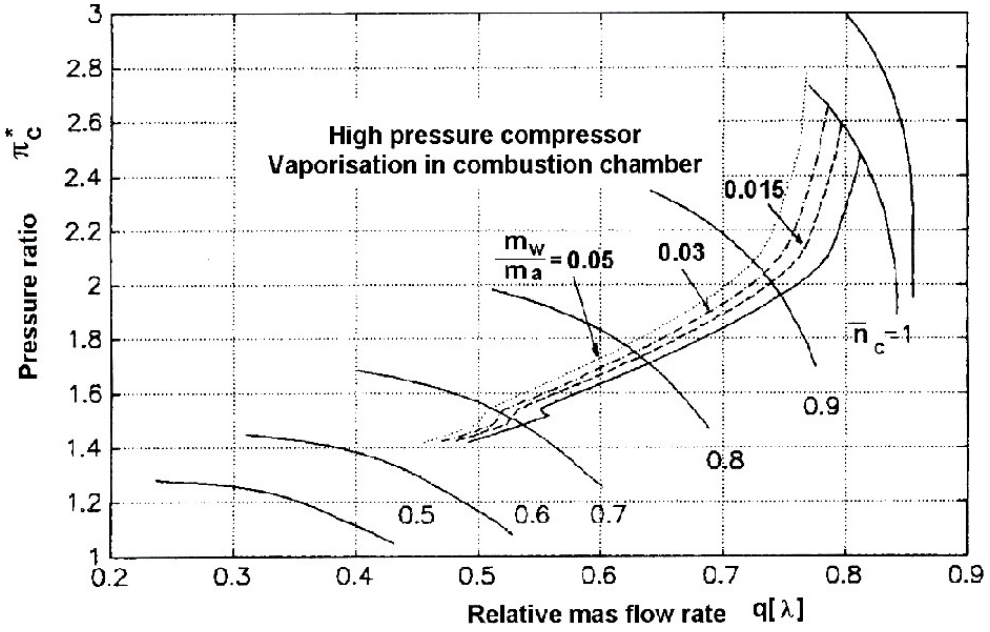

Figure 4-25: HPC Running Line Movement due to Water Ingestion [Santa (2000)]

The aerodynamic effects are investigated theoretically by Park and Chang (2000). The authors, using a numerical method, solve the Lagrangian particle-tracking equations and trace the liquid water droplet in the gas phase. The also use a breakup-impact droplet model to simulate the process of droplet deposition. The authors confirm that the aerodynamic properties of the blade are changed considerably. For the same inlet air velocity or mass flow rate in both dry and wet flow, the static pressure and Mach number distributions on the blade surface are significantly altered. They also argue that the shock wavy moves towards the trailing edge making the blade to operate in off-design conditions. This causes a change to the structural load and the vibration characteristics and consequently the possibility of material failure is bigger.

Hale et al. (2005) conduct a parametric study to determine the effects caused on a gas turbine engine compressor by steam ingestion. The authors focus on the evaporation effects and particularly on the gas properties changes. However, they acknowledge that other effects, which are important as well, accompany the phenomenon. These are the temperature distortion at the compressor due to heat transfer and the aerodynamic effects due to the phase change from liquid water to vapour. The authors confirm that the increase of gas constant R in moist air causes an increase in non-dimensional mass flow and decrease in non-dimensional speed. Hence, they refer that the engine moves toward choke.

Extensive work on the rain ingestion effects is carried out by Williams J. et al. (2005). They investigate the subject both computationally and experimentally. Tests are conducted in a standalone 4-stage compressor plus one row of IGV blades. It is assumed that the water does not evaporate and thus, the non-

dimensional parameters are calculated based on dry air properties. The authors justify this, arguing that at a small compressor in part-speed, there is no time for water to evaporate and it is concentrated in liquid form occupying a negligible fraction the annulus. It seems that this is quite sensible and it is confirmed by their experimental observations. Hence, the effect on the thermodynamic properties of the air is negligible.

The authors remark that small amounts of water appear to have little or no effect on the pressure ratio. On the contrary, larger amounts have a very pronounced effect. Additionally, the mass flow coefficient at stall condition is changed substantially and this declares a loss of surge margin under wet conditions. However, in other tests configurations (droplet mass, size) the onset of stall condition contrasts with the above observation, and consequently, the authors cannot justify the eminent reduction in surge margin due to ingested water.

Williams et al (2005) report that the water rivulets, which are formed on the blade's surface, do not cause the change in blade's performance. They come to this conclusion noting that when the water supply to the compressor is suddenly switched off, the compressor's performance returns to the dry level in less than a second although there are water tracks on the suction side of the stator blades for half a minute or more. They attribute the blade's performance deterioration to the reduction in air axial velocity, which is detected particularly near stall conditions. This change results from the energy exchange between the low-speed water droplet and the high-speed air. Hence, air flows with a lower speed and the aerodynamic efficiency is reduced.

However, in the author's view this is not fully valid for a rotor blade, where the relative speed between air and water is quite bigger than the case on a stator blade. The liquid film, due to the centrifugation, covers the biggest part of the pressure surface forming water rivulets. It is certain that the drag coefficient increases causing a thickening of the boundary layer, resulting in a change of the blade aerodynamic performance.

Williams et al (2005) state that water droplet size has no remarkable effect on compressor's performance. Furthermore, they confirm that water has a pronounced effect on compressor's drive torque. A considerable increase is observed even for small water quantities and the increase is directly proportional to the amount of water ingested. They also present a theoretical method to estimate the demanded torque by the compressor to keep its rotational speed. This is feasible assuming that all the water deposits and it is accelerated up to blade speed by the rotor blade. It gives quite reliable results, considering that the water cannot accelerate tangential and no slip factor between surface and water film has been included. The author adopts this model, for the torque demand calculations.

Walsh and Fletcher (1998) propose a very convenient formula for first order calculations of power per stage (P_w) demand due to water, when the mean blade rotational speed (U) assumed to be constant:

$$P_w = 0.5 \cdot W_w \cdot U^2$$

Equation 4-30: Power Demand due to Water [Walsh and Fletcher (1998)]

In Nikolaidis Th. et al. (2008) the effect of ingested water on the drive torque is investigated. Their analysis extends that of Williams et al (2005) calculating the water droplets torque as they exit from the blade tip or the trailing edge. Hence, the radius is not constant (i.e. mid-span) because the water droplet may exit from the rotor blade near the hub, mid-span or (mainly) at the tip. The results confirm the dramatic increase in torque and for 4%-5% water to air can be 40% assuming that the water droplets are accelerated to the blade rotational speed. However, it is noteworthy that the results are geometric dependent and they should be treated as trends for the described condition.

In conclusion, the work from Williams et al (2005) provides an extended insight of the processes, which take place in a compressor under water ingestion conditions. It covers almost all the aerodynamic and mechanical effects and its experimental data are analysed in detail. Only few published work deals with the extra torque demand and this means that this field has not been fully explored yet.

4.6 Combustor

It has been reported that most of the water entering the core engine will pass to the burner. A part of liquid water evaporates at the last stages of the compressor. The diffuser causes a decrease in both air and water velocity. In the combustor, the high temperature environment increases dramatically the evaporation rate, which absorbs a substantial amount of the released heat. Consequently, evaporation causes a decrease in flame temperature and drops the combustion efficiency. Moreover, the increase of the working fluid volume acts as a throttle to the compressor and this decreases the air mass flow. Hence, assuming a constant fuel rate, there is enrichment in fuel-air mixture, which causes combustion extinction (flameout).

4.6.1 Effects on Combustor Performance

Thorough research has been conducted in Purdue University about the combustor's performance under water ingestion conditions [Laing et al. (1993), Laing et al. (1993), Laing and Murthy (1992), Murthy and Laing (1993), Shastri et al. (1995), and Shastri et al. (1994)]. Their work includes both theoretical and

experimental models and their objective is twofold. Firstly, they aim to establish the redistribution of water in the combustor, and secondly, they intend to investigate the performance deterioration in the combustor, including the flameout occurrences.

Laing, Shastri et al (1993) in their analysis define two principal combustor performance parameters: the Pressure Loss Factor (F_{PL}) and the Temperature Increase Factor (F_{TI}). The Pressure Loss Factor (F_{PL}) is calculated by the following equation for constant values of P_o and T_o for the supplied air:

$$F_{PL} = \frac{\left(\frac{\Delta P_o}{P_o}\right)_m - \left(\frac{\Delta P_o}{P_o}\right)_a}{\left(\frac{\Delta P_o}{P_o}\right)_a} \quad \text{where} \quad \frac{\Delta P_o}{P_o} = \frac{P_{oref} - P_{o4}}{P_{oref}}$$

$$P_{oref} = \text{reference } P_o \text{ upstream of the prediffuser,}$$

$$P_{o4} = P_o \text{ at combustor exit}$$

Equation 4-31: Pressure Loss Factor Definition [Laing et al. (1993)]

It takes values between 0.0 and 1.0 indicating how far the mixture total pressure drop is from the dry condition corresponding value. If F_{PL}=0.0, there is no pressure loss due to water ingestion conditions. It is worth noting that pressure loss across the combustor is affected by the temperature rise and the loss due to the liquid water film, which is formed in the burner. It should be added that the overall temperature rise depends on the amount of energy spent for the liquid water evaporation and is subtracted from the fuel heat release.

Having said this, the relative Temperature Increase Factor (F_{TI}) across the pre-diffuser – combustor unit, can be defined as follows:

$$F_{TI} = \frac{\left(\frac{\Delta T_o}{T_o}\right)_a - \left(\frac{\Delta T_o}{T_o}\right)_m}{\left(\frac{\Delta T_o}{T_o}\right)_a} \quad \text{where} \quad \frac{\Delta T_o}{T_o} = \frac{T_{o4} - T_{oref}}{T_{oref}}$$

$$T_{oref} = \text{reference } T_o \text{ upstream of the prediffuser,}$$

$$T_{o4} = T_o \text{ at combustor exit}$$

Equation 4-32: Temperature Increase Factor Definition Laing et al. (1993)

It takes values between 0.0 and 1.0 indicating the difference in temperature increase between dry and under water ingestion condition. If F_{TI}=0.0, the temperature increase at exit of the combustor is that of dry operation (i.e. the water does not affect the temperature rise).

Experiments in Laing et al. (1993) include both cold and burning flow tests. They take place with water in the form of a liquid film, a spray or a combination of both. The water content of the liquid film is held at the constant value of 2% while the spray value varies from 0% to 8%. Tests conditions involve spray water droplets size of 0.75 mm and 0.025 mm, and water temperature of 7 °C and 20 °C. Finally, although several values for the fuel equivalence ratio (φ: fuel to air ratio divided by the corresponding stoichiometric value) are used in order to establish the performance changes, the results presented in the next paragraph are obtained for φ=0.3.

The authors conclude that the ingested water has a detrimental effect on pre-diffuser – combustor performance. It is evaluated that it causes an increase in total pressure loss across the cascade and simultaneously a drop in combustor's exit temperature. The relevant data are exported and used by the author to produce the following charts, which are shown in figures 4-26 and 4-27.

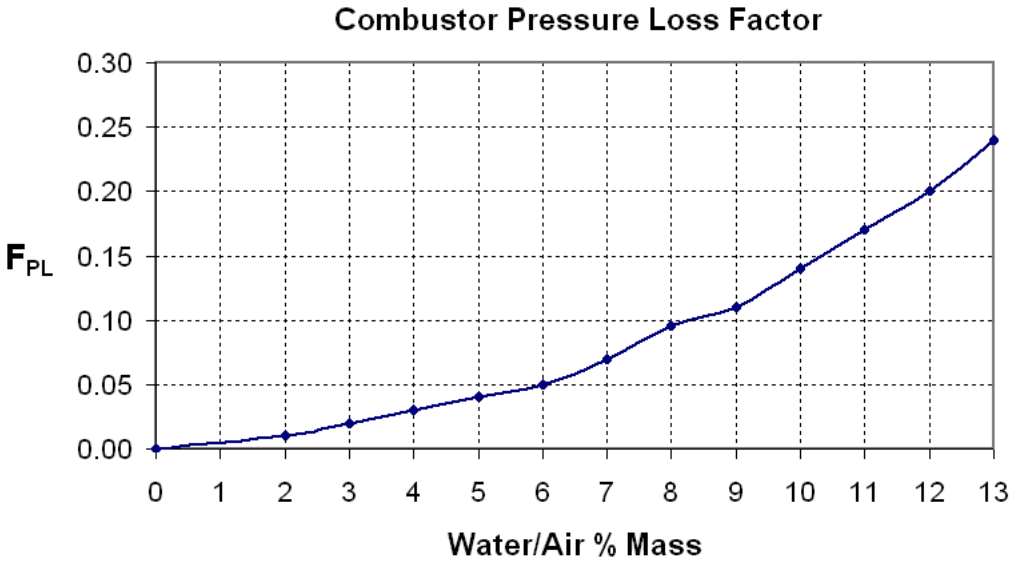

Figure 4-26: Combustor Pressure Loss Factor change [reproduction from Laing et al. (1993)]

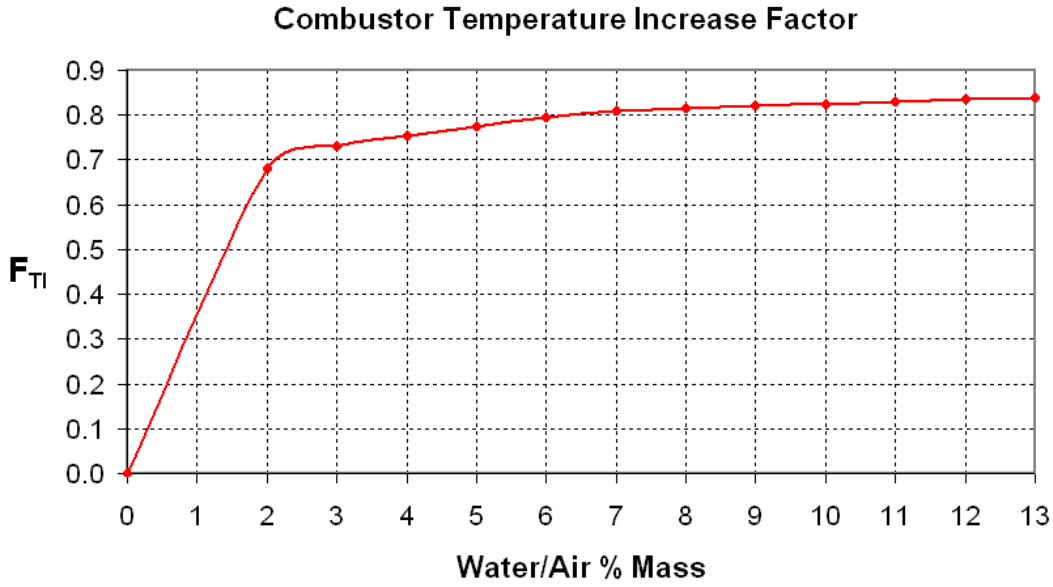

Figure 4-27: Combustor Temperature Increase Factor [reproduction from Laing et al. (1993)]

The authors comment on the combustor's performance deterioration that it is not only a result of water's partial evaporation. Bearing in mind the combustion process, there are effects on fuel – air mixing and the formation of recirculation zones upstream of the primary jets. There are also chemical and mechanical interactions between the flame and the water, which destabilizes the former. Lastly, there are direct effects on reaction kinetics. Consequently, the evaporation of liquid water is not the root for the burner's temperature rise deterioration, which is measured during water ingestion experiments. Figure 4-28 demonstrates the liquid water flow in the combustor.

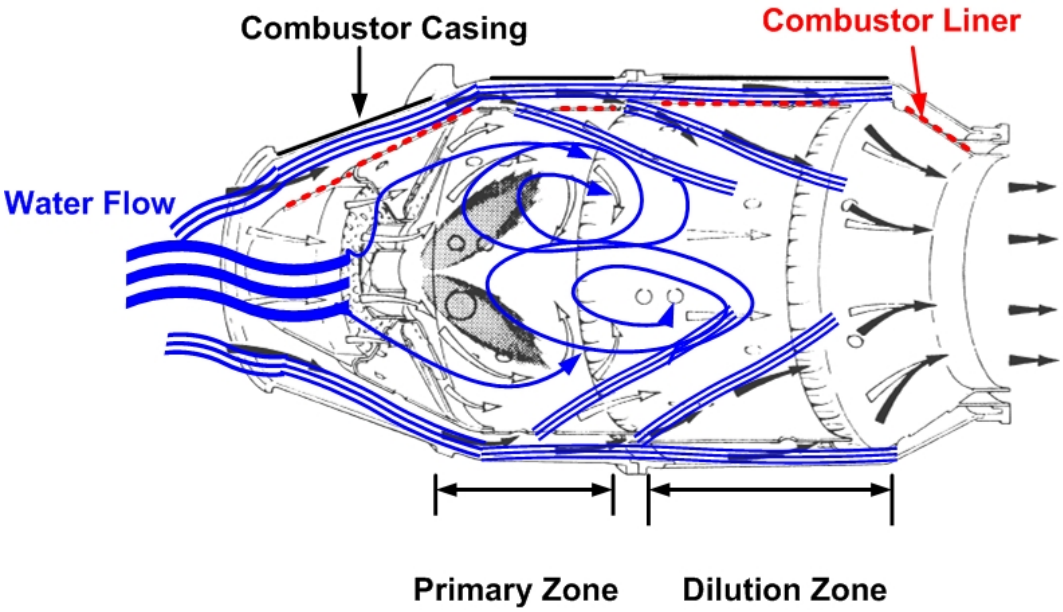

Figure 4-28: Water Flow in the Combustor [initial photo courtesy of Rolls-Royce]

It is worth noting that the drop in total pressure follows the water mass fraction. In combustor exit temperature case, there is a high rate of change for up to 2% water mass fraction and after that value temperature drop is quite smaller. That may be justified by the fact that the amount of water entering the combustor's primary zone may not increase in direct proportion to the amount of water ingested initially into the air stream Laing et al. (1993).

The usefulness of F_{TI} lies to the fact that it can be used to correlate the drop (due to water) in temperature increase ΔT at combustor's exit with its efficiency (ETA) deterioration. Bearing in mind the simplified definition of ETA, which is the ratio of actual to theoretical ΔT for a given fuel/air ratio (f), it can be assumed that deterioration in burner's ETA follows the rate of change of its temperature increase (ΔT) relatively to the dry values, on a percentage basis. However, it seems that this assumption overestimates the combustor's ETA deterioration, giving values in the order of 80%. Hence, the reduction in combustor's exit temperature is not directly connected with the drop in its efficiency.

The authors observe from the tests that the fraction of water entering the combustion zone through the dome and the primary jets depends on the flow split, the airflow rate and the droplet size. They quantify it reporting that this value is nearly 80%-90% of the liquid water.

They also concur that the water mass content influences the temperature in the combustion zone and at the combustor exit. The combustor cannot achieve the expected temperature rise. They note that the reduction in temperature rise becomes larger when the mass fraction of water increases from 0.5% to about

2.0%, but then remains nearly constant even when the initial mass fraction of water increases to 10%-12%.

In AGARD (1995) the water ingestion effects on a gas turbine combustor is examined. Data from Pratt and Whitney internal research is presented. It is confirmed that nearly all the water entered into the core engine will pass into the combustor almost in liquid phase. Burner's flame extinction is expected when large amounts of water are ingested. Data from a combustor rig testing are demonstrated in figure 4-29, in which a semi-logarithmic plot of combustion efficiency is presented. It is observed that the combustion efficiency is decreased with increasing water concentration. Furthermore, flameout occurs when the efficiency is reduced about 40%, which is consistent with the typical dry combustor operating limits.

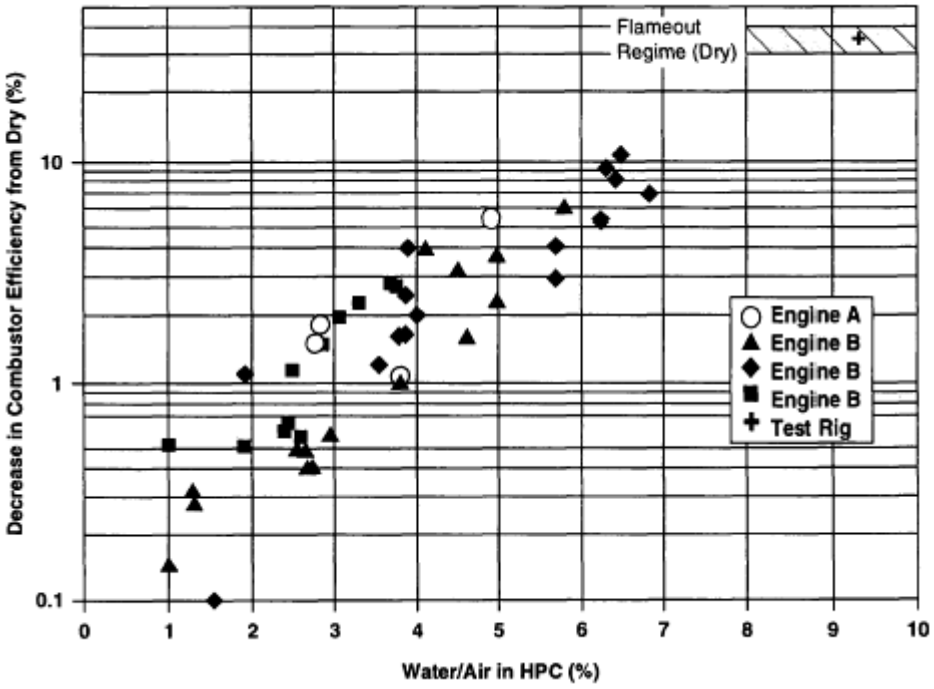

Figure 4-29: Combustor Efficiency Deterioration due to Ingested Water [AGARD (1995)]

It is noteworthy that the author manipulates the data from the above plot to model the combustion efficiency deterioration under water ingestion conditions. Detail description is given in chapter 7.2.3 (figure 7-4). Moreover, the research of the effects of water on the combustion process involves a thorough study of the chemical kinetics, and a deep knowledge of how it influences the flame stabilization. From the literature search, it is found that the topic has not been fully covered yet. Its investigation is beyond the scope of this project and it is recommended for further work.

4.7 Turbine

Turbines (and downstream the nozzles) are the last components of a gas turbine engine, facing the impact of the ingested water. The water is mostly in vapour form because it partially evaporates in the combustor. This results in an increased gas mixture C_p, which has a beneficial effect on turbine's work output. However, there are rivulets of liquid water flowing from the burner's casing. Moreover, temperature and pressure decrease and they enhance the phenomenon of water condensation.

Although it is reported in AGARD (1995) that the effects of the ingested water on turbine's performance are negligible, the author states that turbine performance indeed deteriorates due to the presence of liquid rivulets. Many researchers arrive at the same conclusion about the long-term effects of water presence in the turbine. Erosive wear of turbine's blade surface is expected. Pinpointing published work is given in Khoshaim (1979), Hill et al. (2000), Krzyzanowski et al. (1994), Krzyzanowski (1983), and Krzyzanowski (1974).

4.8 Engine Control

Water ingestion influences the operation of engine's control system. Temperature and airflow rate sensors are affected and they may give false measurements to the computerized control system. A characteristic incident is presented in Russell and Victor (1984), in which the authors describe the compressor stall investigation of CF6-50 General Electric gas turbine engine during operation under water ingestion conditions. They report that a temperature sensor read lower temperature because of the difference between the temperatures of liquid water and air. As a result, the main fuel control component repositioned the Inlet Guide Vanes (IGV) driving the compressor to stall because its operation did not match the airflow conditions.

It is reported in AGARD (1995) that the water may block the pressure sensors and lines making them inoperative. It is recommended that engine rapid transient operation should be avoided due to the destabilizing effect of water. When throttle is position towards max speed, the engine tends to accelerate while the surge margin is reduced (the operating point moves towards stall line). Likewise, when throttle is position towards idle speed, there is a reduction in fuel flow, pressure and temperature. Bearing in mind the destabilizing effects of water, the condition may lead to burner's flameout.

In any case, the effects of water ingestion on engine's control system are significant. Surprisingly, published work is not so extensive. However, internal researches of engine manufacturers are cited in AGARD (1995), which declares

their concern about the subject. Unfortunately, these manuscripts are not available in their full extent. Further investigation is out of the scope of this work.

4.9 Engine Protection against Water Ingestion

It is reported in section 4.1 that engine's manufacturers have taken immediate measures after the repeated incidents of engines in-flight shutdown. They improved inlet's design (figure 4-2) and they revised the schedule for variable bleed valve (VBV) operation. Volk (1992) argues that these improvements increased the CFM56-3 engine water-ingestion capability by 61% and hail ingestion capability by 96%. His results are based on engine ground and flight tests in simulated rain ingestion conditions and combustor rig tests.

Certification tests, which are presented in section 4.1, became stricter than it used to be before the reported incidents. According to amendment 23-18 FAA (2001), the engine should be able to operate without a sustained loss of power for at least three minutes, when it operates at flight idle in rain conditions. The rate of rain ingestion should not be less than 4%, by mass, of the inlet airflow rate. With this amendment, FAA ensures that the engine's installation does not affect the water ingestion tolerance determined by engine certification.

The number of patents, which were issued in the last decade suggesting ways to tackle the water ingestion on gas turbine engines, is indicative of the great concern of the gas turbine community. Bardey et al. (1994) propose the use of a V-shaped guide vane installed in the diffuser, which directs the water in the secondary airflow (i.e. between the combustor outer casing and its liner). Consequently, the vanes prevent the water from entering the core combustion chamber (primary and dilution zone), where the combustion takes place. Figure 4-30 shows the concept of the patent.

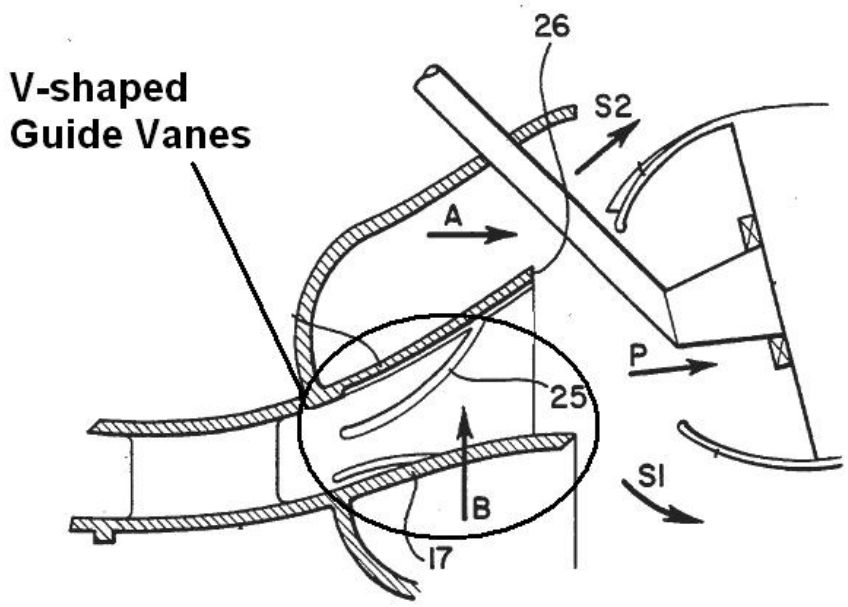

Figure 4-30: V-shaped Guide Vanes at Diffuser [Bardey et al. (1994)]

Rowe (1995) suggests an advance liquid water detection system for gas turbine protection against heavy rain. A number of sensors are installed in the ducted fan of the gas turbine engine. The sensors detect the presence of liquid water and they transmit the data to the main fuel control, which increases the fuel flow to the combustor. Hence, the rotational speed of HPC increases and the engine is more capable of evaporating the liquid water. However, the author thinks that the application of this patent needs additional safety features. This is because engine's auto-acceleration and the subsequent unexpected increase of thrust raise safety issues. The condition may be dangerous especially during landing, where the controlled aircraft speed is of primary importance.

Meher-Homji and Mee (2007) propose a system installed in the air inlet duct. The patent, through a system of ducts and drains, removes the liquid water, which is concentrated on the inlet casing in film, from the inlet duct. It is suggested for ground-based gas turbine engines.

4.10 Concluding Remarks

In conclusion, the literature review reveals that the water ingestion has pronounced effects on engine's operation. Both, the engine's manufacturers and the aviation authorities, have done a considerable effort to address the rain ingestion effects. Engine design and certification tests have changed to enhance aviation safety.

The various forms of environmental water and the probability theory of an airplane to encounter a heavy rain conditions justify the criterion of 4% water-air

chosen for the water-ingestion certification tests. However, further research has to be done in order to include the scoop factor effect in the analysis.

Water droplet accelerates at high-speed air when rain is ingested by a gas turbine engine. Under these conditions, droplets deposit on the compressor blades and the water film, which is formed, develops in rivulets and changes the aerodynamic of the surface. Several researchers have taken into account the roughness effect of water film on the drag coefficient calculation of an airplane, which flights through heavy rain. However, this model has not been applied yet in case of a compressor rotor blade.

The water film thickness has also a great influence in compressor's torque. Few researchers have experimentally measured the torque increase. Its theoretically calculation is based on mean water content, on the blade mean radius and the mean air velocity. However, a more analytical estimation is necessary.

Compressor's and combustor's performance is also affected by the presence of water. Several authors have examined these effects both theoretically and experimentally. Compressor's operation becomes unstable as water is ingested into the engine, followed by a reduction in mass flow and in pressure ratio. Thus, compressor's operating-point moves to the surge line. Furthermore, water has a detrimental effect on combustor's performance. The increase in pressure loss and the reduction in its efficiency are confirmed by several researchers.

The effects of water ingestion on gas turbine engines are aerodynamic (shear force increase, change of velocity triangle in the compressor), thermodynamic (heat and mass transfer, temperature distortion, change of gas properties in the working medium) and mechanical (demanded torque increase, blade vibration, change of structural load). These effects occur simultaneously and affect each other.

5 Project Methodology

This chapter describes the methodology that is used in the context of this research. Bearing in mind the project's objectives and the literature review, a description of the used methods are presented.

The knowledge of the airflow, which exists in a gas turbine compressor, is very important for understanding the water droplet behaviour in it. This is necessary for achieving the milestone of identifying the parameters that affect engine's performance under water ingestion conditions and evaluating their impact. The application of Computational Fluid Dynamics (CFD) is the basic methodology to examine the details of the flow in an axial compressor and how it is affected by the presence of water. A commercial code, called CFX-Tascflow, is used to solve the flow field in a compressor stage. The solver tracks the particle trajectories giving details about their behaviour in the flow field.

CFX-BladeGen program is used to produce the blade's computational domain. The compressor's blading is available in MS Excel spreadsheet including the x, y and z coordinates of the blades in the hub, shroud and three other cuts. As a result, blade's design is optimized and new layers are created to generate the computational grid in detail.

The produced geometries are exported to CFX-Turbogrid for the creation of the computational mesh of the IGV, 1st rotor and 1st stator blades. The computational domain is imported to CFX-Tascflow and several cases are solved. All the parameters, which affect water ingestion, are taking into account, including cases at part speed. Thus, apart from water mass, the effects of droplet's size and its initial speed are investigated. To make the results more obvious and easily understood high values of ingested water mass are chosen for some cases. Thus, although 17% and 30% water/air mass are not met in the gas turbine operating conditions, under those circumstances they really help.

The calculations of water film thickness, which is formed on the rotor blade, its motion (direction and speed) and the extra torque demand, are provided by a code created by the author. The code, called FILM_MOTION, is built in FORTRAN programming language. Data is provided by the CFD calculations and include the deposited water mass, the air shear stress and the water droplets momentum. Having known the film thickness at each node of the grid, the new Cartesian coordinates x, y, z of the blade's pressure surface are calculated and imported again in CFX-Tascflow changing the blade's grid. Therefore, the grid is changed and saved again for the same case. In addition to this, the roughness model of CFX-Tascflow is implemented to account for the drag coefficient increase due to the water film wavy characteristics. The cases run again simulating the performance deterioration under water ingestion

conditions. Hence, pressure ratio, efficiency and mass flow deterioration of the compressor model is calculated by extracted the relevant results. It is highlighted that the method involves analytical data (i.e. the water droplet mass, speed, size and its position) while the relevant researches found in literature involve mean flow values (i.e. the estimated parameters are calculated by assuming that all the water exits from the blade surface at mid-span).

The objective of upgrading Turbomatch code to account for the effects of water ingestion is achieved by using FORTRAN programming language. Several subroutines are developed and described in detail in chapter 7. Firstly, the extra compressor work for given water to air ratio and rotational speed ($N/\sqrt{T}$) is calculated. Secondly, the percentage deterioration in the performance parameters for this $N/\sqrt{T}$ is taken into account and the new values for pressure ratio, mass flow and efficiency are calculated. Furthermore, combustor's pressure loss increase and efficiency reduction is evaluated. Thirdly, the overall performance of the model is computed using the new data.

It is noteworthy that the application of CFD methodology limits the full investigation of the phenomenon because it is strongly dependent on the model geometry. Water deposition, film formation and its motion on the rotor blade surface differs between blades of different profiles or stagger angles. Furthermore, the water ingestion effects cannot be scaled because the parameters vary with engine size (i.e. water distribution under identical ingestion conditions is different for a large engine and a small one). For the time being, there is no simulation tool to extent its capability beyond these limits. However, in this case, the main objective is to evaluate the trends in performance deterioration due to ingested water.

6 CFD of an Axial Flow Compressor

Computational Fluid Dynamics (CFD) is widely used to examine the details of a fluid flow. Over the last few years, the huge increase of the computational resources has contributed to this. CFD is the basic methodology to examine the details of the flow in an axial compressor and how it is affected by the presence of water. The governing internal equations for conservation of mass, momentum and energy are discretized into algebraic equations and can be solved iteratively by several CFD software packages. The flow field within the domain is solved by CFX-Tascflow, which is a commercial CFD code commonly used in turbomachinery.

Afterwards, a numerical approach is used to evaluate the liquid water film thickness and its motion on an axial flow compressor rotor blade under water ingestion conditions. The change in blade's profile and surface is imported in CFD, which calculates the change in the performance parameters of the compressor stage.

This chapter discusses in detail the CFD and the numerical approach used to evaluate the compressor's performance deterioration due to water ingestion. The CFD mesh and its parameters are presented briefly at the beginning. Water film computation follows giving details of the theoretical model, which is used for the numerical approach. Finally, the chapter focuses on the results produced by the simulation.

6.1 Compressor Model – Mesh Generation

CFX-Tascflow is used in order to solve the flow field in a compressor stage. The solver tracks the particle trajectories giving details about their behaviour in the flow field. What is more, the mass of water droplets and their position as they impact on the rotor blade are included in the flow field solution.

The compressor in study was inspired on the compressor fitted in the J79-GE-17 General Electric turbojet aero-engine. The studied engine is a single-shaft turbojet aircraft engine. Its compressor is an example of a constant tip diameter annulus. Its basic performance characteristics are shown in table 6-1.

PARAMETER		VALUE
Pressure Ratio	PR	13.5
Mass Flow	W	76 kgr/sec
Inlet Pressure	P_1	101325 Pa
Inlet Temperature	T_1	288 ° K
Number of stages	n	17
Rotational speed	N	7700 rpm
IGV blade diameter	D_{tip}	0.812 m

Table 6-1: J79-GE-17 Compressor Design Parameters

The compressor blading data were available from Noel (2003) in MS Excel spreadsheet format (Appendix A). To produce the blade's computational domain, CFX-BladeGen program was used AEA (2001a). As a result, blade design was optimized and new layers were created to generate the computational grid in detail. Moreover, the leading and trailing edge of the blades were specified as an ellipse ratio, smoothing any discrepancies in the blade's shape. The work, which has produced the blades used as models, is presented in detail in Appendix A. The produced geometries were exported to CFX-Turbogrid for the creation of the computational mesh of the IGV, 1st rotor and 1st stator blades AEA (2001b) and (2002).

The geometry of each component was exported to CFX-Tascflow where the global domain for the IGV and the 1st compressor stage was set up. The computational domain consists of an IGV blade, a rotor and a stator blade. A total number of 326,000 mesh points (nodes) are finally involved in generating the global computational grid. Dense clustering around the blades and especially in the rotor is used for better resolution of boundary layers.

It is worth noting that due to occupational matters, the project continued by the author based overseas as a part-time student. At the beginning, being off-campus caused log on problems with Cranfield High Performance Computer (HPC), in which CFD software is installed. Apart from this, CFD code works on UNIX systems, which means that the use of Windows Emulators Software is necessary to connect MS Windows with UNIX. There were also problems in viewing CFX Graphical User Interface (GUI), which means that the display of the results was impossible. The above difficulties were overcome by using specific software called PuTTY and Cygwin. The whole procedure was set up in co-operation with Cranfield HPC Team and is presented in Appendix B.

6.1.1 Grid Checks

In order to prove that the obtained solution is grid independent, it is necessary to perform computations at several computational grids differing in the number of nodes. Thus, it is possible to determine the number of nodes, starting with the solution, which does not change with further increase of this number. Bearing that in mind, four computational grids with different number of nodes are tested (150,000 nodes, 326,000 nodes, 415,000 nodes and 623,000 nodes) and the results prove that the grid with 326,000 nodes is sufficient for the computations.

Figure 6-1 shows the 3D computational domain and figure 6-2 a general view of the axial flow compressor model.

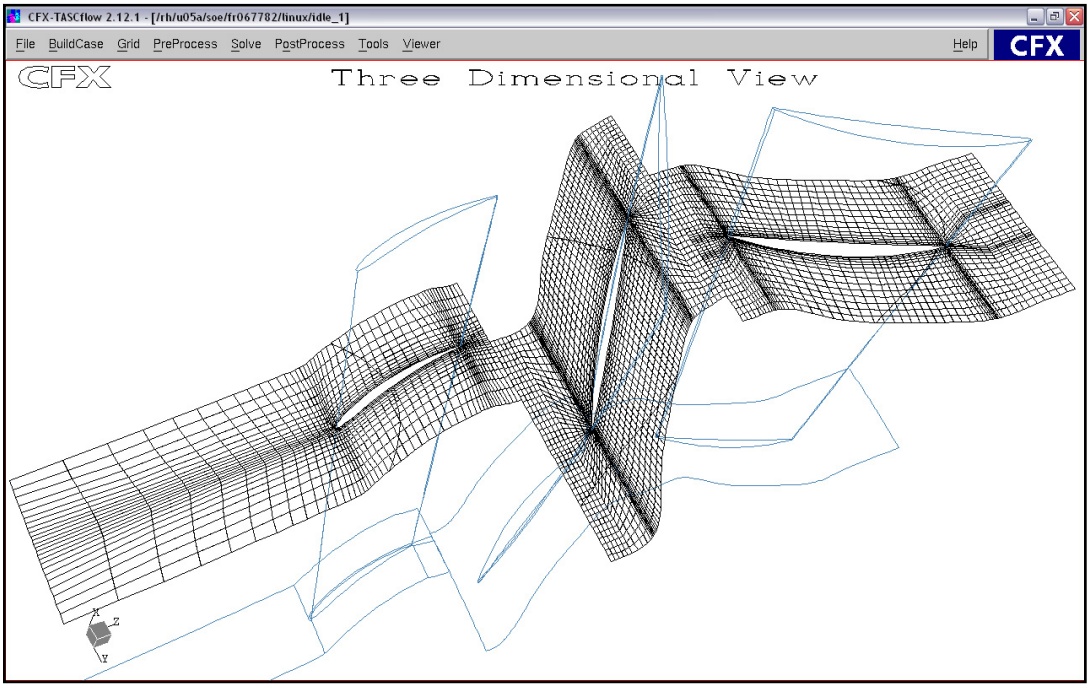

Figure 6-1: 3D View of Compressor IGV & 1st Stage

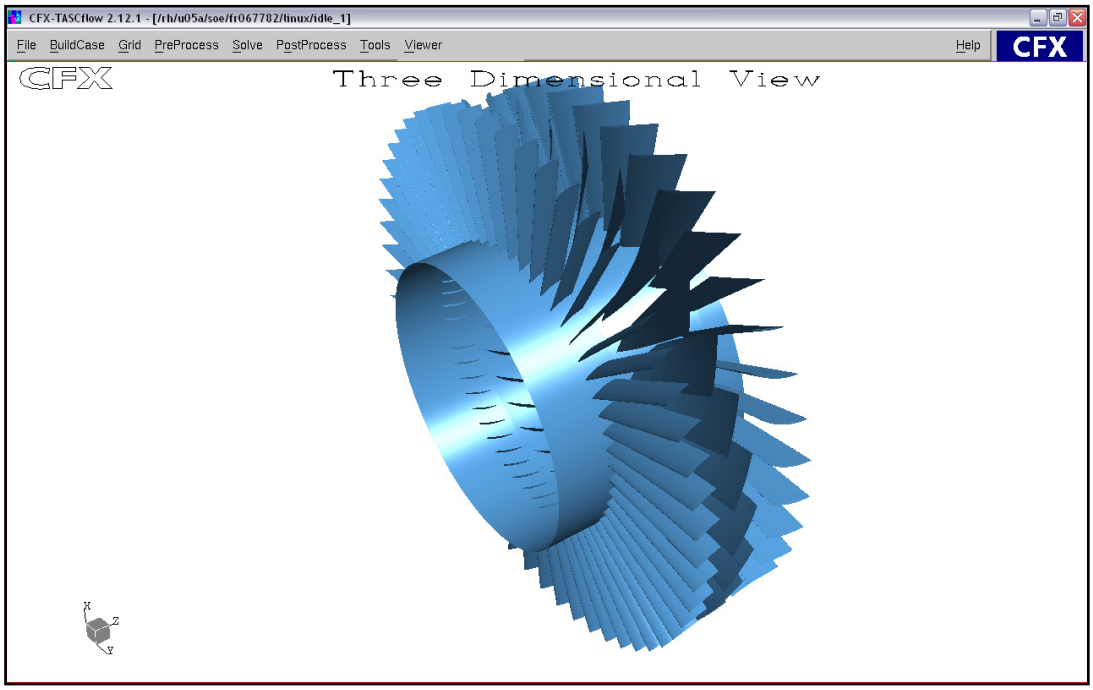

Figure 6-2: 3D View of Axial Flow Compressor Model

Grid check is performed to evaluate the minimum skew angle and maximum element aspect ratio (defined as the ratio of flux element edge lengths) as well. Minimum skew angle is 23.64° and maximum element aspect ratio is 287.04 only in a few elements. For a good convergence, the former should be greater than 20° and the latter lower than 100 [AEA (2002)].

It is worth noting that a detailed description of the work done to create the computational domain is presented in Appendix C. This is part of the project's initial phase. The creation of a robust computational model is necessary for the accuracy of the results. Thus, the process of building a CFD mesh starting from scratch data is time-consuming and requires many tests to ensure model's robustness.

6.2 CFD Parameters

CFD codes are written for several applications and they can be customized for a special case study through the adjustment of their parameters. Setting the CFD parameters is of great importance for the accuracy of the results. The following is an analysis of the factors used to solve the fluid flow in the current simulation.

The k-ε two-equation turbulence model is used with turbulence intensity values of 1.0 (medium intensity values) where k is the turbulent kinetic energy and ε its dissipation rate ("*the amount of k per mass and time converted into internal energy of the fluid by viscous action*", [AEA (2002)]. These two parameters are

introduced to model the equations for turbulent correlations in the Reynolds-averaged Navier-Stokes (RANS) equations. These equations represent transport equations only for the mean flow quantities. Therefore, by using this approach the computational time and resources are reduced compared with the Direct Numerical Simulation (DNS) method.

To model the flow in the near-wall region, the Wall-Function method is used. With this method, empirical formulas are used to provide near-wall boundary conditions for the mean flow and turbulence transport equations. These formulas connect the wall conditions (e.g. the wall-shear-stress) to the dependent variables at the near-wall grid node. This point should lie in the fully turbulent region of the boundary layer (outer sublayer). The use of empirical functions eliminates the necessity of numerically resolving the large gradients in the viscous sublayer region.

Consequently, the location of the point nearest to the wall is very critical, because the predictions, using the log-law wall-functions, are sensitive to the near-wall meshing. For that reason, computational grid is tested and it is found that y+ values (non-dimensional wall distance) range from 20 to 85 at the wall nodes. Therefore, according to the CFX-Tascflow documentation [AEA (2002)], these values ensure that near wall log-law predictions will be fully valid.

Turbulent diffusion deposition is negligible since the droplet's diameter, in most cases, is big enough (1 mm) and it deposits on the blade due to inertial impact. Therefore, turbulent diffusion deposition is not considered at all.

To model the particle trajectory, Lagrangian tracking (separated flow analysis) is implemented. By using this method, the solver tracks several individual particles through the flow field, assuming that each particle represents a sample of particles that follow an identical path. Therefore, the flow path of the tracked particles illustrates the average behaviour of the dispersed phase. In the current work, two-way coupling is implemented, which means that the water droplets affect the fluid behaviour. In this case, the particle source terms are included in the momentum equations.

Since evaporation is taken into account to this simulation, the water interacts with the flow by introducing mass, scalar and energy sources, as well as the usual momentum sources. Additionally, the loss of droplet mass due to evaporation decreases its size. Hence, water droplets have a strong influence to the flow field and when they are injected, it needs to adjust to their new source terms. Using Lagrangian tracking capability, to get a converged solution, three parameters should be adjusted:

- Frequency of particle injection
- Number of particles injected

- Relaxation of the source terms generated by the particles

Therefore, the procedure to get a converged solution with Lagrangian tracking is two-fold: the first step, in which few particles injected very frequent and low relaxation factor and the second step with many particles, infrequent and relaxation factor of 0.35-0.45. At the first step, the low relaxation factor smoothes out the oscillations from this frequent injection of particles, while at the second step, the reduced frequency and the increased relaxation factor allows the solver to adjust the influence of the discrete phase required for convergence.

Evaporation is modelled in this CFD code. It is worth pointing out that, at the first stages of an axial flow compressor under water ingestion conditions, only small water quantities evaporate, because the temperature difference is not big and the residence time is extremely low. The above have been shown in the current research, where it is found that only a tiny fraction of water quantity is evaporated. Consequently, evaporation does not affect the film thickness model.

Boundary Conditions (B.C.) at inlet and outlet of the model are defined in CFX-Tascflow to solve the flow field at D.P. operation. Specifically, $P_{t,in}$=101,325 Pa and $p_{s,out}$=114,680 Pa are set up. Additionally, the rotor blade and hub constitute the rotating surface while the IGV blade, shroud and stator are in the absolute frame. Moreover, the meridional hub to shroud planes is periodic boundaries and all the walls are assumed adiabatic. Furthermore, IGV, rotor and stator blades have been specified block-off grid since they are solid objects in the computational domain.

Finally, Modified Linear Profile (MLP) solver procedure is chosen as the discretization scheme with Physical Advection Correction (PAC). This scheme combines accurate predictions and robustness.

6.3 Application of CFD

To calculate the water ingestion deterioration on the compressor model, CFD co-operates with a FORTRAN computer code created by the author. After finding the fluid flow solution, some of the results are exported to the code; they are further processed and imported again to CFD, where the performance deterioration is estimated.

6.3.1 Process Overview

The computational domain is imported to CFX-Tascflow and several cases are solved. The parameters, which affect water ingestion, are taken into account, including cases at part speed. The results are exported in **.dat* file format and

read by a FORTRAN code, named FILM_MOTION. The program calculates the water film thickness, which is formed on the rotor blade's pressure surface, its motion (direction and speed) and the extra torque demand. Data like build up mass and its position on the blade, shear stress and water droplets momentum are provided by the CFD calculations.

Having known the film thickness at each node of the grid, the new Cartesian coordinates x, y, z of the blade's pressure surface are calculated and imported again in CFX-Tascflow changing the blade's profile. Therefore, the grid is changed and saved again for the same case parameters.

However, using this method the results does not show any significant change in the compressor's performance. This is attributed to the fact that CFX-Tascflow not only smoothes the grid but also it performs several checks for grid suitability avoiding negative volumes and big skew angles. In some nodes, where film thickness takes relatively high values and the adjacent node has a low value, the author manually corrects the errors in order to run the program. Finally, all the cases are run with an altered blade profile to include its effects on compressor's performance.

To tackle the problem of grid automated smoothing, the roughness model of CFX-Tascflow is used. Based on literature, an equation is used (heading 6.4.4), which links the water film with the surface roughness. The water film height determines the equivalent sand-grain roughness for each case. Finally, CFD runs again with modified parameters and the performance degradation is estimated respectively. Figure 6-3 displays the discussed work flowchart.

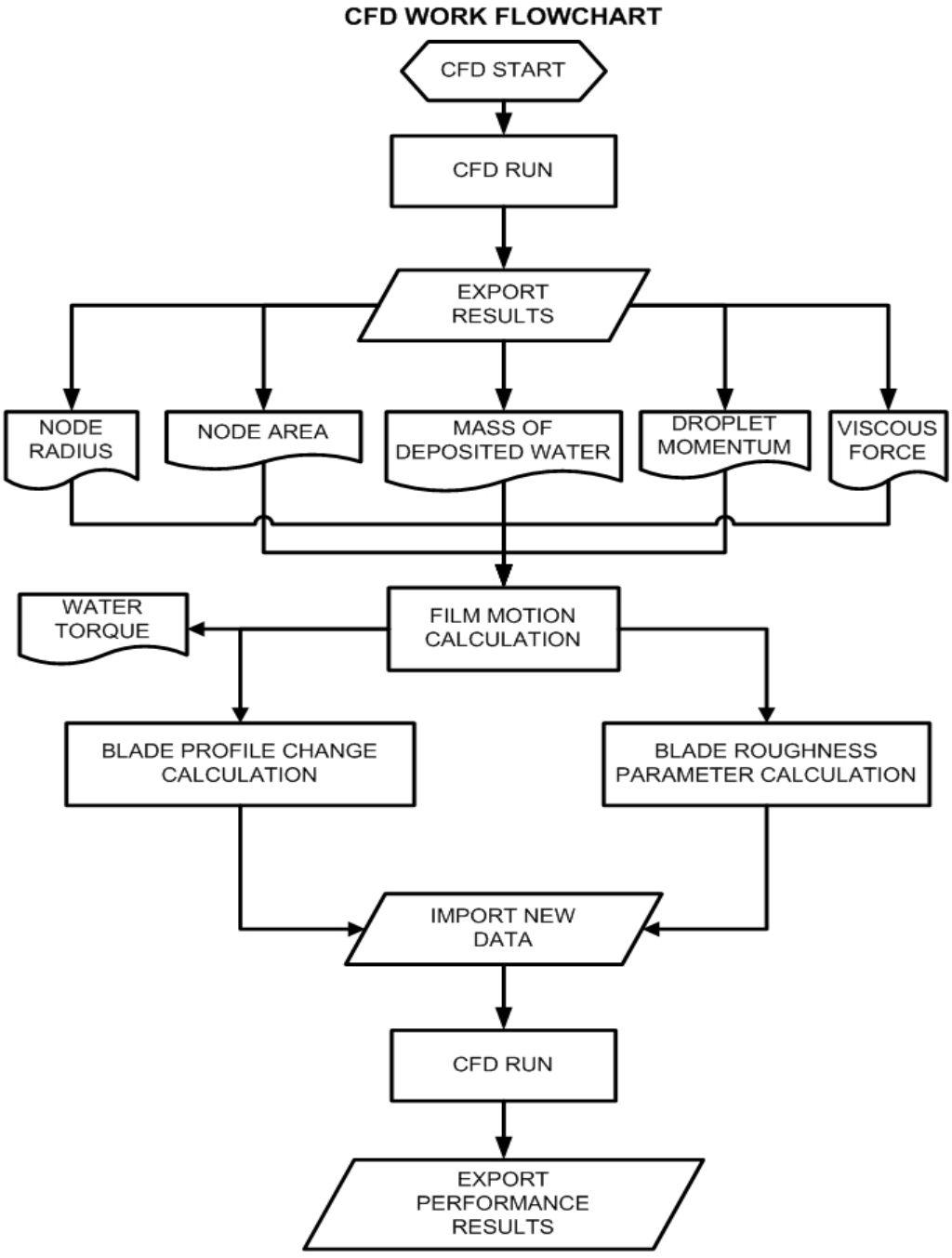

Figure 6-3: CFD Work Flowchart

It is noteworthy that there was an attempt to use the CFX-Tascflow Moving Grid feature, which means that the software can track and model changes in grid node position over time. To do this type of simulation the user must define how the grid moves within time. The grid movement process is controlled by user-coded routines. In view of the above, the concept was to change the blade's pressure surface position simulating the thickening of blade's profile due to the water film formation. Hence, a subroutine was created to determine the

movement of pressure surface grid nodes and run the simulation with a local executable.

However, the attempt was not successful. The software crashed on all trials giving error messages for either memory capacity or FORTRAN compilation process during the run of the local executable. It was thought that CFX-Tascflow was not able to adopt such massive grid changes bearing in mind that each node moved in a different way. Given that, the investigation of the matter was time-consuming and the success of the method was doubtful, the re-orientation was considered as the best choice.

6.3.2 Test Strategy

It is well known that experiments involve several factors. Bearing in mind CFX-Tascflow capability and the knowledge obtained by studying the literature, it is determined that four factors are of primary interest:

- The water mass
- The water droplet speed
- The water droplet diameter
- The blade's rotational speed

For the first three factors, the physics of the phenomenon limits their values. Hence, water droplet diameter varies from 0.001 mm up to 3 mm and droplet ingestion speed from 50 m/sec up to 150 m/sec including cases where that parameter has the same value with air speed (0 relative V_w and T_w). However, some extreme cases are run just to check the code and its results. Although, in adverse weather conditions, there is a possibility of an aircraft to encounter water ingestion of only 3.18% water/air mass [Kissel (1979)] and the gas turbine water ingestion certification test is accomplished with 4% water/air, in this study water mass fraction varied from 2% up to 30%. It is clear that these values are not met in the gas turbine operating conditions but they are necessary in order to make the results more obvious and easily understood. In figure 6-4, the above water ingestion factors are plotted.

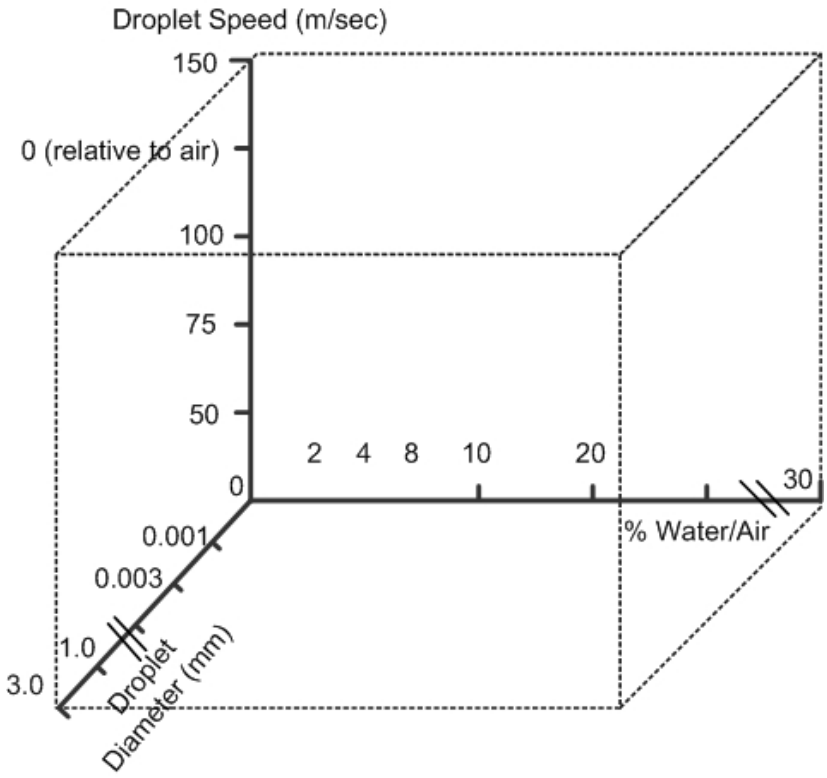

Figure 6-4: Water Ingestion Parameters

The strategy of experimentation is the *one-factor-at-a-time* approach. Using this method involves the selection of a starting point for each factor and then varying it while the other factors are held constant [Montgomery (2005)]. The major disadvantage of this strategy is that it cannot take into account any possible interaction between the factors. In this work, it was found that none of the above parameters produce the same result for different values of the other two (i.e. water mass has different effect for small and large droplets). Consequently, the *one-factor-at-a-time* strategy seems to be inadequate for this type of test. In this case, the *factorial-design* should be involved, which means that all the possible combinations of the parameters should be investigated [Montgomery (2005)]. More specifically, due to the variation of the factors, the planning of the experiment should be based on a scientific statistical model.

However, it is reported that the effects of water droplet diameter and its speed are not so pronounced and they are negligible comparing with the water mass and the blade's rotational speed. Thus, it is decided to perform the CFD calculations based on the *one-factor-at-a-time* strategy and suggest the *factorial-design* for future research due to the complexity of this method.

6.3.2.1 Blade Rotational Speed Factor

Bearing in mind that water ingestion causes serious problems when the engine operates at part load (60-65% rpm), cases at idle speed has to be investigated. To have the most possible realistic flow in the stage, IGV angle at 65% rpm

should be estimated and re-positioned the IGV blades. Because model's compressor map is not available, IGV angle choice is a combination of the author's experience in jet engine maintenance and of many trial cases to find out when flow starts to separate.

Consequently, several IGV angles for good grid skewing and convergence are tested. It is worth noting that is not an easy task, because the outflow boundary condition (B.C.) is not known. Therefore, W_a or p_{st} at outlet should be guessed. In cases where W_a is chosen, Tascflow is very unstable and unable to converge, presumably due to the sensitivity of compressor map over the change of mass flow. For that reason, p_{st} is used as B.C. at the stage outlet. Finally, the IGV angle is set to 20° (towards close-position) with $p_{st,out}$=105 kPa giving a mass flow value of W_a=48.7 kgr/sec. After this, several idle speed cases run with the same water parameters as these for full speed.

For the same reasons, another group of cases with 80% rotational speed are set up. This is necessary for interpolating accurately performance parameters values when rotational speed varies between 65% and 100%. The B.C. for these cases are $p_{st,out}$=110 kPa and W_a=61.9 kgr/sec.

6.4 Water Film Computation

Having solved the flow field for the different water ingestion cases, the water droplets mass is known for each control volume of the computational blade pressure surface. Following Gardner's methodology in Gardner (1963), under the influence of the centrifugal force, in the water film there is a span-wise "mass flow component" m_K. Similarly, air shear force controls the chord-wise "mass flow component" m_l. The two "mass flow components" are linked by the fact that film thickness height δ is the same for both dimensions. It is assumed that the blade chord-wise direction coincides with the axial one. The concept is illustrated in figures 6-5 and 6-6.

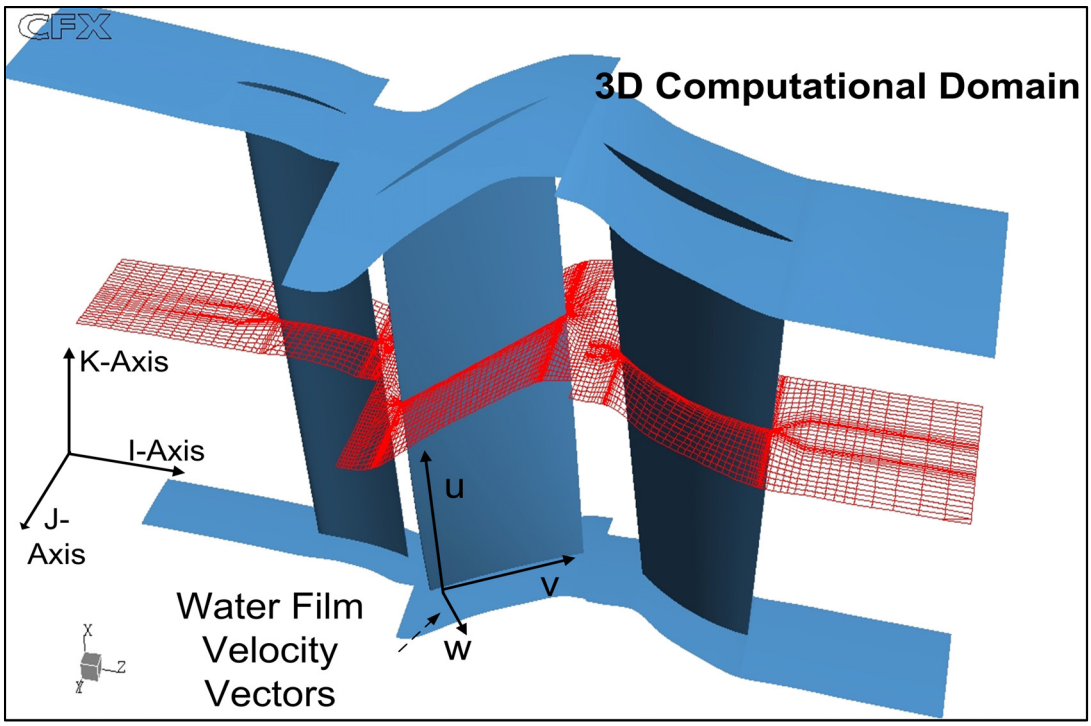

Figure 6-5: 3D Computational Domain

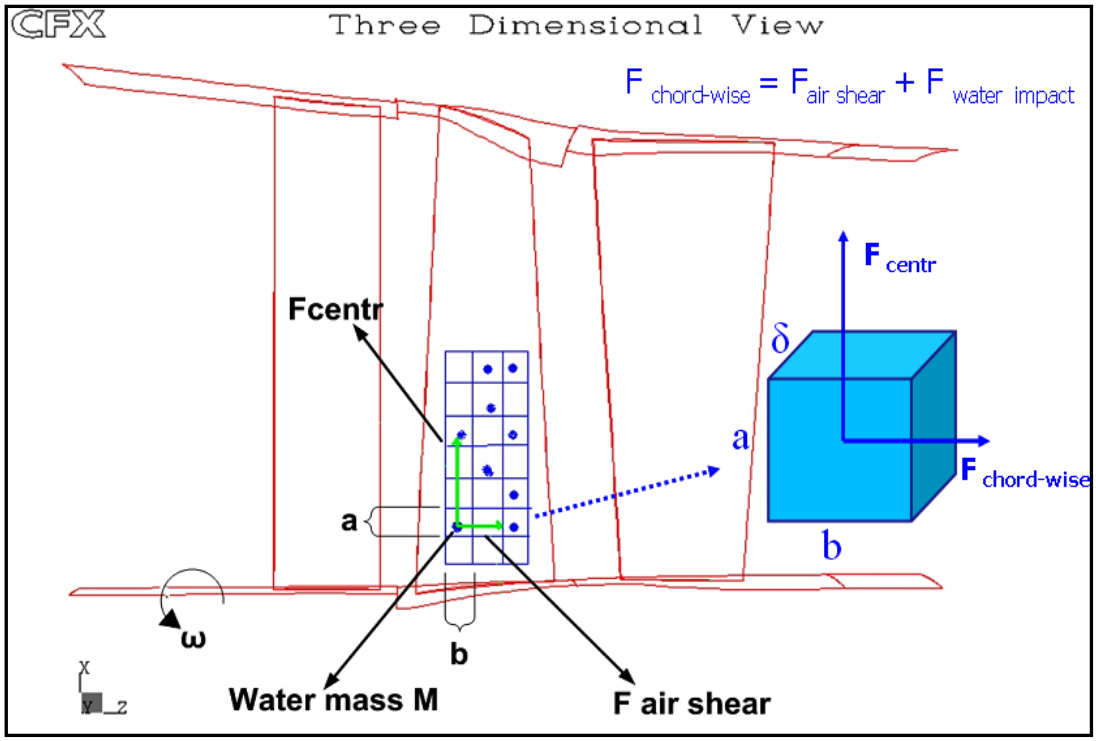

Figure 6-6: Water Mass Deposition on Rotor Pressure Surface

The results from CFX-Tascflow are imported in a FORTRAN program called FILM_MOTION. This program takes data from CFD and calculates the water film thickness and its motion on the rotor blade's pressure surface at the equilibrium condition, through an iterative process. This condition is defined when the water which deposits on the blade equals with that flowing out of the

blade [Freeman (2004)]. In every iteration, water mass deposits on the blade and an amount of water mass extracted since it is flowing out of the blade. The program includes five subroutines, which solve the span-wise and chord-wise motion of the water mass, the total axial shear stress, and the torque. These are:

- The FILM_THICK subroutine, which calculates the water film thickness on the blade's pressure surface,
- The SHEAR_CALC subroutine, which calculates the air shear stress on the blade's pressure surface including the water droplets momentum impacting on the water film,
- The CV_DIMENSION subroutine, which calculates the radius distance of the node in each control volume,
- The EQU_SOLVE subroutine, which solves the equation of water film mass flow, by using the bisection method,
- The ROTOR_TORQUE subroutine, which estimates the extra torque due to water film.

The FILM_MOTION flowchart is presented in Appendix D.

6.4.1 Span-wise (Radial) Movement

Due to the blade rotation, a centrifugal force is applied to the mass of water. This force dominates in the radial direction (figure 6-7).

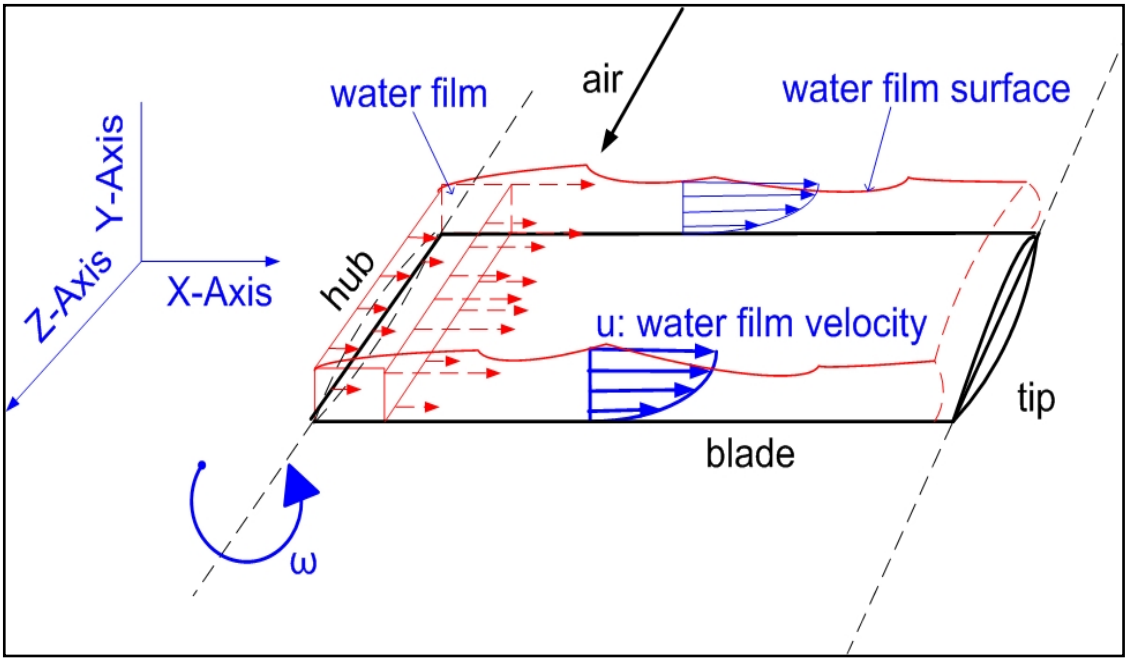

Figure 6-7: Water Film Span-wise Motion

The following assumptions can be made:

a. During the centrifuging of the water film, there is no film motion to any other direction y or z, thus continuity equation becomes:

$$\frac{\partial u}{\partial x}+\frac{\partial w}{\partial y}+\frac{\partial v}{\partial z}=0 \Rightarrow \frac{\partial u}{\partial x}=0$$

Equation 6-1: Mass Continuity Equation

b. The water film flow is steady thus

$$\frac{\partial u}{\partial t}=0, \quad \frac{\partial v}{\partial t}=0, \quad \frac{\partial w}{\partial t}=0$$

Equation 6-2: Water Film Steady Flow Equation

c. There are no pressure gradients to any direction thus

$$\frac{\partial P}{\partial x}=0, \quad \frac{\partial P}{\partial y}=0, \quad \frac{\partial P}{\partial z}=0$$

Equation 6-3: Zero Pressure Gradients Equation

d. Tip clearance effects, due to the concentration of water mass at the outer radius, are not taken into account.

Considering the above assumptions and using Navier-Stokes equations in x Cartesian coordinate (direction of motion), it can be concluded that:

$$\rho\left(\frac{\partial u}{\partial t}+u\frac{\partial u}{\partial x}+v\frac{\partial u}{\partial y}+w\frac{\partial u}{\partial z}\right)=\frac{\partial P}{\partial x}+\mu\left(\frac{\partial^2 u}{\partial x^2}+\frac{\partial^2 u}{\partial y^2}+\frac{\partial^2 u}{\partial z^2}\right)+Fx \Rightarrow Fx=-\mu\frac{\partial^2 u}{\partial y^2}$$

Equation 6-4: Navier-Stokes Equation in Span-wise Direction

Assuming parabolic velocity distribution in the water film and the no-slip wall condition, it can be written that (per unit volume):

$$F_{centr}=-\mu\frac{\partial^2 u}{\partial y^2} \quad \Rightarrow \quad \frac{F_{centr}\,y^2}{2}-F_{centr}\,\delta\,y=-\mu\,u$$

Equation 6-5: Centrifugal Force Equation

Using continuity equation:

$$dm_K=\rho\,b\,u\,dy \Rightarrow u=\frac{1}{\rho\,b}\frac{dm_K}{dy} \quad \therefore$$

$$(6-5)\ \therefore\ \frac{F_{centr}\,y^2}{2}-F_{centr}\,\delta\,y=-\mu\,\frac{1}{\rho\,b}\frac{dm_K}{dy} \Rightarrow \int_0^{\delta}\left(\frac{F_{centr}\,y^2}{2}-F_{centr}\,\delta\,y\right)dy=$$

$$=-\mu\,\frac{1}{\rho\,b}\int_0^{m_K} dm_K \quad \Rightarrow \quad \frac{F_{centr}\,\delta^3}{3}=\mu\,\frac{1}{\rho\,b}\,m_K$$

Equation 6-6: Centrifugal Force – Mass Equation

The centrifugal force equals: $F_{centr}=\rho\omega^2 r \quad \therefore$

$$(6-6) \quad \therefore \quad \frac{(\rho\,\omega^2\,r)\,\delta^3}{3}=\mu\,\frac{1}{\rho\,b}\,m_K \Rightarrow \delta=\left(\frac{3\mu}{b\,\rho^2\,\omega^2\,r}\right)^{1/3} m_K^{\,1/3}$$

Equation 6-7: Film Thickness Equation

$$u=\left(\frac{\omega^2\,r}{3\rho b^2\,\mu}\right)^{1/3} m_K^{\,2/3}$$

Equation 6-8: Water Film Span-wise Velocity

6.4.2 Chord-wise Movement

The water film is moving chord-wise under the influence of air shear stress, the pressure gradient and the momentum transferred by the impinging water droplets on the film. Its viscosity retards its motion. Pressure gradient is supposed to be negligible. If v is the chord-wise velocity at the δ film surface and assuming a linear distribution inside it, then:

$$\tau = \mu \frac{\partial v}{\partial y} \Rightarrow \tau = \mu \frac{v}{\delta}$$

Equation 6-9: Wall Shear Stress Equation

Using continuity equation:

$$m_I = \rho \int_0^{\delta} (\alpha v) dy \Rightarrow m_I = \frac{\alpha \tau \rho \delta^2}{2\mu}$$

Equation 6-10: Continuity Equation in Chord-wise Direction

From the Tascflow results, we can extract the following scalars:

- mass of deposited water per node (build-up array)
- node radius
- node area wall (AREA WALL)
- viscous force per unit area (wall shear stress - TAU_WALL)
- momentum of water droplets (PART_U, PART_V, PART_W)

The wall shear stress (TAU_WALL) is the shear stress due to the airflow. Although the water film on the blade changes the blade surface and consequently the value of this shear stress, it is assumed that TAU_WALL remains unaffected.

However, the total shear stress acting on the blade surface is modified when water droplets momentum is taken into account. Therefore, the total viscous force τ per unit area acting on the airflow (hence, to the water film on the blade) is the sum of wall shear stress TAU_WALL and the shear stress caused by the water droplet momentum (the source of water momentum is modified in force per unit area in SHEAR_CALC subroutine).

The water droplets after the impact on the blade retain only a percentage of their momentum just before the deposition. The collision is highly inelastic. The droplets radial momentum (K computational coordinate) is extremely small and can be neglected during the calculations. Thus, the total water momentum can be defined using the momentum in J and I (chord-wise) computational coordinates and adding them as vectors (figure 6-5). The resulted vector is assumed tangential with the blade chord-wise dimension. Finally, the amount of retained water momentum is added to the water film initial momentum at each time step.

As noted above, the impact is inelastic and the FILM_MOTION user should define the percentage of retained water momentum. For this, literature search

and empirical rules may be applied. It has been observed that when water droplets impact on a surface, they retain only a small amount of their momentum [Murthy (1989), Kennedy and Roberts (1990), Santa (2000)]. Hence, in FILM_MOTION code, the user should define the value of the coefficient of restitution, which should be between 0.1 and 0.3 [Williams (2003), Williams J. et al. (2005)]. Finally, the value of 0.2 was imported, which seems to reflect the phenomenon, [Yarin and Weiss (1995), Sommerfeld and Huber (1999), Mundo et al. (1998), Bussmann M. et al. (2000), Rein (1993)].

Combining equations (6-9) and (6-10):

$$m_I = \frac{\alpha \rho \tau}{2\mu}\left(\frac{3\mu}{b\rho^2\omega^2 r}\right)^{2/3} m_K^{2/3} \Rightarrow m_I = \frac{\rho}{2\mu}\left(\frac{3\mu}{\rho^2\omega^2}\right)^{2/3} \frac{\alpha\tau}{(br)^{2/3}} m_K^{2/3}$$

Equation 6-11: Chord-wise "Mass Component" Equation

But $m_l+m_K=M$ hence

$$m_K + A \cdot B \cdot m_K^{2/3} - M = 0$$

Equation 6-12: "Mass Components" Equation

where E is the area wall, and

$$A = \frac{\rho}{2\mu}\left(\frac{3\mu}{\rho^2\omega^2}\right)^{2/3} \quad \text{and} \quad B = \frac{\alpha\tau}{(br)^{2/3}} = \frac{\alpha\tau}{\left(\frac{E}{\alpha}r\right)^{2/3}} = \frac{\alpha^{5/3}\tau}{(Er)^{2/3}}$$

6.4.3 Torque calculation

Water impinges on the blade and forms a film, which flows radially outwards because of the centrifugal force. Shear force due to airflow and water droplets momentum are low compared with the radial forces. The described impact is highly inelastic. This means that droplets retain only a small amount of their momentum and only in chord-wise direction. However, due to rotor blade rotation they obtain energy and develop relatively high speed in radial direction. Leaving the blade, they have an adequate amount of tangential momentum, which is diminished when they impact on the stator blade.

FORTRAN subroutine ROTOR_TORQUE was built to estimate the torque, which is required to achieve the described energy change. Initially, it is assumed that the water film obtains, in the tangential direction, the blade speed (V_θ) when it exits out of the blade tip or trailing edge. Apart from that, it is assumed that the centrifugal force is the only force that acts on the radial

direction. This approach does not deviate a lot from the real phenomenon because radial shear force and water viscosity are low compared with the centrifugal force. On the other hand, this assumption will give a lower value of film thickness as it will be analyzed in the next sections.

Therefore, at each node (at the blade tip or trailing edge) the torque per stage due to water is:

$$T = F \bullet d = m \bullet \gamma \bullet R \Rightarrow T = m \bullet \frac{dU}{dt} \bullet R \quad \therefore \quad T_{water} = \dot{m} \times R \times V_\theta \times (\text{number of blades})$$

Equation 6-13: Water Torque Equation

$\dot{m}$: is the water mass rate (kgr/sec),

R: is the radius of the node (m),

V_θ is the water tangential speed at the exit of the blade (m/sec).

From the above parameters, R and V_θ are given from CFD calculations, while m is calculated from FILM_MOTION program. Torque depends on the ingestion parameters like the ingested water mass, droplet size, droplet speed and the blade's rotational speed. As it will be shown, these factors affect the build-up mass and the film motion, and consequently the torque due to water.

It should also be highlighted that the aforementioned methodology has been presented in ASME Turbo Expo 2008 and published in Nikolaidis Th. et al. (2008).

6.4.4 Water Film Characteristics

Water film formation has considerable effects on blade's geometric characteristics. Apart from the change in its profile due to thickness increase, air shear force and the water droplets momentum magnify the wavy features of the water film, introducing a kind of "roughness" on blade's surface. The interfacial air speed and the film motion cause waves on the water film, which are not stable and if they are of sufficient amplitude, they will result in water film breakdown and the formation of "dry spots" and/or rivulets. Rough blade surfaces are known to develop considerably larger skin friction coefficients when compared to smooth surfaces. At the same time, roughness at the blade surface creates thicker boundary layers, which result in an increase in blockage reducing the aerodynamic performance of the blade. Consequently, it is necessary to include in the calculations the roughness effect on the blade's performance.

The idea of the roughening effect of water droplets on aircraft wings has widely been used by several researchers Thompson B. et al. (1995), Thompson B. and

Jang J. (1996), Haines and Luers (1983), Luers and Haines (1983),Khodadoust A. and Bragg M.B. (1995), Ashenden R. et al. (1996a), Bilanin (1987); Ashenden R. et al. (1996b). In Haines and Luers (1983), the authors tried to evaluate the aerodynamic penalty of heavy rain on an aircraft wing. Their effort focused on the airfoil roughness caused by the momentum of droplets, which disturb water film surface, and the waves develop on the water film surface under wind shear force. They found that the performance degradation of an aircraft wing under rainfall conditions could be significant. The roughness associated with drop impact produced a 37% loss in maximum lift at 100 mm/h rainfall. Accordingly, film waviness produced losses in maximum lift from 11% to 30%, depending on the rainfall rates. However, their results lack experimental validation. Qualitatively, rain on an airfoil can produce the same aerodynamic deterioration as the fixed-element roughness does.

As far as the numerical simulation is concerned, CFX-Tascflow includes a rough wall model. Because the influence of the roughness on the flow does not only depend on the mean height or grain size but also on the form of the grains and their distribution on the blade, CFX-Tascflow has adopted the equivalent sand-grain roughness k_s. The idea is also used by other CFD codes, like FLUENT 6.0. Sand-grain roughness parameter consists of close-packed natural sand-grains of nominally uniform diameter and their relation are based on measurements made by Nikuradse (1933) of flow over such kind of roughness. The concept of equivalent sand-grain roughness k_s was firstly introduced by Schlichting (1936), and it is the height of standard sand roughness that would produce the same effects on the flow as the roughness of interest. Therefore, the user of CFX-Tascflow should determine a value for k_s.

In case of liquid films and their relation with k_s, Wurz (1976) measured a ratio relationship between the mean water film thickness and equivalent sand-grain roughness [Wurz, (1976)]. He found that the ratio is 1.25 to 2.0 in the subsonic test from 0.18-0.6 Mach number range. However, his experiments were conducted in low rainfall rates, which produced low film thickness values.

Another way of determining the value of k_s was presented by Koch and Smith (1976). They have found that the equivalent sand-grain k_s can be related with the arithmetic centreline average roughness k_{CLA} with the relation:

$$k_s = 6.2 \cdot k_{CLA}$$

Equation 6-14: Equivalent Sand-Grain Roughness Equation [Koch and Smith (1976)]

Their conclusion based on the usage of measurements of k_s values for several standard sandpapers made by Spiedel [cited in Koch and Smith, (1976)]. The above equation is in reasonable agreement with the experimental results of Young [cited in Koch and Smith, (1976)]. Therefore, for this project, the equivalent sand-grain roughness is determined using the above equation. It is

worth pointing out that CFX-Tascflow roughness numerical simulation has been validated and gave quite reliable results Kang et al. (2003).

Another issue, which has to be solved, is the fact that, blade film thickness is not uniform on the pressure surface. That parameter is addressed by dividing the surface in four smaller regions (figure 6-8), taking into account experimental observations in Williams J. et al. (2005) in connection with the results from the current project about water film concentration on the blade pressure surface. After that, the average film thickness for each region is calculated providing data for determining the equivalent sand-grain roughness. These values are imported into CFX-Tascflow rough wall model. Then the cases run again under the new parameters and the results are exported to estimate the changes in performance.

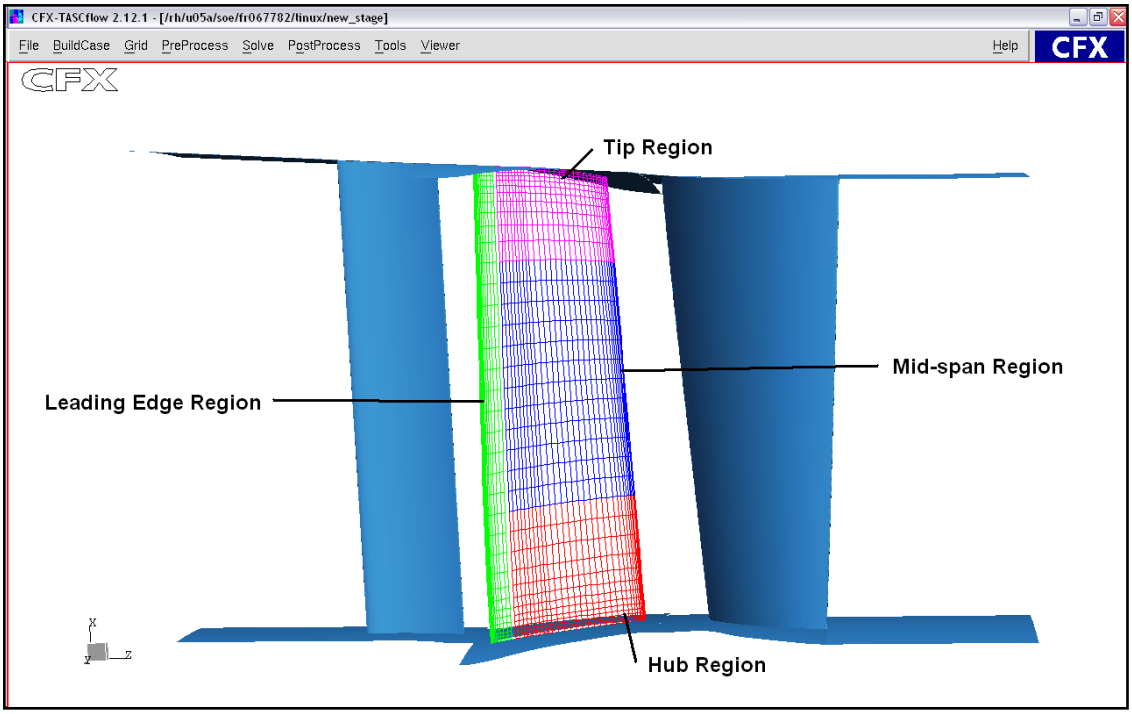

Figure 6-8: Rotor Blade Pressure Surface Regions

6.5 CFD Results

Many cases are solved by using computational analysis. By changing the water ingestion parameters, the results for water film formation on the rotor blade and the demanded water torque are exported. Moreover, performance deterioration is calculated based on blade profile change and surface roughness model. Finally, some remarks are made about CFX-Tascflow Lagrangian Tracking capability and the water deposition on the blade's suction surface.

6.5.1 Lagrangian Tracking Model

Lagrangian method of flow description involves tracking individual fluid particles as they move, and determining how the fluid properties change as a function of time. It means that the fluid particles are identified and tracked as they are moving. This method is widely used in multiphase flows – mixtures such water droplets dispersed in the air. The flow path of the dispersed phase is determined by the tracking of several individual water droplets through the flow field. Each particle represents a sample of particles that follow an identical path. The behaviour of the tracked particles is used to describe the average behaviour of the liquid phase. Therefore, Lagrangian method involves a statistical approach in describing the flow.

Practically, that means that injecting a large number of water droplets can achieve a more accurate solution than injecting few droplets. On the other hand, bearing in mind that each particle is tracked individually, determining the flow of many droplets is extremely time-consuming and is limited by the computational resources. Therefore, it was necessary to define the number of droplets, which can give a realistic statistical result. Several cases have been run to test the accuracy of the results for different number of injected droplets. In the figures 6-9(a), (b), (c), (d) and (e) is the build up water mass for 1000, 5000, 10000, 15000 and 20000 water droplets respectively, for the same water mass flow (30% of air mass). It was found that from the statistical point of view, the case with 20000 droplets gives more accurate results about the deposition water mass than the cases with fewer droplets. However, there is no considerable difference when the number of droplets is bigger than 5000 and that is obvious in figure 6-9 where the regions of the build up scalar has similar values on the blade pressure surface. Consequently, cases with 5000 droplets offer a good balance between accuracy of the results and computational time and that is why this value was chosen for this parameter.

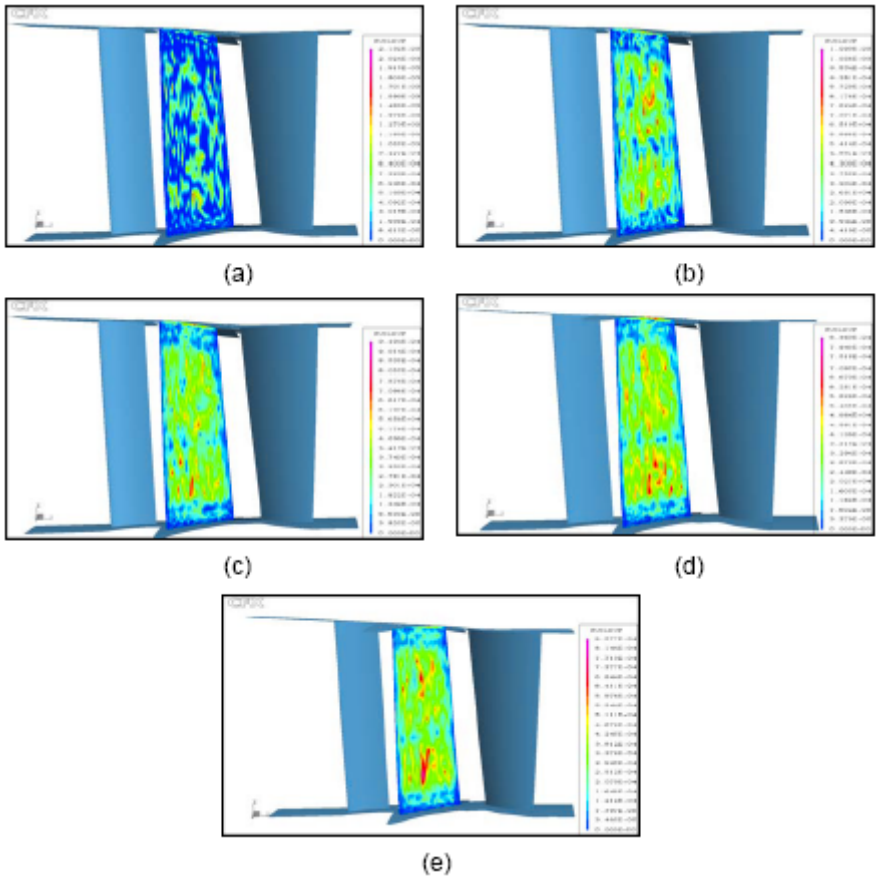

Figure 6-9: Water mass deposition for (a):1000, (b):5000, (c):10000, (d):15000 and (e):20000 water droplets

6.5.2 Water Deposition on Blade Surface

Investigating the amount of water, which is ingested into the compressor, a reasonable question was about the percentage of water impinging on the pressure and the suction surface of the rotor blade.

Deposition mechanisms on a rotor blade depend on the operating conditions and the nature of the injected particles. These mainly include the inertial impact and the diffusion from laminar or turbulent boundary layers. When the particles' inertia is big enough, they deviate from the gas streamlines and they impact on the blade pressure surface and the leading edge. Diffusion from laminar or turbulent boundary layers may occur only when very small particles are present in the gas flow [Moore and Crane (1972)].

By using computational analysis, it was proved that in the case of liquid water ingestion, inertial impact is the dominant mechanism in droplet's deposition. Changing the parameters of water injection speed and mass, the results show that almost all the ingested water impacts on the blade's pressure surface, while on the suction surface there are spots of a few water droplets. Even at very small injection speed (10 m/sec), there is no change in the build up water mass.

Consequently, the liquid water droplets deposit on the blade's pressure surface due to inertial impaction mechanism. When evaporation takes place then, the suction surface of the blade appears to be wet due to the diffusion mechanism. Das et al. (2006) confirm the above conclusions. CFD calculations have been used to produce build-up mass on the rotor blade in figure 6-10.

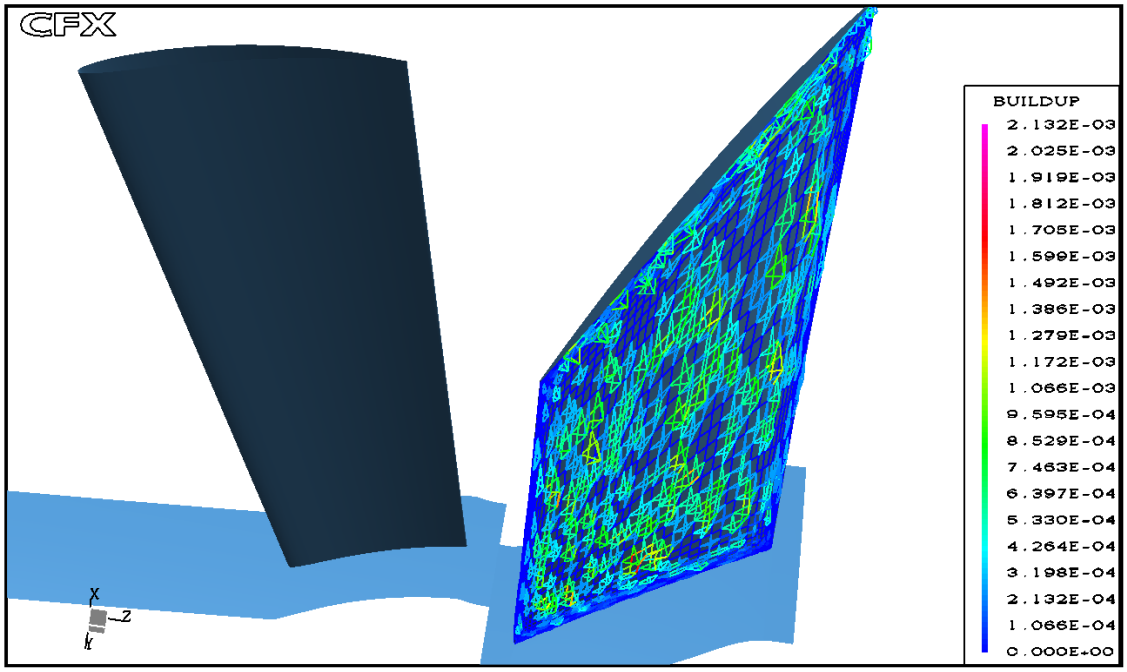

Figure 6-10: Water Mass Deposition on Rotor Blade (BUILDUP units: kgr/sec)

The water film, which is formed on the rotor blades, moves in the inner casing and part of it disintegrates. This water film changes the blade's profile, which results in performance deterioration. It has been found that the water film thickness depends on ingested water mass and the rotational speed of the blade. It is shown that the dominant parameter is the rotational speed, which contributes to the high value of the centrifugal force. In figure 6-11 film thickness is plotted for a case where 30% water/air is ingested with D_w=1 mm. It can be seen that water film reaches values of few hundredths of mm in case of full speed model (ω=898 rad/sec). In the calculations, no friction force has been taken into account. That gave a slightly increased radial force, which has minimized the film thickness. However, according to experiments thickness value approaches a fraction of mm (0.4-0.6 mm for 15% water) [Williams J. et al. (2005)]. Moreover, it is obvious in figure 6-11 that water film is thicker at the tip region and that is in agreement with experimental observations.

Parameters like the ingested water mass and the blade rotational speed affect the film thickness height and they are analyzed in the following paragraphs.

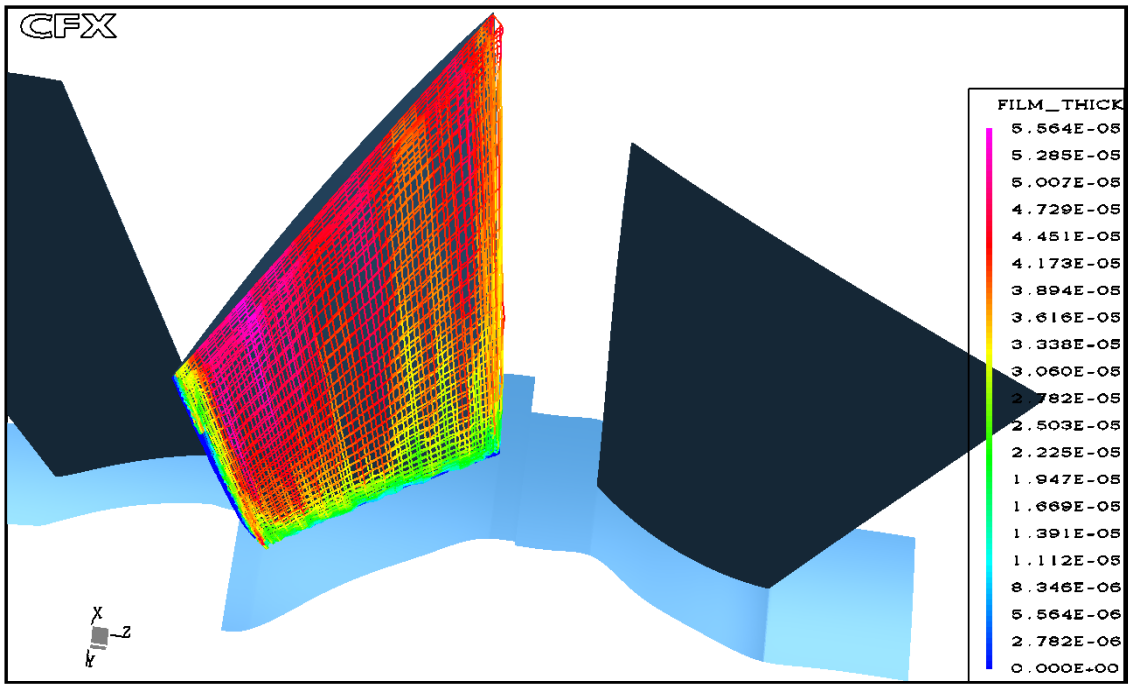

Figure 6-11: Water Film Thickness (m) for 30% water/air, D_w=1 mm

6.5.3 Effects of Water Ingestion Parameters

6.5.3.1 Effect of Ingested Water Mass

The water mass, which deposits on the blade pressure surface per second, is the build-up mass (M_b). Water deposited mass (M) is the mass, which has totally built up on the blade surface at the equilibrium condition, where the water flowing out of the blade equals to that of building up on the blade.

The water mass fraction affects the water film thickness δ. The increase of the former causes an increase of the latter. A plot is given in figure 6-12, where the film thickness change is coloured when the ingested water mass rises from 4% to 30%. It is worth pointing out that there are strips of thick water film across the blade span. These strips are caused by the dominant effect of centrifugal force.

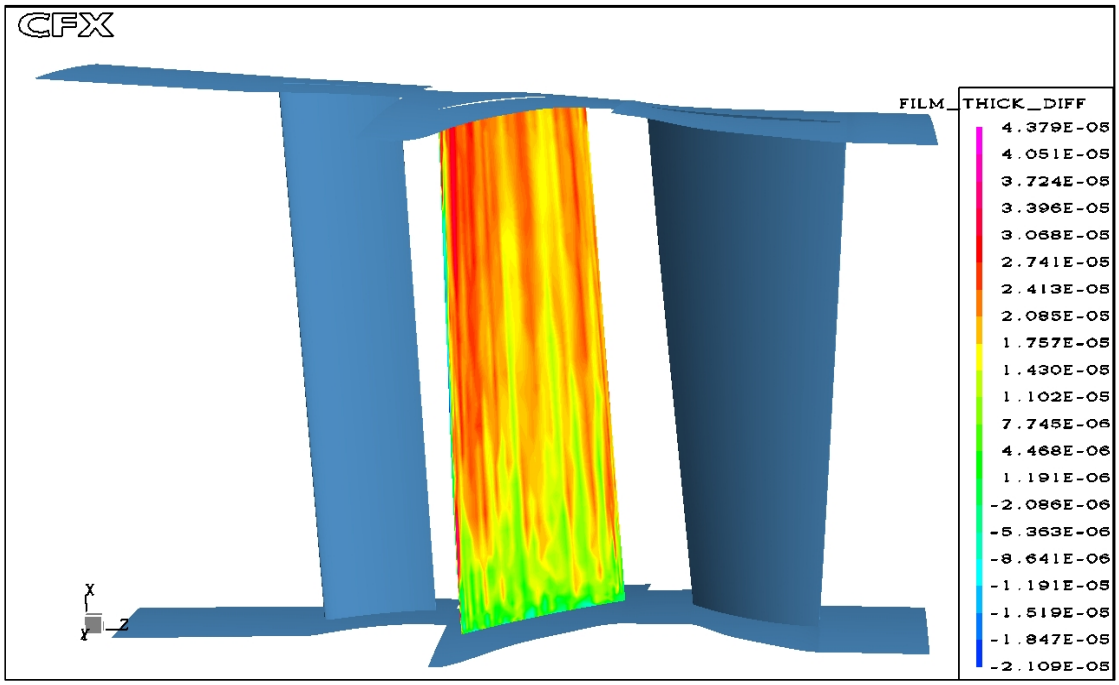

Figure 6-12: Water Film Thickness Change (m) for 4% to 30% Increase of Ingested Water (idle speed, D_{dr}=1 mm, $V_{dr\text{-}rel}$=0)

The influence on film thickness can be seen in figure 6-13; 30% ingested water/air mass flow forms a 0.0377 mm water film thickness in idle speed and 0.0346 mm in full speed. In addition to that, the increase of water mass from 4% to 30% almost doubles the film thickness at both cases of rotational speed (figure 6-14). It should be noticed that, film is thicker in idle speed due to the lower centrifugal force, its speed is smaller and that, in connection with mass continuity, leads to a thicker film.

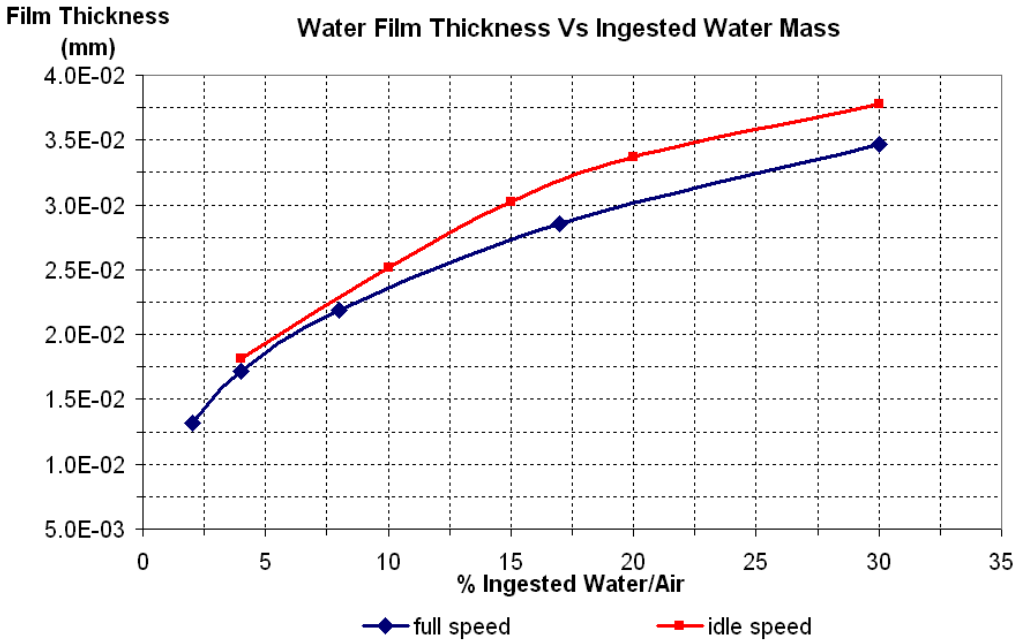

Figure 6-13: Water Film Thickness Increase due to Ingested Water Mass

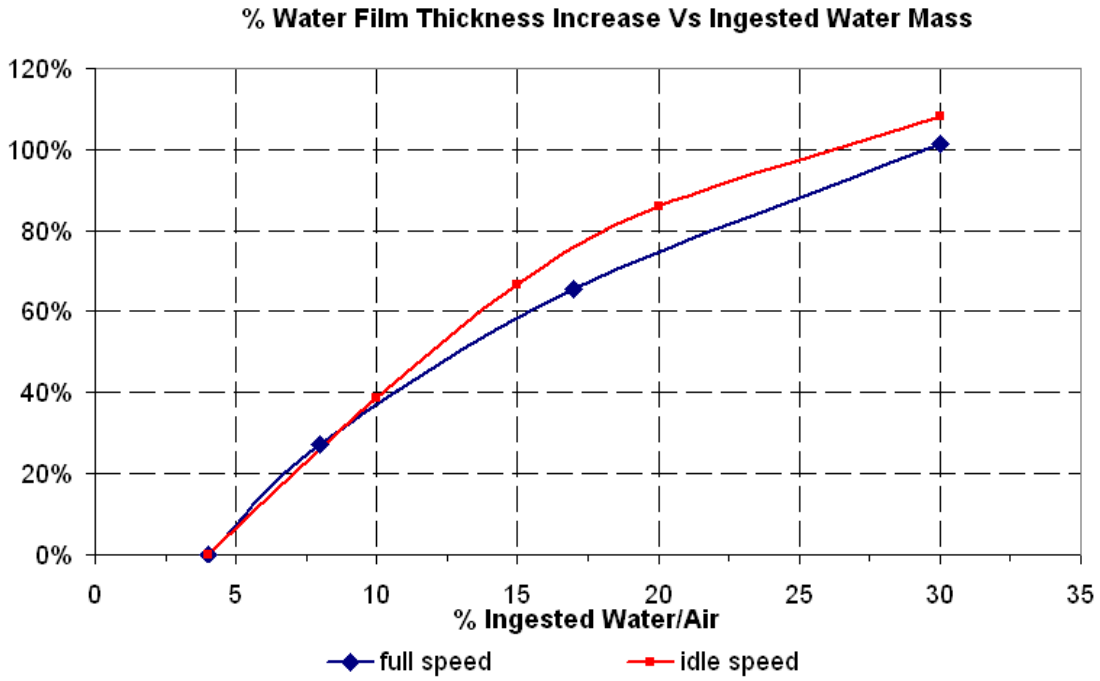

Figure 6-14: Increase of Water Film Thickness (%) due to Ingested Water Mass

The ingested water has an effect on the torque required from the compressor. That is shown in figure 6-15, where the increase in water mass fraction causes an increase in the torque required from the compressor to keep the same rotational speed. The increase in torque is directly proportional to the amount of ingested water. It is obvious that water has a detrimental effect on the blade's performance since the extra torque demand causes a considerable reduction in engine's rotational speed.

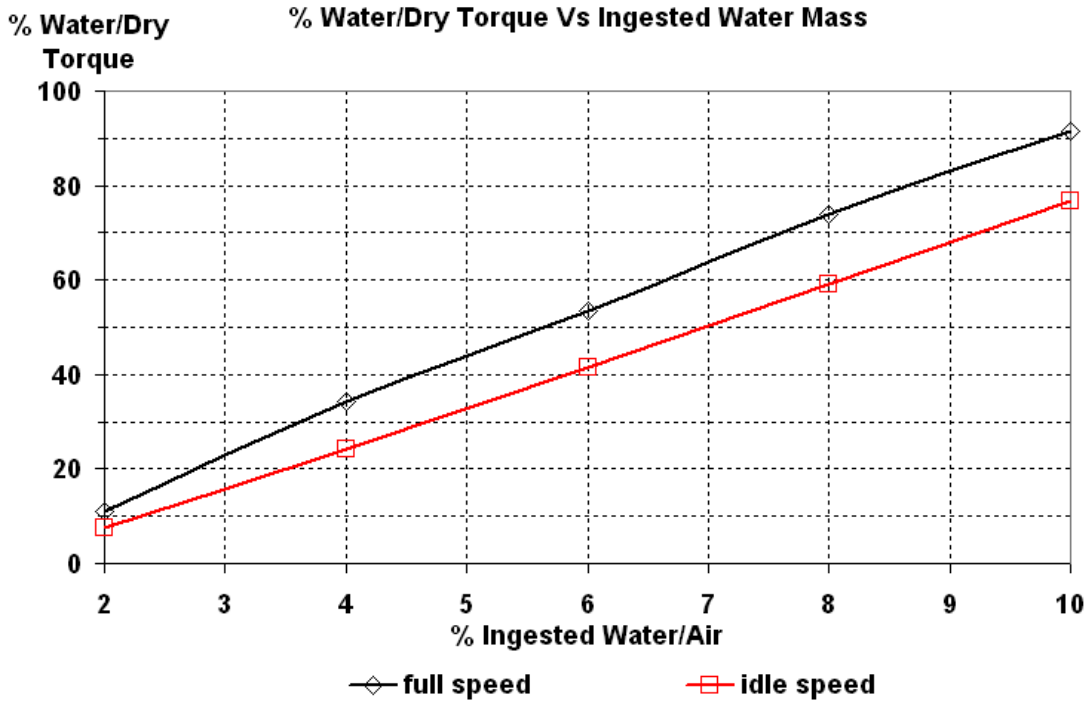

Figure 6-15: Torque Increase due to Ingested Water Mass

In figure 6-15, the percentage torque increase relatively to that of dry operation is displayed. For a water-air mass ratio 4-5%, the torque required by the compressor to keep the same rotational speed increases 40-50%. However, the torque due to the ingested water obtains high values since it is assumed that all the mass of water, which impacts on the blade, builds up on that and forms the water film, without any other effect like water droplet bouncing, splashing or film break up.

6.5.3.2 Effect of droplet diameter

It has been found that water droplet size has a small effect on build-up process and consequently on film formation. Fine droplets evaporate more easily than coarse droplets. Furthermore, fine droplets follow the air path through the blade row and the possibilities of impact on the blade are slightly lower. The results have shown that the majority of water droplets impact on the blade, mainly when they are relatively large.

CFX-Tascflow has been used to produce figure 6-16, which shows the change in build-up scalar for two cases with different droplet diameter. In case 11 the diameter is D_w=3 mm and in case 13 is D_w=0.003 mm. Both refer to 2% water/air mass, V_w=150 m/sec at inlet, T_w=288°K at full speed. BUILDUP_DIFF is a user-defined scalar which is the subtraction of build-up mass (M_w) for D_w=0.003 mm (case 13) from build-up mass (M_w) for D_w=3 mm (case 11). It can be seen that BUILDUP_DIFF scalar has mostly positive values and this means that build-up mass is higher for D_w=3 mm droplets than D_w=0.003 mm. Hence, large droplets deposit more easily than fine droplets, which evaporate quickly

and their tracking in the CFD calculations stops. In addition to this, due to their low inertia, they can follow the air streamlines.

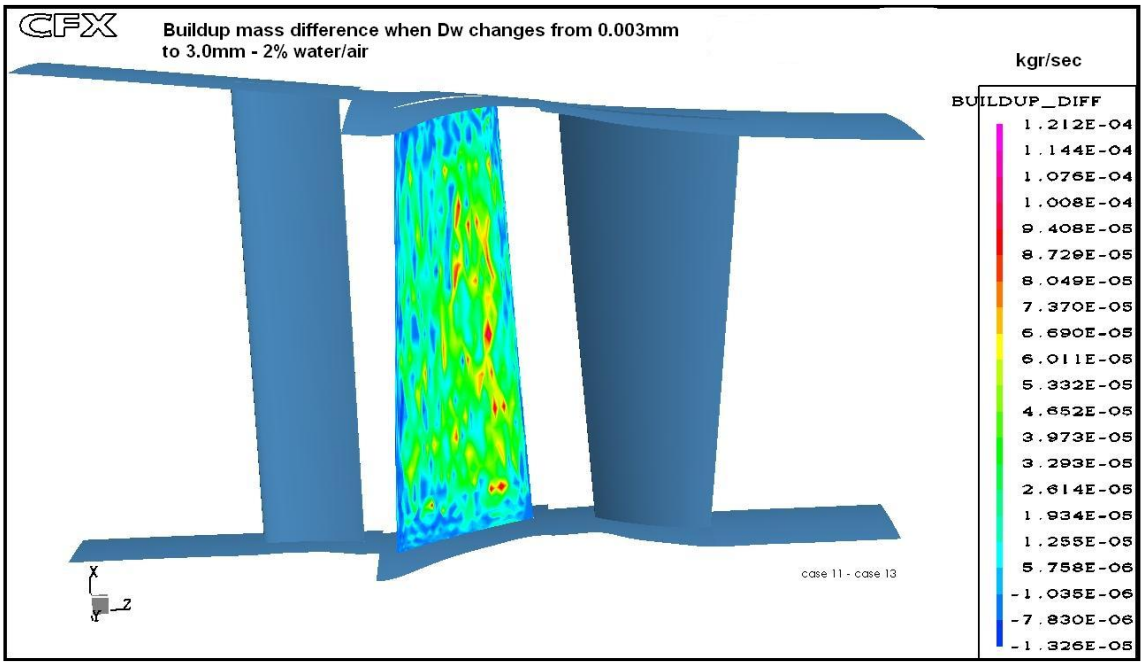

Figure 6-16: Build-up Mass Change for Different Droplets Size (0.003mm to 3mm, for 2% water/air, V_w=150m/sec)

When liquid water is ingested in the compressor, the air supplies the heat of evaporation and the water evaporates. Fine droplets evaporate at a higher rate because evaporative rate depends on the diffusion rate of vapour from the liquid droplet surface (chapter 4, equation 4-15). The high rate of fine droplets' evaporation relatively of this of large droplets is plotted in figure 6-17. For the two already described cases (11 and 13), H2O_VAP_DIFF is a user-defined scalar, which represents the water vapour (H2O_VAP) scalar subtraction of case 11 from case 13. It is worth pointing out that fine droplets of case 13 (D_w=0.003 mm) produce 16 times more water vapour than large droplets of case 11 (D_w=3 mm), at the stage outlet. However, in any case the produced vapour mass is negligible and does not influence the performance of the model. The subject is further analysed in subsection 6.6.4.

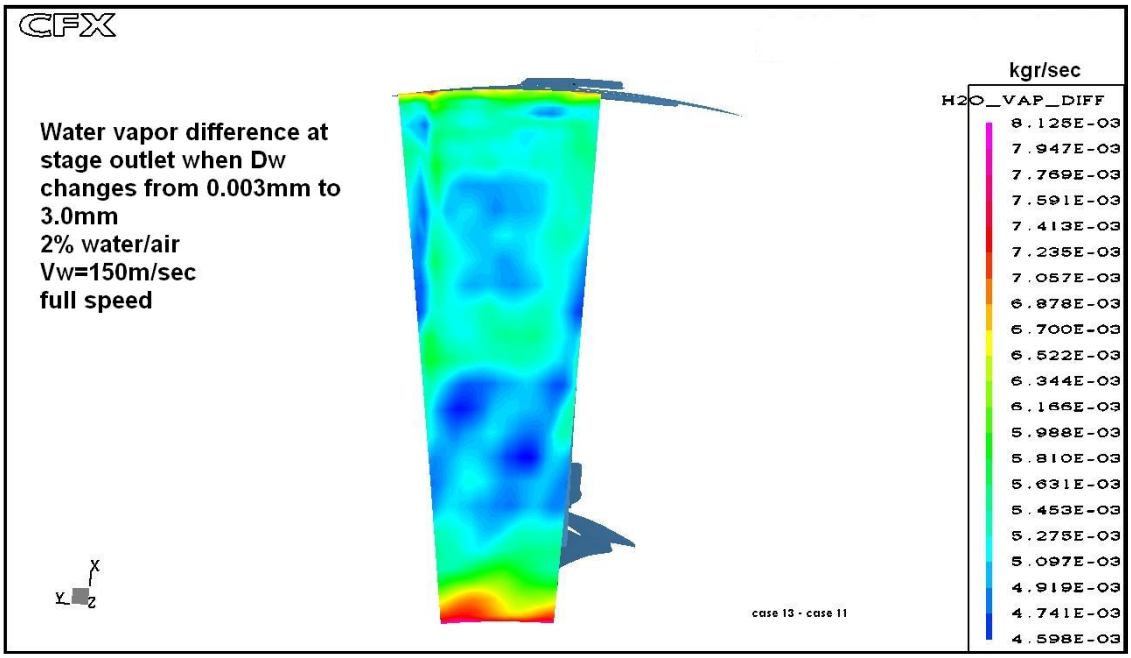

Figure 6-17: Water vapour change for different droplets size (0.003mm to 3mm, for 2% water/air, V_w=150m/sec)

In the CFD calculations, the water droplet size has varied from 1 μm up to 3 mm. As a result, the build-up water mass is minimized for fine droplets and this can be seen in figure 6-18. For 2% and 4% water, the build-up mass increases about 44% and 49% respectively, when the water droplet diameter changes from 1 mm to 3 mm.

It is worth noting that the rate of change in build-up mass does not follow that of droplet diameter. As noted above, fine water droplets follow the air streamlines. In this case, aerodynamic forces are adequate to divert the water mass. Nevertheless, when large droplets (which have higher moment of inertia), flow in the air path, they cannot follow air streamlines and hit on the blade pressure surface.

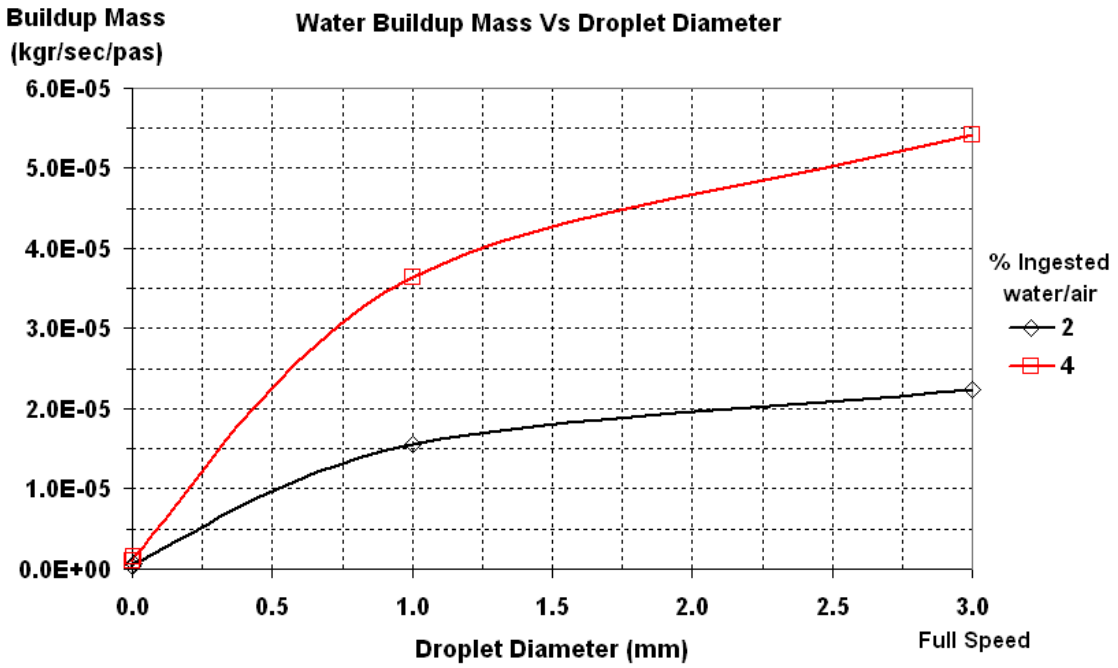

Figure 6-18: Water Build-up Mass Variation for Different Droplet Sizes

Consequently, water film appears to be thicker for large droplets. For constant rotational speed, an increased water build-up mass gives thicker water film. For 2% and 4% water, the film thickness increases about 16% for both cases, when the water droplet diameter changes from 1 mm to 3 mm. What is more, water droplet size has an influence on torque demand. Taking into account its impact on the water build-up mass and the film thickness, then the increase in torque seems to be as expected. The results show 56% torque increase for droplet change from 1 mm to 3 mm for both cases of water/air mass. The above data are presented in table 6-2.

Water Ingestion Parameters when D_w varies from 1mm to 3mm				
		Build-up Mass	**Film Thickness**	**Extra Torque**
Water/Air	2%	43.92%	16.56%	56.78%
	4%	48.82%	16.42%	56.70%

Table 6-2: Water Ingestion Parameters Variation due to change of Water Droplet Diameter

On the other hand, fine droplets seem to have negligible effect on the water ingestion parameters. Several cases ran for droplet sizes from 1 μm to 100 μm. It is shown that no considerable difference in water build-up mass and film thickness is produced over this range of droplet size. What is more, this is verified by experimental measurements in Williams J. et al. (2005), where droplets varied from 51 μm to 97 μm had the same effect on the compressor behaviour. However, in this experiment, there was no considerable change even with large droplets (≈1.5 mm), which contradicts the current simulation.

In the author's view, this can be attributed to the fact that the secondary phenomena, which take place when water flows in the air, are not included in the simulation. Given that large droplets are susceptible to break up or splash, it is concluded that the effects of droplet size increase are less intense when these phenomena take place. Even if large water droplets are ingested in the engine inlet, due to break up, smaller droplets impact on the compressor blades. The rate of droplet's size change requires further investigation with the appropriate software.

6.5.3.3 Effect of water droplet speed

Water initial ingestion speed (V_w) has an influence on build-up mass. Water droplets ingested to the compressor with low speed hit the blade mostly on the leading edge region. These can be clearly viewed in figure 6-19, which shows the water build-up mass alteration for two cases with different water ingestion speed. BUILDUP_DIFF is a user-defined scalar which is the subtraction of build-up mass (M_w) for V_w=50 m/sec (case 19) from build-up mass (M_w) for V_w=150 m/sec (case 10); 4% water/air, D_w=1 mm. It is worth noting that this scalar has negative values only at blade's leading edge region, which means that the droplets with V_w=50 m/sec impact on the leading edge while the droplets with V_w=150 m/sec occupy the majority of the blade pressure surface.

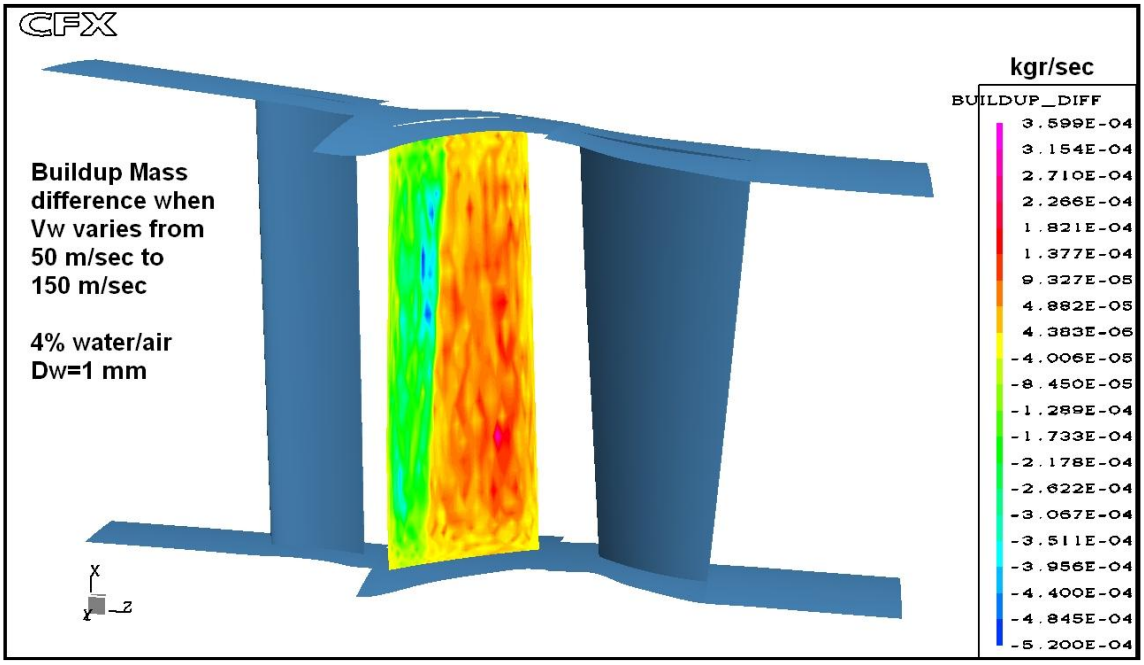

Figure 6-19: Water Build up Mass Difference when Ingestion Speed changes

Another issue is that the water mass, which deposits on the blade, reduces as the droplets' ingestion speed increases. When high-speed water droplets enter the compressor, although it is more difficult to follow the air streamlines (due to their inertia), the time they remain in the blade passage is shorter and the chances to hit on the blade are reduced. Data is exported for 4% water/air,

D_w=1.0mm and varying V_w from 150m/sec to 50 m/sec. In figure 6-20, the data is plotted on a percentage basis, using as initial values these for V_w=150 m/sec. Reducing V_w from 150 m/sec to 50 m/sec, build up mass increases 73% and torque 88%, relatively to values when V_w=150m/sec.

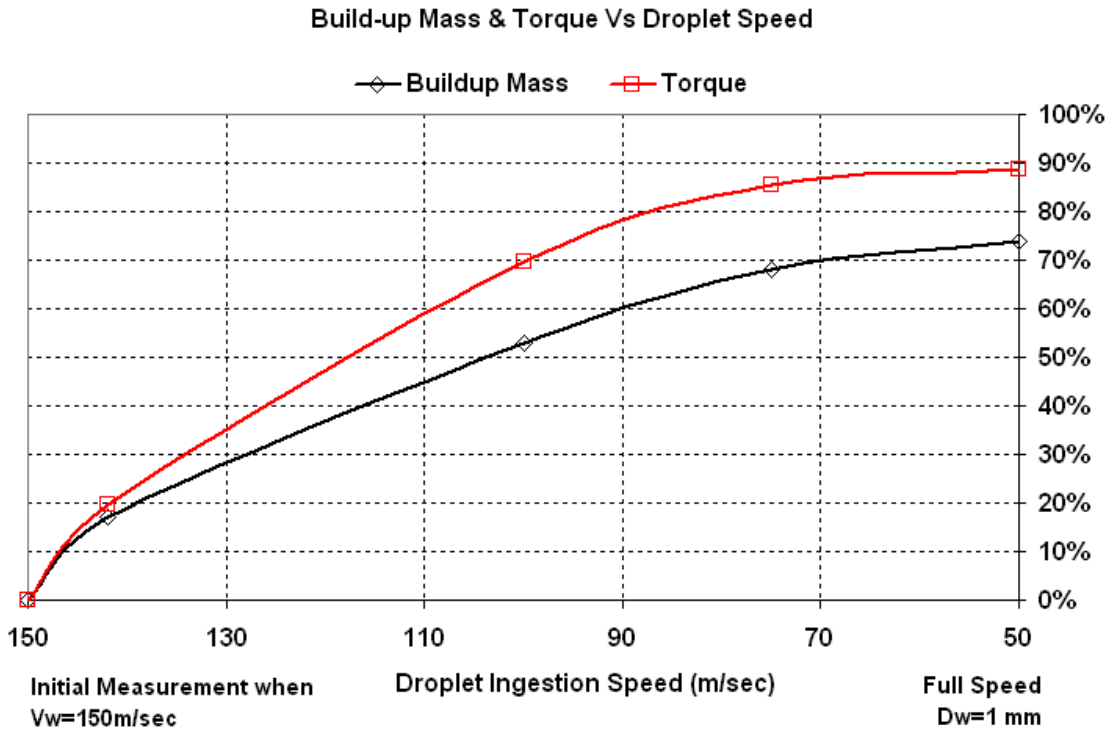

Figure 6-20: Build up Mass and Torque Variation when Droplet Ingestion Speed Reduces

It is noteworthy that the ingestion speeds used above are relatively high when they are compared with the values met in the physics of the phenomenon. Water droplets have significantly lower velocity than the air. This leads to an energy exchange between the water droplets and the air particles, which forces the air to reduced speed. That has an effect on the air velocity distribution and flow direction across the blade span. The attempt to simulate low speed water droplets (1 to 10 m/sec) was unsuccessful due to convergence problems of the code. It is found that the solver oscillates and very often diverges when a discrete phase is used and injected with very low relative speed. The lowest value of V_w, in which the code converged, was 50 m/sec. In this case (4% WAG, D_w=1mm) the air velocity at the rotor inlet was reduced by 3-8 m/sec (its dry value was 90 m/sec, thus the speed reduction ranges from 3.3% to 8.8%). However, the velocity distribution was not affected significantly, due to the uniform injection of water at the inlet. Figure 6-21 demonstrates the air velocity reduction.

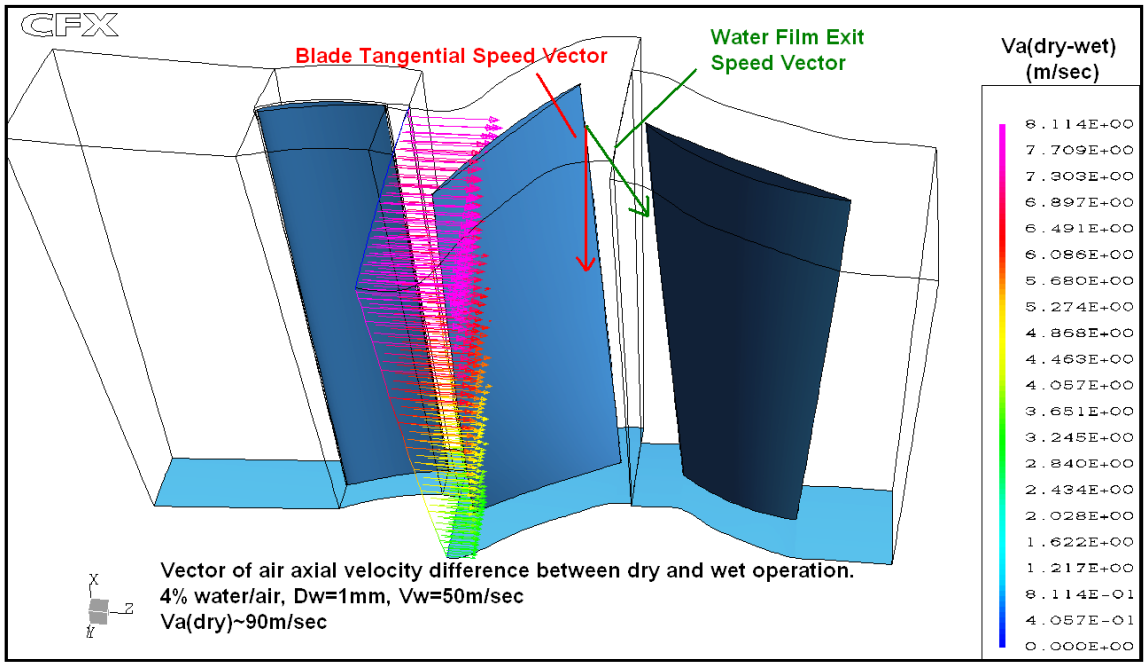

Figure 6-21: Air Axial Velocity Reduction due to Water Ingestion

Ingestion speed parameter has an effect on water film motion. This happens because when the water droplets impact on the already formed film, their momentum is transferred on that. Its direction is almost chord-wise and that gives a rise in total chord-wise force, which is applied on the water film. This force is calculated in the FILM MOTION program and affects water film motion. Consequently, the influence of this parameter is plotted in figure 6-22, where average speed is recorded when the water film leaves the rotor blade. It is shown that when V_w increases high momentum droplets cause an increase in film axial speed. Simultaneously, there is a small reduction in radial speed because, due to quicker axial motion, water exits of the blade and there is no time to obtain the high values of radial speed.

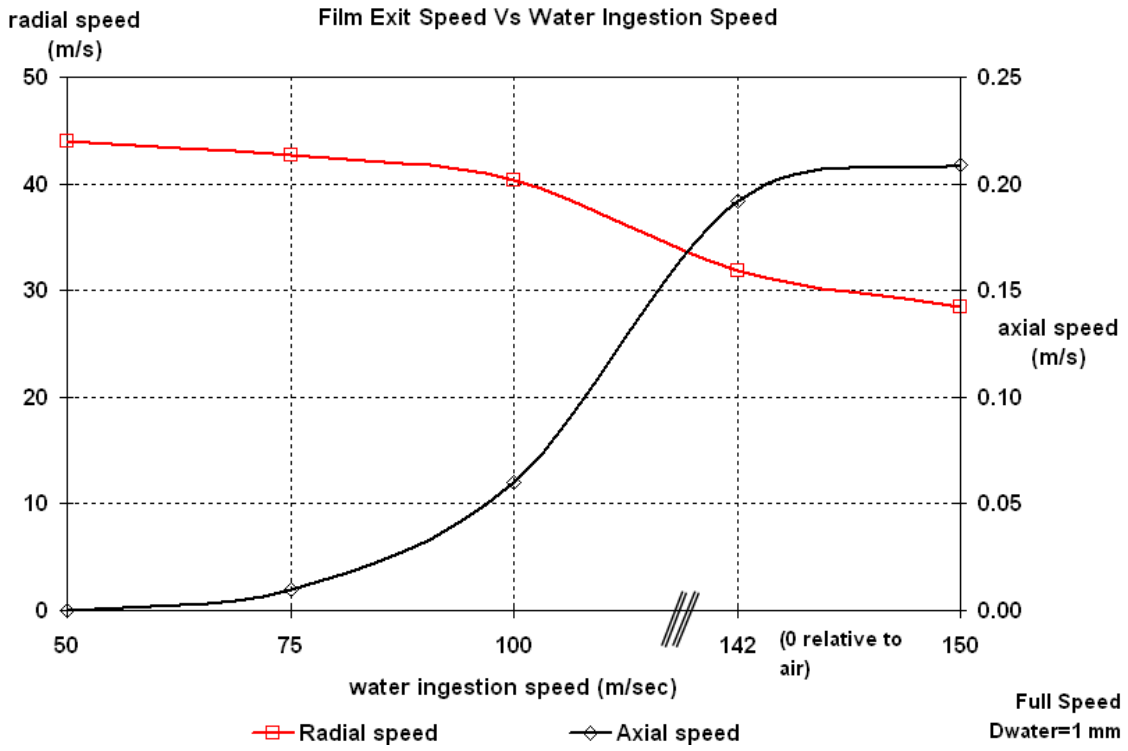

Figure 6-22: Water Film Exit Speed when Droplet Ingestion Speed Varies

6.5.4 Effect of rotational speed

Compressor's rotational speed has a great influence on ingested water. The centrifugal force acting on water film and torque due to water depends on angular speed. Water droplets, which deposit on the blade, are subject to centrifugal force. In addition to that, water droplets are accelerated at high speed in the tangential direction and then are decelerated to axial direction by the stator blades. Generally, at full speeds, the increased air velocities will lead to higher deposition rates. This is a result of the fact that the water droplets will be less able to follow the curved gas streamlines.

A change in the compressor's rotational speed is accompanied by changes in pressure ratio and mass flow. Bearing in mind the IGV angle, the compressor works at a new operating point. Compressor map is more than necessary to calculate the values of the compressor's parameters. In this study, the compressor map is not available for the model. To investigate the effects of the compressor's rotational speed, it is assumed that all the data files (build-up mass, shear stress, water droplets momentum) are kept constant. Therefore, data from full and idle speed cases are used and the angular speed is changed from 20% to 100%. To exaggerate the problem, 30% of water ingestion mass is used (i.e. W_w=0.4056 kgr/sec full speed, W_w=0.2707 kgr/sec idle speed).

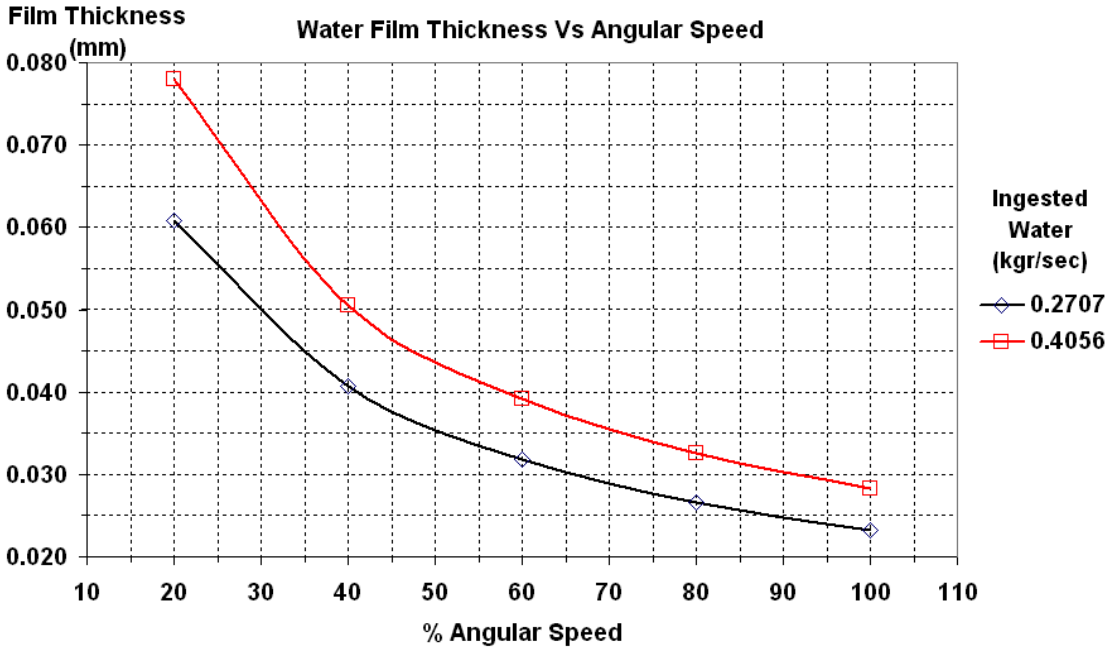

Figure 6-23: Water Film Thickness Change due to Angular Speed

Film thickness is affected by the change of rotational speed. When angular speed reduces, the film becomes thicker. The reason is that the film moves with lower speed (lower centrifugal force) and taking into account the mass continuation, the film thickness increases. Diagram in figure 6-23 shows the change in film thickness with angular speed reduction from 100% to 20%. When W_w=0.4056 kgr/sec (water ingestion conditions at full speed) the reduction of film thickness when angular speed increases from 20% to 100% is 63.7% (from 0.078 mm to 0.028 mm). In idle speed water ingestion conditions W_w=0.2707 kgr/sec the reduction is 61.8% (from 0.06 mm to 0.023 mm). It should be noted that the air mass flow remains unchanged (i.e. build-up data is the same for every angular speed case) for the research purposes.

It is noteworthy that water film thickness reaches values of few hundredths of mm in case of a compressor rotor blade, where the centrifugal force has dominant effects. For the rotor blades, there are not any experimental values, possibly due to the difficulties of obtaining the measurements. Using FILM_MOTION program, the calculations for zero rotational speed (stator case) revealed that in case of a stator blade, the values of water film height counts a fraction of a mm. This has been verified from the relevant literature [Gyarmathy (1962), Kirillov and Yablonik (1968)].

Since water film radial and axial speeds are known at each node, it is easy to plot the speed vector angle, which is shown in figure 6-24. It is worth pointing out that film motion is nearly radial at a big range of angular speed. For speeds higher than 40%, the speed vector angle is above 77°. It is highlighted that Williams and Young (2006) arrive at the same conclusion. In their theoretical approach, they argue that this angle is about 82° (8° from the radial direction).

The small difference is justified by the fact that they include the friction force in their calculations. They also use a high friction factor, which leads to more radial water flow.

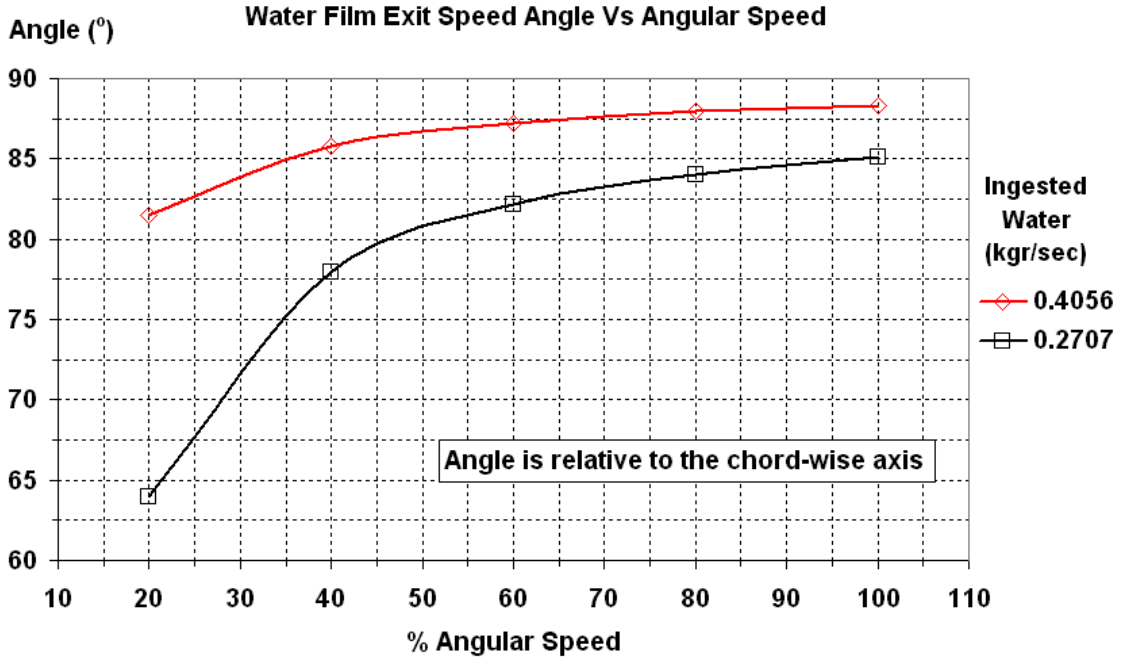

Figure 6-24: Water speed angle change due to angular speed

6.6 Compressor Performance Results

6.6.1 Isentropic Efficiency (ETA)

CFD results for $T_{t,out}$, PR, C_p and C_v are used to calculate for each case the compressor isentropic efficiency (ETA). The calculation is based on the equation 6-15:

$$ETA = \frac{\left(\frac{P_3}{P_2}\right)^{\left(\gamma-1/\gamma\right)} - 1}{\left(\frac{T_3}{T_2}\right) - 1}$$

Equation 6-15: Compressor Isentropic Efficiency Equation

As noted above, water ingestion has a detrimental effect on a compressor's performance. The post-processing of CFX-Tascflow results strengthened the above fact. The results showed deterioration in ETA, which is higher at high quantities of water ingestion mass. The effect is more pronounced at part speed and especially at the idle region of operation (65%). For 30% water the degradation in ETA is 17% at idle speed and 4% at full speed. For 4% water

ingestion, which is the value for gas turbine certification tests, the ETA deterioration is 8.5% for idle speed, 1.6% for full speed (figure 6-25 and 6-26).

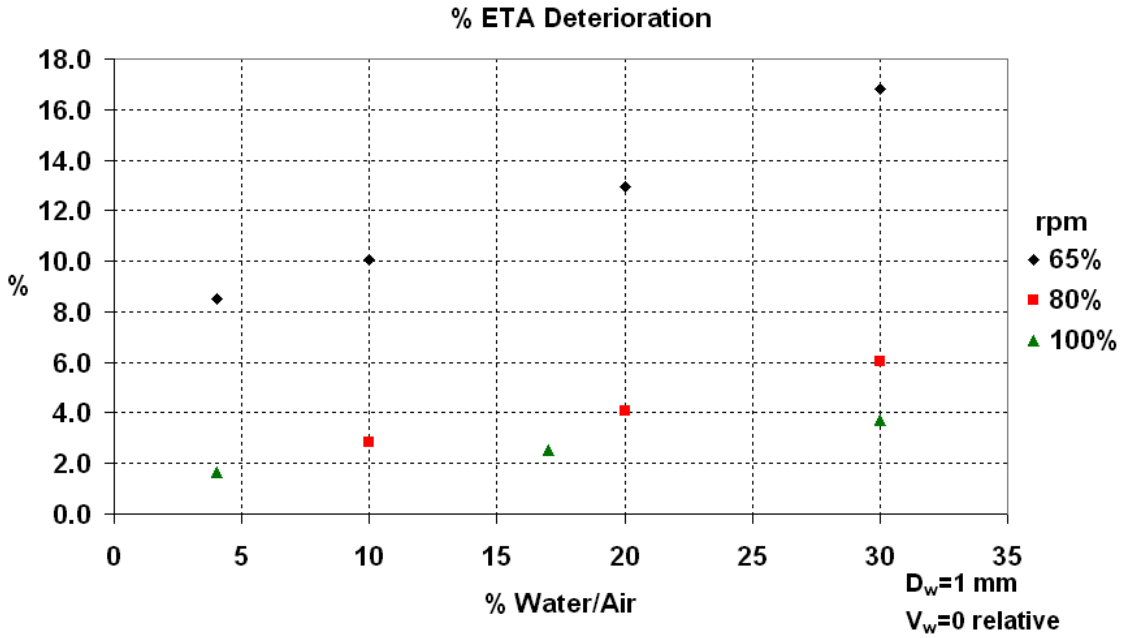

Figure 6-25: Efficiency Deterioration due to Ingested Water Mass

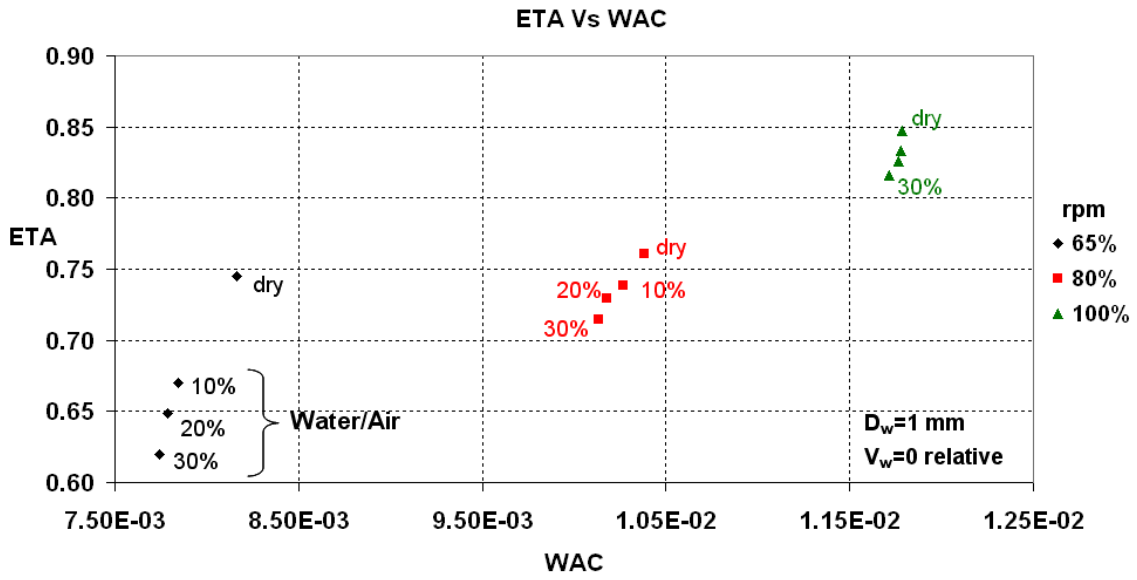

Figure 6-26: ETA – WAC Deterioration due to Ingested Water Mass

Figure 6-26 shows the ETA and WAC deterioration for 10%, 20% and 30% water/air mass. The effects of water ingestion are more obvious at part speed because the water film is thicker due to lower centrifugal force. By considering the mass continuity, the liquid film flows at lower velocities but higher thickness.

In Murthy et al. (1986) water ingestion tests were conducted in a high speed, 6-stage axial flow compressor. It was found that the deterioration in adiabatic

efficiency in a single stage of the above compressor was about 4% for 15% water ingestion.

Similar results were obtained in Williams J. et al. (2005), where the isentropic efficiency was experimentally estimated for a 3-stage axial flow compressor under water ingestion conditions. The authors measured the actual pressure rise for both wet and dry conditions at the 3rd stage of their compressor. Comparing them with the ideal pressure rise, it was observed that the isentropic efficiency in the compression process was reduced about 5% when 17% water/air mass was ingested into the compressor. The measurements were taken from several points along the blade span and the reduction was particularly high in the outer region of the annulus. Possibly, that happened due to the blade tip clearance, which was affected by the presence of water.

6.6.2 Pressure Ratio (PR)

The deterioration in PR is small and above 80% rpm, it was below 1%. For cases with 4% water ingestion mass, the deterioration in PR is negligible (0.4%-0.6%, figure 6-27). The compressor pressure rise, especially at idle speed, further deteriorates with higher quantities of ingested water.

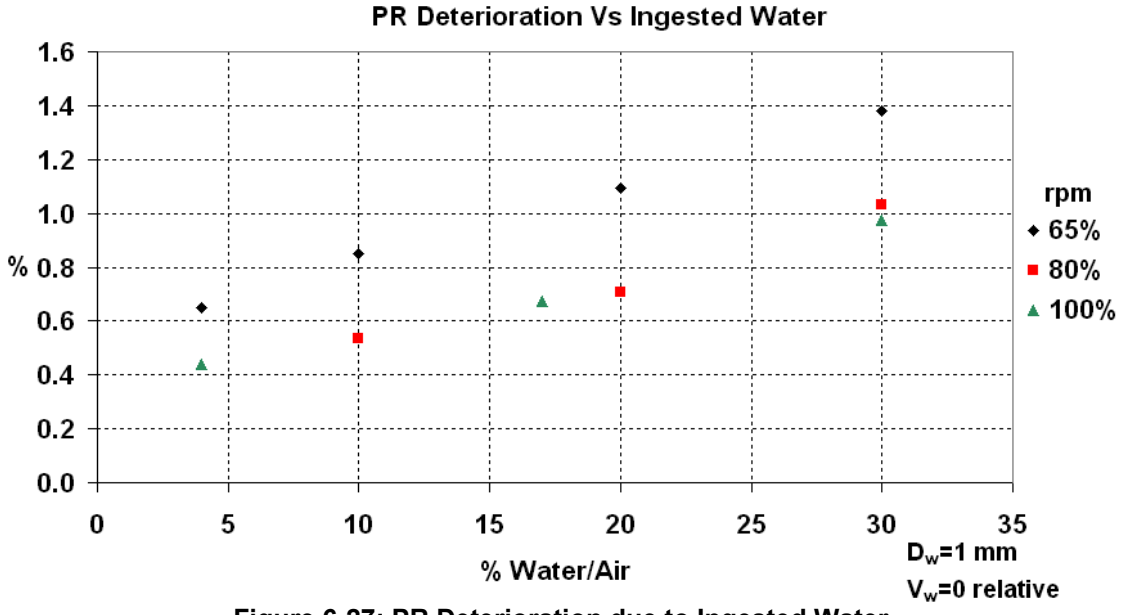

Figure 6-27: PR Deterioration due to Ingested Water

PR deterioration under water ingestion conditions is caused by the same physical mechanisms, which are responsible for ETA and they have been described above. Comparing the values in figure 6-27 and 6-28 with the results in experiments described in Williams J. et al. (2005), it is found that in the numerical simulation there is an underestimation of PR deterioration only at high values of ingested water. In the latter case, PR degraded about 1% and

10% for 4% and 10% water respectively. Both results converge to the point that small amounts of water have little effect on pressure rise coefficient.

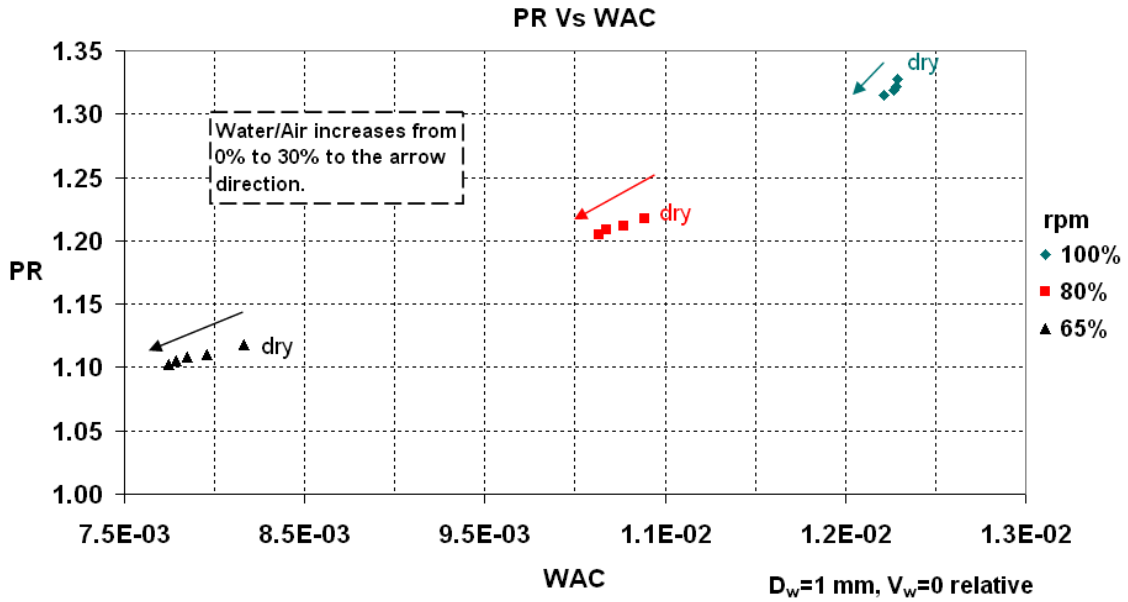

Figure 6-28: PR – WAC Deterioration due to Ingested Water

In addition to that, the experiments described in Murthy et al. (1986) showed that 15% water ingestion caused a reduction in single stage PR of about 5%.

6.6.3 Non-dimensional Mass Flow (WAC)

Having analyzed the effects of water in ETA and PR, the mass flow deterioration is plotted in figure 6-29, using the CFD results. The physical mechanisms responsible for this remain the same. As noted above, water film thickness is added to the blade profile. What is more, air shear stress and water droplets momentum cause waves in water film's surface, increasing the blockage effect. Consequently, the aerodynamic performance of the blade deteriorates reducing the mass flow capacity.

The effects are more pronounced at idle speed, where a 2.4% WAC deterioration is caused by 4% water/air. At high rotational speed, film thickness is extremely low and the effects in aerodynamic performance are almost negligible.

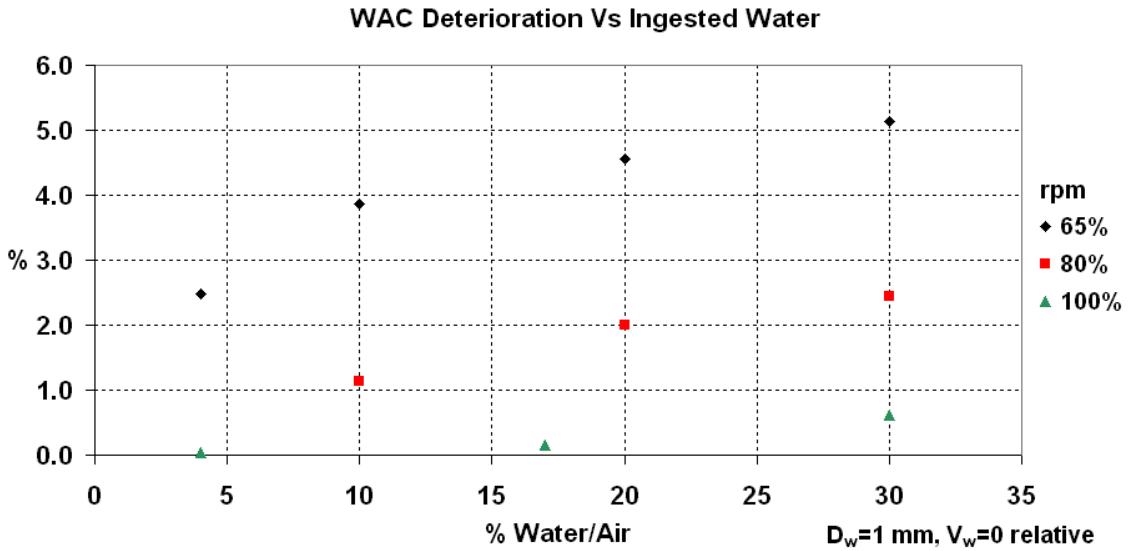

Figure 6-29: WAC Deterioration due to Ingested Water

6.6.4 Water Evaporation

When liquid water is ingested in the compressor, the air supplies the heat of evaporation and the water evaporates. Consequently, there is a reduction in $T_{t,outlet}$ and this is clearly demonstrated in figure 6-30.

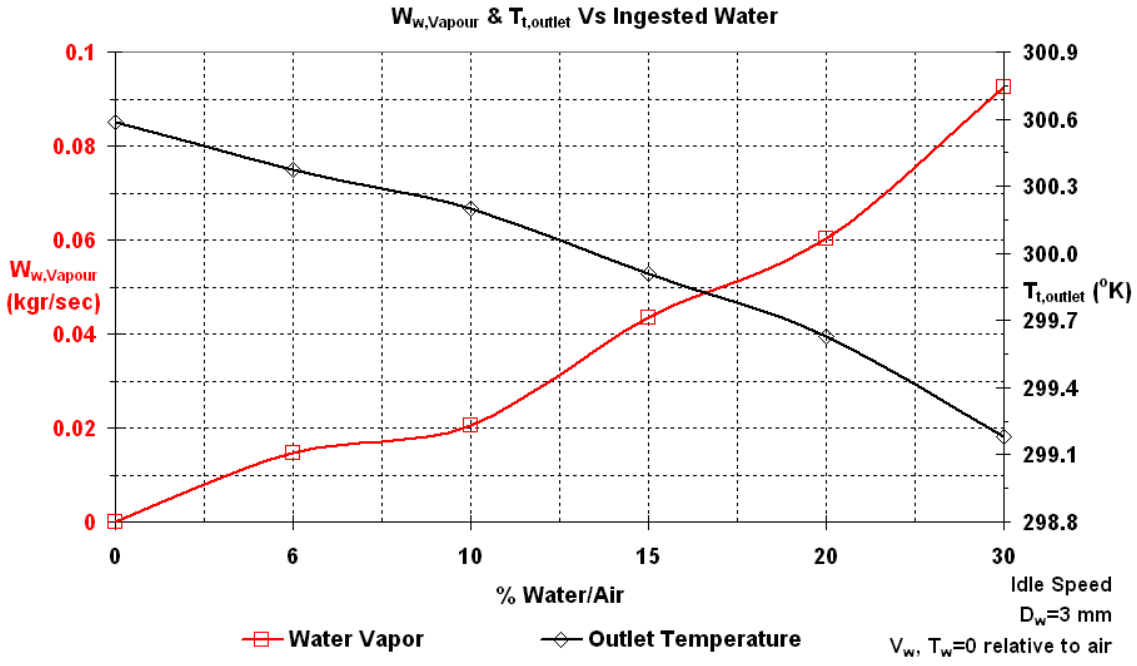

Figure 6-30: Water Vapour, Outlet Total Temperature Change due to Ingested Water

Moreover, water vapour presence causes a change in gas composition. This leads to an increase of C_p and C_v. In the current research, it is found a 0.24% and 0.26% increase of C_p and C_v respectively, taking into account that these values refer to the compressor first stage outlet for D_w=3 mm.

It is noteworthy the water mass, which changes phase from liquid to vapour, is only a tiny fraction of the total water mass. The results confirm the above statement. At part speed, for D_w=3.0 mm, when the water mass varies from 2% up to 30% the produced water vapour is only 0.47% - 0.63% of the ingested liquid mass. At the same time, there is a slight reduction in static temperature of about 1°K. In case of a multistage compressor, water evaporation is more evident in the last stages, where the temperature level is higher. Thus, the phenomenon should be simulated by using a multistage compressor model for more accurate results. However, in case of water ingestion, the thermodynamic effects in the compressor are negligible compared with the aerodynamic or the mechanical effects. Water evaporation takes place mainly in the combustor. The above are supported by published work presented in chapter 4. Hence, investigating this by using CFD methodology is suggested for future work.

6.7 Data Processing

The aforementioned data, according to the project's methodology, is intended to be used as a database in Turbomatch performance simulation code. For this reason, the extent of rotational speed range is necessary. Given that data for 65%, 80% and 100% rpm are available from CFD work, it is decided to use FORECAST function to calculate performance deterioration data for 30% and 120% rpm. Thus, in simulation code, engine rotational speed ranges from 30% to 120%.

The FORECAST function is accessible in MS Excel spreadsheet. It calculates a y-value for a given x-value by using other y and x known values. The calculation is based on linear regression method. Details are given in Appendix E.

Finally, block data is created, which is formatted in FORTRAN computer language file. In figures 6-31, 6-32 and 6-33, the relevant data for compressor ETA, PR and WAC deterioration is plotted.

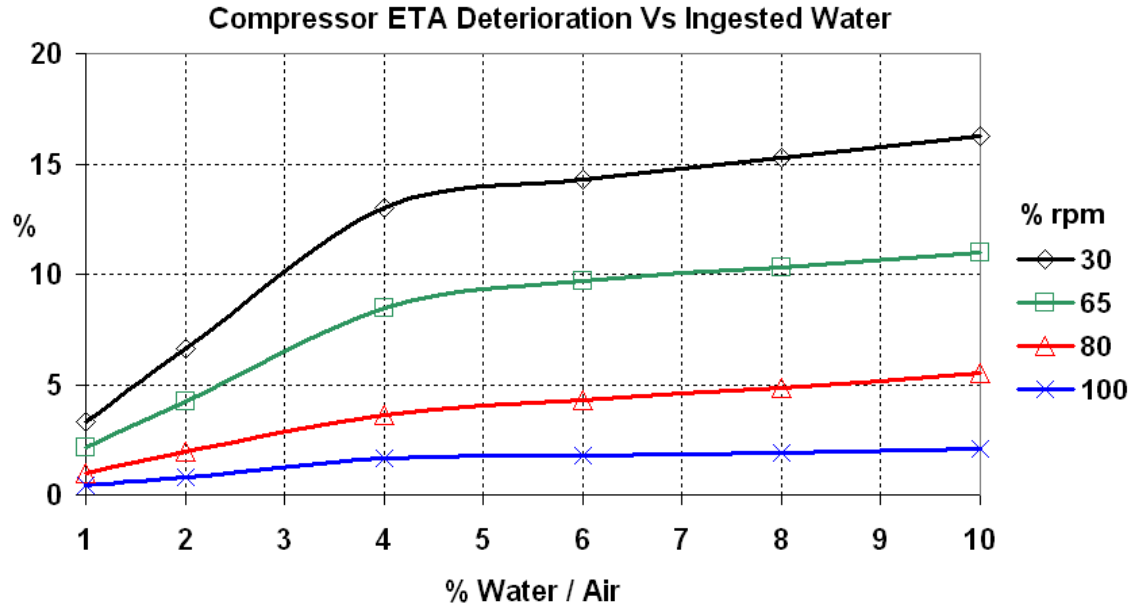

Figure 6-31: Compressor ETA Deterioration Processed Data

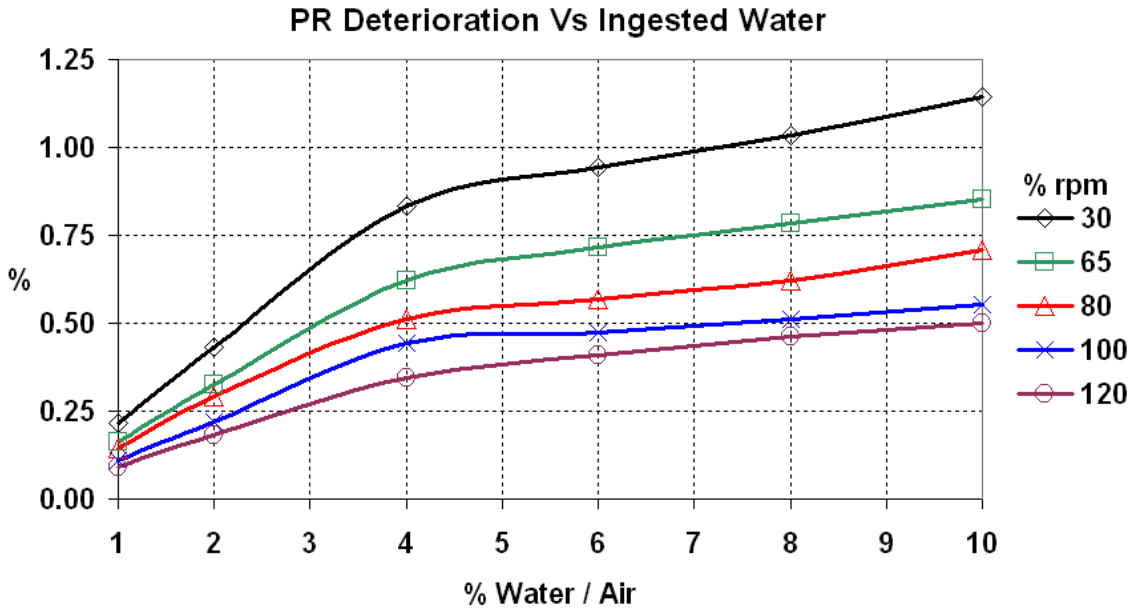

Figure 6-32: PR Deterioration Processed Data

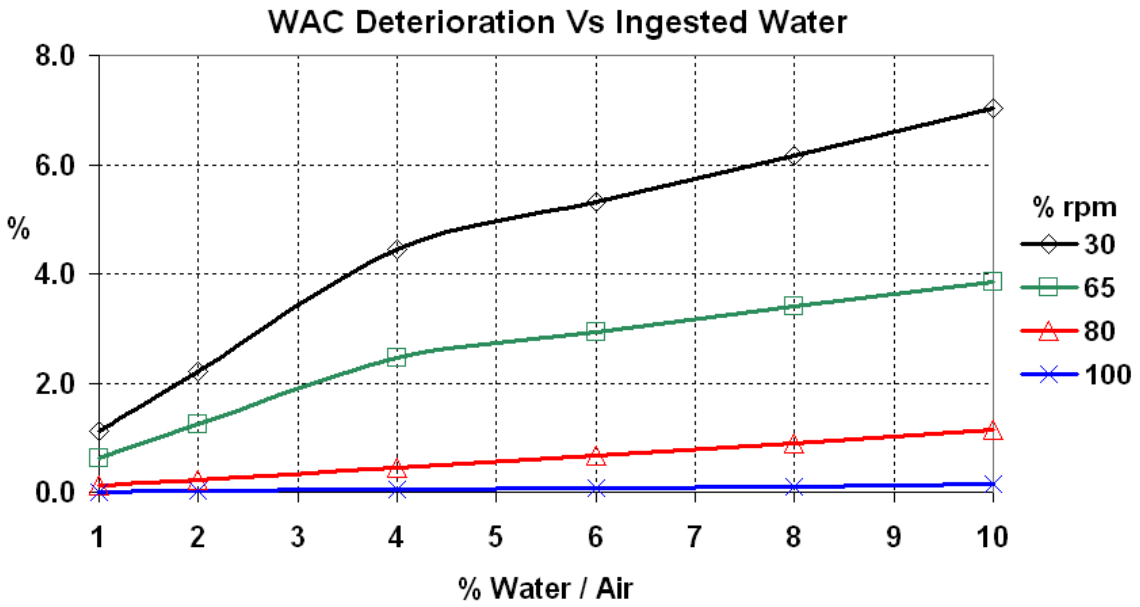

Figure 6-33: WAC Deterioration Processed Data

It is assumed in the theoretical calculation of water torque (subsection 6.4.3) that when the water film exits from the rotor blade, its velocity is equal to that of the blade's speed and in the tangential direction. What is more, no slip condition is assumed and no friction factor has been taken into account in this calculation. However, it is certain that the film exit velocity is not tangential or axial (figure 6-21). In addition to this, when the film thickness reaches a critical height, it collapses, part of it forms rivulets of water and the other re-enters to the airflow. This means that not all the water quantity is subject to centrifuging. Thus, the above assumptions result in overestimating the torque demand, which is considerable especially at full speed calculations [Nikolaidis Th. et al. (2008)].

The torque outcome is imported in the upgraded Turbomatch code described in the next chapter. It is found that the code cannot converge even with tiny ingested water mass and it goes easily out of the standard components map. The cause is the high values of compressor torque introduced in the code through the water ingestion mode.

To alleviate the problem it is decided to approach again torque estimation with the assumption that the water film exit velocity is half of the blade speed. This counterbalances the exclusion of film breakdown, friction force and slip condition of the initial torque calculation. The estimated torque increase due to the mechanical processing of the water droplets is plotted in figure 6-34.

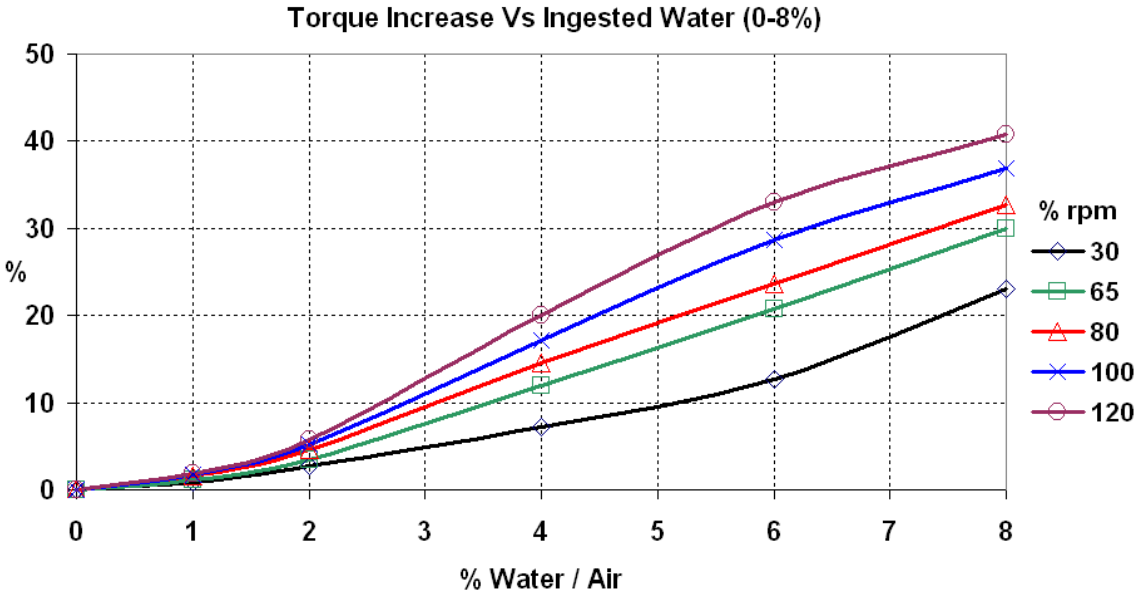

Figure 6-34: Torque Increase Processed Data

It is worth pointing out that the water mass is the dominant factor, which mostly influences the compressor's performance. Consequently, it is chosen to focus on this parameter attempting to model the water ingestion effects, described in the next chapter.

6.8 FILM_MOTION Results Validation

A thorough literature research has been done to explore experimental results about liquid film formation due to gas-liquid flow. It is found that considerable work has been done in Hammitt et al. (1975a), Hammitt et al. (1975b), Hammitt et al. (1981) in a wet steam tunnel in University of Michigan. The tests focused on film thickness measurements caused by liquid water on a flat plate and the effect of a concurrent steam flow. Their objective was to investigate the behaviour and the stability of thin liquid film formed on the turbine blades during high velocity steam flow.

In the above experimental facility, liquid water was injected near the leading edge of the plate at known rates and it flowed under the influence of a steam flow. The film thickness was measured for different liquid film flow rate and steam velocity and its values varied from 50 to 200 μm for water flow rate 5 to 60 cm^3/min. It was observed that the measured film thickness was reduced when the steam velocity was increased.

At the same time, theoretical calculation of film thickness was done by assuming that the gas shear force equals with liquid shear force at the interface, and the velocity profile in the film flow is linear. Both theoretical and experimental results were exported and plotted in figure 6-35. Film thickness measurements were almost double the values of the theoretical calculations.

The error was attributed to the interface shear force estimation. Therefore, it was confirmed that there is indeed a friction factor between liquid film and high-velocity gas, which is influenced by the film wavelet characteristics.

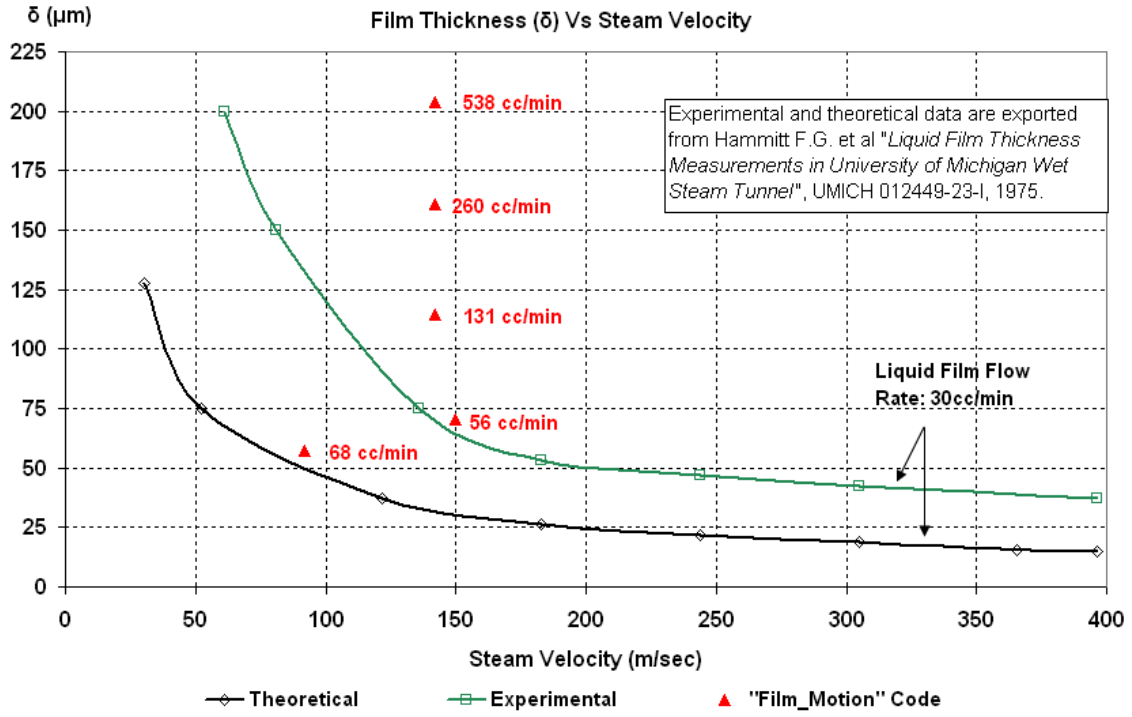

Figure 6-35: Film Thickness Measurements and Theoretical Calculations

Water film thickness on a stator blade calculated by FILM_MOTION code for various flow rates is shown in figure 6-35. Inlet air velocity is known for three group cases (92, 142 and 150 m/sec) and they are displayed at the Steam Velocity axis. Liquid film flow rate is converted to cc/min (cm^3/min) just for comparison purposes. It can be supported that theoretical results either from Hammitt et al. (1975a) or FILM_MOTION code underestimate the film thickness calculation. This is caused by the interface shear-force estimation, as it is discussed above.

On the other hand, it can be argued that there is an agreement between the theoretical results at high air velocities, while at 92 m/sec air speed, FILM_MOTION value is low. In the author's view, the agreement shown in figure 6-35 is significant bearing in mind that, in FILM_MOTION code, not only any friction factor is taken into account but also the interface shear force is assumed equal with this in wall at dry condition. It is reported in Wurz (1976) that during experiments it was measured that the shear-force on a liquid film increases by approximately 30% in comparison with the dry wall condition. The droplets momentum, which is added in the interface shear-force theoretical estimation presented in this work, cannot counterbalance the change of the shear-force from dry wall to liquid film characteristics.

In Wurz (1976), similar tests were conducted but for supersonic air velocities (Ma=1.2 – 2.4). Film thickness measurements range from 20 to 40 μm confirming the asymptotic trend shown in figure 6-35 for high gas flow velocities.

The water film chord-wise (i.e. axial in case of a flat plate) speed is recorded by the FILM_MOTION code. Its value is exported when it exits from the rotor blade. It ranges from 0.2 m/sec to 2.3 m/sec depending on rotational speed and ingested water mass (figure 6-36). Values are higher at idle speed because the centrifugal force is lower and this enhances the film chord-wise motion. Experimental data is extracted from Williams J. et al. (2005) in which the water film axial speed estimated by simply timing how long it takes for the water to exit from the test compressor. The test process is discussed in chapter 4. A velocity of about 1 m/sec was obtained for 15% water mass fraction. It is worth noting that this value lies between the values for idle (1.8 m/sec) and full (0.4 m/sec) speed. There is a significant agreement considering the tip clearance effects, which certainly alters the water flow characteristics.

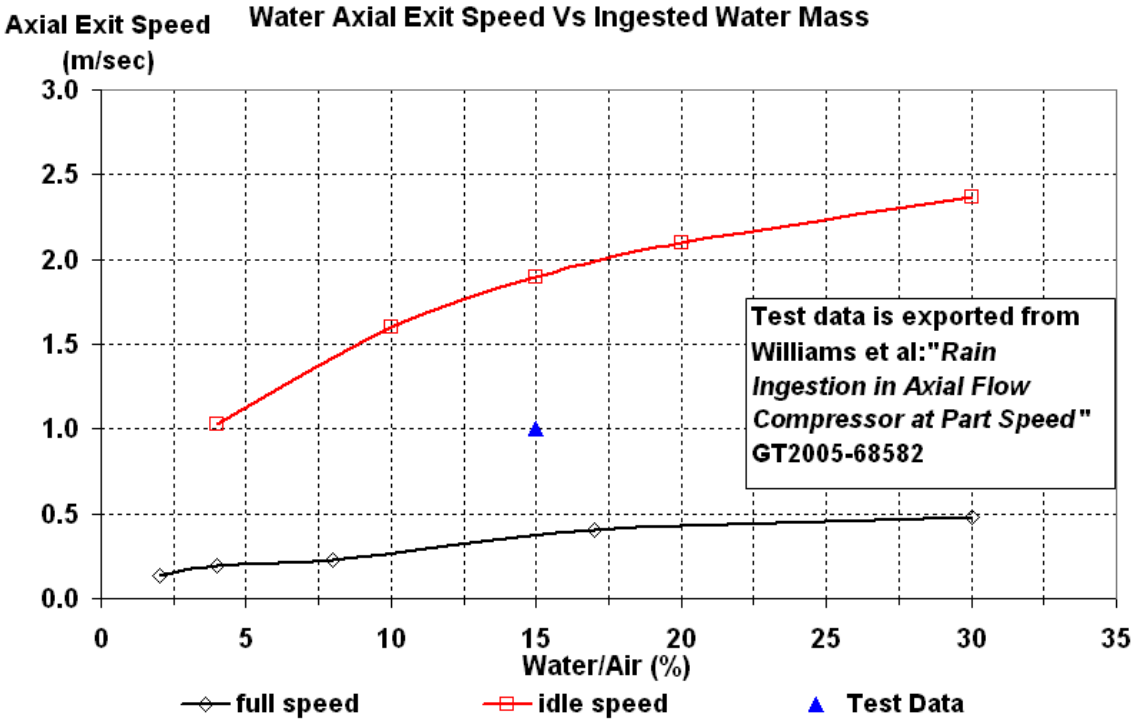

Figure 6-36: Water Axial Exit Speed Vs Ingested Water

Consequently, it is argued that FILM_MOTION code gives relatively reliable results. Although, it has been created for calculating the water film parameters flowing on a rotor blade, its results are compared with these from two-phase flow tests on a flat plate. Its accuracy can be improved by further investigating the interface shear-force between liquid water film and airflow. The latter certainly demands the inclusion of experiments in the research process to validate thoroughly any theoretical calculations.

6.9 Concluding Remarks

Computational analysis presented above proves that inertial impact is the dominant mechanism in droplet's deposition. Water droplets impinge mainly on the blade's pressure surface.

In water ingestion, the dominant parameters are the water mass and the rotational speed of the blade. The latter has a major impact to centrifugal force. Film thickness is affected by the change of rotational speed. When angular speed reduces, film becomes thicker. The reason is that the film moves with lower speed (lower centrifugal force) and taking into account the mass continuation, water mass and consequently film thickness increases.

In the quantitative approach, water film thickness reaches values of a few hundredths of mm in case of a compressor rotor blade, where the centrifugal force has dominant effects. The increased radial force due to the assumption of no friction force and no slip condition, results in underestimating the film thickness. However, using FILM_MOTION program, the calculations for zero rotational speed (stator case) revealed that in case of a stator blade, the values of water film height counts few mm. That has been verified from the relevant literature Gyarmathy (1962), Kirillov and Yablonik (1968).

Fine droplets seem to have negligible effect on the water ingestion parameters. It is shown that no considerable difference in water build-up mass and film thickness is produced for droplet sizes from 1 μm to 100 μm. For larger droplets, there is a contradiction between experimental and theoretical results. This is done because the secondary phenomena, which take place when water flows in the air, are not included in the theoretical approach.

Ingestion speed parameter influences the water film motion. This happens because when the water droplets impact on the already formed film, their momentum is transferred on that. Its direction is almost chord-wise and that gives a rise in total chord-wise force, which is applied on the water film. The ingestion speed values used in the computations are relatively high when they are compared with the values met in the physics of the phenomenon. The attempt to simulate low speed water droplets was unsuccessful due to convergence problems of the code. It was found that the solver oscillated and very often diverged when a discrete phase was used and injected with very low relative speed.

In table 6-3, qualitative results are summarized for the discussed ingestion parameters, while in figure 6-37, torque variation is plotted under the influence of ingested water mass, its droplet size and its speed.

Parameter with increasing value	Build-up	Film Thickness	Torque
Ingested Water Mass ▲	▲	▲	▲
Droplet Diameter ▲	▲	▲	▲
Droplet Speed ▲	▼	▼	▼
Rotational Speed ▲	▲	▼	▲

Table 6-3: Water Ingestion Parameters and Simulation Qualitative Results

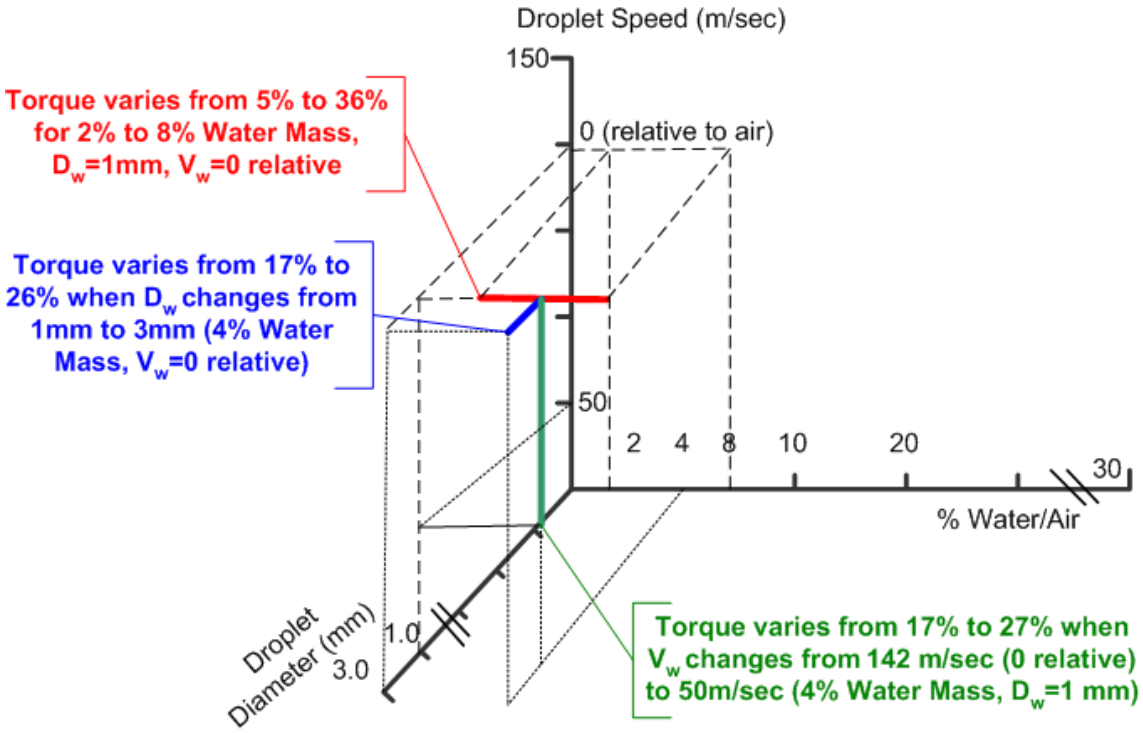

Figure 6-37: Water Ingestion Parameters Influence on Torque Demand

The mechanical processing of water has the greatest influence on compressor performance. The increase in torque demand is considerable and detectable even with small quantities of water. The aerodynamic effects are calculated but their influence is evident only in high values of water ingestion mass. Figure 6-38 displays the change in performance parameters when the ingested water content increases.

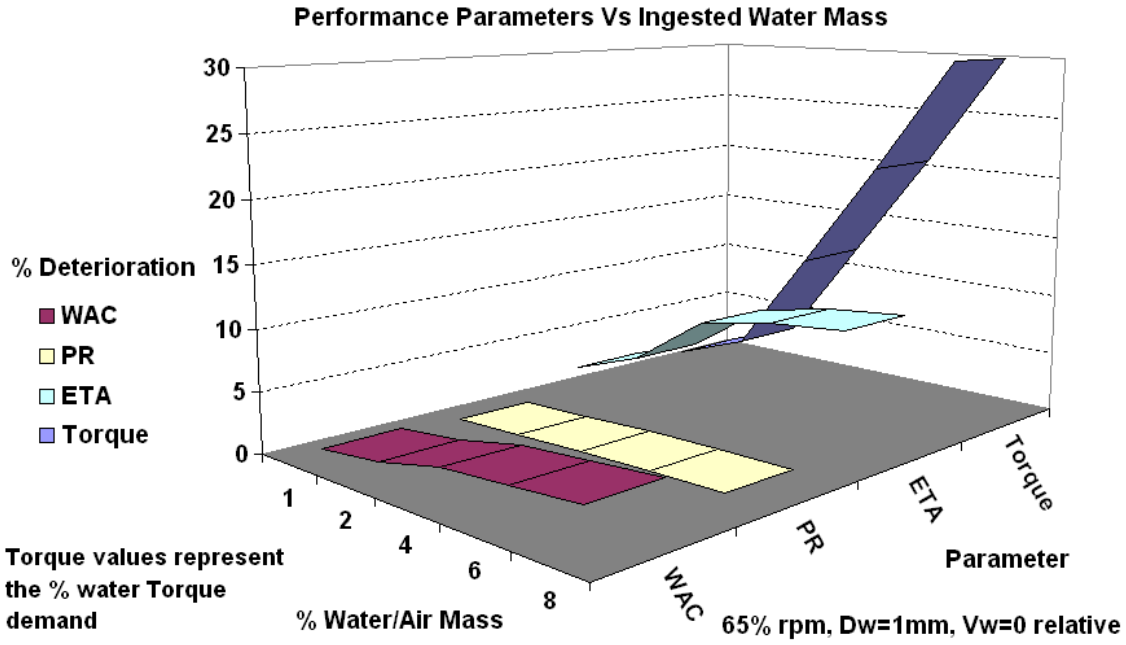

Figure 6-38: Performance Parameters Change due to Ingested Water

As far as the performance results are concerned, the deterioration in compressor ETA, PR and WAC is calculated. The physical mechanism includes the water film centrifugation towards the casing and the disruption of the airflow. In addition to this, water droplets have significantly lower velocity than the air. This leads to an energy exchange between the water droplets and the air particles, which forces the air to reduced speed. That has an effect on the air velocity distribution and flow direction across the blade span. Consequently, there is a reduction in ETA and pressure ratio PR. Tip clearance effects and this energy exchange are not fully simulated in the CFD model.

However, the results in the current research are comparable with these obtained from experiments especially in the high-speed region of operation. They seem that they overestimate the presence of the water on the rotor blade in the idle speed but that was expected since it was assumed that no bouncing, coalescence or rebounding of the water took place. Apart from that, the deterioration is calculated by linking the blade surface roughness with the film thickness. This theory is applied for first time in water ingestion modelling and gives quite significant results. Nevertheless, the correlation between the water film thickness and the equivalent sand-grain roughness needs further study.

Finally, it is noteworthy that the strong points of this study are:

- The inclusion of air shear force in the water droplets motion on the blade pressure surface,

- The incorporation of the water droplets momentum, which deposit on the blade, into the liquid film motion calculations,

- The involvement of liquid film wavy characteristics on the aerodynamic performance of the blade,

- The calculation of the compressor torque demand due to liquid water centrifugation based on the water film mass, its thickness, its velocity and the position (i.e. radius) when it exits from the blade pressure surface.

On the other hand, the weak points of this study are summarised as follows:

- The phenomena of droplet break-up and coalescence under the influence of high-speed air have not been taken into account. Moreover, it has been assumed that if the water droplets impinge on the blade pressure surface, they deposit on it (i.e. no splashing). The point can be improved by using upgraded CFD codes, which incorporate these effects.

- CFD code was unable to converge when low-speed droplets were injected (i.e. Vw≈5-10 m/sec). Thus, the energy exchange between them with the high-speed air has not been completely simulated. It is the author expectation that convergence could be achieved using upgraded CFD codes.

- The friction force between the liquid film and the blade surface has not been included in the model for the water droplet motion. Furthermore, the study has assumed that the blade is a flat plate without considering its geometry (i.e. stagger angle). The model can be improved by integrating Williams and Young (2006) work into the FILM_MOTION code.

- The compressor torque due to water is calculated based on the assumption that the rotor blade accelerates the water film to half of its tangential speed (i.e. this is the liquid film velocity when it exits from the blade surface). In the author's view, assuming that the liquid film obtains the tangential blade speed results in an overestimation of torque due to water. The former assumption gave more sensible results than the latter. In any case, the liquid film exit speed should be examined in detail.

- The tip clearance effects have not been included in this study. In this area, the water is splashed back into the blade span and further deteriorates the compressor's performance. The model can be improved considering the development of liquid film on the compressor

casing (simulated by a flat plate) and its motion under the shearing action of air.

- The model consists of one compressor stage preceded by an IGV blade row. The effects should be examined incorporating a multistage compressor model. The reason is that at the last stages of a multistage compressor some of effects are more intense (like evaporation) while some others (energy exchange between air and water particles) are alleviated. Although the computational resources may currently limit the creation of a fine multistage-compressor grid, it seems that this restriction would be overcome in the near future.

7 Water Ingestion - Engine Performance Simulation

Modelling the effects of water ingestion and integrating it in a gas turbine performance code is not as common as other features which may be included in their capabilities. This is because the phenomenon is complex and affects engine performance in a variety of ways.

The modification of the Turbomatch code in order to simulate the water ingestion phenomenon is presented in this chapter. At the beginning, the basic characteristics of Turbomatch are discussed, followed by an analytical description of the changes in the components performance calculations.

Afterwards, the results of several runs are showed commenting on the changes in performance parameters and how the code behaves. Finally, the chapter focuses on the validation necessary to assess the water ingestion modifications.

7.1 The Turbomatch Code

Turbomatch is a computer program developed by the School of Engineering of Cranfield University, to facilitate design and off-design point performance calculations for gas turbine engines. It is written in FORTRAN computer language and uses component performance maps [Cranfield University (2007)]. The upgraded version of the code (TURBOMATCH_stage04_v2_1/Sept 2007) enables ten maps for the compressor, one for the burner and twelve for the turbine.

Its library includes several subroutines (called “BRICKS” such as “COMPRE”, “BURNER”, “TURBIN” etc), which perform the thermodynamic calculations for the processes occurring in the engine components. Apart from that, there are also subroutines for arithmetic calculations to facilitate the estimation of engine overall performance.

Additionally, all the BRICKS are linked with a number of eight quantities (old version) known as the Station Vector of that station (inlet or outlet). The quantities in the order stated are:

Item 1	Fuel-air ratio	(dimensionless)	α
Item 2	Mass flow	(lb s^{-1} or kg s^{-1})	W
Item 3	Static pressure	(Atm)	p
Item 4	Total pressure	(Atm)	P
Item 5	Static temperature	(°K)	t
Item 6	Total temperature	(°K)	T
Item 7	Velocity	(ft s^{-1} or ms^{-1})	V
Item 8	Area	(ft^2 or m^2)	A

Table 7-1: Turbomatch Station Vector Items

It is worth noting that five of these quantities (α, p or P, t or T and any two of W, V or A) can fully describe the gas state of the station.

The input file includes the several case selectors for defining the characteristics for the simulation. Thus, there are selectors for Design-point (DP) or off-design (OD) calculations, Imperial (IM) or S.I. (SI) units, Kerosene (KE) or Diesel (DI) or Hydrogen (HY) or Natural Gas (type M:GM, type T:GT) fuel, Fixed geometry compressor and turbine (CT) or Variable geometry compressor or turbine (VA) and Full (FP), Short (SP) minimal (NP) printing or (XP) extra print.

The simulation is divided into two parts: the design point (DP) and the off-design point simulation. The former is the starting point for any engine design study. The off-design point includes the effect of changing the engine's parameters (such as compressor pressure ratio, TET, altitude etc). This program has proved to be reliable, accurate and extremely flexible for both amateur and experienced computer program users.

New features were added in the upgraded version of the code in September 2007. This version includes the effects of water injection in the burner and the change of fluid properties due to humidity. Therefore, two new station vector items were added: the injected water to air ratio (item No 9 - WAR) and the "water quality" (item No 10 - X). The latter declares the form of water (liquid, saturated steam or superheated steam) [Mucino (2007)]. Multi-fuel capability was also incorporated in this version.

In addition to that, new brick data in the intake and the combustor allow the user to simulate the engine's performance with different values for relative humidity (RelHum) at the intake and WAR and/or water injection temperature in the burner. To be more explicit, brick data 6 at the intake refers to air relative humidity, while brick data 4, 5 and 6 represent data for WAR, water injection temperature and water quality in the combustor [Mucino (2007)].

7.2 The Turbomatch Code with Water Ingestion Capability

The effects of water ingestion in a gas turbine engine performance are included in the Turbomatch new version (June 2008). A new module, named "*WaterIngestionDeterioration*" and the included new subroutines, has been added and calculates the deterioration, which is caused due to engine's operation in rain conditions. To be more specific, four new subroutines use data for the WAC, ETA and PR deterioration in the compressor and ETA, P loss in the burner due to liquid water. Furthermore, the extra torque TRQW needed by the compressor to accelerate the liquid water film, which is formed on the blade, is also calculated and added to the compressor work. The flowchart of the water ingestion software is presented in appendix G.

The water ingestion subroutines use data, which is stored in a block data file named "*WATERINGESTION*". Its shape is in the form of two-dimensional arrays (one for WAG change and one for the rotational speed N). The concept is based on the fact that, in case of water ingestion, WAG and N are the dominant parameters, which mostly affect the severity of the phenomenon. Thus, the water ingestion subroutines read the engine's rotational speed and taking into account the user's water to air ratio (WAG), calculate the appropriate deterioration percentage for WAC, ETA and PR. Moreover, the extra compressor torque TRQW due to liquid water is estimated using the same technique. It is worth noting that CFD has been used to calculate the performance deterioration data as it has been analysed in the previous chapter of this manuscript.

It has been written that the September 2007 version of Turbomatch incorporates the use of ten fluid properties as Station Vector items. To facilitate the water ingestion capability, one more property has been added as item No11 and this is the water to air ratio of liquid ingested water (WAG). Following this methodology, it is confirmed that this fluid property is available for any component (BRICK) in the engine model. Therefore, the programmer can handle the WAG in a way which depends on the component. For example, in the compressor, the water film formation on the blades is of primary importance while in the combustor evaporation is the dominant effect. WAG property is displayed in the result file (figure 7-1).

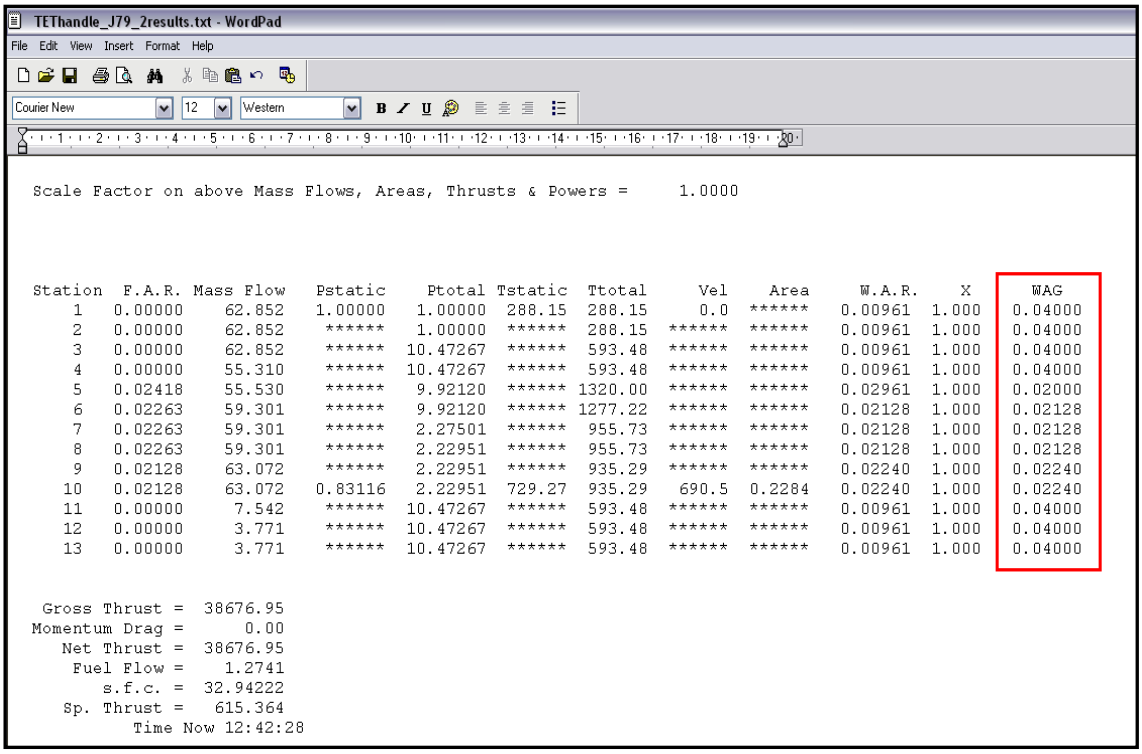

TEThandle_J79_2results.txt - WordPad

File Edit View Insert Format Help

Courier New 12 Western

Scale Factor on above Mass Flows, Areas, Thrusts & Powers = 1.0000

Station	F.A.R.	Mass Flow	Pstatic	Ptotal	Tstatic	Ttotal	Vel	Area	W.A.R.	X	WAG
1	0.00000	62.852	1.00000	1.00000	288.15	288.15	0.0	******	0.00961	1.000	0.04000
2	0.00000	62.852	******	1.00000	******	288.15	******	******	0.00961	1.000	0.04000
3	0.00000	62.852	******	10.47267	******	593.48	******	******	0.00961	1.000	0.04000
4	0.00000	55.310	******	10.47267	******	593.48	******	******	0.00961	1.000	0.04000
5	0.02418	55.530	******	9.92120	******	1320.00	******	******	0.02961	1.000	0.02000
6	0.02263	59.301	******	9.92120	******	1277.22	******	******	0.02128	1.000	0.02128
7	0.02263	59.301	******	2.27501	******	955.73	******	******	0.02128	1.000	0.02128
8	0.02263	59.301	******	2.22951	******	955.73	******	******	0.02128	1.000	0.02128
9	0.02128	63.072	******	2.22951	******	935.29	******	******	0.02240	1.000	0.02240
10	0.02128	63.072	0.83116	2.22951	729.27	935.29	690.5	0.2284	0.02240	1.000	0.02240
11	0.00000	7.542	******	10.47267	******	593.48	******	******	0.00961	1.000	0.04000
12	0.00000	3.771	******	10.47267	******	593.48	******	******	0.00961	1.000	0.04000
13	0.00000	3.771	******	10.47267	******	593.48	******	******	0.00961	1.000	0.04000

Gross Thrust = 38676.95
Momentum Drag = 0.00
Net Thrust = 38676.95
Fuel Flow = 1.2741
s.f.c. = 32.94222
Sp. Thrust = 615.364
Time Now 12:42:28

Figure 7-1: WAG property in the Turbomatch Result File

From the computer-programming point of view, the supplements of the new features (like humidity, water injection and ingestion) drove the code to be more complicated. What is more, the effects of water injection in the combustor and water ingestion due to operation of the engine under rain conditions, are completely different and there was a demand to separate the performance calculations. More to this point, the two phenomena refer to different types of gas turbine engines (water injection for power generation gas turbines and rain ingestion in aero-engines).

Consequently, it was necessary to distinguish the cases and provide the user the capability of choosing whatever he/she wants to simulate. Thus, a new case-selector set was developed in the new version of Turbomatch (June 2008) input file. For this reason three new set of character were added: DR for dry or only humidity case, WG for the water ingestion and IJ just for the water injection cases. The new code word string is: "*DPODIMSIKEDIHYGMGTCTVADRWGIJFPSPNPXP*" (the underlined letters are the new additions). If the user mistakenly declares a water injection case and the code tracks that there is an input value for WAG which is not zero, then an appropriate error message informs the user (figure 7-2).

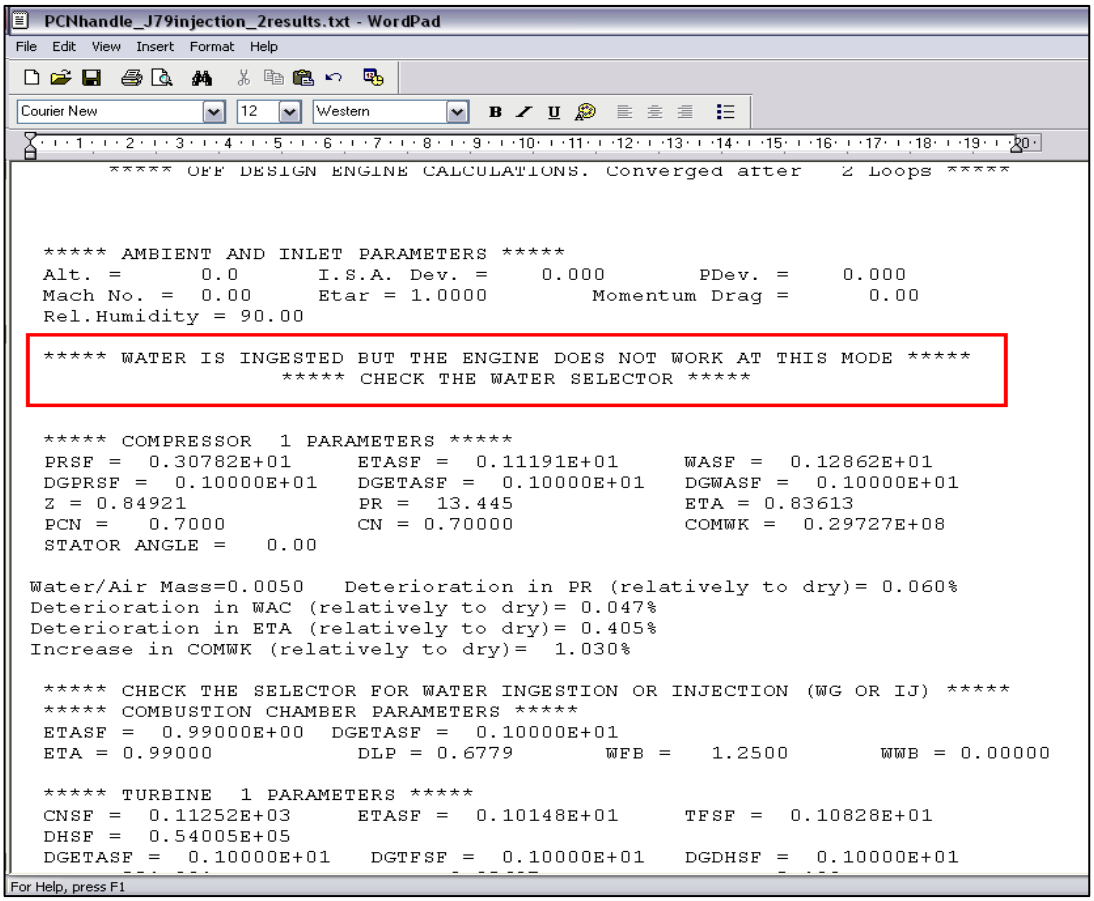

Figure 7-2: Turbomatch Case Selector Error Message

For the same reason, the “SELECT CASE” structure, which is a FORTRAN programming practice, was frequently used in new Turbomatch code. Therefore, sections of the subroutines TURBOMAT, INTAKE, combinedCOMPRE and BURNER were reorganized to accommodate the different mode of operation.

7.2.1 Intake

The INTAKE brick is used to estimate free stream static and total conditions at a given altitude and flight Mach number. For the calculations, the International Standard Atmosphere (ISA) is used and the code allows the user to include a deviation from standard static temperature and pressure. Moreover, at the intake exit, pressure recovery can be either stated explicitly, or calculated from the U.S.A.F. Standard Pressure Recovery - Flight Mach Number relations. Furthermore, the RelHum value is imported in No6 brick data item.

As far as the water ingestion is concerned, in the new version (June 2008) of Turbomatch, the user defines the ingested liquid water to air ratio at the intake. That can be done through the Station Vector item No11. Afterwards, the code uses this value for the subsequent water ingestion calculations.

It has been shown that the effects of humidity in the fluid properties are included in the Turbomatch code (September 2007 version). The new version (June 2008) incorporates the rain ingestion capability. Bearing in mind that humidity is strongly affected by the presence of rain, there was a need for the code to adjust humidity parameter with the rain meteorological conditions. In physics, RelHum inside a rain-cloud is 100% (i.e. the air cannot contain more water vapour and the water is in liquid form) and can be lower outside of it (depending on water content, pressure and temperature of the air). For the simulation purposes, it is assumed that, under similar conditions, this parameter is about 90% in the nearby atmosphere. Consequently, the Turbomatch modifies the value of RelHum and sets it to 90% when the simulation runs in the water ingestion mode (case-selector is “WG”) and the WAG value is slightly above zero (>0.001 arbitrary). It is worth noting that the user is informed for the condition by a message in the result file (figure 7-6).

It has been written in the previous chapter that apart from the liquid water to air ratio (WAG), two other parameters can influence the fluid flow on a gas turbine engine under water ingestion conditions. These are the water droplet diameter and its initial speed relative to the air. It was showed that their impact on the flow is not so pronounced comparatively with WAG. For this reason, they are not taken into account at this primary stage of the water ingestion capability development.

Furthermore, the phenomenon of droplet break-up or splashing is not simulated in the code. These dynamically change the water droplet diameter as it has been analyzed in chapter 4. However, WAG is the dominant parameter in the water ingestion phenomenon and as a result, the inclusion of droplet break-up or splashing was not regarded as necessary. The CFD codes the author espoused did not include droplet’s break-up and coalescence phenomena. In his effort to keep up with CFD, he found that their latest upgrade incorporates these effects (for example CFX-10.0). Unfortunately, the progress of this work and the time restrictions did not allow the author to get back and re-design the simulation. This is an area for further work.

7.2.2 Compressor

The compressor (or fan) outlet conditions and its work demand are calculated in the COMPRE brick. This subroutine reads data for the inlet conditions, design-point PR, ETA and CN. In addition to this, other subroutines provide data for off-design values of the above parameters based on the scaling of standard compressor maps. It is worth noting that is the code includes the capability of simulating the influence of compressor degradation on engine’s performance, using appropriate scaling factors.

In the new version of Turbomatch (June 2008), the degradation due to liquid water of compressor's performance is estimated. This is of great importance because the compressor in a gas turbine engine is the component, which suffers firstly the effects of water ingestion. Deterioration in its WAC, PR, ETA and TRQW as well, has been calculated using CFD. These values have been worked out on a percentage basis taking into account two fundamental factors: PCN and WAG. Deterioration in WAC, PR, ETA and TRQW due to water was estimated for PCN 0.3, 0.65, 0.8, 1.0 and 1.2 and WAG of 1%, 2%, 4%, 6%, 8%, 10% and 20%. The method has been thoroughly described in chapter 6. Finally, these values were used to build a block data in Turbomatch code.

Having said this, a subroutine, named "*SEARCHWATERDETER*" in the water ingestion module, reads the current value of PCN and WAG and utilizing the aforementioned block data, calculates the deterioration parameters by using the linear Lagrange interpolation method (equation 7-1 and figure 7-3). This gives the linear Lagrange polynomial by the equation:

$$f(x) = \frac{x - x_1}{x_o - x_1} f_o + \frac{x - x_o}{x_1 - x_o} f_1$$

Equation 7-1: Linear Lagrange polynomial

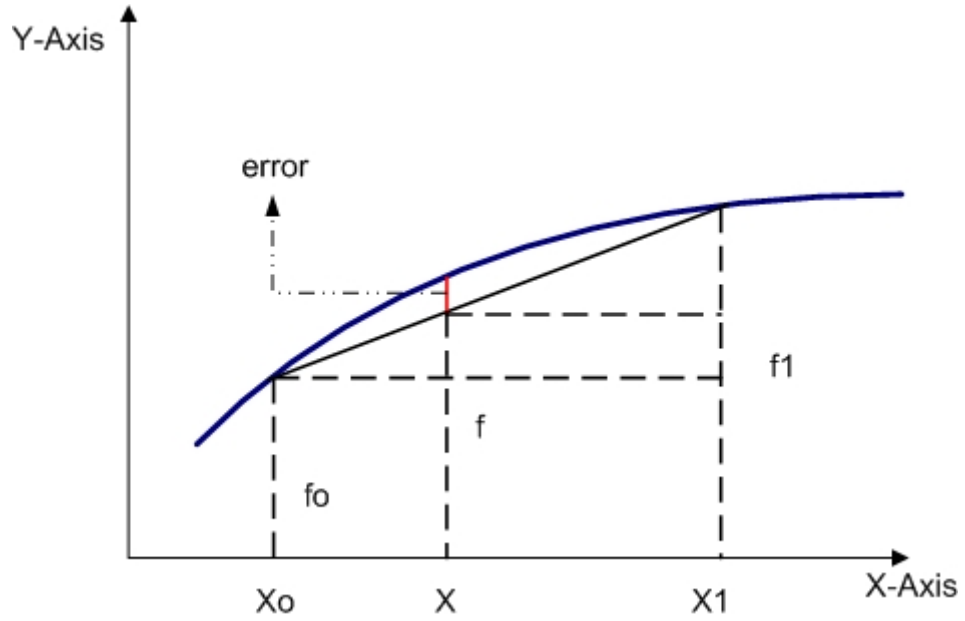

Figure 7-3: Linear Lagrange Interpolation [reproduction from Kreyszig (1999)]

Therefore, new values for compressor PR, WAC, ETA and the relevant work as well are computed in the COMPRE brick, resulting in a considerable alteration of compressor's performance. The latter is expressed by the compressor map, which is plotted on a non-dimensional basis, i.e. PR and ETA against WAC or corrected mass flow (CM) for fixed values of CN. The described method was tested using several existing engine models. The code run for both PCN and TET as handles. The results show that, in each case, there is deterioration in

compressor's characteristics. Section 7.3, in which the performance results are discussed, clarifies that point.

It is worth noting that an assumption has been made about the water evaporation in the compressor. In this case, it is assumed that there is no evaporation in the compressor. Ingested water concentrates in liquid form and occupies a negligible fraction of the annulus. Although a small quantity of water may evaporate in the last stages of a multistage compressor, it can be assumed that it has an insignificant effect on thermodynamic properties of the air. The author's view can be supported by the results found on CFD simulation analysed in chapter 6, subsection 6.6.4, where it is shown that only a tiny fraction (≈ 0.5%) of the ingested liquid water changes to the vapour phase. In addition to this, literature review in chapter 4 (subsection 4.3.3) reveals that the evaporation rate of the rain droplets in the compressor is low and can be neglected when rain ingestion effects are investigated. Evaporation takes place mainly in the combustor and the phenomenon is examined in the following subsection. In conclusion, the author argues that there is no need to modify the thermodynamic calculations, which take place in the compressor brick.

Another key point is the way, in which the compressor work COMPW is calculated based on the torque increase (TRQW). In Turbomatch, the compressor work is estimated by using the enthalpy property. Enthalpy difference between inlet and outlet is multiplied by the air mass flow and the result is the compressor work. In chapter 6, the extra torque due to the water centrifugation has been calculated. The author assumes that the increase in COMPW equals with this of TRQW on a percentage basis. This gives a very good approximation considering that water does not evaporate in the compressor and the gas properties do not change due to water. Hence, enthalpy is not affected and by following the aforementioned assumption the results are not changed appreciably.

7.2.3 Combustor

It has been analyzed in chapter 4 that liquid water has a detrimental effect on combustor's performance. The presence of water especially in the primary zone, affects the combustion process and consequently the combustor faces a drop in its efficiency while engine's operation demands a fuel flow (m_f) rescheduling. In the worst case, flame out and unsuccessful relight may be possible. It is justified in chapter 4 that the effects of water ingestion on a gas turbine burner are quite dramatic.

Therefore, for the Turbomatch completion as far as the water ingestion is concerned, it was necessary to introduce the combustor's performance deterioration into the code. For the simulation purposes, the burner

performance was expressed by two parameters: the total pressure loss and the efficiency.

As far the total pressure loss is concerned, its simulation was feasible by using the experimental results from work done in Purdue University Laing et al. (1993), Laing et al. (1993), Minster and Murthy (1991), Shastri et al. (1994), Shastri et al. (1995). In this analysis, the Pressure Loss Factor (F_{PL}), which is a principal combustor performance parameter, was experimentally estimated (the analysis is presented in chapter 4, subsection 4.6.1). The relevant data (chapter 4, figure 4-26) were exported and used by the author to create the appropriate block data for Turbomatch library.

Another important parameter of combustor's performance is its efficiency (ETA), which is simply defined as the ratio of actual to theoretical ΔT for a given fuel/air ratio (f). It has been highlighted that water ingestion has a detrimental effect on combustor's ETA. Evaporation takes place in the combustor primary zone due to the high temperature environment. This results in a reduction in exit temperature. Moreover, water addition on a gas turbine combustor has several effects apart from the evaporation of liquid water. Firstly, there are effects on fuel – air mixing and the formation of recirculation zones upstream of the primary jets. Secondly, there are chemical – mechanical interactions between the flame and the water. Thirdly, there are direct effects on reaction kinetics. Consequently, combustor's ETA deterioration should be taken into account in any case of water ingestion simulation.

This was feasible in upgraded version of Turbomatch (June 2008) by using experimental data found in AGARD, (1995) and analytically presented in chapter 4, subsection 4.6.1. The data was worked out and for 1% up to 10% water/air by mass the deterioration in combustor' ETA was estimated as shown in figure 7-4. It is worth noting that the combustor' ETA drop is characterized by a curve in exponential form especially for values above 3% of water mass fraction. This declares a high rate of change for these values of ingested water. This may be justified by the fact that the amount of water entering the combustor's primary zone may not increase in direct proportion to the amount of water ingested initially into the air stream Laing et al. (1993).

The author agrees with this guess and it can be justified by considering that the liquid water film enters into the combustor, it flows mostly across the combustor casing and its thickness develops with the ingested water mass (figure 4-28 in chapter 4 illustrates the flow). When its thickness reaches a critical value, it enters to the primary and dilution zone through the combustor liner. At this phase, the water has a great impact on flame and destabilizes the whole process. Hence, combustor's performance deterioration is higher. However, the threshold that the water enters to the combustor primary-dilution zone is strongly dependent on the combustor type, its geometry and its position on the

combustor section. More liquid water is expected to concentrate at the lower sections of the engine due to gravity.

Apart from that, the water mass does not affect linearly the aforementioned effects of water addition into the combustor's primary zone (fuel-air mixing, chemical kinetics etc).

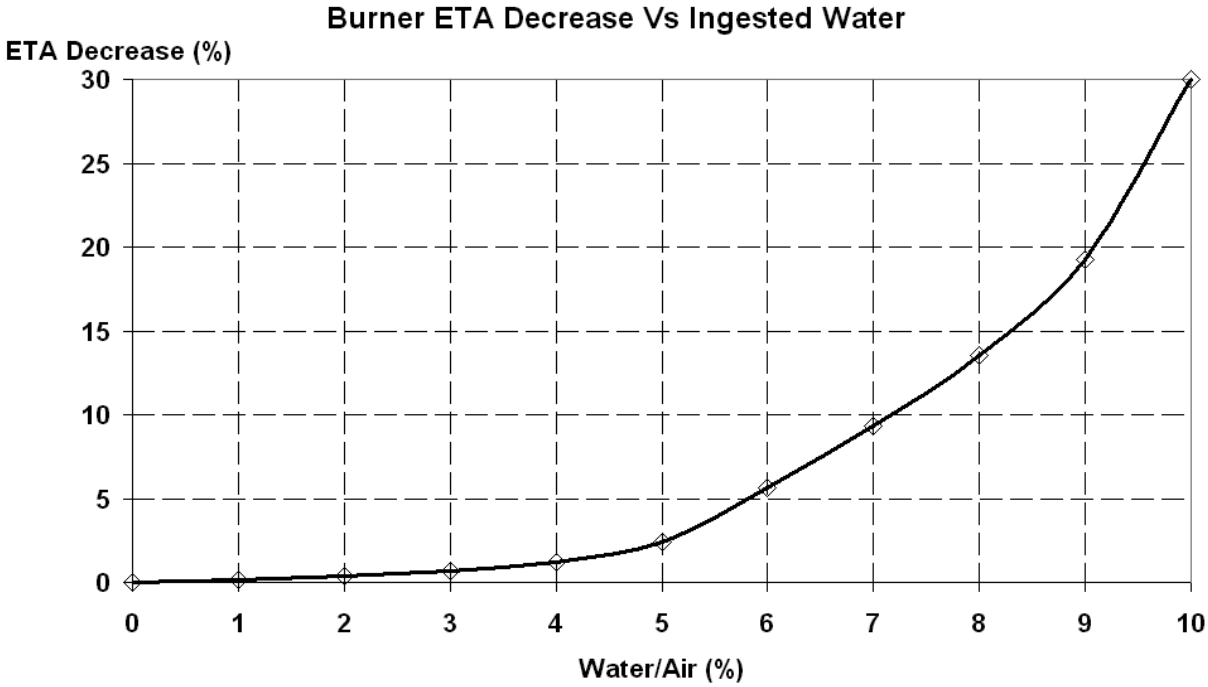

Figure 7-4: Burner ETA Deterioration due to Ingested Water (based on AGARD (1995))

Hence, the relevant data (F_{PL}, ETA deterioration and predefined values of water/air ratio), was imported in the new Turbomatch version (June 2008) in the "*WATERINGESTION*" block data. The burner deterioration subroutines, named "*BurnerWaterDeter*" and "*SearchBurnerParametersDeter*", take into account the water to air ratio and by means of the linear Lagrange interpolation method, their outcome is the percentage of ETA deterioration and the total pressure loss as well, for water mass fraction specified by the user. As a result, the reduced ETA is responsible for an increased m_f or a drop in combustor's exit temperature.

An example from pressure loss calculation, using the PCN parameter as handle, is shown in figure 7-5. The expected detrimental effect of water is obvious. In this case, water in any form (liquid or spray) disturbs the air flow field. Moreover, the discreteness of liquid phase contributes to the pressure loss. Numerically, there is a 4% increase of total pressure loss when 6% water/air is added to the burner. It seems that a key feature of total pressure loss change is the linearity, which is obvious in figure 7-5. This can be justified by the fact that pressure loss depends on the form in which the water is present (either liquid, spray or a combination) as well as its mass. The author supports

that liquid water has a greater impact on pressure loss than spray or vapour. This is because it flows mainly in the combustor's casing wall, which is the area where the boundary layer develops. Bearing in mind that liquid water film thickness depends almost linearly in water mass content (this is analysed in chapter 6, subsection 6.5.3, figure 6-13), this linearity is valid for the pressure loss calculation.

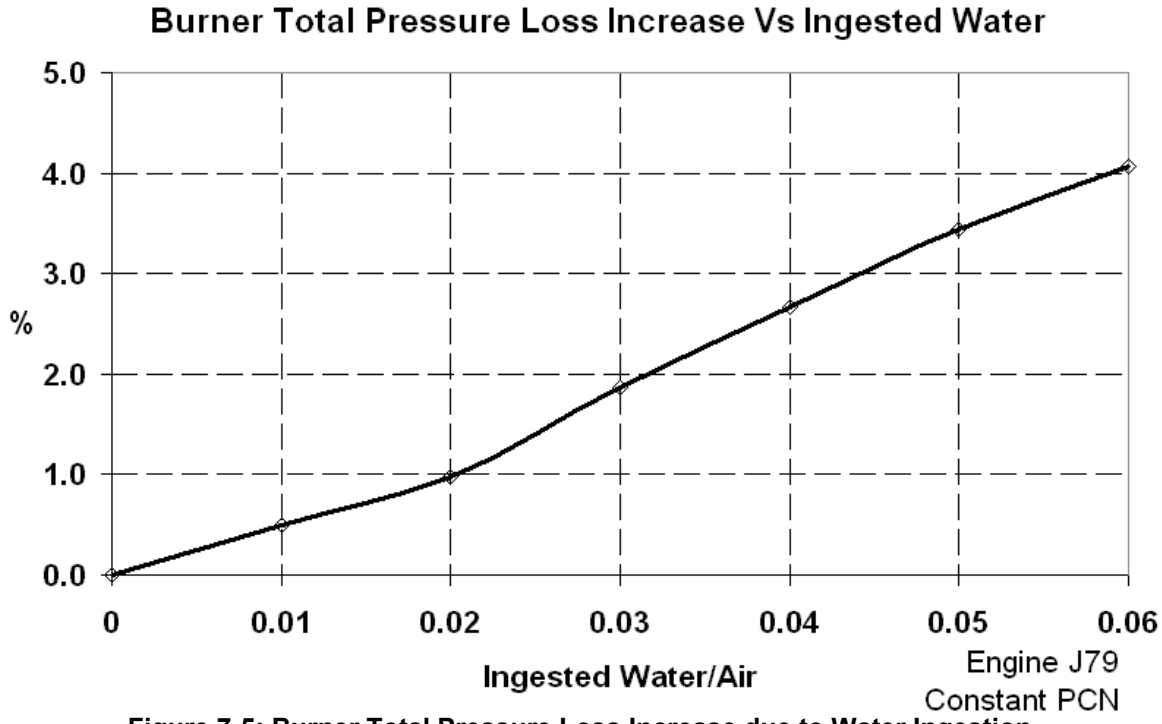

Figure 7-5: Burner Total Pressure Loss Increase due to Water Ingestion

It should be emphasized that, in the combustor brick, it is assumed that all the ingested liquid water mixes with any other form of water like the one calculated at the intake from the air humidity and finally evaporates. Evaporation calculations are based on a process built and clarified by Mucino (2007). In this analysis, the combustion chamber was regarded to be an open thermodynamic system with three inlets [main air flow (m_a), fuel flow (m_f) and water flow (m_w)] and two outlets mass streams [the combustion products (m_g) and outlet water flow]. Assuming that there are not heat losses or inputs from the combustor environment and no work is being done by or to the system, the mass and energy balance equation is:

$$m_a \theta_a + m_f \theta_f + m_w \theta_{w,in} = m_g \theta_g + m_w \theta_{w,out}$$

Equation 7-2: Combustor Mass and Energy Balance Equation

In the above equation, θ is the total energy of the fluid (θ=h+ke), expressed as the sum of kinetic energy ke and enthalpy h, which involves the state (h_{state}) and chemical energy ($h_{chemical}$) of the fluid ($h=h_{state}+h_{chemical}$). Bearing in mind that the

inlet velocities of water and fuel is relatively low and that the fuel state energy h_{state} is negligible compared to its $h_{chemical}$, it can be written that

$$m_a \theta_a + m_f h_{chemical} + m_w h_{w,in} = m_g \theta_g + m_w h_{w,out}$$

Equation 7-3: Manipulated Formula of Mass and Energy Balance Equation

Finally, the fuel chemical energy can be expressed by its low-heating value (LHV) corrected by the combustor's efficiency ETA. Thus, for a given combustor outlet temperature, which declares a known energy demand θ_g, equation 7-3 can be solved for m_f:

$$m_f = \frac{\left(m_g \theta_g - m_a \theta_a\right) + m_w\left(h_{w,out} - h_{w,in}\right)}{(LHV)(ETA)}$$

Equation 7-4: Combustor Fuel Flow Equation

From the above equation, θ_a and θ_g are estimated by TRM subroutine, which is a function that calculates the thermodynamic properties (enthalpy, calorific heat and entropy) for the working fluid. Similarly, water inlet and outlet enthalpy is calculated by WTP function for given T - P conditions.

Therefore, at the burner exit the water is only in vapour form. That is not completely true and it has been analyzed that, in reality, a part of water leaves the combustor in liquid form. This is caused by the fact that not all the water quantity enters to the combustor primary zone, where high temperature values characterize the area. Furthermore, the residence time in the combustor is relative low and heat transfer is limited by this parameter.

However, it is written above that evaporation is not the only effect of water addition on combustor. Chemical – mechanical interactions between the flame and the water, fuel – air mixing and reaction kinetics contribute to a great extend to drop the combustor's ETA. Consequently, the burner's ETA deterioration, which is measured during experimental water ingestion conditions, cannot be attributed solely to the evaporation of liquid water. The aforementioned phenomena are also important and it is necessary to include the ETA deterioration to simulate gas turbine engine performance under water ingestion conditions.

Hence, the fuel consumption calculation is based on the combustor's efficiency deterioration (as plotted in figure 7-4) and on the partial evaporation (50%) of liquid water mass. Partial evaporation in a combustor under water ingestion conditions has been verified by experimental observations (presented in chapter 4, section 4-6-1). What is more, the author has conducted a relevant parameter study described in page 143, proposing that partial evaporation is the most realistic option. On the contrary, for small water quantities full evaporation is expected. Thus, the topic is strongly suggested for further work.

It is worth noting that, after the evaporation calculations, air, fuel and water mass flow parameters are referred back to air in order to avoid combustion products overestimation. The total working fluid flow is calculated taking into account the fuel mass and the total water flow. Hence, WAG parameter is included in the working fluid flow.

Another assumption, which was necessary to be made, was about the temperature of water entering into the combustor. This value was needed for the evaporation calculations (necessary to calculate water inlet enthalpy $h_{w,in}$ – equation 7-4), because the process absorbs an amount of energy released by the fuel burn. Bearing in mind the small residence time of water in the compressor and the nature of rain droplet (relatively large droplets resulting in lower water surfaces for the same mass, thus lower heat transfer – the subject is analyzed in chapter 4), the value of water temperature entering into the burner was chosen to be 295.0 °K. The author tried several values within the range 290°K to 300°K and found out that the impact of this factor depended mainly on the water mass (i.e. high water temperature has minor impact when it refers to small water quantities). In any case, the water temperature entering the combustor should be examined based on heat and mass transfer processes and it is suggested for further work.

It is noteworthy that this value is model dependent because heat transfer is progressively higher to the last stages of the compressor. Hence, the number of compressor stages plays an important role to heat transfer rate. There is also another characteristic, which should be pointed out. From the inception of this work, the combustor data is based on experimental work, which, in several respects, is model geometry-dependent. Thus, the results must be considered from the point of view of the trends, which are expected during water ingestion conditions.

In conclusion, it can be said that after these modifications in Turbomatch BURNER subroutine, the code simulates the effect combustor deterioration due to the presence of water. Total pressure loss across the combustor and the drop in its ETA are calculated and are taken into account to the overall engine performance simulation.

7.2.4 Turbine - Nozzles

Turbines and nozzles are the last components of a gas turbine engine, facing the impact of ingested water. It enters into them mostly as vapour due to the evaporation in the preceding combustor. That results in an increased gas mixture C_p, which has a beneficial effect on turbine's work output. It has been reported that, the effects of water ingestion on the turbine and nozzle operability and performance are benign [AGARD (1995)]. However, bearing in mind that water does not fully evaporate in the combustor, it impacts the first turbine stage

being in liquid form. Similar phenomena with these in compressor take place (centrifuging, splashing etc). Therefore, it is believed that turbine work is certainly affected by liquid water and that should be a matter for further investigation.

Currently at this code, there is no any major change to these component bricks apart from the change to the mass flow of working fluid. All the water content is in vapour form and is treated as an additional component in the gas mixture. Hence, the change in gas properties is taken into account without any other modification.

7.2.5 Mixing Components

Turbomatch makes possible to calculate the outlet conditions, resulting from the constant-area mixing of two flows, with given inlet conditions. When one inlet flow is much smaller than the other (e.g. cooling air bleed back), the MIXEES brick should be used, in which there is no allowance for total pressure loss. In different case, MIXFUL brick allows total pressure change resulting from momentum balance between the two streams.

When water is present in the flow, the value of air mass flow from the working fluid is changed. Mixing expressions were modified and the ingested water content was included in the calculations.

It should be noted that a uniform water distribution is assumed when the air-water flow splits or mixes. That may generate an error in water flow value, especially in turbofan engine simulations, in which fan blades centrifuging the water droplets and a higher value of water mass than the estimated may pass through the secondary flow. However, for the time being, mixing and splitting flow calculations regarded to be more than adequate.

7.3 Performance Results

The final phase of Turbomatch modification included the code verification. For this reason, it was thoroughly tested in aero gas turbine engine configurations. Generally, the code has adopted the changes and the results were qualitatively correct taking into account the limitation of using the parameter PCN or TET as handle (constant). This is a compromise because water ingestion affects both PCN and TET of a gas turbine engine. Of course, the dominant effect is the reduction in engine's rotational speed and this is understandable from the water torque charts presented previously since the increase in torque is noticeable from the inception of water ingestion phenomenon. In any case the user can spot the difference between dry and wet operation. By using PCN as handle, an increase in m_f (hence and TET) is expected although combustor's performance

degrades. Currently, m_f cannot be used as handle, which would be more appropriate (i.e. no movement of the throttle but reduction in rotation speed). Thus, this option is suggested for further work.

At this point, it is worth highlighting the improvement of an MS excel-spreadsheet used in earlier versions of Turbomatch. This software, by using several macros, reads performance parameters data from Turbomatch output file and imports them into an MS excel-spreadsheet. This is extremely helpful since the user is able to visualize the results and plot any data in a parametric analysis (i.e. change of gross thrust with the altitude variation). However, after the inclusion of humidity effects and water injection at the burner this option was no longer available because the output file contained more data than excel macros could read. Making the appropriate modifications the described software is accessible again and includes data for the water ingestion mode. The entire work is presented in appendix F.

Regarding the test of the code, the model of J79-GE-17, a single spool turbojet engine produced by General Electric, is used here as an example for the performance results. Its compressor PR is 13.5 for 76 kgr/sec air mass flow while TET is 1320 °K at design point (DP) conditions. The maximum thrust at sea level is 52,800 Nt and SFC is 23.8 mgr/Nt·sec. The engine is characterized by a specific thrust of 690.2 Nt/kgr/sec. It is worth noting that Turbomatch D.P. calculations for the above model are in close agreement with the performance data given by General Electric.

Choosing the water ingestion mode of simulation and having the WAG value slightly above zero (>0.001) the user is informed of the rain condition (RelHum is set to 90%) via a message in the result file (figure 7-6). Similarly, compressor and burner deterioration parameters are presented.

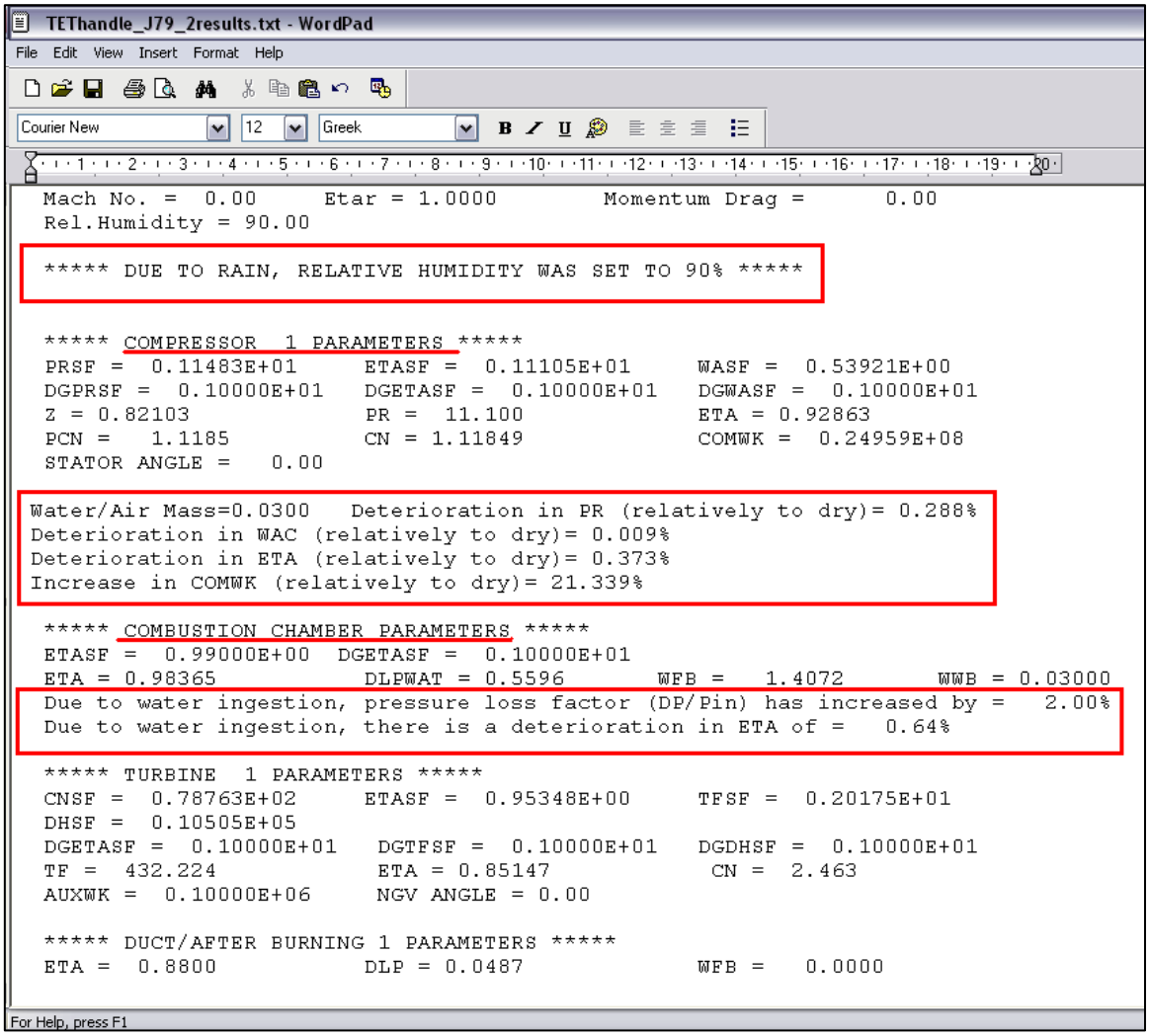

TEThandle_J79_2results.txt - WordPad

File Edit View Insert Format Help

Courier New 12 Greek

```
 Mach No. =   0.00      Etar = 1.0000        Momentum Drag =       0.00
 Rel.Humidity = 90.00

 ***** DUE TO RAIN, RELATIVE HUMIDITY WAS SET TO 90% *****


 ***** COMPRESSOR  1 PARAMETERS *****
 PRSF =  0.11483E+01      ETASF =  0.11105E+01      WASF =  0.53921E+00
 DGPRSF =  0.10000E+01    DGETASF =  0.10000E+01    DGWASF =  0.10000E+01
 Z = 0.82103              PR =  11.100              ETA = 0.92863
 PCN =   1.1185           CN = 1.11849              COMWK =  0.24959E+08
 STATOR ANGLE =   0.00

Water/Air Mass=0.0300   Deterioration in PR (relatively to dry)= 0.288%
Deterioration in WAC (relatively to dry)= 0.009%
Deterioration in ETA (relatively to dry)= 0.373%
Increase in COMWK (relatively to dry)= 21.339%

 ***** COMBUSTION CHAMBER PARAMETERS *****
 ETASF =  0.99000E+00  DGETASF =  0.10000E+01
 ETA = 0.98365            DLPWAT = 0.5596       WFB =   1.4072       WWB = 0.03000
 Due to water ingestion, pressure loss factor (DP/Pin) has increased by =   2.00%
 Due to water ingestion, there is a deterioration in ETA of =   0.64%

 ***** TURBINE  1 PARAMETERS *****
 CNSF =  0.78763E+02      ETASF =  0.95348E+00      TFSF =  0.20175E+01
 DHSF =  0.10505E+05
 DGETASF =  0.10000E+01   DGTFSF =  0.10000E+01    DGDHSF =  0.10000E+01
 TF =  432.224            ETA = 0.85147             CN =  2.463
 AUXWK =  0.10000E+06     NGV ANGLE = 0.00

 ***** DUCT/AFTER BURNING 1 PARAMETERS *****
 ETA =  0.8800            DLP = 0.0487              WFB =   0.0000
```

For Help, press F1

Figure 7-6: Turbomatch Result File

7.3.1 PCN Handle

In case of using PCN as handle (fixed value), although the compressor work due to water is increased, engine is forced to keep a constant rotational speed. This, combined with the fact that energy is absorbed to evaporate the liquid water in the burner, results in TET and m_f increase.

To be more specific, there is a noticeable movement of compressor's operating point towards the surge line. In figure 7-7, a compressor map from a J79-GE-17 engine model is presented. The code run for constant PCN value of 0.7 and, for up to 6% WAG, the operating point approaches to surge. Compressor centrifuges the water and its work demand is increased while there is deterioration in PR, ETA and WAC. Downstream, water evaporates in the combustor and m_f - TET are increased to provide energy for the turbine to keep the engine at PCN=0.7. It is noteworthy that the deterioration factors depend on the water mass content (WAG) and model's rotational speed. Details are

showed in figure 7-8, in which the deterioration of standard PR, WAC for PCN=0.7 is evident. WAC degrades 12.5% and PR 3.5% for 6% WAG.

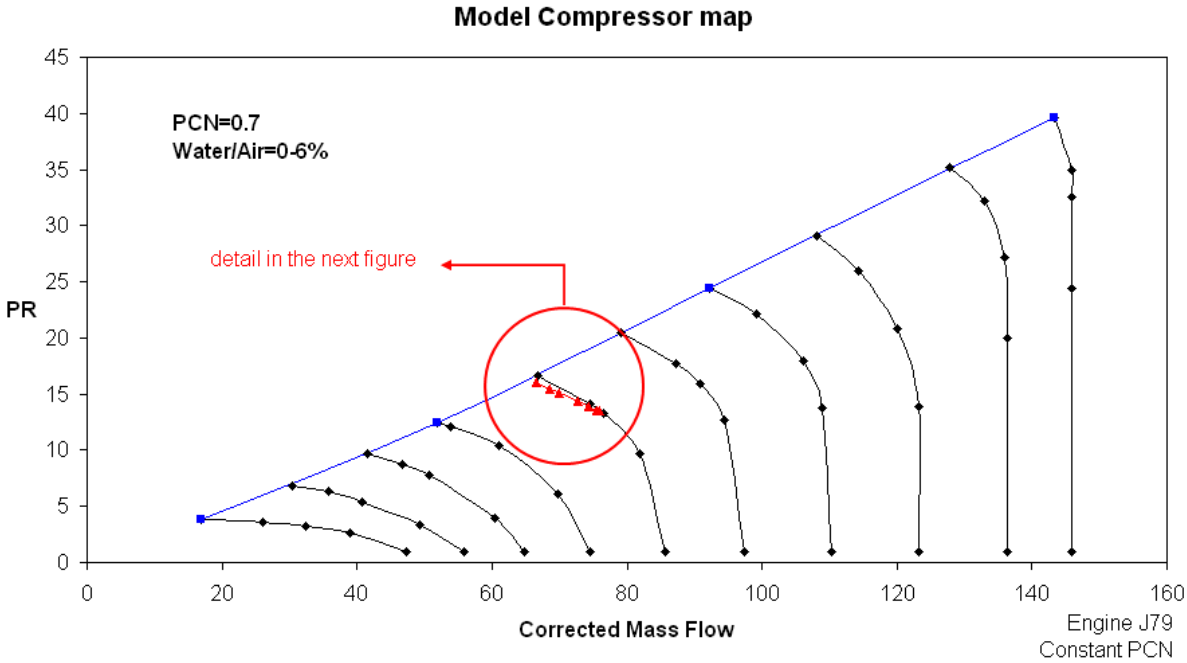

Figure 7-7: Compressor Map under Water Ingestion Condition (PCN handle)

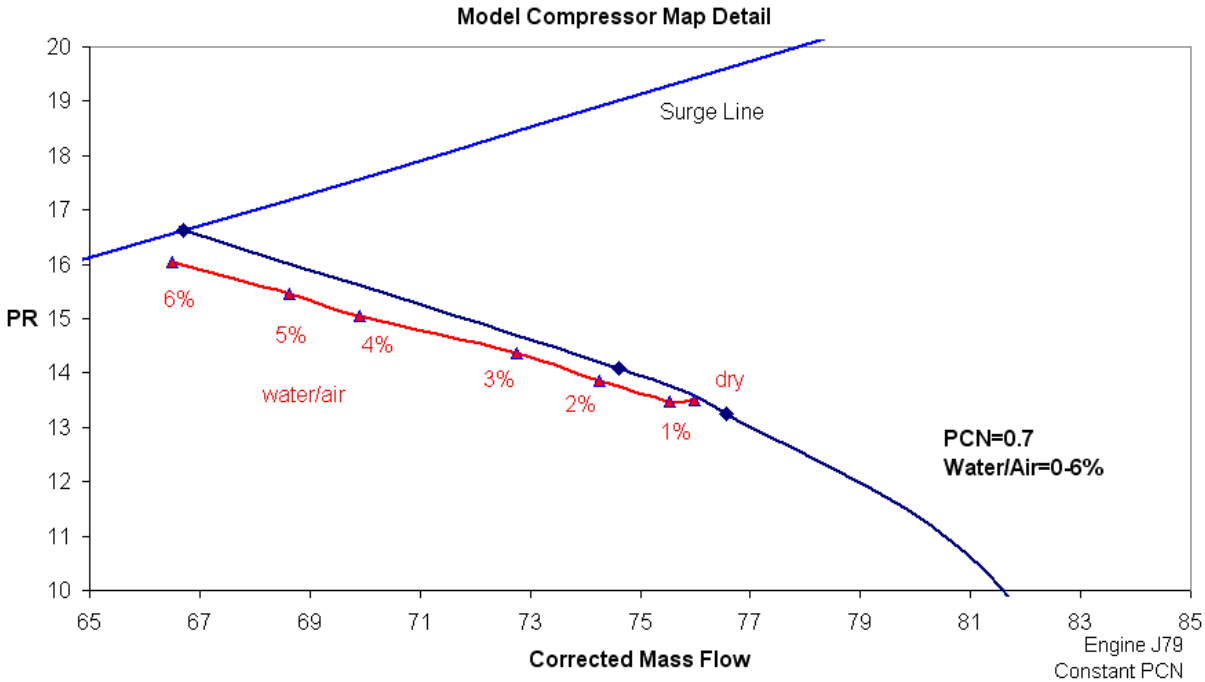

Figure 7-8: Operating Point Movement due to Water Ingestion

It is worth pointing out that the surge line is assumed unaffected by the water ingestion although this is not true. Liquid water has an effect on stall inception and it has been proved that compressor is more susceptible to stall under these conditions Williams J. et al. (2005). In the author's view, this is a key point for determining compressor's performance in the limit of surge line. Thorough study

is necessary for the effects of water ingestion on the stall inception and is recommended for further work. However, stall margin (SM), which is defined by equation 7-5, is affected by water because PR approaches PR_{surge} values. Figure 7-9 shows the decrease of surge margin due to ingested water. For dry conditions, SM is 0.23 and it reduces to 0.04 for 6% WAG (i.e. this compressor for 6.3% WAG cross the surge line and the simulation stops). Large water quantities have a pronounced effect on surge margin. It has been shown in chapter 6, figure 6-32 that small water quantities have a negligible effect on PR. This has been also observed in tests by Williams J. et al. (2005) and have been analysed in chapter 4. It seems that the very thin liquid film, which is formed by small water quantities, cause air disturbances of low amplitude and their effect are not detectable. At larger water content, the liquid film obtains wavy characteristics due to the shear action of air and their aerodynamic impact is evident.

$$SM = \frac{PR_{surge} - PR}{PR}$$

Equation 7-5: Surge Margin Definition

There is also a slight raise in PR since the WAC deteriorates and the compressor approaches to surge (figure 7-8). The energy exchange between the water droplets and the air particles results in reduced air speed, thus lower values of air enter the compressor (deteriorated WAC). Considering the velocity triangles, the air incidence angle onto rotor blades is increased and so does PR until flow separation inception drives the compressor to stall. However, the compressor cannot achieve PR values, which were obtained during its operation in dry conditions. This is attributed to the fact that air speed does not change in a uniform way. Water affects both air velocity-distribution and the flow direction across the blade span. This results in PR and ETA reduction, relatively to the dry values for the same WAC.

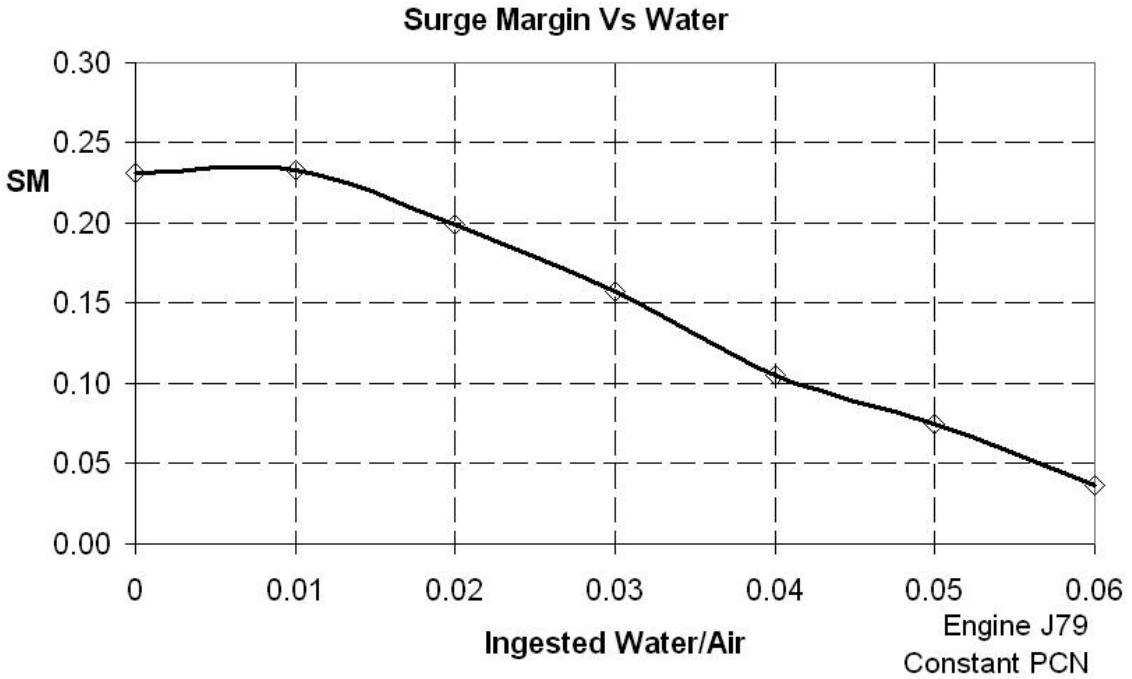

Figure 7-9: Surge Margin Decrease due to Water Ingestion

Similarly, liquid water has an effect on compressor's ETA, which is reduced under these conditions. The new version of Turbomatch (June 2008) corresponds to this effect in a representative way as it is showed in figures 7-10 and 7-11, where the deterioration in compressor's ETA is obvious as the water mass increases (ETA degrades 11.5% for 6% WAG). The physical mechanism for the compressor's ETA reduction incorporates the disruption of the airflow due to energy exchange between the water droplets and the air particles, as it has been analysed in the previous paragraph. It is noteworthy that the effects cannot be isolated and they influence each other acting towards blade's performance deterioration.

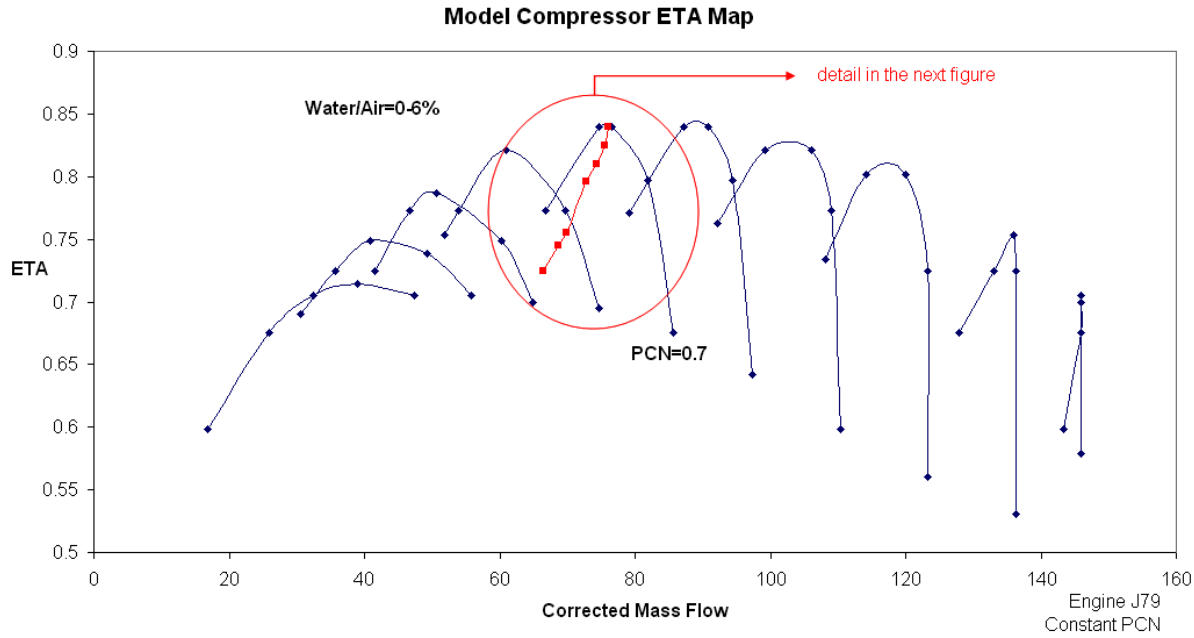

Figure 7-10: Compressor ETA deterioration due to water ingestion (PCN handle)

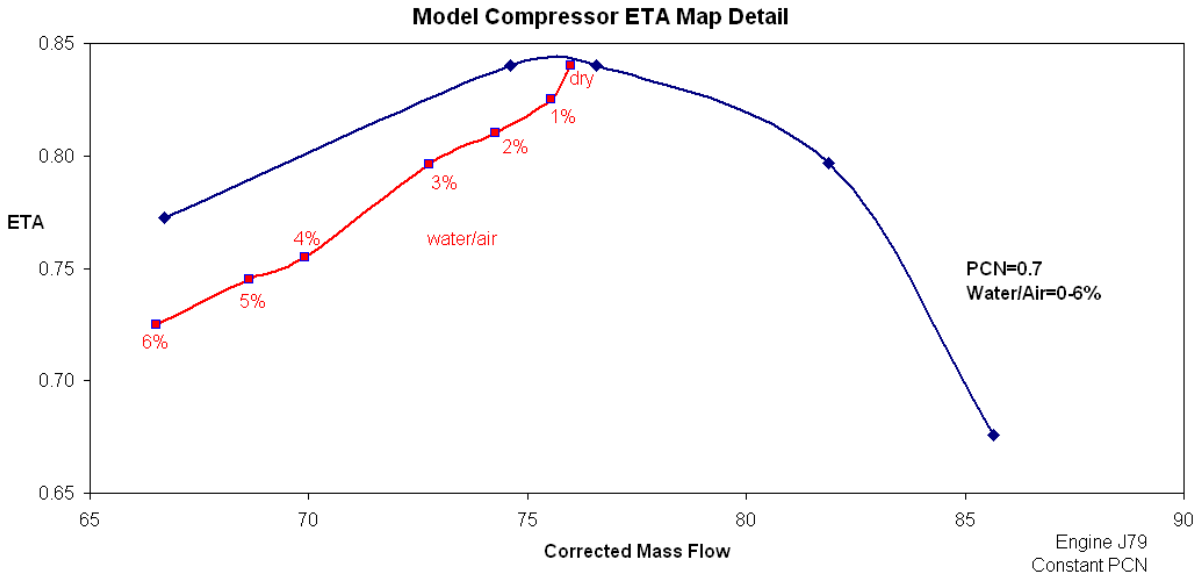

Figure 7-11: Detail of Compressor ETA deterioration (PCN handle)

It has been written that the increase in compressor work is quite dramatic and this is obvious in figure 7-12. For WAG values up to 6%, COMPW increases about 30% at PCN=0.7. It should be underlined that this value is a result from the combined effect of torque due to water centrifugation and the deterioration in compressor ETA since the latter affects enthalpy calculations at the compressor exit (i.e. enthalpy property is used for the compressor work calculation). Neither the reduction in WAC nor the PR increase can counterbalance the percentage of torque increase. In any case, a message in the results file informs the user of the effect caused in PR, ETA, WAC and COMPW merely by the ingested water (figure 7-6).

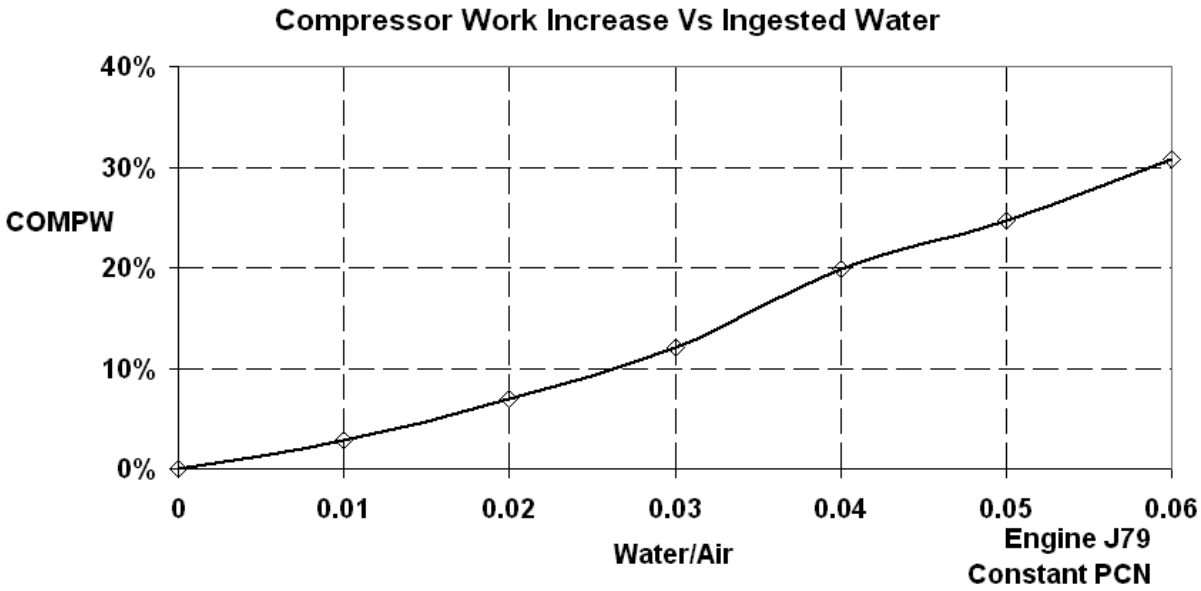

Figure 7-12: Compressor Work Increase due to Ingested Water

It is mentioned above that the engine keeps constant PCN although the COMPW increases. The excess energy is provided by the fuel, which increases dramatically. However, the initial assumption that all the water evaporates in the combustor drives the simulation code to overestimate the increase in m_f and consequently the specific fuel consumption SFC. In order to limit this, a parametric analysis was conducted. Three cases were simulated with full, 50% and no evaporation of water in the burner. The results reveal that, in any case, there is an increase in m_f, which is bigger when full evaporation is assumed in the burner (figure 7-13). For increased water content, m_f values for full and no evaporation in the burner diverge progressively as it is obvious in figure 7-13.

From another point of view, the percentage difference of the m_f values between full and no evaporation are presented in figure 7-14. It is showed that for 6% water/air this difference can be up to 45%. In the extreme case, which full evaporation is assumed but no evaporation actually takes place, the error in m_f estimation could be 45%. Similarly, assuming 50% of water evaporation in the burner the maximum error can be ±22% for 6% water/air. Therefore, to minimize the possible error, evaporation in the combustor has been limited to 50% of ingested water. Of course, this point and generally heat transfer process in the combustor under water ingestion condition should be studied in detail and it is suggested as further work.

It is worth noting that the percentage difference in m_f between full and no evaporation varies almost linearly (figure 7-14) because water mass and consequently the energy absorbed to evaporate it, affects linearly m_f, as it is proved with equation 7-4.

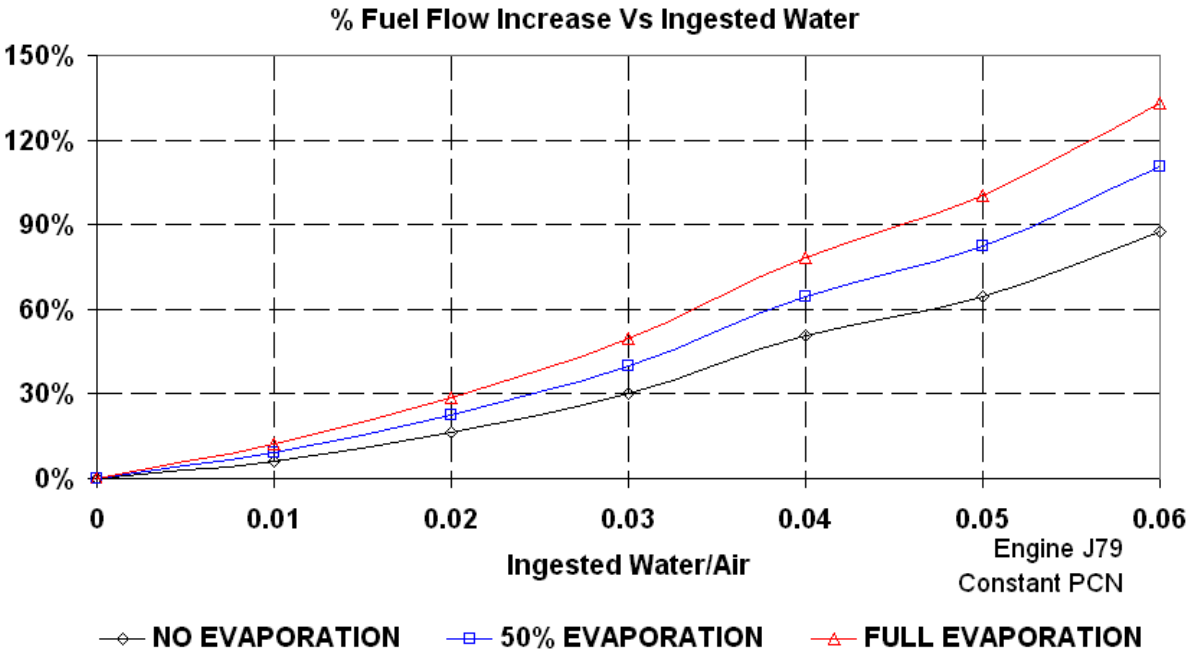

Figure 7-13: Fuel Flow Increase due to Ingested Water for % of Evaporation

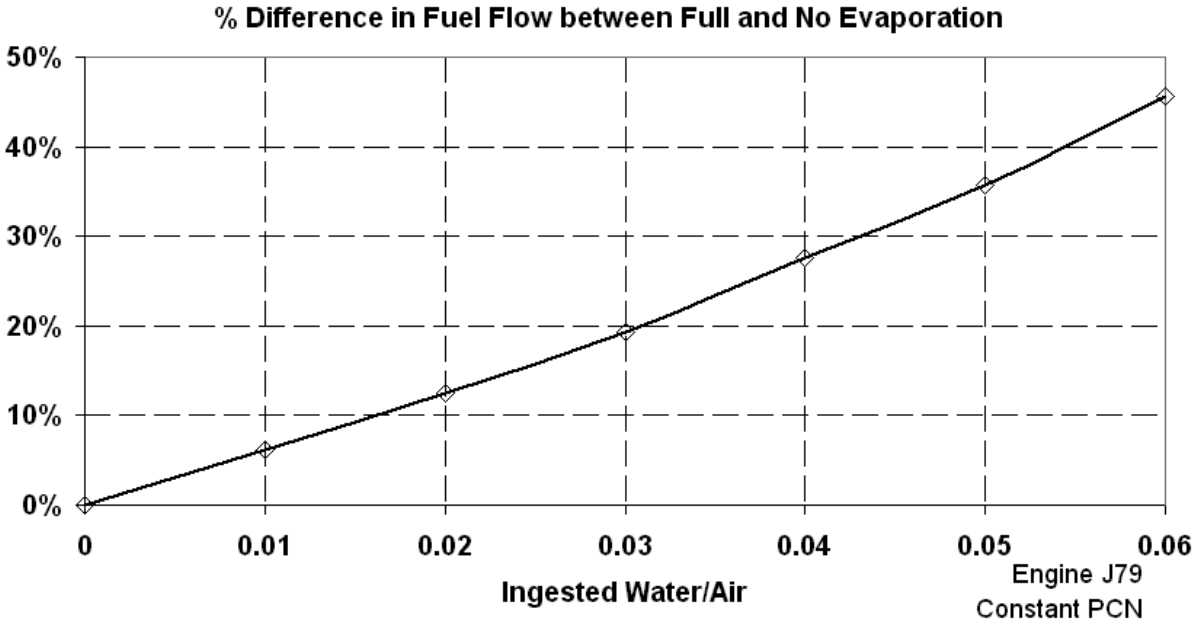

Figure 7-14: % Difference in Fuel Flow between Full and No Water Evaporation Cases

Thus, evaporating all the water in the burner has a detrimental effect on fuel consumption. Even in no evaporation cases, 5% water/air forces the engine to work with m_f almost 90% above its dry value and this is explained by the fact that keeping the PCN constant while COMPW increases, the turbine demands higher TET, which is offered by the combustor through m_f increase.

7.3.2 TET Handle

In the same way, when TET is used as handle, the change in compressor map is characterized by a reduction in PCN due to the increased compressor work. To be more specific, in that model a 10% reduction in PCN has been estimated for 4% ingested water/air. This change in engine's rotational speed is caused mainly by water centrifugation.

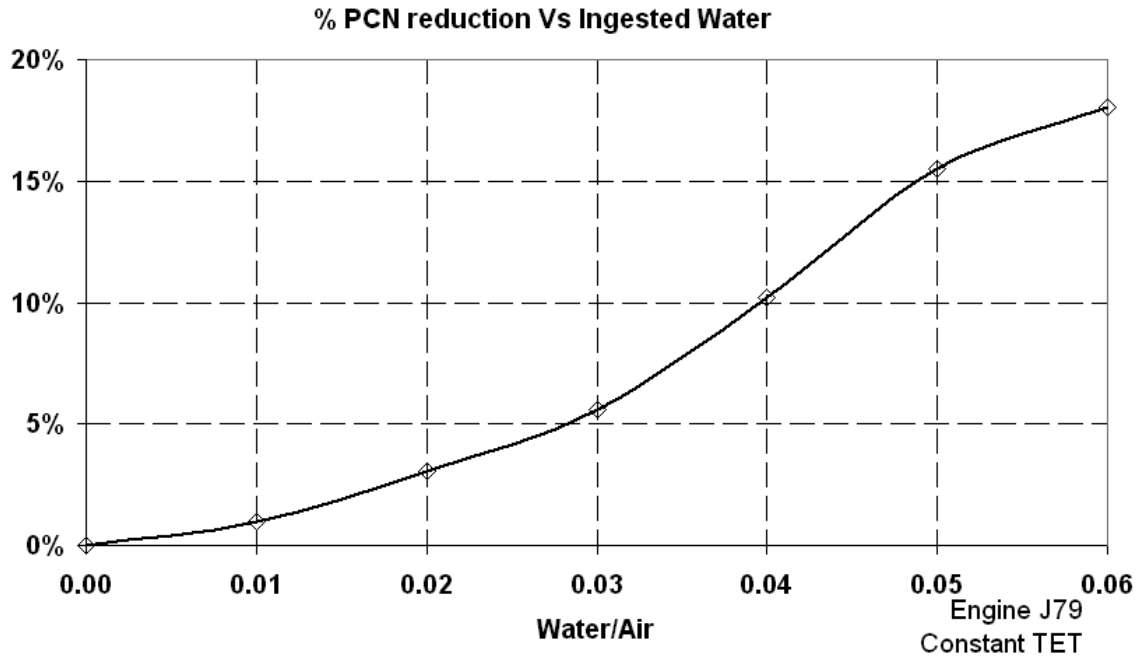

Figure 7-15: Engine Speed Reduction under Water Ingestion Condition (TET handle)

Moreover, PR and WAC are reduced and this is a result of the combined PCN change and their deterioration due to water ingestion (figure 7-16). The aforementioned behaviour of the code agrees to a certain extent with the physical phenomenon of ingested water in a gas turbine engine because the loss of rotational speed is the first and most important effect of water ingestion in a gas turbine engine.

In figure 7-17, the variation in compressor ETA is demonstrated under water ingestion condition. Bearing in mind that TET value is fixed, the available turbine work TURBW cannot balance anymore the increased COMPW and the engine is forced to work at part speed. Thus, WAC reduces and ETA follows the compressor map for the reduced CM-PCN. It is worth noting that water evaporation in the burner alters the gas properties of the mixture. That has a beneficial effect on turbine's work output, which is taken into account in the simulation through the turbine enthalpy calculations, as it has been reported in section 7.2.4. Nevertheless, this parameter cannot counterbalance the increase in COMPW, which has a quite higher detrimental effect.

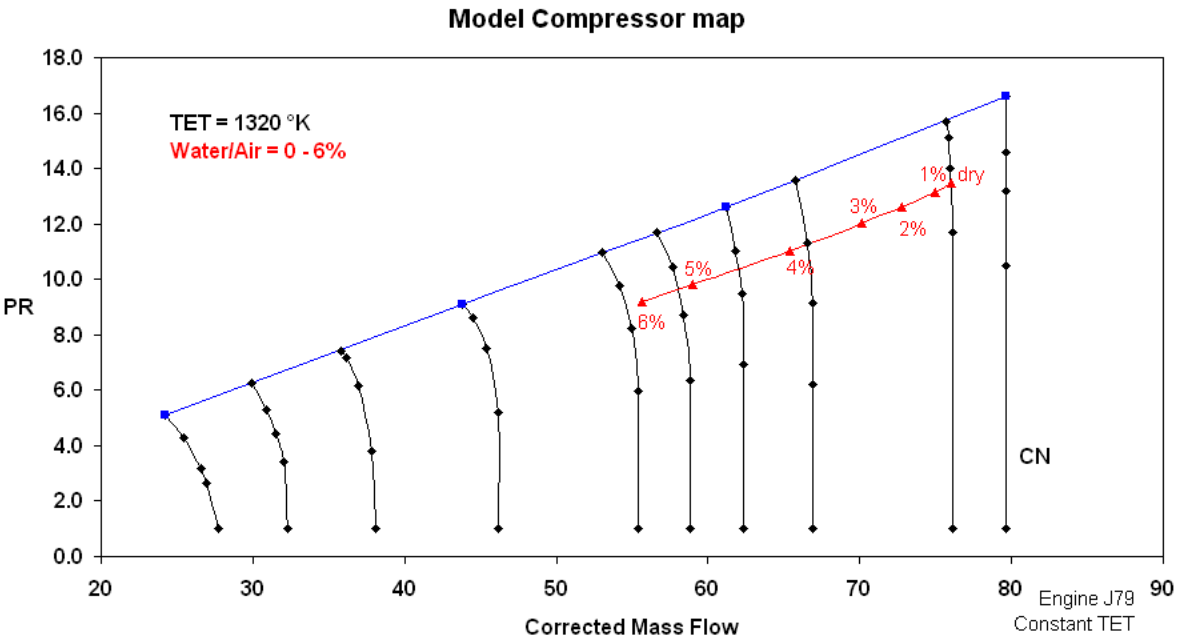

Figure 7-16: Compressor Map under Water Ingestion Condition (TET handle)

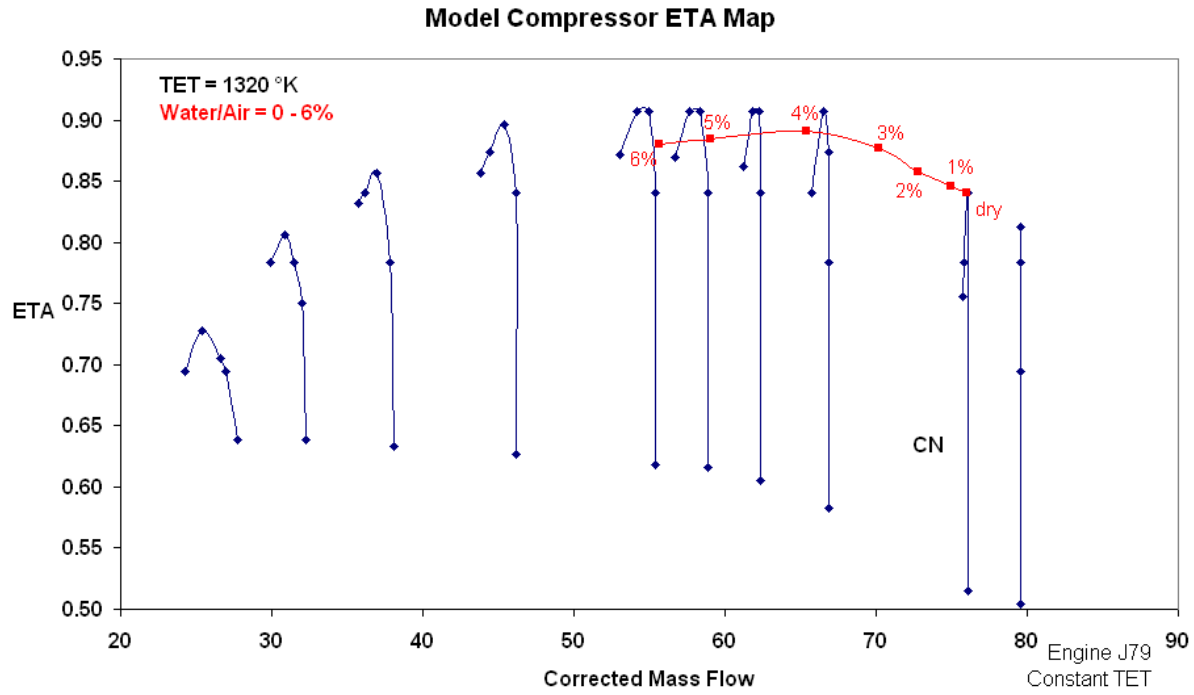

Figure 7-17: Compressor ETA Variation under Water Ingestion Condition (TET handle)

The ingested water also affects engine's performance parameters like the SFC, Net Thrust FN and Specific Thrust SFN. Engine performance deteriorates (SFC increase and FN, SFN decrease) because of the simultaneous decrease in engine PCN, TET and the increase in m_f. However, Turbomatch simulates this degradation with the limitation that, in the input file, it is necessary to use as handle either model's PCN or TET (i.e. using PCN as handle, TET increases with water ingestion and this result in an increased FN and SFN).

When the user handles the simulation with TET, in case of water ingestion, Net Thrust (FN) and Specific Thrust (SFN) deteriorate (figure 7-18). A key feature of this plot is that the reduction in these parameters is sharper when WAG>3%. This is a result of engine's operation at part speed (i.e. low PCN) with deteriorated compressor (WAC, PR and ETA) and burner (DLP, ETA) parameters. It has already been pointed out that high values of water content have a more pronounced effect on the engine component parameters.

Another characteristic demonstrated in figure 7-18 is that at very low water/air values (≈1%), FN is almost unaffected and SFN shows a slight increase (note: percentage refers to reduction). This is an effect of the assumption that engine operates in rain and atmosphere Relative Humidity is set to 90% after the DP calculations. Therefore, there is a water content, which passes to the subsequent engine components and finally evaporates in the combustor. Up to this point, engine "benefits" from that change in gas properties without suffering considerable deterioration due to rain condition. However, for 4% WAG, the deterioration value is 3.15% for SFN and 16.6% for FN.

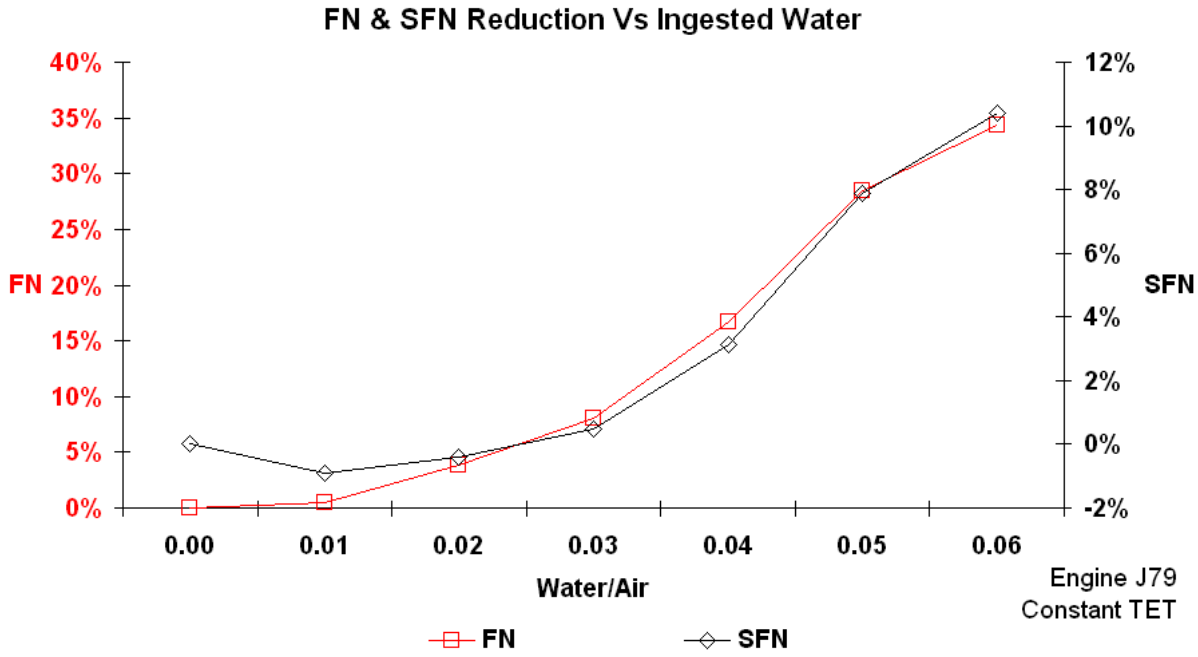

Figure 7-18: Percentage Deterioration of Net and Specific Thrust with Water Ingestion (TET handle)

Another engine parameter, which deteriorates under water ingestion condition, is the SFC and that is demonstrated in figure 7-19. The combined effect of m_f increase and FN reduction results in SFC rise of about 33% for 4% ingested water. In the author's view, in a real case, water will cause a reduction in engine's PCN and TET regardless of the throttle position (i.e. fuel flow). The pilot's reaction to engine's deceleration is to move the throttle forward trying to accelerate by increasing the fuel flow. This makes things worse because further

power loss occurs due to rich flame extinction. However, improved engine control systems may protect engine from off-schedule operation. Main Fuel Control component, assisted by computerised sensors, can detect the low PCN, low air mass flow and reduced TET and it may limit the fuel flow accordingly.

It is of great importance to draw attention to the fact that the fuel used for these simulations was kerosene and in the calculations, LHV (43,124 kJ/kgr) was used. Changing the fuel type will alter the aforementioned percentages on the engine performance parameters. However, the trends towards engine's deterioration will remain unaffected.

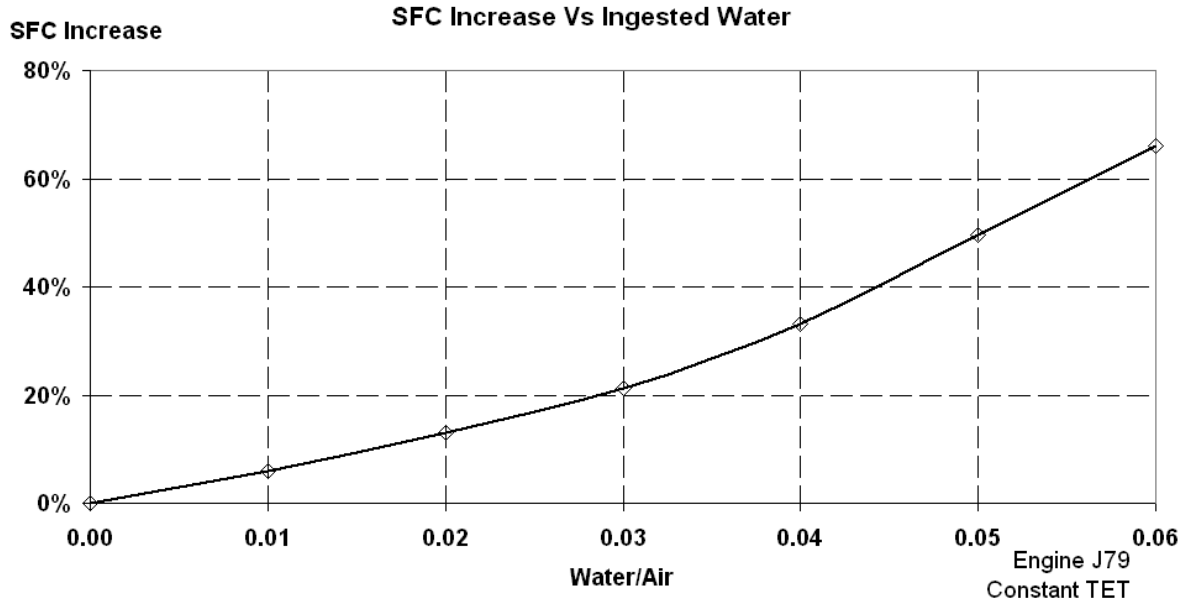

Figure 7-19: SFC Increase due to Water Ingestion (TET handle)

7.4 Code's Limitations

In view of the above, it is noteworthy that there are some limitations in the use of the code when it simulates water ingestion cases. Analytically, the compressor or turbine operating point may go off their standard map while there is no problem in dry computations. The reason for that is the dramatic increase of compressor work, which forces the component to work far from its design value.

This problem can be tackled by simply changing the compressor (BD 6) or turbine map (BD 7). A second option is by adjusting compressor or turbine CN values accordingly. For example, when TET is used as handle, the design value of compressor PCN should be relatively high (i.e. 1.0 – 1.2). This will allow the code to stay inside the compressor map and adjust accordingly the operating point of the compressor. On the contrary, when PCN is used as handle the design value of PCN should be relatively low (i.e. 0.7 – 0.9) to force the

operating point staying inside the compressor map. Thus, in water ingestion mode, user should handle the code with care.

For the reason described above, there is a limitation in the ingested water mass. Although block data files contain WAG values up to 20%, it is observed that the code terminates its operation for WAG=5% to 9%. This value depends on the model and the operating conditions chosen by the user. It should be reminded that the gas turbine certification tests in the water ingestion field take place for WAG up to 4%.

It is noteworthy that any assumption, which has been made in the context of this modelling, is stated above at each components section.

7.5 Code Validation

One of the most important parts of the current work was the code validation under water ingestion mode of operation. To do this, experimental data or/and the use of results by other simulation software, were necessary for comparison purposes. At the particular field of water ingestion operation, experimental work has mainly involved whole engine tests. In these tests, the mechanical, aerodynamic and thermodynamic effects of water addition, which alters engine performance, not only occur simultaneously but all influence each other. When standalone components are tested, the aforementioned effects can be isolated.

In chapter 4 of the current manuscript, a detailed description of the published work about water ingestion tests is presented. From the onset of this project, author has insisted on collecting constructive experimental data about water ingestion tests. This has been proved a difficult task for several reasons.

Firstly, performance data of the engine rigs is not revealed in the relevant papers, so it is impossible to simulate their dry performance. Consequently, the comparison of measured and simulated absolute values of performance deterioration is not feasible.

Secondly, the majority of the experimental results refer to the transient operation of the test engine because, as it has been analyzed, the severity of the effects is time-dependent. On the contrary, this project focuses on simulating the steady state performance under water ingestion condition. However, an attempt was made to extract data from the work presented in Warwick (1963), in which altitude water ingestion tests were carried out on a J79-GE-8 engine at the U.S. Naval Air Turbine Test Station (NATTS). Flight conditions with 0.9 Mach speed at 40000 ft altitude were simulated in the test cell and the engine was ingested with various quantities of water in an effort to investigate reported incidents of engine's stall and flame out during deliberate

thunderstorm penetration tests. Engine's performance was recorded as a function of time and ingested water content up to a point when stall or flame out occurred. In most runs, the engine showed an unstable behaviour after a short period of water ingestion but, in some cases, the engine performance was stabilized before the final stall or flameout (detailed description of the test is presented in Chapter 4). Hence, data was exported for this phase of tests and the % change of PR and N were calculated. Figure 7-20 shows the PR versus N change for four different cases in which stall or flame out occurred about 72 sec after the initiation of water ingestion, for constant water rate.

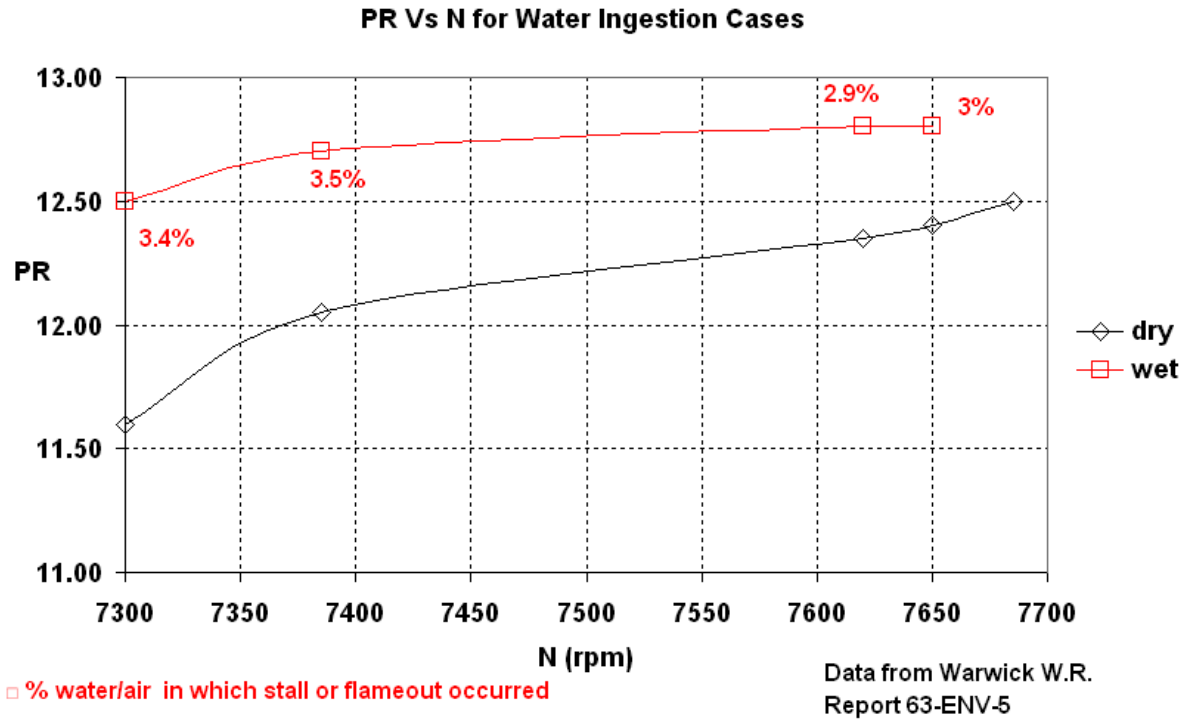

Figure 7-20: PR Vs N due to Water Ingestion [Test Data from Warwick (1963)]

A J79-GE-8 engine model was simulated by Turbomatch at the test cell conditions (0.9 Mach speed at 40,000 ft altitude and 2.9%, 3%, 3.4% and 3.5% WAG). The results were compared with these in the aforementioned test. The difference between the simulated and test data in the percentage change of PR and N is displayed in figure 7-21. Error in N change estimation varies from 3.2% up to 7% and in PR from -1.7% up to 3.9%. The variation can be justified by considering the assumptions made to build the water ingestion mode in the simulation code. It is certain that compressor blade clearance, the change in surge line, the geometry of the engine's compressor and the engine control system influences engine performance in the test cell. The above parameters were not included in the simulation software calculations.

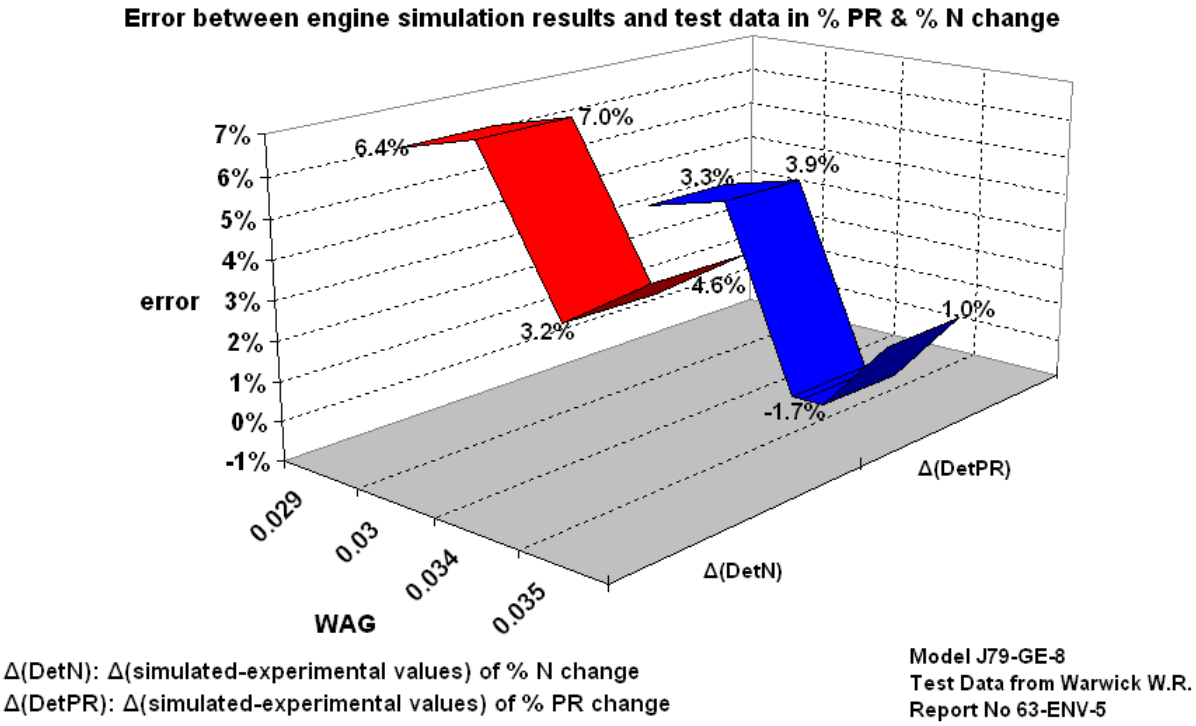

Figure 7-21: Error in %PR and %N change due to Water Ingestion between Simulated and Experimental Results

It is well understood that this error can give considerable deviation in the results of engine performance simulation under water ingestion condition and one may think that this error is unacceptable for a contemporary simulation tool. However, it should be acknowledged that many difficulties emerge when attempting to simulate water ingestion. It has been highlighted that the phenomenon is geometry and time dependent. This means that under identical atmospheric conditions water distribution at a small gas turbine engine inlet will be different from that in a large turbofan engine. Moreover, the centrifugal force to the liquid water droplets affects their motion and film formation in different ways when the size of the compressor is changed appreciably. Finally yet importantly, water distribution differs in the combustors of different size. Consequently, the results from the Turbomatch software must be considered from the point of view of the engine performance trends, as far as the water ingestion phenomenon is concerned.

Another set of data were derived from the experimental work done by Williams J. et al. (2005) described in chapter 4. In this project, water ingestion effects were investigated in a standalone compressor at part speed. The key feature, of this experimental set up was that, the aerodynamic and mechanical effects were far more important that the thermodynamic effects. The standalone compressor working at part speed kept the evaporation to a minimum, thus, there were not considerable changes in the gas properties or temperature distortion. For clarity, the compressor consisted of four stages preceded by a row of Inlet Guide Vanes (IGV's). Its rotational speed was 3000 rpm. In this

experiment, measurements showed a dramatic increase in torque required to keep the compressor speed at the same level. The change is proportional to the amount of ingested water. The measurements were used to plot the percentage change in compressor torque (figure 7-22).

The above measurements were compared on a percentage basis with the results produced by the CFD model presented in chapter 6. The reason for using the CFD model was that the experimental data derived from a standalone compressor. Figure 7-22 shows that there is a reasonable agreement between the experimental and calculated change in compressor torque required for constant speed. Error varies from -1.66% up to 4.3% for 10% water/air.

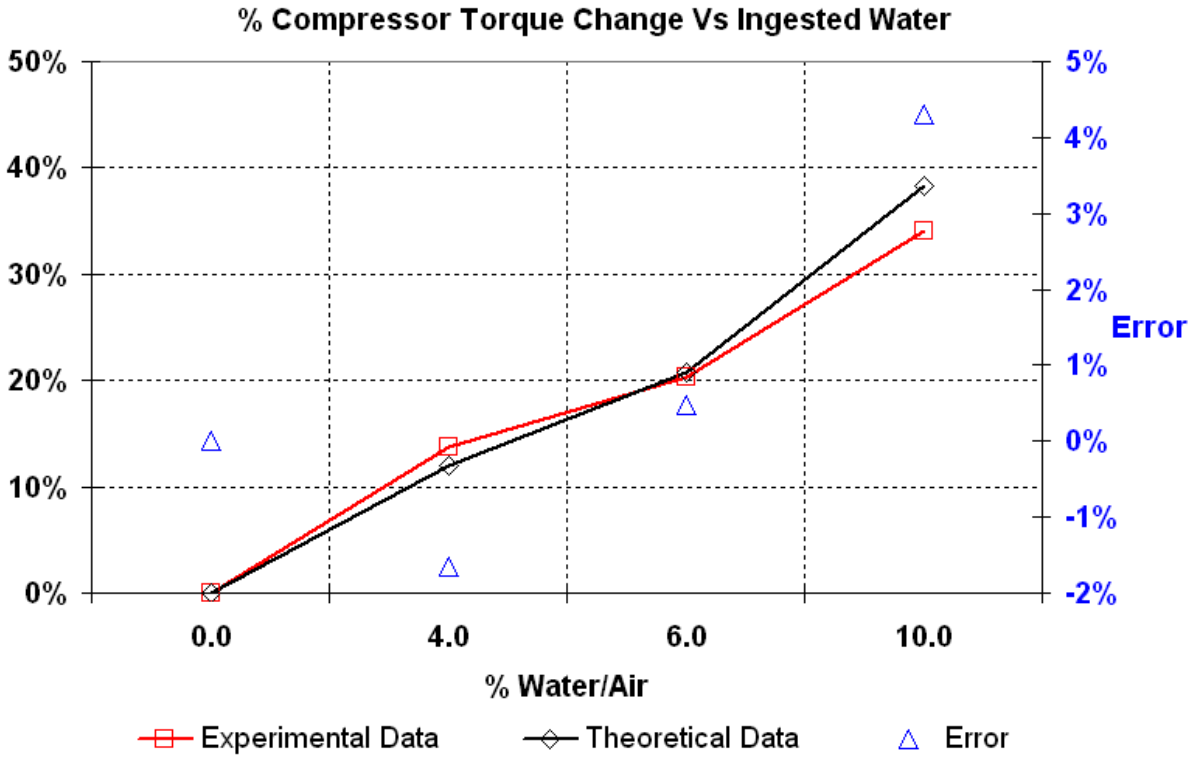

Figure 7-22: Torque Experimental Measurements Williams J. et al. (2005) and Simulation Results under Water Ingestion Condition

The assumption that the water droplets obtain the 50% of blade's rotational speed as they leave its pressure surface has been highlighted in the theoretical calculation of water torque. That was done because no friction factor was taken into account. Moreover, the water flow speed is never full tangential or axial as it exits from the rotor blade. In the context of the above experimental work, the torque increase was calculated by assuming that all the water passing through a stage was accelerated up to the blade speed. Hence, for 13% water/air, the calculated torque was 40 Nt·m. For the same water quantity, the measured value was 32 Nt·m, which means that the error between the test and the calculated value for the same compressor is 22%. This error is considerable bigger than the error estimated by the current work and that justifies the

assumption that the water flow accelerates tangentially up to 50% of the rotor blade speed.

Working in a similar way, the loss of pressure rise at stall condition were measured and calculated on a percentage basis (figure 7-23). Test rig values showed that small amount of water have little effect on pressure rise while larger amounts increase rapidly the loss of pressure rise. The deterioration compared with the CFD results. Figure 7-23 shows that there is an agreement up to 4% of water mass (error≈0.5%). However, for higher water quantities, the simulation underestimates the deterioration. It is supported in Williams J. et al. (2005) that the aerodynamic losses in the compressor come from the air deceleration due to presence of the low speed water droplets. It has been written above that when the water droplets entrain to the airflow there is an energy exchange between them. Thus, the low speed water droplets force air to decelerate, affecting at the same time the velocity distribution on the blade. These result in an increase of the aerodynamic losses.

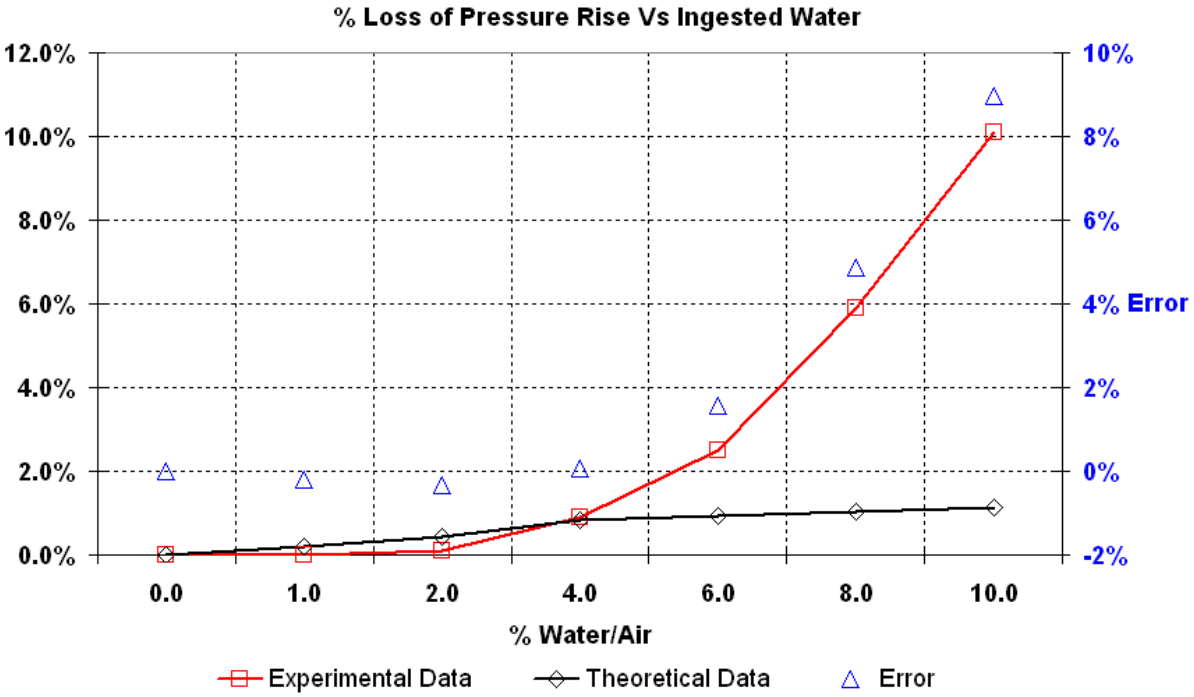

Figure 7-23: Loss of Pressure Rise due to Water Ingestion–Experimental and Theoretical Data

However, in the CFD cases, the water droplet initial speed was relatively high and in many runs was equal to that of air. That happened because there were convergence problems when water droplets entered the airflow with low velocity. The author tried several cases with a variety of water velocities but it was impossible for the CFX-Tascflow to find a solution. It was found that there is a limitation when a discrete phase is used and injected with very low relative speed. Hence, CFD did not simulate the aerodynamic losses emerged from the

water – air energy exchange. In view of the above, it is supported that CFD limitation is the cause for the error showed in figure 7-23 for WAG>6%. For small water quantities, the effect is not so pronounced and the compressor seems that it can copy with air deceleration. Of course, the whole point requires further investigation by using a test rig designed for this purpose.

Due to the difficulties of validating the Turbomatch performance results under water ingestion condition, an attempt was made to compare them with these of other gas turbine simulation tools. The effort focused on four codes: GasTurb developed by Kurzke (2004), AEDsys and EOP PERF programs which are based on the design tools found in Mattingly et al (2005) and Mattingly (2006) respectively, and the National Aerospace Laboratory (NLR) Gas turbine Simulation Program (GSP) [National Aerospace Laboratory (2004)].

GasTurb simulates the effects of inlet fogging and water injection upstream of the fan. Wet compression process is involved when water injected directly in front of the fan because it has no chance evaporating before it enters the engine. The calculations based on an empirical constant evaporation rate of water. Therefore, only the thermodynamic effects of water addition are considered.

AEDsys can perform mission and engine performance analysis It includes fourteen (14) constraint types, thirteen (13) mission types, seven (7) aircraft drag models, seven (7) engine thrust models, and seven (7) engine fuel consumption (TSFC) models. It can run engine performance calculations (variation in an engine's uninstalled performance with changes in engine flight conditions (altitude and Mach number) and engine throttle. A similar but newer program, the EOP PERF has eight (8) engine models, two (2) gas models and two (2) unit systems. However, neither of them takes into account possible water ingestion at the inlet of the engine due to atmospheric conditions.

Finally, NLR GSP is a tool for performance prediction and off-design analysis. By establishing a specific arrangement of engine component models, both steady state and transient simulation can be performed. The code includes the capability of water injection in the combustor but it is not extended to the water ingestion effects.

Consequently, it should be reported that water ingestion is simulated in a limited number of codes, which have been developed in-house mainly by the gas turbine industry. The complexity of the phenomenon has driven to the conclusion that only simulation combined with experimental testing can assure the accurate prediction of gas turbine performance.

7.6 Concluding Remarks

It should be acknowledged that the water ingestion capability built in Turbomatch is not generic. Several factors, which have not taken into account in this code, may affect in a different way the gas turbine simulation. Parameters like the water droplet size and its speed, the evaporation rate in the compressor and mainly in the burner, the compressor tip clearance and generally the compressor and combustor geometry should be included in contemporary gas turbine software to simulate precisely the engine's performance.

In the author's view only a tool, which integrates the CFD capabilities and the gas turbine performance simulation, can achieve this. The complexity of the phenomenon makes its simulation a difficult task. This is proved by the fact that, according to the published work, the gas turbine community has dealt with it mostly experimentally. At the same time, it has made considerable progress simulating computationally the water injection, evaporation or the air humidity phenomenon.

On the other hand, Turbomatch water ingestion code can be the basis for further development. The software is built with FORTRAN modules and allows supplements. Thus, subroutines calculating several other factors can be added improving its accuracy. For the time being, it can be written that Turbomatch can simulate and provide to the user a fundamental view of the detrimental effect of water ingestion phenomenon.

8 Discussion

This chapter includes the discussion of the results produced by the theoretical approach. It also presents experimental values, which compared with the simulation outcome, provide the relevant justification. It should be highlighted that in the writing process of this manuscript, the author has expressed his view when each result was presented. Thus, many comments are displayed in chapter 6 and 7 while in this chapter are grouped together.

8.1 Compressor

8.1.1 Water Deposition

It has been written that when a jet engine operates under rain conditions, the majority of water droplets, which enter the engine, impact on the compressor blades and form a liquid film. The computational analysis has revealed that the inertial impact is the dominant mechanism in droplet deposition. Even by changing the parameters of water injection speed and mass, the results show that almost all the ingested water impacts on the blade's pressure surface, while on the suction surface there are spots of a few water droplets (chapter 6, subsection 6.5.2). Fine droplets, due to their small inertia, may follow the air streamlines and avoid impingement at the first compressor stages. When evaporation takes place then, the suction surface of the blade appears to be wet due to the diffusion mechanism. The results are in complete agreement with these of Das et al. (2006).

8.1.2 Liquid Water Film Thickness

The thickness of the liquid film, which is formed on the blade pressure surface, depends on the droplet mass, its diameter, its initial ingestion velocity and the blade rotational speed.

The increase of the water mass fraction (WAG) causes an increase of the water film thickness δ. It was found that 30% WAG forms a 0.0377 mm water film thickness in idle speed and 0.0346 mm in full speed. In addition to this, the increase of WAG from 4% to 30% almost doubles the film thickness for both cases of rotational speed. It should be noticed that, film is thicker in idle speed due to the lower centrifugal force, its speed is smaller and that, in connection with mass continuity, leads to a thicker film (chapter 6, subsection 6.5.3.1).

The study has also shown that water droplet size has an effect on build-up process and consequently on film formation. As expected, fine droplets evaporate more easily than coarse droplets. Large droplets deposit more easily than fine droplets, because they have higher inertia than air particles and they cannot follow the air streamlines. Consequently, large droplets develop a thicker

water film. It was shown that for 2% and 4% WAG, δ increases about 16% when the D_w changes from 1 mm to 3 mm, for both idle and full speed cases.

The cases, which ran for fine droplet sizes from 1 μm to 100 μm, proposed that there was no considerable difference in water build-up mass and δ (chapter 6, subsection 6.5.3.2). These results are verified by experimental observations in Williams J. et al. (2005), where droplets, varied from 51 μm to 97 μm, had the same effect on the compressor's behaviour. However, Williams et al. (2005) observed that there was no considerable change even with large droplets (≈1.5 mm), which contradicts with the current simulation. In the author's view, this is a result of droplet's secondary phenomena, which take place when water flows in the air. Their effects (break-up and splashing) were not included in the simulation. Hence, the effects of droplet size are magnified. In tests, droplet's break-up results in smaller droplets, which impact on the compressor blades. The rate of droplet's size change requires further investigation with the appropriate software (chapter 6, subsection 6.9).

It has been shown that droplet's initial speed (V_w) affects the deposited water mass fraction. High-speed injected droplets can avoid the rotor blade row although it is more difficult to follow the air streamlines due to their high inertia. The reason lies to the small residence time they remain in the blade passage. Hence, the chances to hit on the blade are low (chapter 6, subsection 6.5.3.3). It was found that reducing V_w from 150 m/sec to 50 m/sec, build up mass increases 73% and torque 88%, relatively to values when V_w=150 m/sec. Data refers to 4% water/air, D_w=1.0 mm. Nevertheless, the results are strongly affected by the compressor's features. In a multistage compressor, the water droplets may avoid impingement on the first blade row but they will deposit on the downstream stages. In the author's view, all the water droplets influence the compressor torque value regardless of the impingement location (1^{st}, 2^{nd} or 3^{rd} rotor blade).

The compressor's rotational speed has a great influence on ingested water. Water film is moving mainly under the influence of centrifugal and air shear force. These forces depend on the blade's angular speed. Furthermore, water droplets are accelerated at high speed in the tangential direction and then are decelerated to axial direction by the stator blades. Generally, at full speeds, the increased air velocities will lead to higher deposition rates. This is a result of the fact that the rain droplets will be less able to follow the curved gas streamlines. This study showed that when angular speed (ω) reduces, the film becomes thicker. The reason is that the film moves with lower speed (lower centrifugal force) and taking into account the mass continuation, δ increases. It was found that when ω varies from 20% to 100%, δ reduces about 63 % (chapter 6, subsection 6.5.4). In the author's view, the effect of this parameter is very important because, as it has been emphasized, the majority of power-loss incidents have occurred during descent flight, where the power settings are at

idle region. Consequently, the calculation of δ alteration with the engine's rotational speed is of primary importance. However, there are not experimental results about the effect of ω in the rate of change of δ.

This study has also shown that in a rotor blade, δ could reach the values of few hundredths of mm. For the rotor blades, there are not any experimental values, possibly due to the difficulties of obtaining the measurements. The calculations for stator blade (zero rotational speed) revealed that the values of water film height counts a fraction of an mm. This has been verified from similar theoretical calculations by Gyarmathy (1962), Kirillov and Yablonik (1968). Considerable work has been done in Hammitt et al. (1975a), Hammitt et al. (1975b), Hammitt et al. (1981) in a wet steam tunnel at the University of Michigan for experimentally measuring the film thickness caused by liquid water on a flat plate and the effect of a concurrent steam flow. They also calculated theoretically the film thickness assuming that the gas shear force equals with liquid shear force at the interface, and the velocity profile in the film flow is linear. They found that their theoretical calculations underestimated δ measurements because the friction factor between liquid film and high-velocity gas was not included in their model. The results from FILM_MOTION code for various flow rates were compared with these and it was found that the theoretical results either from Hammitt et al. (1975a) or FILM_MOTION code underestimate the film thickness calculation (chapter 6, subsection 6.8, figure 6-35). Hence, the inclusion of friction force between liquid film and high-velocity gas should be considered in any case and its estimation is suggested for further work.

In the author's view, the agreement with Hammitt et al (1975) results is significant bearing in mind that, in this study, not only any friction factor is taken into account but also the interface shear force is assumed equal with this in wall at dry condition. It is reported in Wurz (1976) that during experiments it was measured that the shear-force on a liquid film increases by approximately 30% in comparison with the dry wall condition. The droplets momentum, which is added in the interface shear-force theoretical estimation presented in this work, cannot counterbalance the change of the shear-force from dry wall to liquid film characteristics.

8.1.3 Liquid Water Film Motion

It has been shown that film motion is nearly radial at a big range of angular speed. For speeds higher than 40%, the speed vector angle is above 77°. It is highlighted that Williams and Young (2006) arrive at the same conclusion. In their theoretical approach, they argue that this angle is about 82° (8° from the radial direction). The small difference is justified by the fact that they include the friction force in their calculations. They also use a high friction factor, which leads to more radial water flow (chapter 6, subsection 6.5.4).

It has also been observed that water initial speed (V_w) has an effect on water film motion. The momentum of deposited droplets is transferred on the already formed film. Its direction is almost chord-wise and that gives a rise in total chord-wise force, which is applied on the water film. This force was calculated in the FILM MOTION program and affects water film motion. It was shown that when V_w increases, high momentum droplets cause an increase in film chord-wise speed. Simultaneously, there is a small reduction in radial speed because, due to quicker axial motion (i.e. with a low stagger angle chord-wise and axial direction are coincident), water exits from the blade and there is no time to obtain the high values of radial speed.

Another noticeable point has been the liquid film chord-wise speed. It was found that it ranges from 0.2 m/sec to 2.3 m/sec depending on rotational speed and ingested water mass (chapter 6, subsection 6.8, figure 6-36). Values are higher at idle speed because the centrifugal force is lower and this enhances the film axial motion. Williams et al (2005) confirm this estimation by conducting water ingestion tests on a compressor model. They measure a velocity of about 1 m/sec for 15% water mass fraction. It is worth noting that this value lies between the values for idle (1.8 m/sec) and full (0.4 m/sec) speed. There is a significant agreement considering the tip clearance effects, which certainly alters the water flow characteristics.

In conclusion, the author states that FILM_MOTION code gives relatively reliable results. Although, it has been created to calculate the water film parameters flowing on a rotor blade, its results are compared with these from two-phase flow tests on a flat plate. Its accuracy can be improved by further investigating the interface shear-force between liquid water film and airflow. The latter certainly demands the inclusion of experiments in the research process to validate thoroughly any theoretical calculations.

The combined application of Computational Fluid Dynamics on a compressor model with FILM_MOTION code has achieved the first two milestones of the primary objective, set in chapter 2. The parameters that affect the water flow in a jet engine under water ingestion conditions have been indentified and their impact on the engine's operation has been estimated.

8.1.4 Compressor's Performance

According to the project's methodology, CFD has been applied again taking into account the change in the blade's profile due to water deposition and the liquid film wavy-characteristics effect caused by the air shear force (chapter 6, subsection 6.3.1). The results showed that there is a considerable deterioration in compressor's performance. The values of WAG were exaggerated to make the outcomes more pronounced. It has been analysed in chapter 4 that under extreme weather conditions there is a possibility for a gas turbine engine to

ingest about 4% water to air by mass. However, higher quantities may be possible, taking into account the scoop effect.

Compressor efficiency (ETA) was reduced when the model ran under water ingestion conditions. For 4% water ingestion, which is the value for gas turbine certification tests, the ETA deterioration was 8.5% for idle speed, 1.6% for full speed (chapter 6, subsection 6.6.1 and section 6.7, figure 6-31). At part speed, the effects were more obvious because the water film is thicker due to lower centrifugal force. Considering the mass continuity, the liquid film flows at lower velocities but higher thickness. Murthy et al. (1986) conducted water ingestion tests in a high-speed, 6-stage axial flow compressor. They confirmed that the deterioration in adiabatic efficiency in a single stage of the above compressor was about 4% for 15% water ingestion. Moreover, Williams et al (2005) experimentally estimated the isentropic efficiency for a 3-stage axial flow compressor under water ingestion conditions. The authors measured the actual pressure rise for both wet and dry conditions at the 3rd stage of their compressor. Comparing them with the ideal pressure rise, it was observed that the isentropic efficiency in the compression process was reduced about 5% when 17% water/air mass was ingested into the compressor. For 15% WAG, the calculated ETA deterioration simulation varied from 3% (full speed) to 12% (idle speed). Consequently, there is a significant agreement with the experimental results in compressor ETA deterioration.

The code also showed that the ingested water affected the compressor pressure ratio (PR). However, the effects were almost negligible for a wide range of water mass. For 4% WAG, PR deteriorated 0.44% (full speed) and 0.62% (idle speed). For 10% WAG, these values became 0.55% and 0.82% respectively (chapter 6, subsection 6.6.2). The experiments performed by Murthy et al. (1986) showed that 15% water ingestion caused a reduction in single stage PR of about 5%.

For further validation, the author has used experimental results published in Williams et al (2005). Test rig values showed that small amount of water have little effect on pressure rise while larger amounts increase rapidly the loss of pressure rise. PR deterioration was calculated at 1% for 4% water/air content. Both results converge to the point that small amounts of water have little effect on pressure rise coefficient. It was observed that there is a significant agreement in pressure ratio deterioration for up to 4% WAG (error≈0.5%, chapter 7, figure 7-23). However, for large water quantities (>6%), PR deterioration measured in the experiment was quite higher than this calculated by the theoretical model (error≈9% for WAG=10%). In the author's view, the difference is attributed to the tip clearance effects, which were not taken into account in the theoretical model. On the other hand, in the experiment, water film is flowing towards the compressor casing and it is gathered at the tip clearance. Increasing the water mass, it becomes filled and any additional water

will be splashed back into the blade span. This further disrupts the airflow and affects the aerodynamic performance of the blade. Hence, at high water content the effect of tip clearance magnifies the pressure loss.

The non-dimensional mass flow (WAC) deterioration was also estimated. It was found that WAC deteriorates about 2.4% for 4% water/air at idle speed. At high rotational speed, film thickness is extremely low and the effects in aerodynamic performance are almost negligible (chapter 6, subsection 6.6.3).

The physical mechanism for the compressor's deterioration due to water ingestion is summarised as follows:

- Water droplets are ingested with significantly lower velocity than the air. This leads to an energy exchange between the water droplets and the air particles, which forces the air to reduced speed. The disturbance of airflow has an effect on the air velocity distribution and flow direction across the blade span. Hence, the blade aerodynamic performance is changed.

- Water droplets deposit on the blade pressure surface and form a liquid film. Thus, the blade's profile is dynamically changed (i.e. the effect is water mass and time dependent).

- The tip clearance is filled with water, which splashes back to the airflow. Therefore, the air boundary layer is further influenced by the presence of water.

- Air shear force and water droplets momentum magnify the wavy characteristics of liquid film's surface. These waves are not stable and if they are of sufficient amplitude, they will result in water film breakdown and the formation of "dry spots" and/or rivulets. Hence, the blade's surface develops roughness features, which means that its skin friction coefficient is increased and the developed boundary layer is thicker. As a result, there is an increase in blockage reducing the air mass flow and consequently the aerodynamic performance of the blade.

- There is a reduction in engine's rotational speed due to the centrifugation of liquid water. Simultaneously, water evaporates mainly in the combustor, which reduces the exit temperature. Hence, the compressor is forced to work at speed conditions, which are not matched with the engine control schedule. This means that the blade's velocity triangle is further affected deteriorating its aerodynamic performance.

Apart from the aerodynamic effects of water ingestion, the mechanical effects are also very important. When the water impinges on the blade pressure

surface, it forms a film, which flows radially outwards under the influence mainly of the centrifugal force. Air shear force and water droplets momentum, which act in the chord-wise direction, are low compared with the radial forces (chapter 4, subsection 4.5.3). In Nikolaidis Th. et al. (2008) the effect of ingested water on the drive torque was investigated. Their analysis extended that of Williams et al (2005) calculating the water droplets torque as they exit from the blade tip or the trailing edge. Hence, the radius was not taken in mid-span because the water droplet may exit from the rotor blade near the hub, mid-span or (mainly) at the tip. The results confirmed the dramatic increase in torque and for 4%-5% WAG, it can be 20%-25% assuming that the water droplets are accelerated to half of the blade rotational speed (chapter 6, subsection 6.7).

The author holds the view that this assumption was necessary because the water-film exit velocity is not full tangential or axial (chapter 6, figure 6-21). In addition to this, when the film thickness reaches a critical height, it collapses, part of it forms rivulets of water and the other re-enters to the airflow. This means that not all the water quantity is subject to centrifuging. Considering that in torque calculations only the tangential component should be taken into account, the aforementioned estimation of the water-film exit velocity was done. However, it is noteworthy that the results are geometric dependent and they should be treated as trends for the described condition.

The simulation results were compared with the measurements from an experiment conducted by Williams et al (2005). The study showed that the theoretical results are in significant agreement with the test observations, giving small deviation. For up to 10% WAG the error varied from -1.66% up to 4.3% (chapter 7, subsection 7.5, figure 7-22). In the context of the above experimental work, the torque increase was calculated assuming that all the water passing through a stage was accelerated up to the blade speed. Hence, for 13% water/air, the calculated torque was 40 Nt·m. For the same water quantity, the measured value was 32 Nt·m, which means that the error between the test and the calculated value for the same compressor is 22%. This error is considerable bigger than the error estimated by the current work and that justifies the assumption that the water flow accelerates tangentially up to 50% of the rotor blade speed. Furthermore, both test and theoretical results arrive at the same conclusion that water mass affects in a linear way the compressor torque.

In the context of this study, the application of CFD showed that only a tiny fraction (≈ 0.5%) of the ingested liquid water changed to the vapour phase at the first compressor stages. Ingested water concentrates in liquid form and occupies a negligible fraction of the annulus. Although a small quantity of water may evaporate in the last stages of a multistage compressor, it was concluded that it has an insignificant effect on thermodynamic properties of the air. In addition to this, the literature review in chapter 4 (subsection 4.3.3) revealed

that the evaporation rate of the rain droplets in the compressor is low and can be neglected when rain ingestion effects are investigated. Evaporation takes place mainly in the combustor.

8.2 Combustor

It has been analysed that under water ingestion conditions most of the water entering the core engine will pass to the burner. Evaporation process starts from the first compressor stages due to higher air temperature. However, at these stages heat transfer rate is low. A part of liquid water evaporates at the last stages of the compressor. The diffuser causes a decrease in both air and water velocity. In the combustor, the high temperature environment increases dramatically the evaporation rate, which absorbs a substantial amount of the released heat. Consequently, evaporation causes a decrease in flame temperature and drops the combustion efficiency. Moreover, the increase of the working fluid volume acts as a throttle to the compressor and this decreases the air mass flow. Hence, assuming a constant fuel rate, there is enrichment in fuel-air mixture, which causes combustion extinction (flameout).

However, evaporation is not the only effect of water addition on combustor. Chemical – mechanical interactions between the flame and the water, fuel – air mixing and reaction kinetics contribute to a great extend to drop the combustor's ETA. Consequently, the burner's ETA deterioration, which is measured during experimental water ingestion conditions, cannot be attributed solely to the evaporation of liquid water. The aforementioned phenomena are also important.

Data for combustor's ETA estimation were exported from experimental test rig presented in AGARD (1995). These data are demonstrated in figure 4-29, in which a semi-logarithmic plot of combustion efficiency is presented. It is observed that the combustion efficiency is decreased with increasing water concentration. Furthermore, flameout occurs when the efficiency is reduced about 40%, which is consistent with the typical dry combustor operating limits.

When the liquid water film enters into the combustor, it flows mostly across the combustor casing and its thickness develops with the ingested water mass (chapter 4, figure 4-28). When its thickness reaches a critical value, it enters to the primary and dilution zone through the combustor liner. At this phase, the water has a great impact on flame and destabilizes the whole process. Hence, the combustor's performance deterioration is higher. In addition to this, the total pressure loss across the burner is increased. In this case, water in any form (liquid or spray) disturbs the airflow field. Moreover, the discreteness of liquid phase contributes to the pressure loss.

The total pressure loss estimation was based on the experimental results from work done in Purdue University Laing et al. (1993), Laing et al. (1993), Minster and Murthy (1991), Shastri et al. (1994), Shastri et al. (1995). In this analysis, the Pressure Loss Factor (F_{PL}), which is a principal combustor performance parameter defined by equation 4-31, was experimentally estimated (chapter 4, subsection 4.6.1, figure 4-26).

Both data for combustor's pressure loss increase and its ETA deterioration were imported to the simulation code (Turbomatch) and were used to calculate combustor's performance for given quantity of water mass. The results are discussed in the following subsection. Due to the extent of work, the author has used experimental results for the simulation code and he did not proceed to an independent numerical investigation for the combustor's performance under water ingestion conditions. This part of the study is suggested for further work.

It is concluded that the application of the aforementioned methodology for both compressor and combustor resulted in the estimation of their performance deterioration under operation with water ingestion. Hence, the third milestone of the primary objective has been achieved, as set in chapter 2. The milestone was the investigation of engine's major components performance deterioration due to water ingestion. The compressor and the combustor were examined because the water presence affects mostly them. However, the effects on turbine should not underestimated and a thorough investigation is proposed in further work.

8.3 Engine Performance Simulation

8.3.1 PCN Handle

The effects of water ingestion in a gas turbine engine performance are included in the Turbomatch new version (June 2008). New subroutines calculate the deterioration, which is caused due to engine's operation in rain conditions. Furthermore, the extra torque needed by the compressor to accelerate the liquid water film, which is formed on the blade, is also calculated and added to the compressor work. The code was tested by simulating the performance of a J79-GE-17 single spool turbojet engine produced by General Electric.

When the rotational speed is kept constant (PCN handle), although the compressor work due to water is increased, the engine is forced to keep a constant rotational speed. Moreover, energy is absorbed to evaporate the liquid water in the burner. Consequently, TET and m_f are increased. In the compressor, there is a noticeable movement of the compressor's operating point towards the surge line. The compressor centrifuges the water and its work demand is increased while there is deterioration in PR, ETA and WAC. Downstream, water evaporates in the combustor and m_f - TET are increased to

provide energy for the turbine to keep the engine at PCN=0.7. The combined effects of components deterioration is expressed by 12.5% WAC degradation and PR 3.5% for 6% WAG (chapter 7, subsection 7.3.1).

In the same case, a slight raise in PR is observed since the WAC deteriorates and the compressor approaches to surge. The energy exchange between the water droplets and the air particles results in reduced air speed, thus lower values of air enter the compressor (deteriorated WAC). Considering the velocity triangles, the air incidence angle onto rotor blades is increased and so does PR until flow separation inception drives the compressor to stall. However, the compressor cannot achieve PR values, which were obtained during its operation in dry conditions. This is attributed to the fact that air speed does not change in a uniform way. Water affects both air velocity-distribution and the flow direction across the blade span. This results in PR and ETA reduction, relatively to the dry values for the same WAC.

It is also observed a decrease in surge margin (SM). For dry conditions, SM is 0.23 and it reduces to 0.04 for 6% WAG (CN=0.7). Large water quantities have a pronounced effect on SM. It has been shown that small water quantities have a negligible effect on PR. It seems that the very thin liquid film, which is formed by small water quantities, cause air disturbances of low amplitude and their effect are not detectable. At larger water content, the liquid film obtains wavy characteristics due to the shear action of air and their aerodynamic impact is evident.

Similarly, the compressor's ETA deteriorates under water ingestion conditions. The physical mechanism for the compressor's ETA reduction incorporates the disruption of the airflow due to energy exchange between the water droplets and the air particles, as it has been analysed in the previous paragraph. It is noteworthy that the effects cannot be isolated and they influence each other acting towards blade's performance deterioration. It was observed an 11.5% ETA degradation for 6% WAG (chapter 7, figure 7-10).

The study also showed a dramatic increase in compressor work. For WAG values up to 6%, COMPW increases about 30% at PCN=0.7. This value is a result from the combined effect of torque due to water centrifugation and the deterioration in compressor ETA since the latter affects enthalpy calculations at the compressor exit (i.e. enthalpy property is used for the compressor work calculation). Neither the reduction in WAC nor the PR increase can counterbalance the percentage of torque increase. In any case, a message in the results file informs the user of the effect caused in PR, ETA, WAC and COMPW merely by the ingested water.

8.3.2 TET Handle

When TET is used as handle, the change in compressor map is characterized by a reduction in PCN due to the increased compressor work. In that model a 10% reduction in PCN has been estimated for 4% ingested water/air. This change in engine's rotational speed is caused mainly by water centrifugation. Moreover, PR and WAC are reduced and this is a result of the combined PCN change and their deterioration due to water ingestion (chapter 7, figure 7-16). The aforementioned behaviour of the code agrees to a certain extent with the physical phenomenon of ingested water in a gas turbine engine because the loss of rotational speed is the first and most important effect of water ingestion in a gas turbine engine.

Warwick (1963) conducted water ingestion tests in a J79-GE-8 engine to investigate the power loss occurrences during operation in rain conditions. Turbomatch was used to simulate engine's performance at the test cell conditions (0.9 Mach speed at 40,000 ft altitude and 2.9%, 3%, 3.4% and 3.5% WAG, TET handle). The results were compared with test data and the difference of PR and N, between simulated and test data was recorded (chapter 7, figure 7-21). The error in N change estimation varies from 3.2% up to 7% and in PR from -1.7% up to 3.9%. The variation can be justified by considering the assumptions made to build the water ingestion mode in the simulation code. It is certain that compressor blade clearance, the change in surge line, the geometry of the engine's compressor and the engine control system influences engine performance in the test cell. The above parameters were not included in the simulation software calculations.

The simulation of the described model showed that in the combustor there was a 4% increase of total pressure loss when 6% WAG. The expected detrimental effect of water was obvious. A key feature of total pressure loss change was the linearity (chapter 7, figure 7-5). This was justified by the fact that pressure loss depends on the form in which the water is present (either liquid, spray or a combination) as well as its mass. The author supports that liquid water has a greater impact on pressure loss than spray or vapour. This is because it flows mainly in the combustor's casing wall, which is the area where the boundary layer develops. Bearing in mind that liquid water film thickness depends almost linearly in water mass content (chapter 6, subsection 6.5.3, figure 6-13), this linearity is valid for the pressure loss calculation.

As far as the combustor's ETA is concerned, Turbomatch has calculated its deterioration as well. For 6% WAG combustor's ETA deteriorates about 5% (chapter 7, figure 7-4). The change has exponential characteristic, which are pronounced for values above 3% of water mass fraction. This declares a high rate of change for these values of ingested water. This may be justified by the fact that the amount of water entering the combustor's primary zone is not

increased in direct proportion to the amount of water ingested initially into the air stream. The flow features in the combustor is analysed in the previous subsection.

The study has shown that the ingested water affects engine's performance parameters like the Specific Fuel Consumption (SFC), Net Thrust (FN) and Specific Thrust (SFN). This is an expected result from the performance deterioration of engine's major components. Engine performance deteriorates (SFC increase and FN, SFN decrease) because of the simultaneous decrease in engine PCN, TET and the increase in m_f. However, Turbomatch simulates this degradation with the limitation that, in the input file, it is necessary to use as handle either model's PCN or TET (i.e. using PCN as handle, TET increases with water ingestion and this result in an increased FN and SFN). The code simulated the FN and SFN reduction when TET was used as handle. For 4% WAG, the deterioration value is calculated 3.15% for SFN and 16.6% for FN (chapter 7, figure 7-18). Engine is forced to work at part speed with deteriorated compressor (WAC, PR and ETA) and combustor (DLP, ETA). Air mass flow and its speed is reduced resulted in a reduction in FN and consequently in SFN.

Another engine parameter, which deteriorates under water ingestion condition, is the SFC. The combined effect of fuel flow (m_f) increase and FN reduction results in SFC rise of about 33% for 4% ingested water. The behaviour of m_f when PCN is used as handle is straightforward. It is increased to provide the energy for both water evaporation in the burner and the extra compressor work due to the water centrifugation. However, when TET is used as handle, m_f is increased for low WAG (<3%) to provide energy for the water evaporation in the burner while PCN is reduced. For larger WAG values, engine works at very low rotational speed and m_f gets lower values because this effect counterbalances the demand due to evaporation.

In the author's view when a jet engine ingests water, there is a reduction in PCN and TET (PCN comes first due to water centrifugation in the compressor) regardless of the throttle position. The pilot's reaction to engine's deceleration is to position the throttle forward trying to accelerate. Consequently, the fuel flow is increased and this makes things worse because further power loss occurs due to rich flame extinction. However, improved engine control systems may protect engine from off-schedule operation. Main Fuel Control component, assisted by computerised sensors, can detect the low PCN, low air mass flow and reduced TET and it may limit the fuel flow accordingly.

It should be acknowledged that not many experimental data were available for adequate validation of water ingestion simulation (chapter 7, subsection 7.5). Furthermore, in some cases the exported data compared with the theoretical results produced errors, which may be unacceptable for a contemporary simulation tool. However, it is noteworthy that many difficulties emerge when

attempting to simulate water ingestion. More specifically, the phenomenon is geometry and time dependent. This means that under identical atmospheric conditions water distribution at a small gas turbine engine inlet will be different from that in a large turbofan engine. Moreover, the centrifugal force to the liquid water droplets affects their motion and film formation in different ways when the size of the compressor is changed appreciably. Finally yet importantly, water distribution differs in the combustors of different size. Consequently, the results from the Turbomatch software must be considered from the point of view of the engine performance trends, as far as the water ingestion phenomenon is concerned.

In table 8-1, all the theoretical and experimental results are grouped together:

WATER INGESTION RESULTS			
Parameter	**This study**	**Experimental Results**	**Source**
Effect of droplet size	fine droplets (1 μm to 100 μm): no considerable difference in water deposited mass and film thickness	droplets from 51 μm to 97 μm: had the same effect on the compressor behaviour.	Williams et al (2005)
Film thickness	rotor blade: few hundredths of mm, stator blade: a fraction of an mm	rotor blade: few hundredths of mm, stator blade: a fraction of an mm (only theoretical results)	Gyarmathy (1962), Kirillov & Yablonik (1968), Hammitt, Hwang, et al. (1975), Hammitt, Krzeczkowski, et al. (1981)
Film motion velocity vector angle	For model rotational speeds higher than 40%, the speed vector angle is higher than 77°.	82° (8° from the radial direction)	Williams et al (2005)
Film motion velocity	0.2 m/sec to 2.3 m/sec for WAG=2% to 30%	1 m/sec for 15% WAG	Williams et al (2005)
Compressor ETA	For 15% WAG, ETA deteriorates from 3% (full speed) to 12% (idle speed). Engine simulation: 11.5% for 6% WAG (PCN handle).	5% when 17% WAG	Williams et al (2005)
		4% for 15% WAG	Murthy, Ehresman, et al. (1986)
PR	Compressor: for 4% WAG, PR deteriorated 0.44% (full speed) and 0.62% (idle speed). For 10% WAG, these values became 0.55% and 0.82% respectively. Engine simulation: PR deteriorated 1.15% for 10% WAG.	5% PR deterioration for 15% WAG	Murthy, Ehresman, et al. (1986)
		1% for 4% WAG, 10.1% for 10% WAG	Williams et al (2005)
		The error in PR change calculation between theoretical and experimental results varies from -1.7% up to 3.9%.	Warwick (1963)
WAC	Compressor: 2.4% for 4% WAG. Engine simulation: 12.5% for 6% WAG.	-	-
Torque	20%-25% for 4%-5% WAG. 38% for 10% WAG. Engine simulation:30% for 6% WAG (PCN handle).	34% for 10% WAG	Williams et al (2005)
		The error in N calculation between theoretical and experimental results varies from 3.2% up to 7%.	Warwick (1963)
Combustor Pressure Loss	4% increase for 6% WAG	The simulation results are based on the experiments.	Laing, Shastri et al (1993)
Combustor ETA	5% for 6% WAG	The simulation results are based on the experiments.	AGARD AR-332 (1995)
Net Thrust	16.6% for 4% WAG	-	
Specific Net Thrust	3.15% for 4% WAG	-	
Specific Fuel Consumption	33% rise for 4% WAG	-	

Table 8-1: Theoretical and Experimental Results

The described results indicate that the fourth milestone of the primary objective has been achieved, as set in chapter 2, which was to develop a simulation code to account for the effects of water ingestion and its integration with the

Turbomatch simulation tool. The work included thorough tests of the code under extreme water ingestion cases. The latter accomplished the scope of this study, which was to investigate and quantify the performance deterioration of a gas turbine engine due to water ingestion.

9 Conclusions – Further Work

This chapter focuses on the conclusions and observations of this study. A number of recommendations for the potential further work are also suggested, which the author believes that they will strengthen a relevant future study.

9.1 Conclusions

In the context of this study, the computational grid of a compressor stage was created. The work included blade optimization by using CFD software. The grid was imported in a CFD code and the details of the flow in an axial compressor and how it is affected by the presence of water were examined.

An important outcome of this work was the creation of a computer code to evaluate the liquid water film thickness and its motion on an axial-flow compressor rotor blade under water ingestion conditions. The change in blade's profile and surface was imported in CFD, which calculated the change in the performance parameters of the compressor stage.

This study also achieved the upgrade of a gas turbine engine performance-simulation code to account for the effects of water ingestion. The improved software can now simulate engine's deterioration when water is ingested.

Furthermore, the author's research work in this subject resulted in one conference paper while two more papers are about to be submitted.

Lastly, in the author's view, this study constitute a significant contribution to knowledge because the results of the jet engine components deterioration due to water ingestion can be utilized by any existed or under development simulation code. Moreover, the outcome can be used to conduct on-ground and in-flight engine tests. During these tests the water ingestion parameters (droplet mass, size, speed) should be clearly defined because they affect the intensity of the phenomenon.

9.1.1 Methodology

The analysis conducted by this study showed that Computational Fluid Dynamics (CFD) is a powerful tool to track the water droplets and explore their behaviour under the influence of a high-speed airflow.

The methodology followed in this study proved that changing the blade's profile (by importing new Cartesian coordinates x, y, z of the blade's pressure surface) cannot simulate the compressor's performance deterioration. This is attributed to the fact that CFD code not only smoothes the grid but also it performs several checks for grid suitability avoiding negative volumes and big skew angles.

Hence, the wavy characteristics of the liquid film cannot be simulated by only thickening the blade's profile.

The methodology also revealed that the CFX-Tascflow Moving Grid feature is not suitable for changing the blade's pressure surface simulating the thickening of blade's profile due to the water film formation. With this feature, the code is capable of tracking and modelling the changes in grid node position over time. To do this type of simulation the user must define how the grid moves within time. The grid movement process is controlled by user-coded routines.

For the first time, this work attempted successfully to incorporate the roughening effect of water droplets on a blade surface. It was considered that the momentum of water droplets disturbs the liquid film surface and the air shear force develops waves on it. Hence, the increase in drag coefficient was related with the equivalent sand-grain roughness making possible performance deterioration calculations by CFD. Data for water film motion were provided by the FILM_MOTION code created by the author.

Another original point in this study was the calculation of the compressor torque due to the water centrifugation. An analytical method was used considering for each one droplet its mass and its exit position from the blade, as the liquid film flows towards the blade tip or the trailing edge.

9.1.2 Application of CFD

This work demonstrated through several case studies that almost all the ingested water impacts on the blade's pressure surface, while on the suction surface there are spots of a few water droplets. The computational analysis revealed that the inertial impact is the dominant mechanism in droplet's deposition. Fine droplets, due to their small inertia, may follow the air streamlines and avoid impingement at the first compressor stages. When evaporation takes place then, the suction surface of the blade appears to be wet due to the diffusion mechanism.

It was proved that the thickness of the liquid film, which is formed on the blade pressure surface, depends on the droplet mass, its diameter, its initial ingestion velocity and the blade rotational speed. The ingested water mass and the blade rotational speed are the most dominant factors.

More analytically, the increase of the water mass fraction causes an increase of the water film thickness. In addition to this, the increase of water content from 4% to 30% almost doubles the film thickness in case of a rotor blade. It was also shown that, film is thicker in idle speed because the centrifugal force is lower, its speed is smaller and that, in connection with mass continuity, leads to a thicker film.

The study also showed that water droplet size has an effect on build-up process and consequently on film formation. Fine droplets evaporate more easily than coarse droplets. Large droplets deposit more easily than fine droplets, because they have higher inertia than air particles and they cannot follow the air streamlines. Consequently, large droplets develop a thicker water film. It was shown that film thickness increases about 16% when the droplet diameter changes from 1 mm to 3 mm. However, the effect is almost negligible when fine droplets are considered.

It was shown that droplet's initial speed affects the deposited water mass fraction. High-speed injected droplets can avoid the rotor blade row although it is more difficult to follow the air streamlines due to their high inertia.

The analysis carried out by this study showed that when engine works at part load (i.e. reduced rotational speed) the water film becomes thicker. It was calculated a 63% reduction of film thickness when engine goes from 20% (i.e. extreme case) to 100% speed. Water film is moving mainly under the influence of centrifugal and air shear force. These forces depend on blade's angular speed. Furthermore, water droplets are accelerated at high speed in the tangential direction and then are decelerated to axial direction by the stator blades.

The study also showed that in a rotor blade, film thickness could reach the values of few hundredths of mm. For the rotor blades, there are not any experimental values, possibly due to the difficulties of obtaining the measurements. The calculations for stator blade (zero rotational speed) revealed that the values of water film height counts a fraction of an mm.

It was shown that film motion is nearly radial at a big range of angular speed. For speeds higher than 40%, the speed vector angle is above 77°. Another noticeable point was the liquid film chord-wise speed. It was found that it ranges from 0.2 m/sec to 2.3 m/sec depending on rotational speed and ingested water mass.

The analysis conducted by this study revealed that water ingestion cause a deterioration in compressor and combustor performance. It was calculated that compressor efficiency degrades about 8.5% for idle speed, 1.6% for full speed when 4% water is ingested. At part speed, the effects are more obvious because the water film is thicker due to lower centrifugal force.

Similarly, the code showed that the ingested water affects slightly the compressor's ability to raise the pressure of the airflow. The effects are almost negligible for a wide range of water mass. For 4% WAG, PR deteriorates 0.44% (full speed) and 0.62% (idle speed). For 10% WAG, these values become 0.55% and 0.82% respectively. The results agree with other experimental

results for up to 4% water mass content. However, for large water quantities (>6%), it seems that the theoretical results underestimate the deterioration in pressure ratio. In the author's view, the difference is attributed to the tip clearance effects, which were not taken into account in the theoretical model. It was also found that the non-dimensional mass flow is reduced about 2.4% due to 4% water content.

This work also demonstrated the mechanical effects of water ingestion. When the water impinges on the blade pressure surface, it forms a film, which flows radially outwards under the influence mainly of the centrifugal force. Air shear force and water droplets momentum, which act in the chord-wise direction, are low compared with the radial forces. The results confirm the dramatic increase in compressor torque demand and for 4%-5% water content, it can be 20%-25%. Furthermore, this change is directly proportional to the amount of ingested water.

In the context of this study, the application of CFD showed that only a tiny fraction (≈ 0.5%) of the ingested liquid water changed to the vapour phase at the first compressor stages. Ingested water concentrates in liquid form and occupies a negligible fraction of the annulus. Although a small quantity of water may evaporate in the last stages of a multistage compressor, it was concluded that it has an insignificant effect on thermodynamic properties of the air.

9.1.3 Engine Performance Simulation

The analysis carried out by this study showed that there is a noticeable movement of compressor's operating point towards the surge line, when engine's rotational speed is kept constant (PCN handle). In this case, although the compressor work due to water is increased, engine is forced to keep a constant rotational speed. Consequently, it was demonstrated that turbine entry temperature (TET) and the fuel flow (m_f) are increased. Compressor centrifuges the water and its work demand is increased while there is deterioration in PR, ETA and WAC. Downstream, water evaporates in the combustor and m_f - TET are increased to provide for the turbine to keep the engine at PCN=0.7. The combined effects of components deterioration is expressed by 12.5% WAC, 11.5% ETA and PR 3.5% degradation for 6% WAG. For the same water quantity, the compressor work is increased by 30%.

It was also observed a decrease in surge margin (SM). It reduces from 0.23 (dry conditions) to 0.04 for 6% WAG. Large water quantities have a pronounced effect on SM. It has been shown that small water quantities have a negligible effect on PR. It seems that the very thin liquid film, which is formed by small water quantities, cause air disturbances of low amplitude and their effect are not detectable. At larger water content, the liquid film obtains wavy characteristics due to the shear action of air and their aerodynamic impact is evident.

When TET was used as handle, the simulation tool showed deterioration in engine's performance. In this case, the change in compressor map is characterized by a reduction in PCN due to the increased compressor work. In that model a 10% reduction in PCN has been estimated for 4% ingested water content. This change in engine's rotational speed is caused mainly by water centrifugation. Moreover, PR and WAC are reduced and this is a result of the combined PCN change and their deterioration due to water ingestion. The aforementioned behaviour of the code agrees to a certain extent with the physical phenomenon of ingested water in a gas turbine engine because the loss of rotational speed is the first and most important effect of water ingestion in a gas turbine engine.

The analysis carried out by this study showed that combustor's ETA is reduced about 5% for 6% water mass content. The change has exponential characteristic, which are pronounced for values above 3% of water mass fraction. This declares a high rate of change for these values of ingested water. This is justified by the fact that the amount of water entering the combustor's primary zone is not increased in direct proportion to the amount of water ingested initially into the air stream. Moreover, it was demonstrated that the pressure loss across the combustor is increased when water is ingested. It was calculated a 4% increase of total pressure loss when 6% WAG.

The deteriorated performance of the engine's major components, results in reduced performance parameters like the Specific Fuel Consumption (SFC), Net Thrust (FN) and Specific Thrust (SFN). This study showed that SFC is increased and FN, SFN are decreased because of the simultaneous decrease in engine PCN, TET and the increase in m_f. For 4% WAG, the deterioration value is calculated to 3.15% for SFN and 16.6% for FN (TET handle). Engine is forced to work at part speed with deteriorated compressor (WAC, PR and ETA) and combustor (DLP, ETA). Air mass flow and its speed is reduced resulted in a reduction in FN and consequently in SFN.

Furthermore, the analysis demonstrated that the combined effect of fuel flow (m_f) increase and FN reduction results in SFC rise of about 33% for 4% ingested water. The behaviour of m_f when PCN is used as handle is straightforward. It is increased to provide the energy for both water evaporation in the burner and the extra compressor work due to the water centrifugation. However, when TET is used as handle, m_f is increased for low WAG (<3%) to provide energy for the water evaporation in the burner while PCN is reduced. For larger WAG values, engine works at very low rotational speed and m_f gets lower values because this effect counterbalances the demand due to evaporation.

In the context of this work, it was revealed that the simulation of water ingestion phenomenon is a difficult task due to the fact that it is geometry and time

dependent. This means that under identical atmospheric conditions water distribution at a small gas turbine engine inlet will be different from that in a large turbofan engine. Moreover, the centrifugal force to the liquid water droplets affects their motion and film formation in different ways when the size of the compressor is changed appreciably. Finally yet importantly, water distribution differs in the combustors of different size. Consequently, the results from any simulation software must be considered from the point of view of the engine performance trends, as far as the water ingestion phenomenon is concerned.

9.2 Further Work

In this subsection, the author discusses his recommendations for potential further work on the subject of water ingestion.

The use of an upgraded CFD code should be enabled because:

- The phenomena of droplet break-up and coalescence under the influence of high-speed air have been neglected.
- It has been assumed that if the water droplets impinge on the blade pressure surface, they deposit on it (i.e. no splashing).
- CFD code was unable to converge when low-speed water droplets were injected (i.e. Vw≈5-10 m/sec). Thus, the energy exchange between these droplets with the high-speed air has not been completely simulated.

It is expected that these points can be improved by using upgraded CFD codes, which incorporate these effects.

The intensity of scoop effect should be further examined. It was referred that this results in an increase of the water concentration, which enters the engine. Furthermore, the proposed values for rain certification tests do not account for the scoop effects. Hence, it will be of primary importance the investigation of this topic. CFD capabilities can be utilized to determine the water concentration in the engine intake.

The subroutine in FILM_MOTION code for calculating the force acting on a water droplet can be expanded to include the friction force between the liquid film and the blade surface. Furthermore, the study has assumed that the blade is a flat plate without considering its geometry (i.e. stagger angle). The model can be improved by integrating Williams and Young (2006) work into the FILM_MOTION code. Thus, the code will be able to model the water film motion on a blade of arbitrary shape.

It has already been explained that the tip clearance effects have not been included in this study. In this area, the water is splashed back into the blade span and further deteriorates the compressor's performance. The model can be improved considering the development of liquid film on the compressor casing (simulated by a flat plate) and its motion under the shearing action of air.

It has been analysed that the compressor torque due to water was calculated based on the assumption that the blade accelerates the water film to half of its tangential speed (i.e. this is the liquid film velocity when it exits from the blade surface). In the author's view, assuming that the liquid film obtains the tangential blade speed results in an overestimation of torque due to water. The former assumption gave more sensible results than the latter. In any case, the liquid film exit speed should be examined in detail. The FILM_MOTION code can be improved to calculate the liquid film velocity when it exits from the rotor blade domain (relative frame of reference) and enters the stator blade domain (absolute frame of reference).

As it was thoroughly described before, the model consisted of one compressor stage preceded by an IGV blade row. It would be advisable to examine the effects of water ingestion incorporating a multistage compressor model. The reason is that at the last stages of a multistage compressor some of effects are more intense (like evaporation) while some others (energy exchange between air and water particles) are alleviated. Although the computational resources may currently limit the creation of a fine multistage-compressor grid, it seems that this restriction would be overcome in the near future.

In this study, the method of *one-factor-at-a-time* was used for the design of the simulation. Using this approach involves the selection of a starting point for each factor and then varying it while the other factors are held constant. The major disadvantage of this strategy is that it cannot take into account any possible interaction between the factors. In this work, it was found that none of the above parameters produce the same result for different values of the other two (i.e. water mass has different effect for small and large droplets). Consequently, the *one-factor-at-a-time* strategy seems to be inadequate for this type of test. In this case, the *factorial-design* should be involved, which means that all the possible combinations of the parameters should be investigated. More specifically, due to the variation of the factors, the planning of the experiment should be based on a scientific statistical model.

In the context of this work the surge line was assumed unaffected by the water flow in the compressor. However, it was analysed that compressor is more susceptible to stall under water ingestion conditions. In the author's view, this is a key point for determining compressor's performance in the limit of surge line. It would be extremely helpful to investigate the effects of water on stalling conditions and the consequences on the surge line by utilizing CFD capabilities.

Another point, which should be further examined is the temperature of water when it enters the burner. This value is needed for the evaporation calculations in the TURBOMATCH subroutine, which performs the combustor's thermodynamic calculations. In this study, the author tried several values within the range 290°K to 300°K and found out that the impact of this factor depended mainly on the water mass (i.e. high water temperature has minor impact when it refers to small water quantities). Finally, the value of 295°K was chosen based. In any case, the water temperature entering into the combustor should be examined based on heat and mass transfer processes.

It has been discussed that the evaporation model adopted in this study assumed that only half of the water mass evaporated in the combustor. The rest flows downstream to the turbine as liquid. This was a result of a parametric analysis, which was needed to investigate the amount of vapour water mass fraction produced in the combustor. The author stated that only part of the water evaporates in the combustor although its high-temperature environment. The heat transfer process in the combustor and the subsequent water evaporation affects the combustor's performance and should be examined in detail.

Furthermore, in this work the combustor's performance calculation (i.e. pressure loss and efficiency) was based on published experimental measurements. The evaporation, which takes place in the combustor primary zone results in a reduction in exit temperature. Moreover, water addition on a gas turbine combustor has several effects apart from the evaporation of liquid water. Firstly, there are effects on fuel – air mixing and the formation of recirculation zones upstream of the primary jets. Secondly, there are chemical – mechanical interactions between the flame and the water. Thirdly, there are direct effects on reaction kinetics. Consequently, combustor's ETA deterioration and pressure loss rise should be taken into account in any case of water ingestion simulation. The application of CFD methodology would be advisable to investigate the effects of water ingestion. This would also cast light on the way the water flow affects the chemical kinetics and the flame stability.

In the context of this study, the effects of water ingestion on the turbine were almost neglected. The change in fluid properties was only taken into account. However, the author argued that turbine performance indeed deteriorates due to the presence of liquid water rivulets. Many researchers arrive at the same conclusion about the long-term effects of water presence in the turbine like the erosion. Thus, an analysis should be performed in order to investigate the turbine's performance under water ingestion conditions. Methodology similar to this of the current work can be utilized.

As it has been thoroughly discussed, the TURBOMATCH code uses either PCN or TET as handle (constant). In case of water ingestion, this is a compromise because water ingestion affects both PCN and TET of a gas turbine engine. In

the author's view when a jet engine ingests water, there is a reduction in PCN and TET (PCN comes first due to water centrifugation in the compressor) regardless of the throttle position. The pilot's reaction to engine's deceleration is to position the throttle forward trying to accelerate the engine. Thus, the fuel flow is increased and this makes things worse because further power loss occurs due to rich flame extinction. Hence, the use of fuel flow as handle would be more appropriate (i.e. no movement of the throttle but reduction in rotation speed). In the old versions of the TURBOMATCH code, the fuel flow was directly related to TET. In the upgraded version, water evaporation alters TET for the same amount of fuel. Thus, it is recommended that the TURBOMATCH's user should be able to use as a handle the fuel flow of the simulated engine.

REFERENCES

[A]

AEA Technology Engineering Software, *CFX-BladeGen User's Guide version 4.1*, 2001a.

AEA Technology Engineering Software ,*CFX-Turbogrid Documentation version 1.6*, 2001b.

AEA Technology Engineering Software, *CFX-Tascflow Theory documentation version 2.12*, 2002.

AGARD Advisory Report No 332 (1995): Recommended Practices for the Assessment of the Effects of Atmospheric Water Ingestion on the Performance and Operability of Gas Turbine Engines, Neuilly-sur-Seine, France.

Anderson W.H. and Wolfe H.E.: Aerodynamic Breakup of Liquid Drops. In: *Proceedings of 5th International Shock Tube Symposium,* 1965, White Oak.

Ashenden R., Lindberg W., Marwitz J. and Hoxie B. Airfoil Performance Degradation by Supercooled Cloud, Drizzle, and Rain Drop Icing. *Journal of Aircraft,* **33** (6), 1996a, p. 1040-1046.

Atlas D. *Advances in Radar Meteorology*, N.Y.: Academic Press, 1964.

[B]

Bardey X., Desaulty M., Jolu J., Meunier M. and Mouton P., Inventors, SNECMA, F., (1994) Gas Turbine Engine with Improved Water Ingestion Prevention. U.S. Patent. 5,339,622.

Bilanin A.J., Scaling Laws for Testing Airfoils Under Heavy Rainfall. *Journal of Aircraft* **24** (1), 1987, 31-37, [AIAA 85-0257].

Bong-Hwa S. and Gene S.: Temperature and surface behaviour of water film driven by co-current steam flow. In: *1st International Symposium on Transport phenomena, Heat transfer and fluid flow in rotating machinery,* 1987, Honolulu, USA.

Bose T. K. and Murthy S. N. B.: Blade Clearance Estimation in a Generic Compressor with Air-Water Mixture Operation. In: *30th AIAA, ASME, SAE, and ASEE Joint Propulsion Conference,* 1994, Indianapolis, IN, AIAA 94-2693, p. 30-40.

Bussmann M., Chandra S. and Mostaghimi J., Modelling the splash of a droplet impacting a solid surface. *Journal of Physics of Fluids,* **12** (12), 2000, p. 3121-3132.

[C]

Chandra S. and Avedisian C.T. On the collision of a droplet wih a solid surface. *Proceedings of Royal Society of London part A,* **432,** 1991, p. 13-41.

Cohen L. and Hanratty T. Effect of waves at a gas-liquid interface on a turbulent air flow. *Journal of Fluid Mechanics* **31** (3), 1968, p. 467-479.

Cranfield University (2007) The Turbomatch code, Cranfield University, UK.

[D]

Das K., Hamed A., and Basu D.: Droplet trajectories and collection on fan rotor at off-design conditions. In: *Proceedings of ASME Turbo Expo 2006 Power for Land, Sea and Air,* 2006, Barcelona, Spain, GT-2006-91214.

[E]

EASA (2007), Certification Specifications for Engines CS-E 790: Ingestion of Rain and Hail

[F]

FAA (1998), Federal Aviation Regulation Part 33.78, Airworthiness Standards: Aircraft Engines, USA.

FAA (2001), Policy Statement Number ACE-00-23.901, **66** (4), FAA.

Freeman, C. (2004), private communication.

[G]

Gardner G.C., Viscous flow of a liquid over a rotating surface with gas drag. *Journal of Applied Mechanics,* **30**, 1963, p. 7-12.

Gelfand B.E., Droplet Break up Phenomena in Flows with Velocity Lag. *Progress in Energy Combustion Science,* **22** (3), 1996, p. 201-265.

Gyarmathy G., (1962), Bases of a theory for wet steam turbines, Zurich: Institute for thermal turbomachines, Federal Technical University,

Translation T-781.

[H]

Haines P. and Luers J. Aerodynamic penalties of heavy rain on landing airplanes. *Journal of Aircraft,* **20** (2), 1983, p. 111-119.

Hale A., Klepper J., and Hurwitz W.: A Numerical Capability to Analyze the Effects of Water Ingestion on Compression System Performance and Operability. In: *ASME TURBO EXPO 2005: Power for Land, Sea and Air,* 2005, ASME, Reno, USA.

Hammitt F.G., Hwang J.B., and Kim W., (1975a), Liquid film thickness measurements in university of Michigan wet steam tunnel, PB-247804/8, Michigan, USA: The University of Michigan.

Hammitt F.G., Hwang J.B., Manguso A., Krause D., and Blome S., (1975b), Liquid film thickness tests: wet steam tunnel, Michigan, USA: The University of Michigan.

Hammitt F.G., Krzeczkowski S., and Krzyzanowski J., Liquid film and droplet stability consideration as applied to wet steam flow. *Forschung im Ingenieurwesen,* **47** (1), 1981, p. 1-14.

Haykin, S. and Murthy, S.N.B. (1987a) Jet engine simulation with water ingestion through compressor (Final Report).

Haykin T. and Murthy S.N.B. Transient Engine Performance with Water Ingestion. *Journal of Propulsion and Power,* **4** (1), 1988, p. 81-88.

Hill P.G., Miyagawa K. and Denton J.D., Fast and accurate inclusion of steam properties in two- and three-dimensional steam turbine flow calculations. *Proceedings of Institution of mechanical engineers, Part C: Journal of Mechanical Engineering Science,* **214,** 2000, p. 903-919.

Horlock J. H.: Compressor performance with water injection. In: *Proceedings of ASME Turbo Expo 2001,* New Orleans, ASME 2001-GT-0343.

Hsiang L.P. and Faeth G.M., Near-limit drop deformation and secondary breakup. *International Journal of Multiphase Flow* **18** (5), 1992, p. 635-652.

[J]

Jackson N.: Certification issues and their impact on the design of the Trent 800. In: *1997 European Propulsion Forum - Design of Aero Engines for Safety, Reliability, Maintainability and Cost,* 1997, Technische Univ. Berlin, Germany, p. 46-53.

Joseph D.D., Belanger J. and Beavers G.S. Break up of a Liquid drop suddenly exposed to a high-speed air stream. *International Journal of Multiphase Flow,* **25**, 1999, p. 1263-1303.

[K]

Kang Shin-Hyoung, Kang Young-Seok, and Han Kyung-Ho: Numerical Study on blade roughness effect on the performance of turbomachines. In: *International Gas Turbine Congress 2003,* Tokyo.

Kennedy J. B. and Roberts J.: Rain Ingestion in a Gas Turbine Engine. In: *4th Annual Conference ILASS-AMERICAS Institute of Liquid Atomization and Spray Systems,* 1990, Hartford, USA, p. 154-162.

Khodadoust A. and Bragg M.B. Aerodynamics of a finite wing with simulated ice. *Journal of Aircraft,* **32** (1), 1995, p. 137-144.

Khoshaim B. H.: Hydrodynamics of rivulet flow over steam turbine blades. In: *IEEE/Engineering in medicine and biology society annual conference, Proceedings of the multiphase flow and heat transfer symp-workshop,* 1979, Miami, USA.

Kirillov I.I. and Yablonik R.M. (1968), Fundamentals of the theory of turbines operating on wet steam, English translation by NASA No TTF-611, Leningrad: Mashinostroyeniye Press.

Kirk Devine: Inclement Weather Induced Aircraft Engine Power Loss. In: *26th AIAA/SAE/ASME/ASEE Joint Propulsion Conference,* 1990, Orlando, FL.

Kissel G.: Rain and Hail Extremes at Altitude. In: *15th AIAA Annual Meeting and Technical Display,* 1979, Washington, DC, AIAA 79-0539.

Koch C.C. and Smith L.H. Loss sources and magnitudes in axial-flow compressors. *Journal of Engineering for Power,* 1976, p. 411-424.

Kreyszig E., *Advanced Engineering Mathematics*, 7th edn. N.Y.: Wiley, 1999.

Krzyzanowski J., The correlation between droplet steam structure and steam

turbine blading erosion. *Journal of Engineering for Power,* 1974, p. 256-266.

Krzyzanowski J.,: Comments on accuracy in predicting steam turbine blading erosion . In: *6th international conference on erosion by liquid and solid impact,* 1983, Cambridge, England.

Krzyzanowski J., Kowalski A.E. and Shubenko A.L., Some aspects of erosion prediction of steam turbine blading. *Journal of Engineering for Gas Turbines and Power,* **116**, 1994, p. 442-451.

Kurzke J, GasTurb10:Gas Turbine Performance Calculations, 2004, Germany

[L]

Laing P., Ehresman C. M., and Murthy S. N. B.: Two and Three-Dimensional Prediffuser Combustor Studies with Air-Water Mixture. In: *31st Aerospace Sciences Meeting and Exhibit,* 1993, Reno, NV, AIAA 93-0240.

Laing P. and Murthy S.N.B., (1992), Gas turbine prediffuser-combustor performance during operation with air-water mixture, FAA-92-G-002 NASA.

Laing P., Shastri R. P., Ehresman C. M., and Murthy S.N.B.: Three-dimensional prediffuser combustor studies with air-water mixture. In: *29th AIAA, SAE, ASME, and ASEE, Joint Propulsion Conference and Exhibit,* 1993, Monterey, CA, AIAA 93-2474, p. 25.

Lee C.H. and Reitz R.D., An Experimental Study of the Effect of Gas Density on the Distortion and Break up Mechanism of Drops in High Speed Gas Stream. *International Journal of Multiphase Flow,* **26**, 2000, p. 229-244.

Liu H. *Science and Engineering of Droplets*, 1st edn. N.Y.: Noyes Publications, 2000.

Loebig J., Vittal B., and Booher M.: Numerical Simulation of Water/Methanol Evaporation in an Axial Flow Gas Turbine Compressor. In: *34th AIAA/SAE/ASME/ASEE Joint Propulsion Conference & Exhibit,* 1998, Cleveland, USA, AIAA 98-3559.

Luers J. and Haines, P., Heavy rain influence on airplane accidents. *Journal of Aircraft,* **20** (2), 1983, p. 187-191.

[M]

Mathioudakis K. and Roumeliotis I. Evaluation of Interstage Water Injection Effect on Compressor and Engine Performance. *Journal of Engineering for Gas Turbines and Power,* **128**, 2006, p. 849-856.

Mattingly J. (2004), EOP PERF Program: Gas Turbine Performance, version 4.2, Virginia, USA.

Mattingly J. (2002), AEDsys: Gas Turbine Performance, Virginia, USA.

Mattingly J., *Elements of Propulsion: Gas Turbines and Rockets*, Virginia, USA: AIAA, 2006.

Mattingly J., Heiser and Pratt, *Aircraft Engine Design*, Virginia, USA: AIAA, 2005.

Meher-Homji C. and Mee T. Inventors Mee Industries, I.C., (2007) Water Removal from a Compressor Air Inlet Duct. U.S. Patent 7,204,670.

Minster T. and Murthy, S.N.B.: Prediffuser-combustor model studies under conditions of water ingestion in engines. In: *27th AIAA, SAE, ASME, and ASEE, Joint Propulsion Conference,* 1991, Sacramento, CA, p. 20.

Montgomery D., *Design and Analysis of Experiments*, USA: John Wiley & Sons, 2005.

Moore M.J. and Crane R.I., (1972) Aerodynamic Aspects of Gas Turbine Blade Corrosion, London: Applied Science Publishers

Moran M.J. and Shapiro, N. *Fundamentals of Engineering Thermodynamics*, N.Y.: John Wiley & Sons, 2000.

Moravec B. and Patnoe, M.: Recommended Values of Rain and Hail Concentrations to be Considered in the Design of Turbine Engines. In: *1996 World Aviation Congress,* 1996, L.A., USA, AIAA 96-5596.

Morsi S.A. and Alexander A.D., An investigation of particle trajectories in two-phase flow systems. *Journal of Fluid Mechanics* **55**(2), 1972, 193-208.

Mucino M., (2007), CCGT Performance Simulation and Diagnostics for Operations Optimisation and Risk Management. PhD Thesis, Cranfield University.

Mundo C., Sommerfeld M. and Tropea C. On the modelling of liquid sprays impinging on surfaces. *Journal of atomization and sprays,* **8**, 1998, p.

625-652.

Mundo Chr., Sommerfeld M. and Tropea C. Droplet-Wall Collisions: Experimental Studies of the Deformation and Break Up Process. *International Journal of Multiphase Flow,* **21**(2), 1995, p. 151-173.

Murthy S.N.B.: Effect of Heavy Rain on Aviation Engines. In: *27th Aerospace Sciences Meeting and Exhibit,* 1989, Reno NV, AIAA 89-0799, p. 19.

Murthy S.N.B. (1996a) Dynamic Performance of High Bypass Ratio Turbine Engines With Water Ingestion, NASA-CR-4703.

Murthy S.N.B.: Effect of Atmospheric Water Ingestion on the Performance and Operability of Flight Gas Turbines. In: *32nd AIAA/ASME/SAE/ASEE Joint Propulsion Conference and Exhibit,* 1996, Lake Buena Vista, FL, AIAA 96-3059.

Murthy S.N.B. and Ehresman C.M.: Effects of water ingestion into jet engine. In: *22nd American Institute of Aeronautics and Astronautics, Aerospace Sciences Meeting,* 1984, Reno, NV, p. 12.

Murthy S.N.B. and Ehresman C. M.: Water Ingestion Simulation-Test Needs. In: *9th International Symposium on Air Breathing Engines,* 1989, Athens, Greece, p. 1133-1141.

Murthy S.N.B., Ehresman, C. M., and Haykin, T.: Direct and system effects of water ingestion into jet engine compressors. In: *Turbomachinery performance deterioration; Proceedings of the Fourth Joint Fluid Mechanics, Plasma Dynamics, and Lasers Conference,* 1986, Atlanta, GA, p. 127-141.

Murthy S.N.B. and Laing P.: Two and three-dimensional prediffuser combustor studies with air-water mixture. In: *11th ISABE - International Symposium on Air Breathing Engines,* 1993, Tokyo, Japan, p. 276-291.

Murthy S.N.B. and Mullican A. (1990) WINCOF-I code for prediction of fan compressor unit with water ingestion (Interim Report).

Murthy S.N.B. and Mullican A. (1993a) Transient performance of fan engine with water ingestion (Interim Report), NASA NAG3-481.

Murthy S.N.B. and Mullican A., (1993b), The WINCOF-I Code: Detailed Description, NASA CR-190779, NASA.

[N]

National Aerospace Laboratory, (2004), GSP 10: Gas turbine Simulation Program, NLR version 10, The Netherlands.

Nikolaidis Th., Pilidis P., Teixeira J.A., and Pachidis V.: Water Film Formation on an Axial Flow Compressor Rotor Blade. In: *Proceedings of ASME Turbo Expo 2008,* 2008, Germany, ASME, GT2008-50137.

Nikuradse J., (1933), Laws of flow in rough pipes, NACA TM 1292.

Noel S. (2003), Siemens V94.3A compressor blading data, (unpublished work).

NTSB, (1980), Aircraft Accident Report: Air Wisconsin Swearingen SA-226 Metro, 12 June 1980, 1980, NTSB-AAR-80-15.

NTSB, (2005), Chairman Letter: Safety Recommendation A-05-19, -20, 31 Aug 2005, USA.

[O]

Oliveira L.A., Costa, V.A.F. and Baliga, B.R., A Lagrangian-Eulerian model of particle dispersion in a turbulent plane mixing layer. *International Journal for numerical methods in fluids,* **40**, 2002, p. 639-653.

[P]

Park K. and Chang K., Computation of Gas-Liquid Droplet Cascade Flows Using Multigrid Adaptive Unstructured Grid. *Journal of Propulsion and Power,* **16** (6), 2000, p. 1002-1010.

Patnoe, M. and Moravec B.: Rain and Hail Threat to Aviation: A Probability Analysis of Extreme Rain/Hail Concentrations Aloft. In: *1996 World Aviation Congress,* 1996, L.A., USA, AIAA 96-5595.

Pinkus O., Liquid Particle Dynamics and Rate of Evaporation in the Rotating Field in Centrifugal Compressors. *Journal of Engineering for Power,* **105**, 1983, p. 80-87.

[Q]

Quandt E., (1996), Water Droplet Evaporation in Air During Compression in a Gas Turbine Engine, NSWCCD-TM-80-96/06.

Qun Z., Yufeng S., Shuying Li and Yunhui W., Thermodynamic Analyses of

Wet Compression Process in the Compressor of Gas Turbine. *Journal of Turbomachinery* **125** (3), 2003, p. 489-496.

[R]

Rein M., Phenomena of liquid drop impact on solid and liquid surfaces. *Fluid Dynamics Research,* **12** (2), 1993, p. 61-93.

Rioboo R., Tropea C. and Marengo M., Outcomes from a drop impact on solid surfaces. *Journal of atomization and sprays,* **11**, 2001, p. 155-165.

Rowe A., Inventor Rolls-Royce plc, (1995), Gas Turbine Engine Water Ingestion Compensation System, U.K. Patent 5,471,831.

Russell R.E. and Victor I.W.: Evaluation and Correction of the Adverse Effects of (i) Inlet Turbulence and (ii) Rain Ingestion on High Bypass Engines. In: *AIAA/AHS/ASEE Aircraft Design Systems and Operating Meeting,* 1984, San Diego, California, AIAA 84-2486,

[S]

Samenfink W., Elsaber A., Dullenkopf K. and Wittig S., Droplet interaction with shear-driven liquid films: analysis of deposition and secondary droplet characteristics. *International Journal of Heat and Fluid Flow* **20** (5), 1999, p. 462-469.

Santa I.: The effect of water ingestion on the operation of the gas turbine engine. In: *22nd International Congress of Aeronautical Sciences,* 2000, Harrogate, United Kingdom,

Schlichting H., (1936), Experimental investigation of the problem of surface roughness, NACA TM 823.

Shastri R.P., Ehresman C.M., and Murthy S.N.B.: Effect of Water Addition on Combustor Performance. In: *30th AIAA, ASME, SAE, and ASEE, Joint Propulsion Conference and Exhibit,* 1994, Indianapolis, IN, AIAA 94-3273.

Shastri R.P., Ehresman C.M., and Murthy S.N.B.: Water Vapor, Water, and Slush Effects on Combustor Performance. In: *31st AIAA/ASME/SAE/ASEE Joint Propulsion Conference and Exhibit,* 1995, San Diego, CA, AIAA 95-3118.

Sikalo S., Marengo M., Tropea C. and Ganic E.N. Analysis of Impact of Droplets on Horizontal Surfaces. *Experimental Thermal and Fluid Science* **25**, 2002, p. 503-510.

Sommerfeld M. and Huber N. Experimental analysis and modelling of particle-wall collisions. *International Journal of Multiphase Flow,* **25** (6-7), 1999, p. 1457-1489.

Spalding D., *Combustion and Mass Transfer*, Pergamon Press, 1979.

Stow C.D. and Hadfield M.G. An experimental investigation of fluid flow resulting from the impact of a water drop with an unyielding dry surface. *Proceedings of Royal Society of London part A* **373**, 1981, p. 419-441.

[T]

Tan S.C. and Barlett P.G.: An experimental study of droplet breakup using a wind tunnel. In: *41st Aerospace Sciences Meeting and Exhibit,* 2003, Reno, Nevada, AIAA 2003-391.

Tattelman P. and Willis P., (1985), Model Vertical Profiles of Extreme Rainfall Rate, Liquid Water Content and Drop-Size Distribution, AFGL-TR-85-0200.

Thompson B. and Jang J., Aerodynamic efficiency of wings in rain. *Journal of Aircraft,* **33** (6), 1996, p. 1047-1053.

Thompson B., Jang J. and Dion J.L., Wing Performance in Moderate Rain. *Journal of Aircraft,* **32** (5), 1995, p. 1034-1039.

[U]

Ulrichs E. and Joos F.: Experimental investigations of the influence of water droplets in compressor cascades. In: *Proceedings of ASME Turbo Expo 2006 Power for Land, Sea and Air,* 2006, Barcelona, Spain, GT-2006-90411.

[V]

Valentine J. and Decker R., Tracking of raindrops in flow over an airfoil. *Journal of Aircraft,* **32** (1), 1995a, p. 100-105.

Valentine J.R. and Decker R., A Lagrangian-Eulerian scheme for flow around an airfoil in rain. *International Journal of Multiphase Flow* **21** (4), 1995b, p. 639-648.

Varga C.M., Lasheras J.C. and Hopfinger E.J., Initial breakup of a small-diameter liquid jet by a high-speed gas stream. *Journal of Fluid Mechanics,* **497**, 2003, p. 405-434.

Volk L.: Power Loss in Inclement Weather. In: *Proc. of Flight Safety Foundation 45th Annual International Air Safety Seminar,* 1992, Long Beach CA, USA, p. 238-248.

[W]

Wallis G.B., *One Dimensional Two-Phase Flow*, London: McGraw-Hill, 1969.

Walsh P. and Fletcher P., *Gas Turbine Performance*, London: Blackwell Science, 1998.

Warwick W. R.: Effect of Water Ingestion on J79-GE-8 Altitude Performance. In: *3rd Annual Conference on Environment and Propulsion Systems,* 1963, Trenton, New Jersey, 63-ENV-5, p. 103-137.

White A. J. and Meacock A. J.: An evaluation of the effects of water injection on compressor performance. In: *Proceedings of ASME Turbo Expo 2003 Power for Land, Sea and Air,* 2003, Atlanta, USA, ASME 2003-GT-38237.

White F., *Viscous Fluid Flow*, NY: McGraw-Hill, 2006.

Williams J. (2003), Water ingestion in jet engines, PhD Thesis, University of Cambridge.

Williams J., Freeman C., and Day I.: Rain Ingestion in Axial Flow Compressors at Part Speed. In: *ASME Turbo Expo 2005: Power for Land, Sea, and Air,* 2005, Reno, USA, GT2005-68582.

Williams J. and Young J. B.: Movement of deposited water on turbomachinery rotor blade surfaces. In: *Proceedings of ASME Turbo Expo 2006 Power for Land, Sea and Air,* 2006, Barcelona, Spain, GT2006-90792.

Wurz D.E.: Flow Behaviour of Thin Water Films under the Effect of a co-current Air Flow of Moderate to High Subsonic Velocities; Effect of the Film on the Airflow. In: *Proceedings of 3rd International Conference on Rain Erosion and Associated Phenomena,* 1970, Farnborough, England, RAE, p. 727-750.

Wurz, D.E., Experimental investigation into the flow behaviour of thin water films; Effect on a concurrent airflow of moderate to high supersonic velocities. Pressure distribution at the surface of rigid wavy reference structures. *Archives of Mechanics,* **28** (5-6), 1976, p. 969-987.

[Y]

Yarin A.L. and Weiss D.A., Impact of drops on solid surfaces: self-similar capillary waves, and splashing as a new type of kinematic discontinuity. *Journal of Fluid Mechanics,* **283**, 1995, p. 141-173.

APPENDICES

A. Compressor Blading Data

The model in study was inspired on the compressor fitted in the J79-GE-17 General Electric turbojet aero-engine. Its compressor map was produced by manipulating the blading data of a Siemens V94.3A compressor, which was scaled according to the way described in appendix C of this manuscript. Siemens V94.3A compressor data were available from Noel (2003) in MS Excel spreadsheet format. Compressor's basic characteristics are shown in table A-1, while its geometric characteristics are illustrated in table A-2 and figure A-1.

Pressure Ratio	PR	16.6
Mass Flow	W	621 Kgr/sec
Inlet Pressure	P_1	101325 Pa
Inlet Temperature	T_1	288 ° K
Number of stages	n	17
Rotational speed	N	3000 rpm
Power output	P	260 MW
IGV blade diameter	D_{tip}	1.32 m
	D_{hub}	2.48 m
OGV blade diameter	D_{tip}	1.4 m
	D_{hub}	1.58 m

Table A-1: Siemens V94.3A design parameters

Axial Flow Compressor Siemens V94.3A					
		centreline axial (mm)		radius hub (mm)	radius tip (mm)
IGV		0.0		660	1240
R1		241.7		660	1227
S1		435.0		665	1201
R2		555.8		670	1174.9
S2		725.0		676.3	1153.2
R3		845.8		682.5	1131.6
S3		978.8		686.3	1111.6
R4		1087.5		690	1091.6
S4		1196.3		692.5	1073.2
R5		1305.0		695	1054.8
S5		1401.7	bleed gap	697	1039.3
R6		1522.5		699	1023.9
S6		1619.2		699.5	1007.2
R7		1703.8		700	990.4
S7		1788.3		700	975.8
R8		1860.8		700	961.2
S8		1933.3		700	948.7
R9		2017.9		700	936.1
S9		2090.4		700	925.2
R10		2150.8		700	914.3
S10		2223.3	bleed gap	700	904.8
R11		2344.2		700	895.3
S11	2	2461.6		700	887
R12	3	2520.3		700	878.6
S12	4	2578.9		700	871.3
R13	5	2637.6		700	863.9
S13	6	2696.3		700	857.5
R14	7	2755.0		700	850.9
S14	8	2813.7		700	845.2
R15	9	2872.4		700	839
S15	10	2931.1		700	834
R16	11	2989.7		700	829
S16	12	3048.4		700	824
R17	13	3107.1		700	820
S17	14	3165.8		700	816

Table A-2: Siemens V94.3A Geometric Characteristics [Noel (2003)]

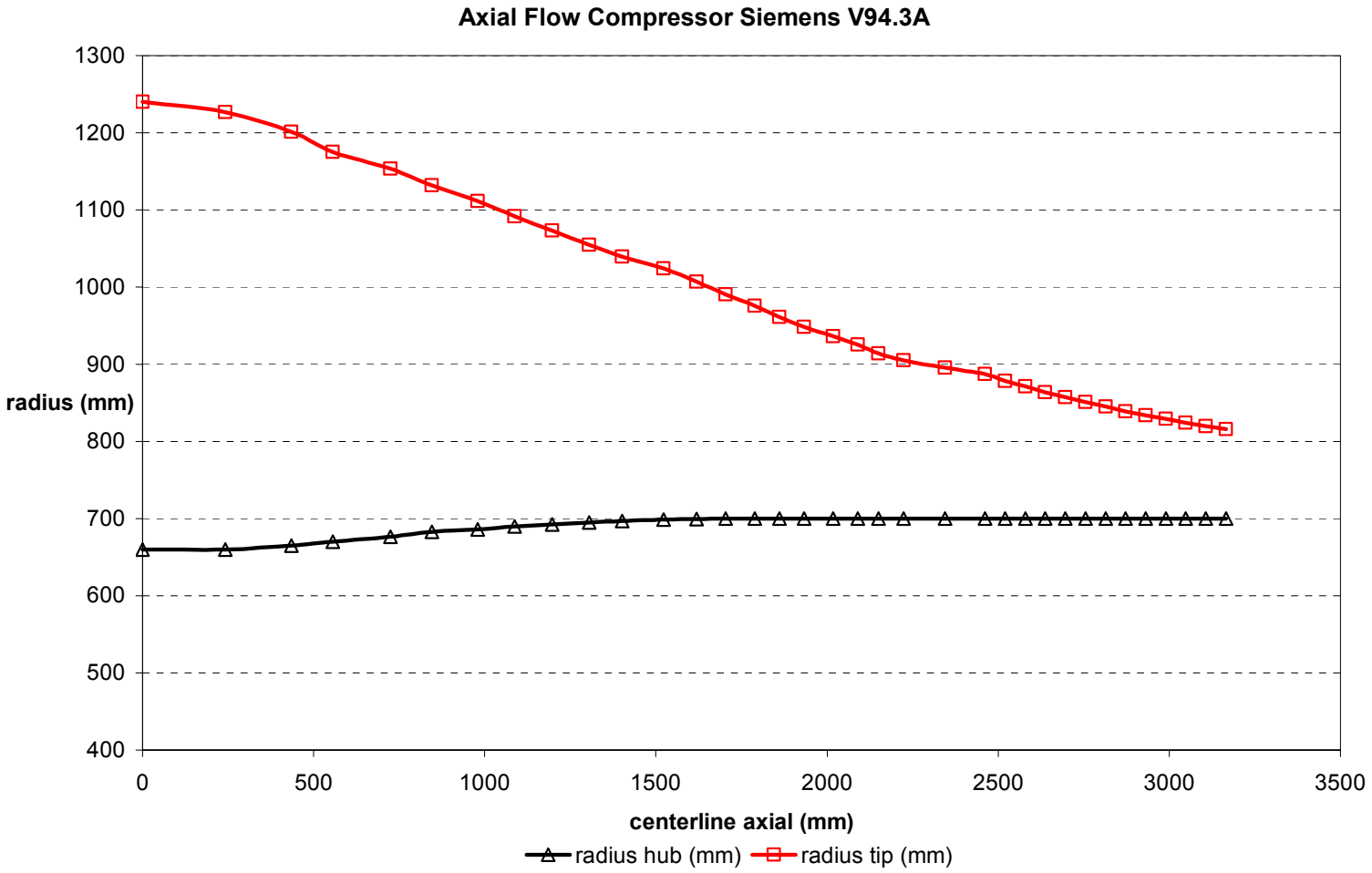

Figure A-1: Siemens V94.3A Geometry

The studied engine is a heavy-duty single shaft industrial engine. Its compressor is an example of a constant hub diameter annulus. The compressor's blading was provided in a MS Excel spreadsheet including the x, y and z coordinates of the blades in the hub, shroud and three other layers. The Double Circular Arc (DCA) blade profile was enabled. This is composed of two circular arcs, one for each surface (suction and pressure). Its fundamental blading data for the 1st rotor and 1st stator are presented in table A-3 while the five layers from the 1st rotor scratch data are illustrated in figure A-2.

aT17 BLADED COMPRE	MASS FLOW (kg/sec): 621.00									
Stage	1.00					1.00				
Station [in]	ROTOR					STATOR				
Radius rotor / stator [in]	660.00	801.75	943.50	1085.25	1227.00	665.00	799.00	933.00	1067.00	1201.00
Blockage factor	0.98					0.98				
Temp. in (total)	288.00	288.00	288.00	288.00	288.00	306.00	306.00	306.00	306.00	306.00
Temp. rise stage	18.00									
Press in (total)	100.70	100.70	100.70	100.70	100.70	122.43	122.43	122.43	122.43	122.43
Press ratio rotor / stage			1.22					1.21		
Efficiency rotor / stage			0.91					0.88		
Reaction	0.71	0.89	1.00	1.07	1.13					
U 0 U 3	207.35	251.88	296.41	340.94	385.47	208.92	251.01	293.11	335.21	377.31
Va 0 Va 3	183.71	182.08	180.48	178.85	177.17	180.87	176.14	171.79	167.68	163.70
a 0	13.76	13.35	13.39	13.72	14.25					
a 1 a 3	41.47	48.89	54.54	58.97	62.51	36.12	33.39	31.62	30.54	29.95
a 2 a 4	23.04	37.45	47.48	54.64	59.95	17.06	16.73	16.86	17.28	17.93
e	18.43	11.45	7.07	4.33	2.56	19.06	16.66	14.77	13.25	12.02
M 0	0.57	0.57	0.56	0.56	0.55					
M 1 M 3	0.75	0.84	0.94	1.05	1.16	0.67	0.63	0.60	0.57	0.56
M2 M4	0.59	0.70	0.75	0.85	0.96	0.61	0.60	0.59	0.58	0.57
de Haller No	0.80	0.80	0.82	0.84	0.85	0.91	0.96	0.99	1.01	1.03
No of Blades			31.00					39.00		
Aspect Ratio			2.54					2.71		
Taper Ratio			1.20					1.50		
Chord	197.47	207.34	217.21	227.09	236.96	153.61	172.81	192.01	211.21	230.41
Camber	19.75	12.21	7.38	4.38	2.56	21.61	20.61	20.24	20.36	20.80
Stagger	-28.59	-40.29	-48.86	-55.28	-60.23	-23.32	-22.59	-22.50	-22.86	-23.55
s / c	0.68	0.78	0.88	0.96	1.04	0.70	0.75	0.79	0.82	0.83
t / c	0.07	0.06	0.05	0.04	0.03	0.06	0.07	0.07	0.08	0.08
Incidence	3.00	2.50	2.00	1.50	1.00	2.00	0.50	-1.00	-2.50	-4.00
deviation	4.37	3.59	2.90	2.79	1.00	4.58	4.57	4.70	4.93	5.20
deflection	18.38	11.12	6.47	3.09	2.56	19.03	16.54	14.55	12.93	11.60
E/E*	0.90	0.67	0.43	0.21	0.20	0.90	0.81	0.73	0.66	0.59
[i stall - i]	8.93	10.94	12.88	15.22	13.07	9.53	11.04	12.37	13.53	14.68
DF	0.30	0.26	0.21	0.13		0.27	0.24	0.21	0.19	0.18
CRITICAL MACH No	0.69	0.72	0.71	0.71	0.00	0.71	0.70	0.69	0.66	0.62
THROAT CHOKE MARGIN %	9.41	7.05	5.94	6.17	0.00	13.82	15.25	16.38	17.23	17.67
Blade Analysis	OK	OK	OK	OK	OK	OK	OK	OK	OK	OK

Table A-3: Blading Data for the 1st rotor and 1st stator [Noel (2003)]

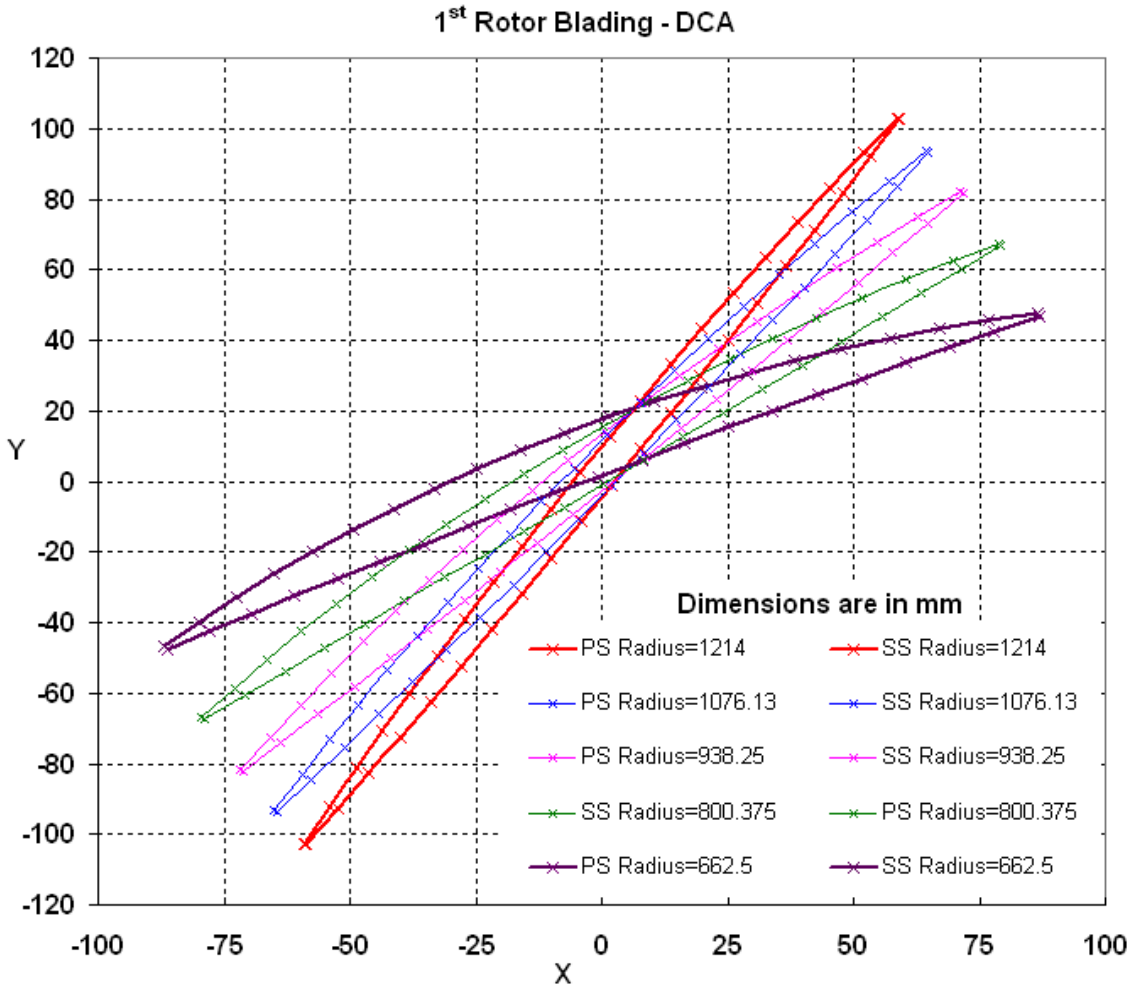

Figure A-2: 1st Rotor DCA Blading Scratch Data

To produce the blade's computational domain, CFX-BladeGen program was used [AEA (2001a)]. As a result, blade's design was optimized and new layers were created to generate the computational grid in detail. Figures A-3 and A-4 show the 1st rotor blade theta angle and thickness respectively, after their optimization.

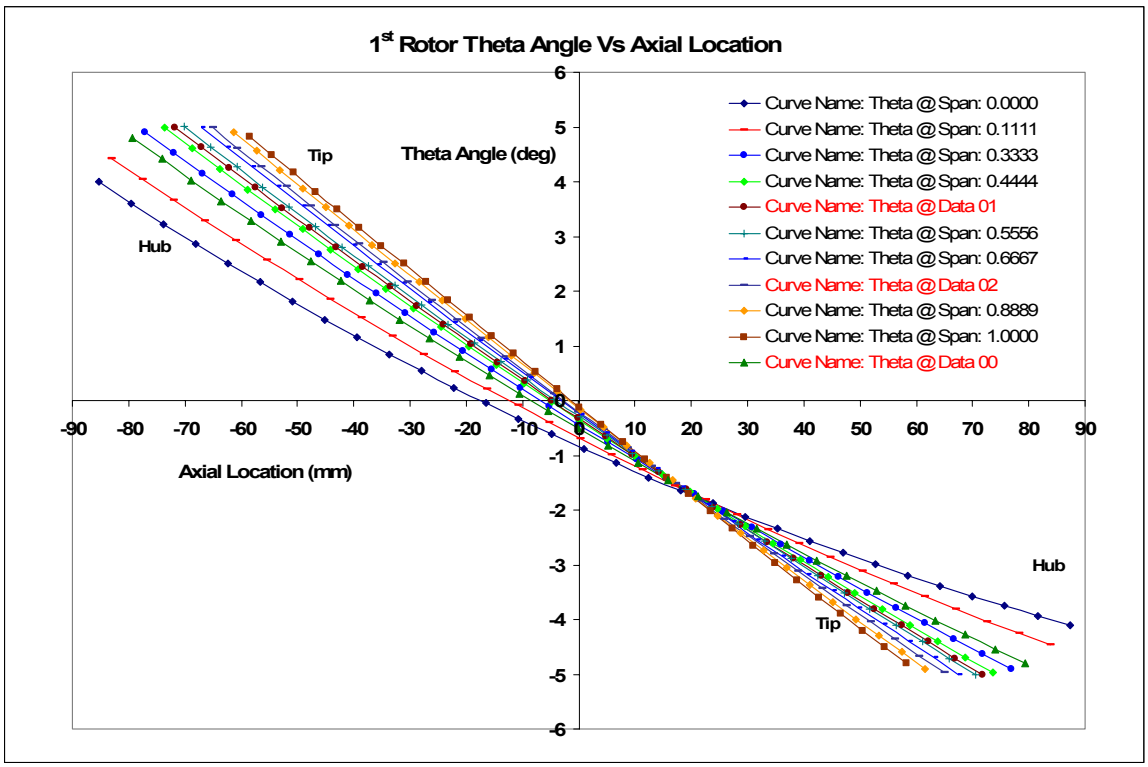

Figure A-3: 1st Rotor Blade Theta Angle Vs Axial Location

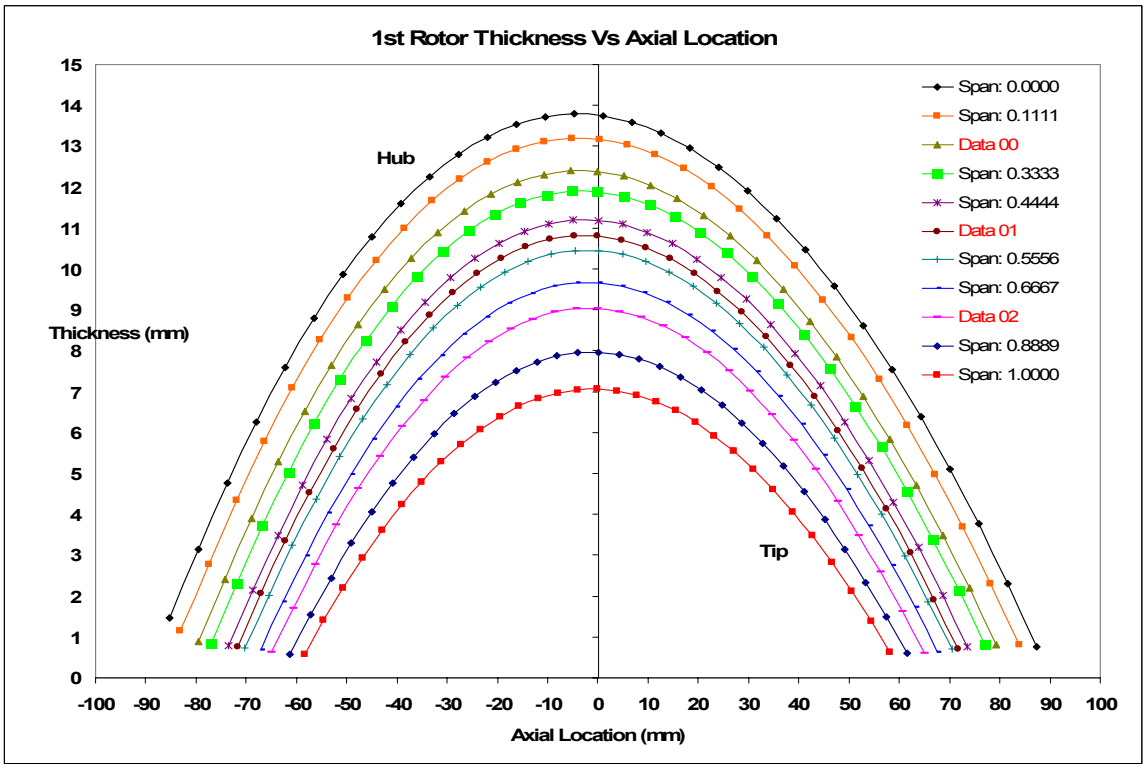

Figure A-4: 1st Rotor Blade Thickness Vs Axial Location

Moreover, the leading and trailing edge of the blades were specified as an ellipse ratio, smoothing any discrepancies in the blade's shape (figure A-5).

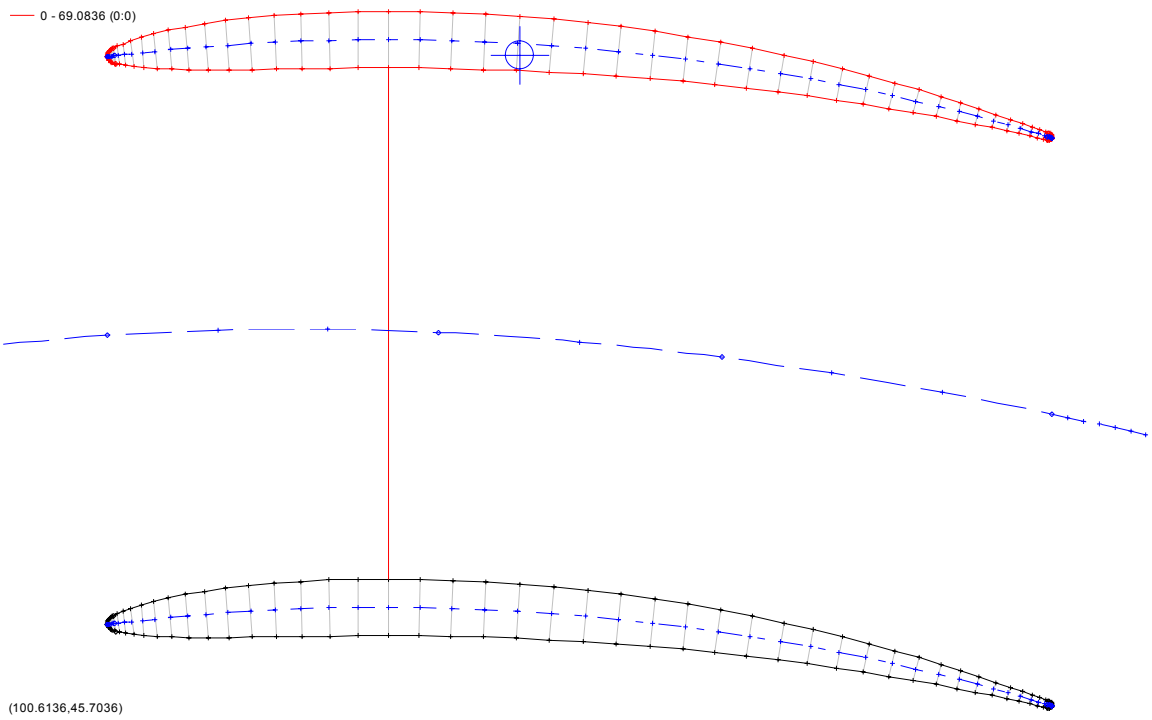

Figure A-5: IGV Blade Smoothing

CFX-BladeGen has been used to create the IGV, rotor and stator blades showed in figures A-6, A-7 and A-8 respectively.

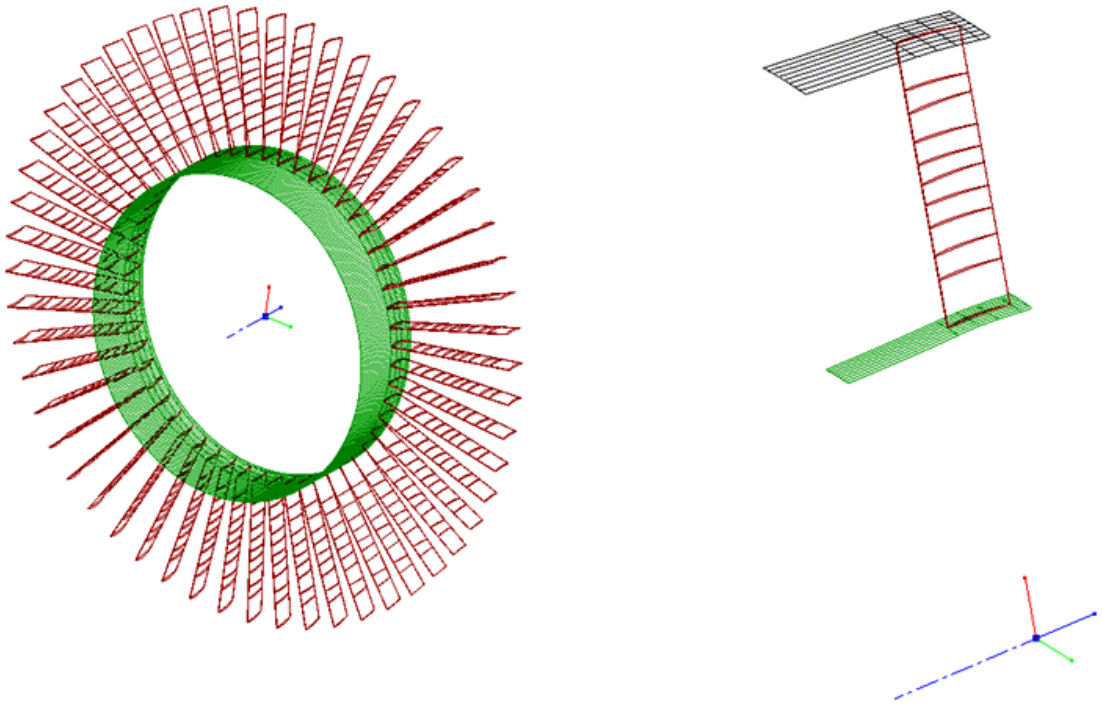

Figure A-6: IGV Blade 3D View

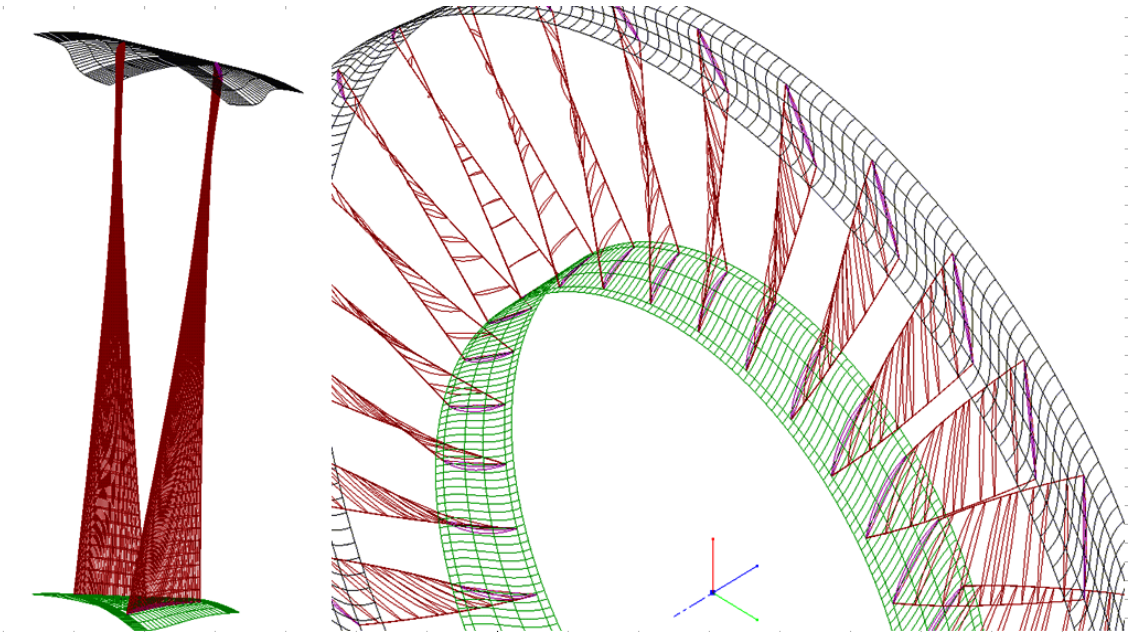

Figure A-7: 1st Rotor 3D View

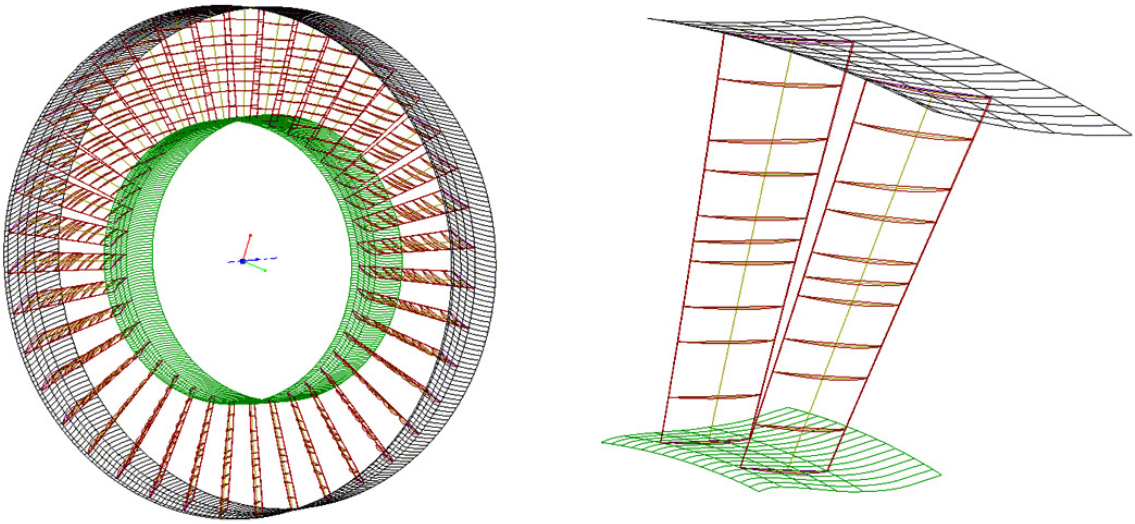

Figure A-8: 1st Stator 3D View

The produced geometries were exported to CFX-Turbogrid for the creation of the computational mesh of the IGV, 1st rotor and 1st stator blades. For each component, an interface for the inlet and outlet was created in order to eliminate any alignment errors when their matching was attempted. Figures A-9 and A-10, show the IGV and rotor computational grid created by CFX-Turbogrid.

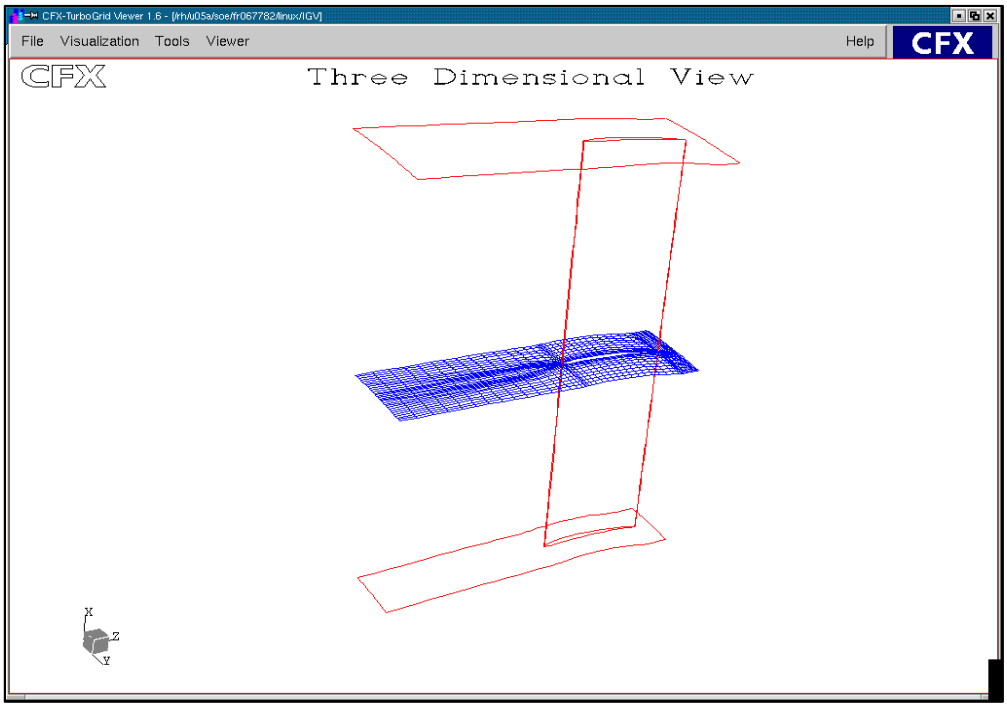

Figure A-9: IGV Blade Grid

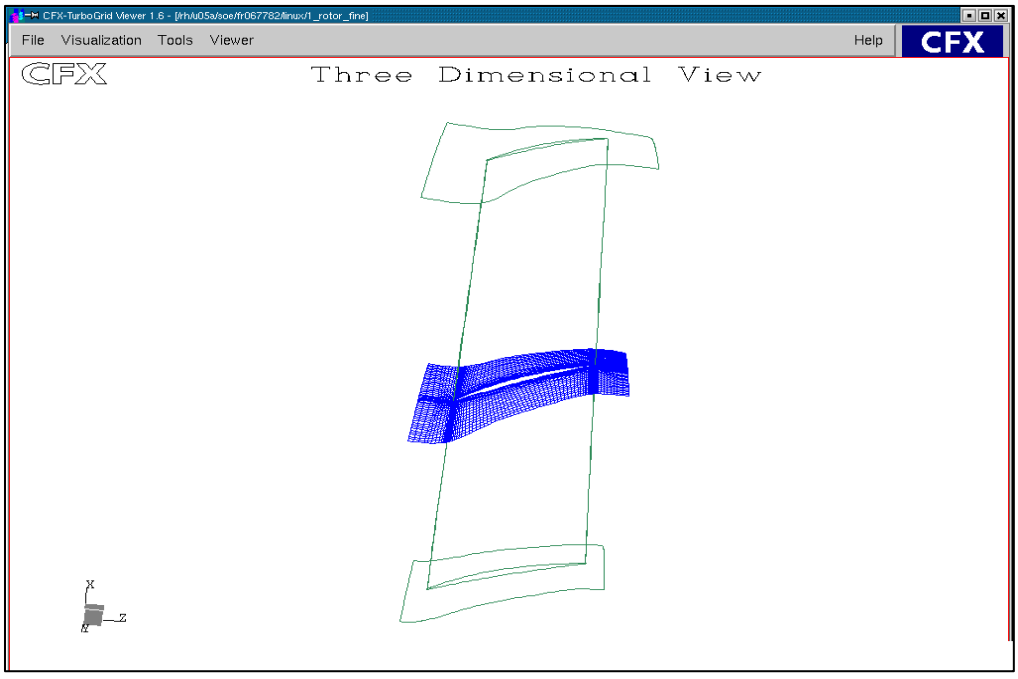

Figure A-10: 1st Rotor Blade Grid

The geometry of each component was exported to CFX-Tascflow where the global domain for the IGV and the 1st compressor stage was set up. It is noteworthy that BladeGen and Turbogrid have been integrated in the new CFX code providing a powerful tool for the Turbomachinery.

B. Off-campus Connection with Cranfield HPC

Working off-campus caused log on problems with Cranfield High Performance Computer (HPC), in which CFD software is installed. Apart from this, CFD code works on UNIX systems, which means that the use of Windows Emulators Software was necessary to connect MS Windows with UNIX. There were also problems in viewing the program's Graphical User Interface (GUI), which means that the display of the results was impossible. The above difficulties were overcome by using specific software called PuTTY and Cygwin. The whole procedure was set up in co-operation with Cranfield HPC Team. What follows is the procedure the author used to connect to Cranfield HPC.

Firstly, the user should have to install PuTTY software, which is a Windows Emulator Software. View in figure B-1 will greet the user. In the Hostname box enter the address: "home.central.cranfield.ac.uk" for ssh (or scp/sftp) connections. Make sure that port 22 (SSH) is chosen. This will connect you to one of the Cluster Grid front-end servers, which run Linux.

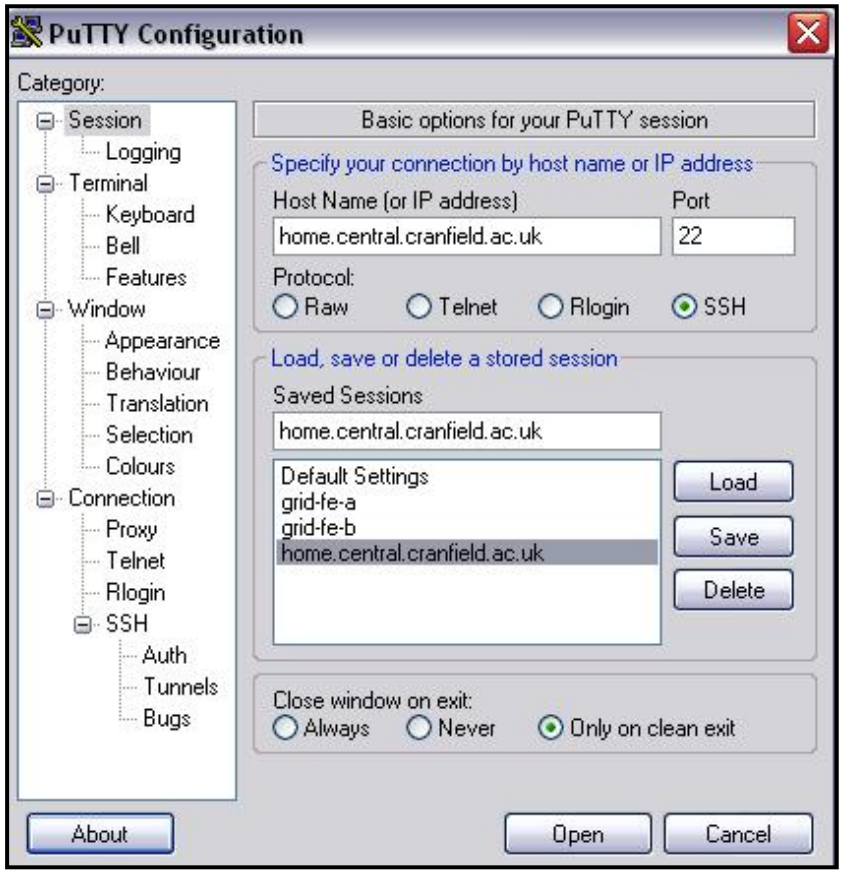

Figure B-1: PuTTY Log on Screen

Now select the SSH item on the Category list and check that "Enable compression" is selected. Furthermore, either "2" or "2 only" should be chosen as protocol version (figure B-2).

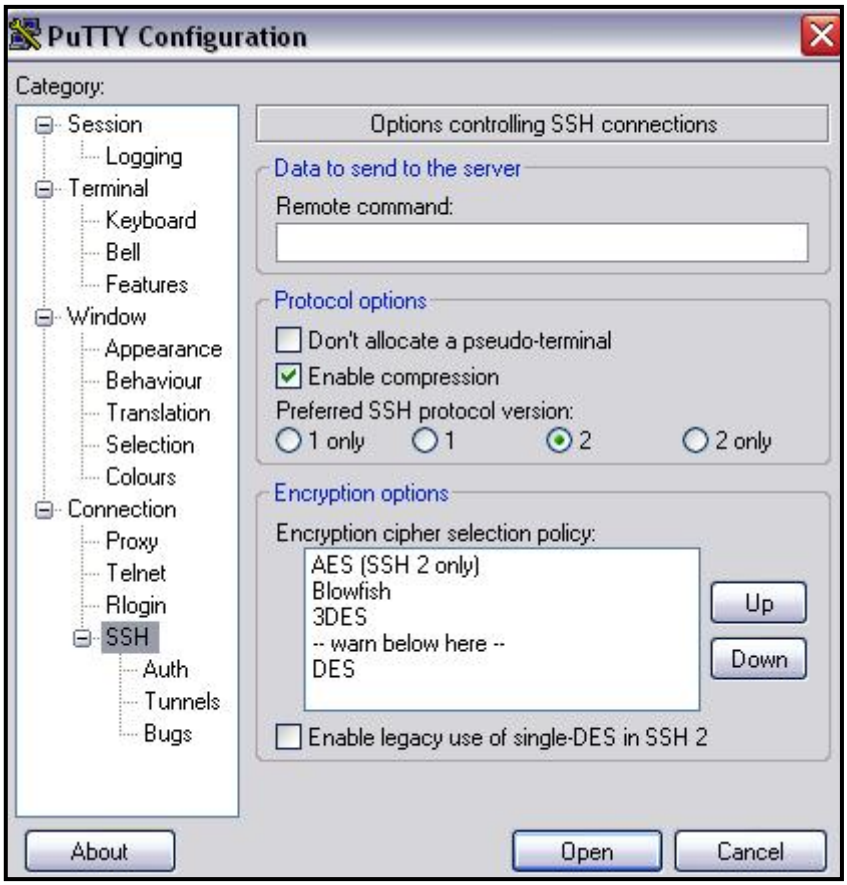

Figure B-2: PuTTY SSH Protocol

The next step is to click the Tunnels category under SSH, in which “Enable X11 forwarding” should be selected (figure B-3).

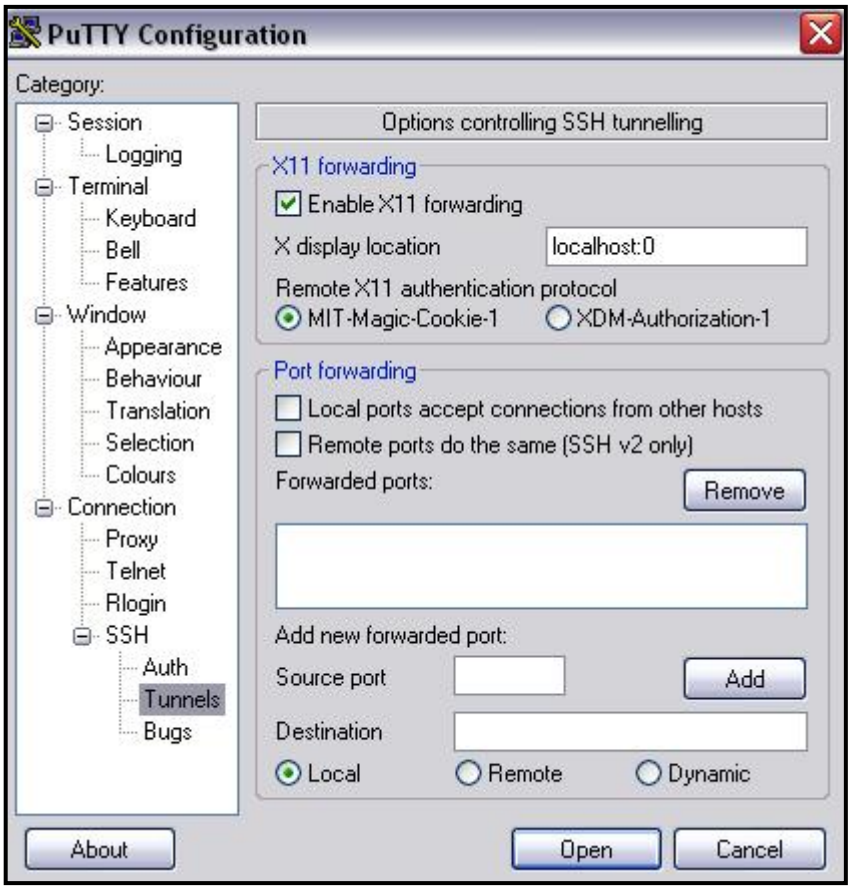

Figure B-3: PuTTY SSH Tunnelling

Now, the user should install Cygwin software. In the welcome screen, the user should write the command “startx”. This step should be done before the use of PuTTY in the connection process. File transfers can be done using Winscp361, which is similar to PuTTY. It does not need any special configuration apart from setting a log on session with the address: “home.central.cranfield.ac.uk" and giving the appropriate username and password.

It is noteworthy that the above steps are the author’s experience in the special case of being off-campus and try to log on HPC. It is strongly suggested that the potential user should seek advice from the Cranfield HPC team when he faces any difficulties.

C.Creation of Computational Domain

Since this project focuses on the aero-engines performance field, the Siemens V94.3A compressor model should have to be scaled to match the dimensions and the performance parameters of a typical gas turbine aero-engine. Moreover, the blade tip speed should be kept constant so as the blading data would be valid in the scaled model as well. A compressor with similar design characteristics with these in Siemens V94.3A is fitted in J79-GE-17 General Electric single turbojet aero-engine (table C-1).

PARAMETER		VALUE
Pressure Ratio	PR	13.5
Mass Flow	W	76 kgr/sec
Inlet Pressure	P_1	101325 Pa
Inlet Temperature	T_1	288 ° K
Number of stages	n	17
Rotational speed	N	7700 rpm
IGV blade diameter	D_{tip}	0.812 m

Table C-1: J79-GE-17 Design Parameters

To pass the mass flow of 76 kgr/sec at this reduced inlet area (i.e. Q function unchanged), the compressor with the given blade design should operate at higher rotational speed to keep the blade speed constant. At both cases, it is assumed that the air inlet speed remains constant. Thus, using the following equations for the compressor inlet area and Q function and applying them in both cases, the scaling factor $D_{tJ79}/D_{tSiemens}$ can be calculated:

$$A_{1Siem} = \frac{\pi}{4} Dt^2 \left[1 - \left(\frac{Dh1}{Dt} \right)^2 \right] = \frac{\pi}{4} \cdot (2.454)^2 \cdot \left(1 - 0.538^2 \right) \Rightarrow A_{1Siem} = 3.3607 \, m^2 \quad \text{Equ. (C-1)}$$

$$Q_o = \frac{W \sqrt{T}}{K_B \, A \, P} = \frac{621 \sqrt{288}}{0.98 \cdot 3.3607 \cdot 101325} \Rightarrow Q_o = 0.03158 \qquad \text{Equ. (C-2)}$$

For W_{J79}=76 kgr/sec and the same Q function, equations C-1 and C-2 are applied again and A_{1J79} and D_{tJ79} are calculated:

$$(C\text{-}2) \Rightarrow A_{1J79} = 0.4113\,m^2$$

$$(C\text{-}1) \Rightarrow D_{tJ79} = 0.8585\ m, \qquad \text{scaling factor} = \frac{D_{tJ79}}{D_{tSiemens}} = 0.35$$

To keep the same blade tip speed for the reduced tip diameter the rotational speed should be increased:

$$N_{Siemens} = \frac{U_{tSiemens}}{\pi\, D_{tSiemens}} \Rightarrow \frac{3000}{60} = \frac{U_{tSiemens}}{\pi\, 2.454} \Rightarrow U_{tSiemens} = 385.5\ {}^{m}\!/_{sec} \qquad \text{Equ.}\,(C-3)$$

Hence,

$$N_{J79} = \frac{U_{tJ79}}{\pi\, D_{tJ79}} = \frac{385.5}{\pi \cdot 0.8585} \Rightarrow N_{J79} = 8576\,rpm$$

Therefore, the compressor model was scaled by a factor of 0.35 setting the PRM=8576 at Design Point (DP). Table C-2 compares design values for the Siemens, J79 and scaled compressor.

Siemens V34.3A – J79 Compressor Scaling				
	Siemens V34.3A	**J79**	**scaled dim**	**%**
W (kgr/sec)	621	76		
PR	16.5	13.5		
stages	17	17		
D_{tip} 1R (m)	2.454	0.812	0.8585	5.4
D_{hub} 1R (m)	1.32	-	0.4619	
D_h/D_t	0.538	-	constant	
N_{DP} (rpm)	3000	7650	8576	10.8
$U_{tip\ 1R}$ (m/sec)	385.5	325.25	constant	
Va_0 (m/sec)	180			
K_B	0.98			
P_1 (Pa)	101325			
T_1 (oK)	288			

Table C-2: Siemens V34 – J79 Compressor Scaling Parameters

The computational domain consists of an IGV blade, a rotor and a stator blade. Figure C-1 shows the 3D computational domain while figures C-2 and C-3 show respectively mid span and meridional grid surfaces. A total number of 326,000

mesh points are involving in generating the global computational grid. Dense clustering around the blades and especially in the rotor is used for better resolution of boundary layers. Figure C-4 shows a general view of the axial flow compressor model.

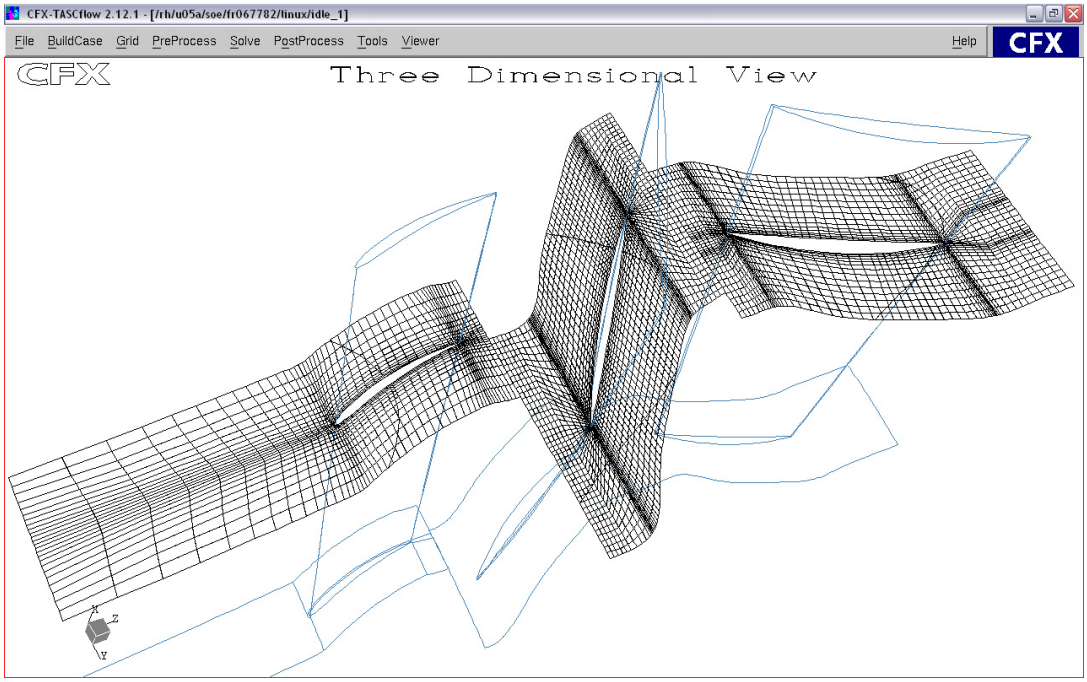

Figure C-1: 3D View of Compressor IGV & 1st Stage

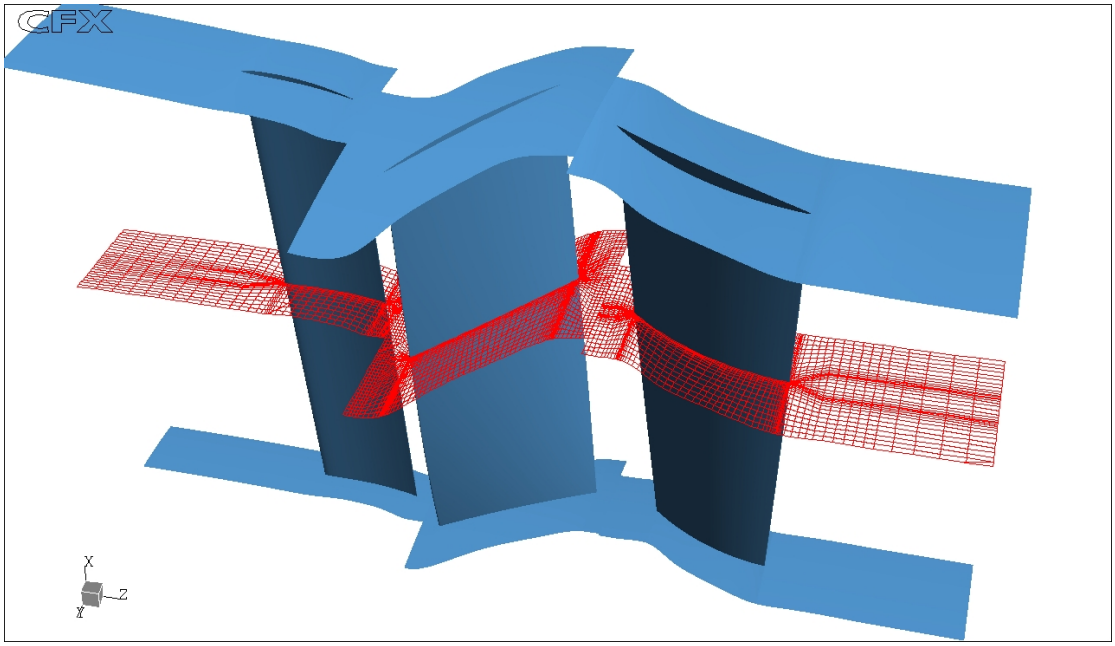

Figure C-2: Mid Span Grid Surface

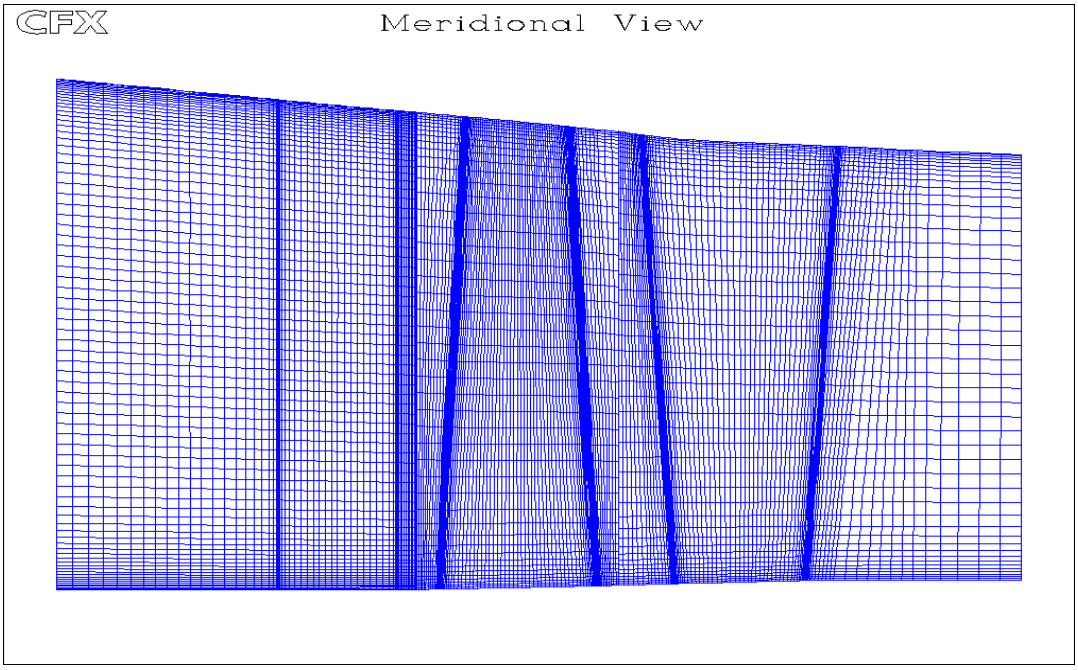

Figure C-3: Meridional Grid Surface

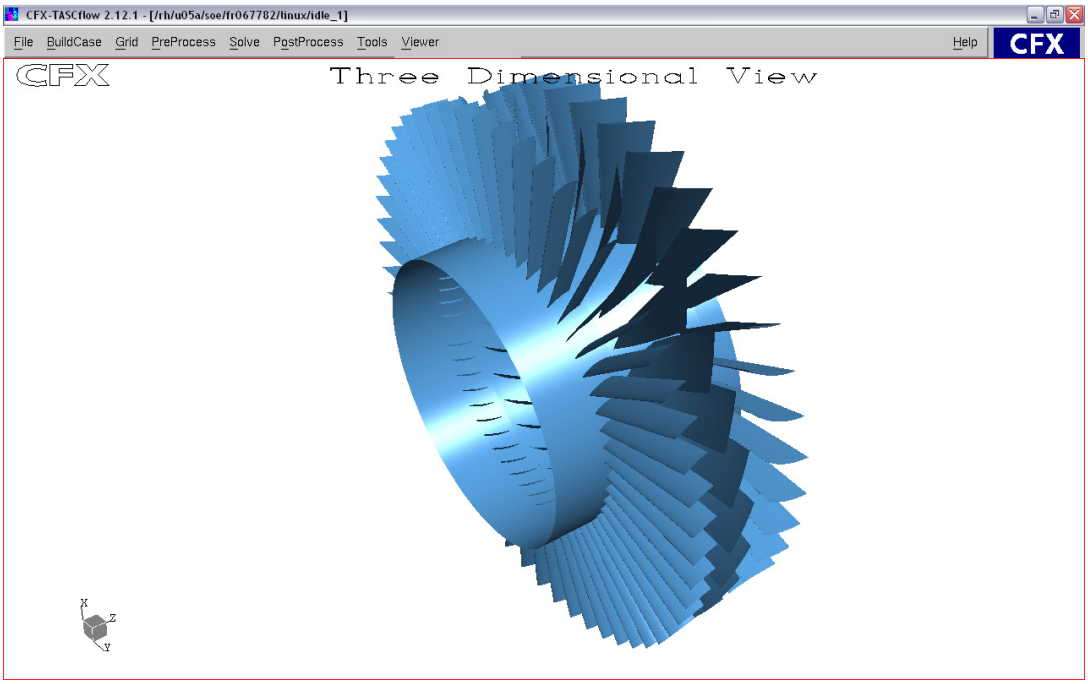

Figure C-4: 3D Axial Flow Compressor Model

For the boundary conditions, uniform constant total pressure is applied at the inlet, ISA conditions, Pt_{in}=101325 Pa and Tt_{in}=288.15 °K. At the outlet, the static pressure at DP operation can be calculated based on the design PR of the 1st stage. From the compressor design data (appendix A) it is known that Pt_1=122.43 KPa, PR_{stator}=1.21 and M_4=0.59. Hence Pt_3=148.14 KPa. Using the isentropic flow equations, the static pressure at stator outlet can be calculated:

$$\frac{P}{p} = \left[1 + \frac{\gamma - 1}{2} M^2\right]^{\frac{\gamma}{\gamma - 1}} \qquad \text{Equ.} \quad (C-4)$$

Therefore, p_{4st}=117.049 KPa at D.P.

At the outlet of the computational grid (boundary condition, B.C. #5), the tip diameter is smaller than that at the stator outlet. As a result, the static pressure at B.C.#5 is bigger than the calculated p_{st}. This pressure can be estimated by using Q function, compressible tables of flow and assuming isentropic process. Since the area changes and assuming isentropic flow (i.e. Pt, Tt : constant), the product Q·A should remain constant for the same mass flow.

From the grid creation process, the geometrical parameters of the domain are known:

R_{t4}=1.1847 m R_{h4}=0.6709 m, $A = \pi\left(R_t^2 - R_h^2\right)$ A_4=2.9952 m^2

R_{t5}=1.174 m R_{h5}=0.6709 m, A_5=2.9209 m^2

From the design data, M_4=0.59, which gives from the compressible flow charts, Q_4=33.625 10^{-3}. Since $W\sqrt{T_t}/K_B P_t$ remains constant, the new Q function for the A_5 area is Q_5=34.48 10^{-3}, which gives for isentropic flow M_5=0.616. So, using again equation (C-4) the static pressure in B.C.#5 is p_s=114.680 KPa. This boundary condition was specified in CFX-Tascflow to solve the flow field at D.P. operation.

D.FILM_MOTION Flowchart

The results from CFD are imported in a FORTRAN program called FILM_MOTION. This program calculates the water film thickness and its motion on the rotor blade's pressure surface at the equilibrium condition, through an iterative process. This condition is defined when the water which deposits on the blade equals with that flowing out of the blade. In every iteration, water mass deposits on the blade and an amount of water mass extracted since it is flowing out of the blade. The program includes five subroutines, which solve the span-wise and chord-wise motion of the water mass, the total axial shear stress, and the torque. These are:

The FILM_THICK subroutine, which calculates the water film thickness on the blade's pressure surface,

The SHEAR_CALC subroutine, which calculates the air shear stress on the blade's pressure surface including the water droplets momentum impacting on the water film,

The CV_DIMENSION subroutine, which calculates the radius distance of the node in each control volume,

The EQU_SOLVE subroutine, which solves the equation of water film mass flow, by using the bisection method,

The ROTOR_TORQUE subroutine, which estimates the extra torque due to water film.

The FILM_MOTION flowchart is presented in figure D-1.

"FILM MOTION" CODE FLOW CHART

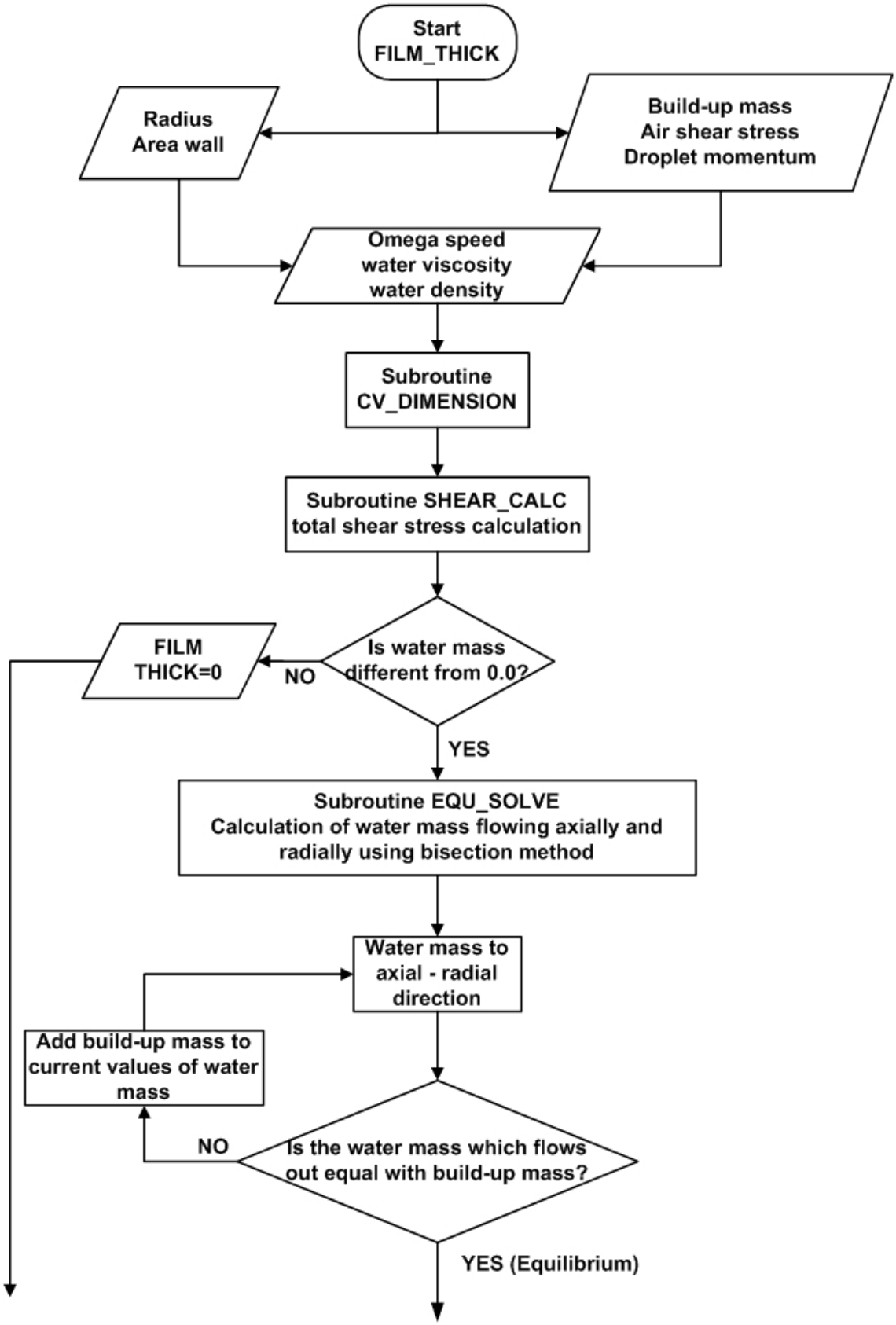

(Continued in the next page)

"FILM MOTION" CODE FLOW CHART

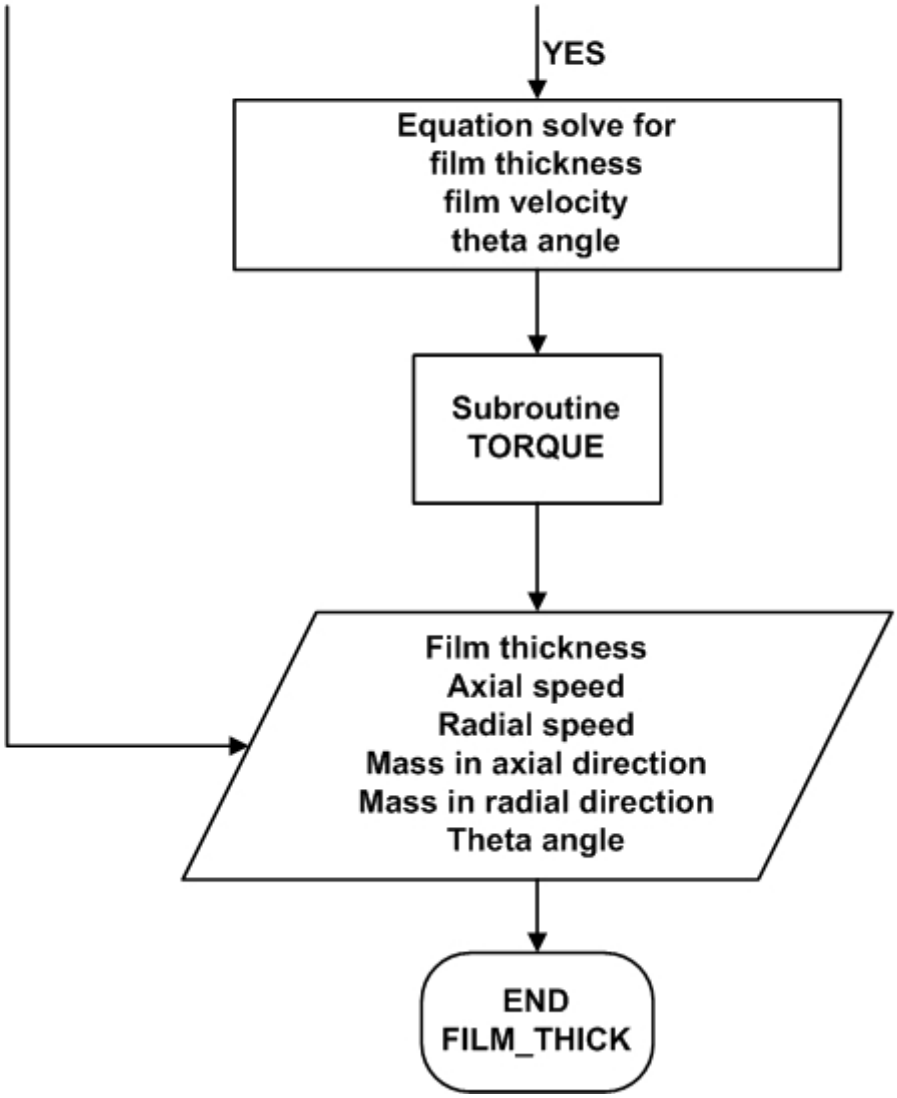

Figure D-1: FILM_MOTION Flowchart

A view of the FILM_MOTION screen is displayed in figure D-2:

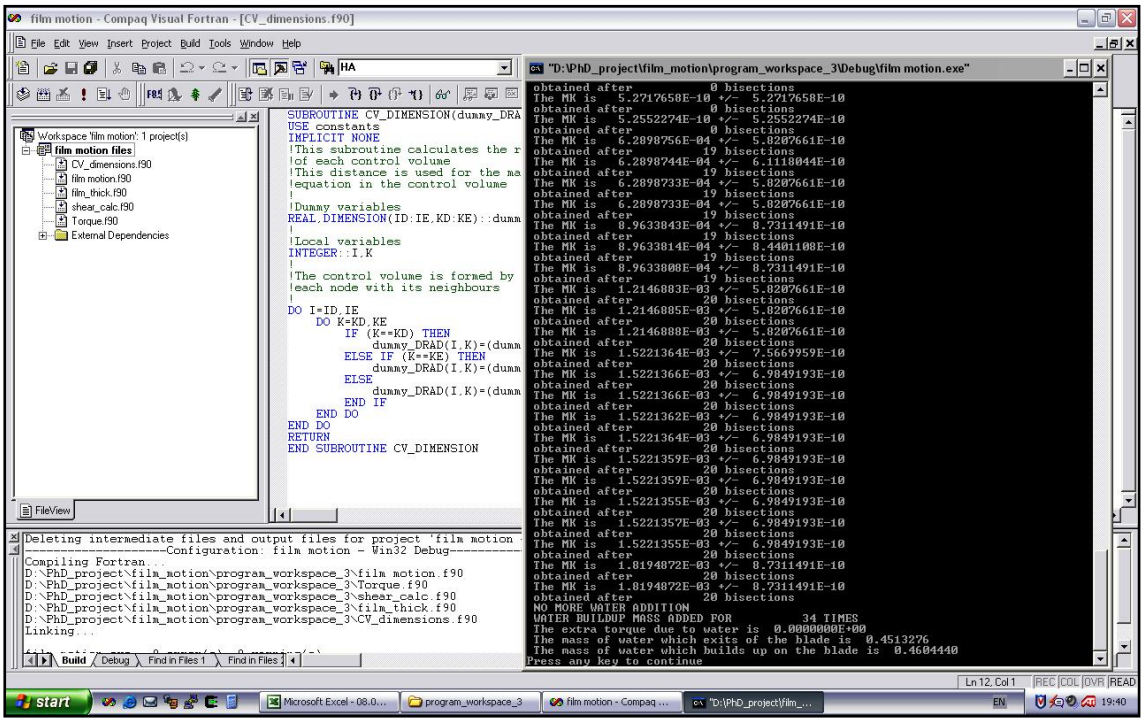

Figure D-2: FILM_MOTION Screen View

E. Forecast Function

The FORECAST in MS Excel calculates a value by using existing values. The predicted value is a y-value for a given x-value. The known values are existing x-values and y-values, and the new value is predicted by using linear regression. In this analysis, the dependence of y on x values is a dependence of the mean y values on x. When a straight line represents this dependence then it is called linear regression [Kreyszig (1999)].

The equation for FORECAST is y=a+bx, where:

$$\alpha = \bar{y} - b\bar{x} \qquad \text{and} \qquad b = \frac{\sum\left(x - \bar{x}\right)\left(y - \bar{y}\right)}{\sum\left(x - \bar{x}\right)^2}$$

x and y are the sample means AVERAGE (known_x's) and AVERAGE (known y's).

F. Turbomatch Results Spreadsheet

In earlier versions of Turbomatch, an MS excel-spreadsheet was used to visualize the results. This software, by using several macros, read performance parameters data from Turbomatch output file and imported them into an MS excel-spreadsheet. This was extremely helpful since the user was able to visualize the results and plot any data in a parametric analysis (i.e. change of gross thrust with the altitude variation). However, after the inclusion of humidity effects and water injection at the burner this option was no longer available because the output file contained more data than excel macros could read. Making the appropriate modifications the described software is accessible again and includes data for the water ingestion mode. The code was firstly developed by Dr. Junfei Yin in School of Engineering of Cranfield University.

In the definition section of the macro, the variables of water to air ratio (WAR) for injection or humidity, the water quality (vapour, liquid, superheated steam) and the water to air ratio (WAG) for water ingestion are defined (figure F-1).

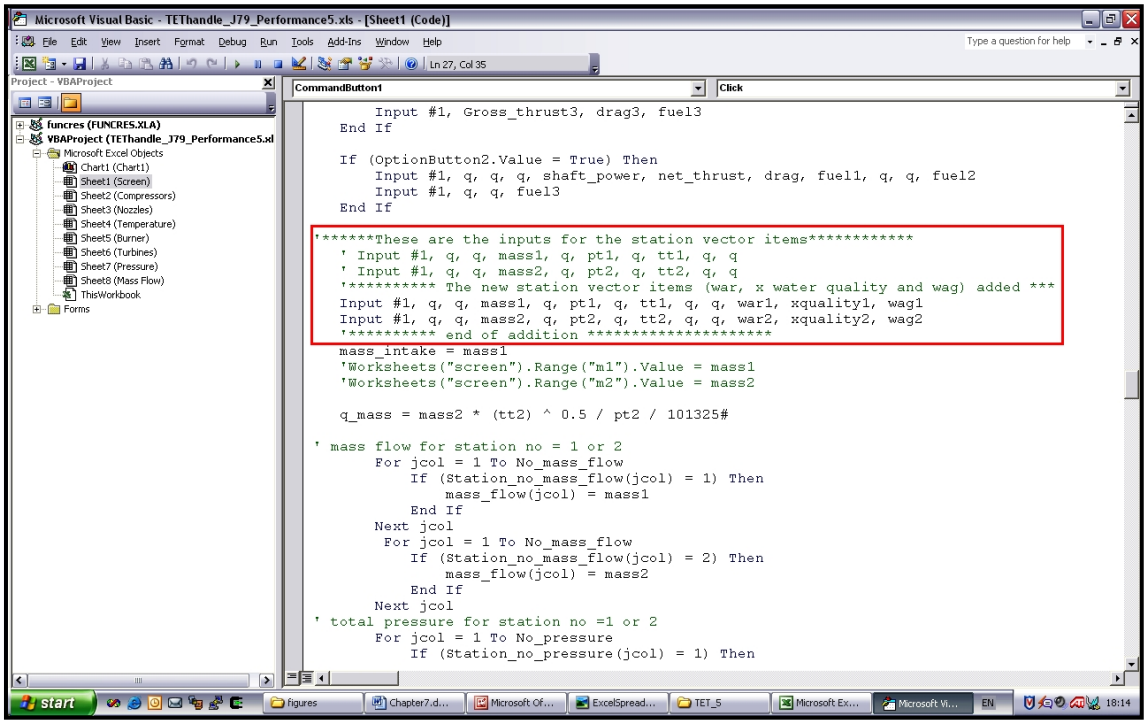

Figure F-1: Turbomatch Spreadsheet File – Water Ingestion Variables Definition

For the INTAKE brick, the variables of pressure deviation and relative humidity are defined. These properties were imported in the Turbomatch code from a previous upgrade without updating the spreadsheet. Similarly, in the BURNER brick, the variables of ingested water mass fraction and the pressure loss are imported (figure F-2).

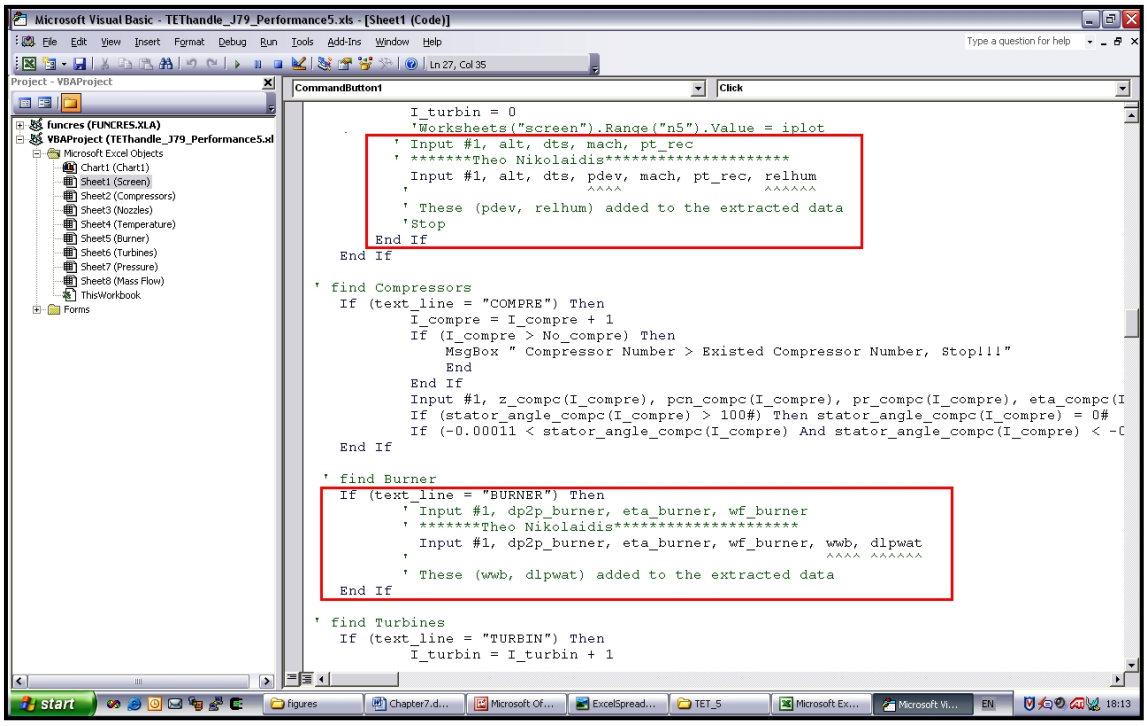

Figure F-2: Turbomatch Spreadsheet File – Variables Definition for Intake and Burner

Finally, the variables of water to air ratio (for both injection and ingestion), the water quality, and the water, pressure loss in the burner are displayed with the relevant values in the spreadsheet (figure F-3).

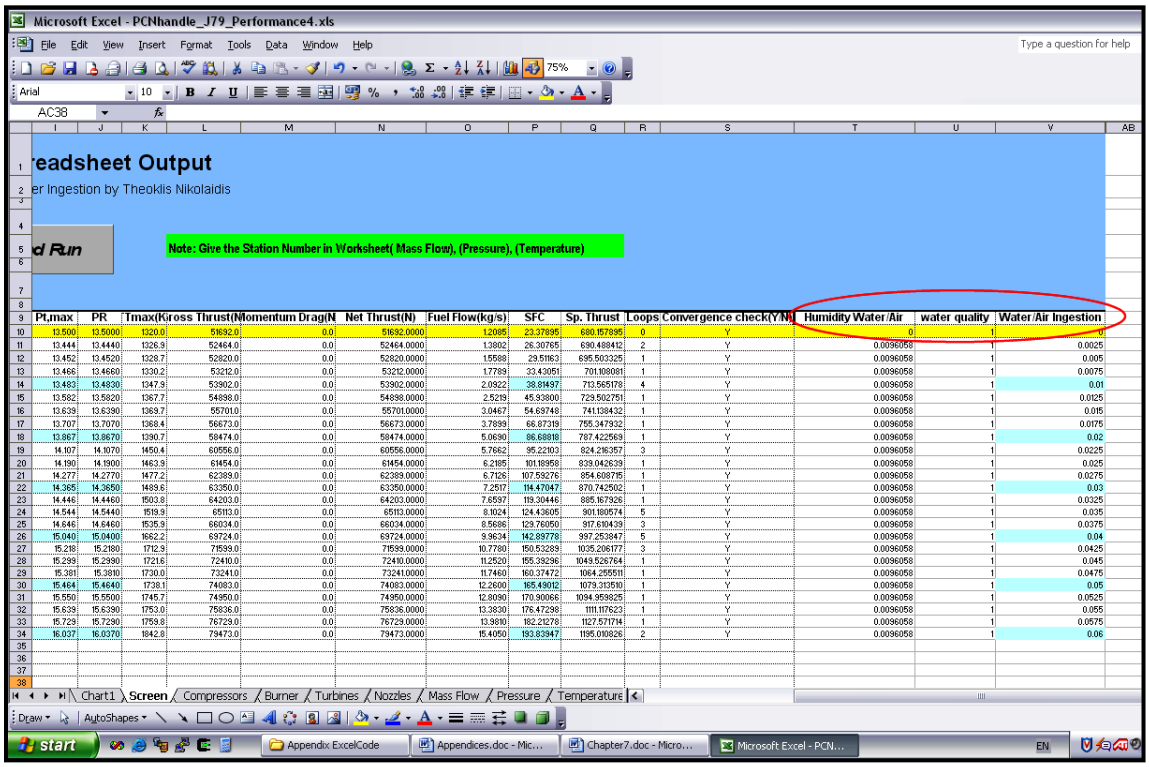

Figure F-3: Turbomatch Spreadsheet File

G. Water Ingestion Module Flowchart

The effects of water ingestion in a gas turbine engine performance are included in the Turbomatch new version (June 2008). A new module, named “WaterIngestionDeterioration” and the included new subroutines, has been added and calculates the deterioration, which is caused due to engine’s operation in rain conditions. To be more specific, four new subroutines use data for the WAC, ETA and PR deterioration in the compressor and ETA, P loss in the burner due to liquid water. Furthermore, the extra torque TRQW needed by the compressor to accelerate the liquid water film, which is formed on the blade, is also calculated and added to the compressor work. The flowchart of the water ingestion software is presented in figure G-1.

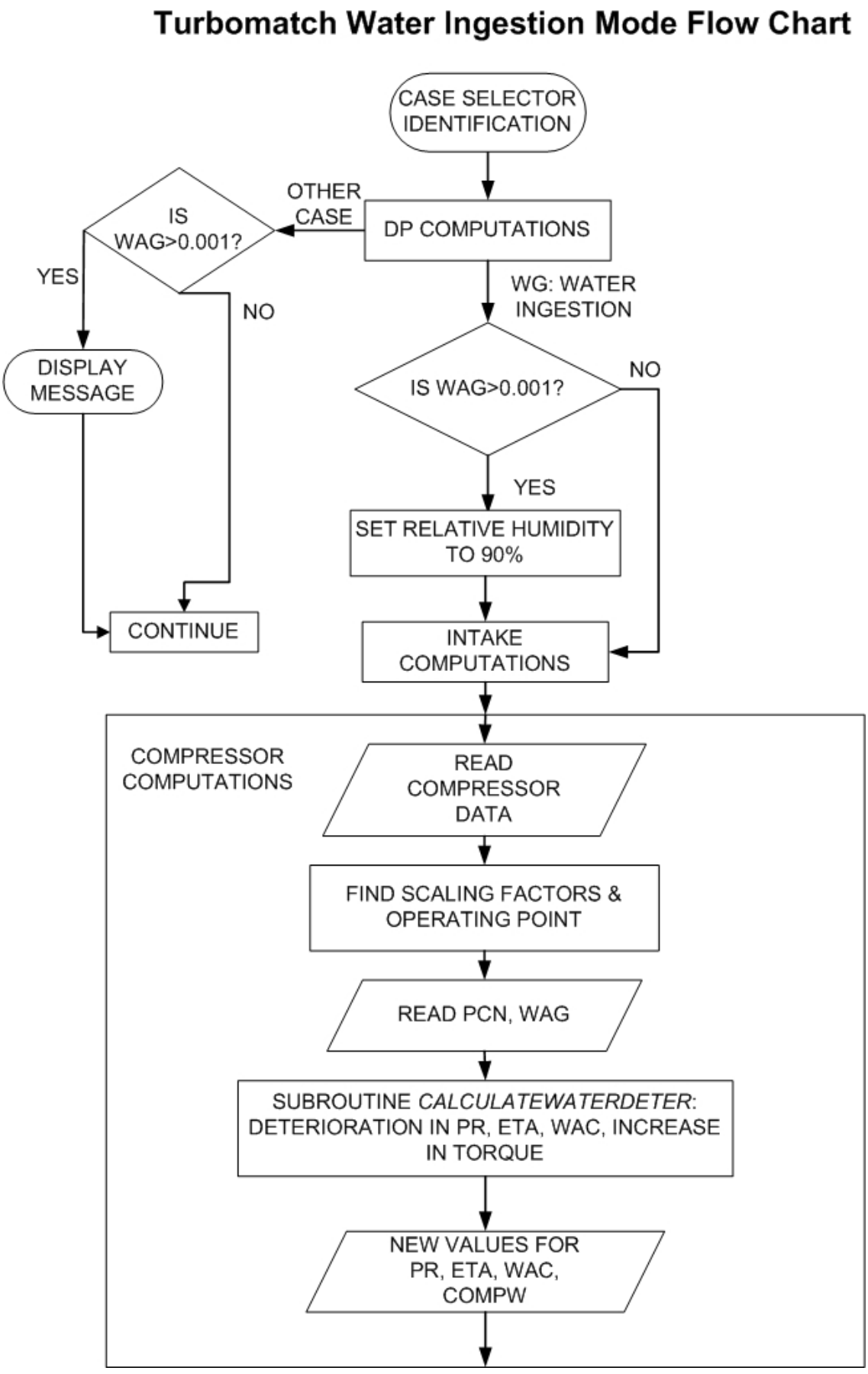

(Continued in the next page)

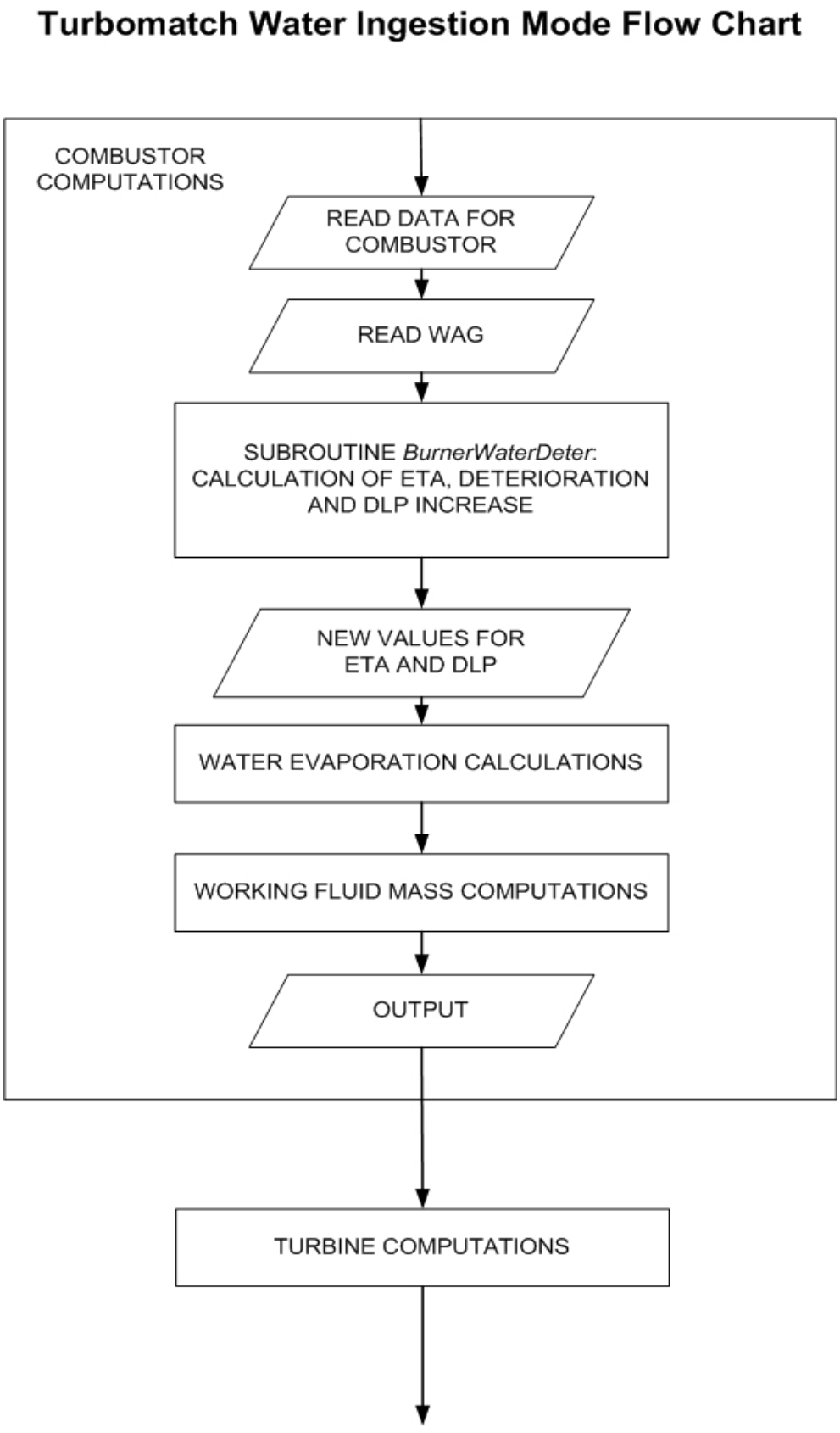

Figure G-1: Turbomatch Water Ingestion Flowchart